University of Glasgow

Nelson, D. James (1976) *On the mechanics of discontinuous fibre reinforced composite materials (with particular reference to damping).* PhD thesis.

http://theses.gla.ac.uk/1520/

Copyright and moral rights for this thesis are retained by the author

A copy can be downloaded for personal non-commercial research or study, without prior permission or charge

This thesis cannot be reproduced or quoted extensively from without first obtaining permission in writing from the Author

The content must not be changed in any way or sold commercially in any format or medium without the formal permission of the Author

When referring to this work, full bibliographic details including the author, title, awarding institution and date of the thesis must be given

Glasgow Theses Service
http://theses.gla.ac.uk/
theses@gla.ac.uk

ON THE MECHANICS OF

DISCONTINUOUS FIBRE REINFORCED COMPOSITE MATERIALS

(WITH PARTICULAR REFERENCE TO DAMPING)

D. James Nelson B.Sc. (Edinburgh)

Department of Mechanical Engineering

University of Glasgow

A thesis submitted to the University of Glasgow
for the degree of Doctor of Philosophy

September 1976

SUMMARY

On the mechanics of discontinuous fibre composite materials - (with particular reference to damping).

Ph.D. thesis by D. James Nelson B.Sc. (Edinburgh).

To further the understanding of the behaviour of discontinuous fibre composite materials with particular reference to their damping properties, model materials were made from stub steel rod of 0.4 mm diameter as fibres (set out in brickwork pattern) and a proprietary silicone rubber matrix. A good bond at the matrix/fibre interface was achieved by use of a special primer on the fibres while little or no bonding occurred if the primer were not used. In some of the unbonded specimens, the fibre surfaces were etched which caused a significant change in properties relative to the unetched case.

Current theory yields reasonable predictions of the Young's modulus for the bonded specimens although non-linearity in the stress-strain characteristic of the silicone rubber makes exact prediction difficult. The unbonded specimens exhibited yield phenomena due to interfacial sliding and the etched specimens also showed the unusual characteristic of returning to the zero load and displacement position even after gross sliding had occurred. An explanation for this behaviour was sought in modifications to the theory used for the prediction of bonded specimen modulus.

Tests were also conducted at low frequency (0.83 Hz) under imposed sinusoidal displacement conditions. Large hysteresis loops were produced in the case of the unbonded specimens - the interfacial sliding increasing the energy lost per cycle but reducing the stiffness.

This combined effect led to large increases in specific damping capacity (the ratio of energy lost per cycle to maximum strain energy in the cycle). It was also found that the specimen properties both bonded and unbonded were broadly dependent upon the amplitude of the hysteresis loops although stress history also played some part. The characterisation of these results was not found to be simple.

The specimens, which were in the form of rods, were also tested as the spring/damper element in a one degree of freedom system (resonance at $\sim$ 20 Hz). The results were treated in a quasi-linear fashion since the incidence of harmonics was generally low. The acceptability of this method seems dependent upon the fact that the material properties depend on the amplitude of vibration rather than the instantaneous value. Broadly speaking the vibration experiment results were in agreement with the 0.83 Hz tests although in the case of the unbonded specimens there was a rate effect which caused the specimens to be stiffer and have less damping at the higher deformation rates.

It was concluded that the discontinuous reinforcement of a matrix material such that shear strain in the matrix is amplified can be an important source of damping and stiffening. If there is little or no bonding at the matrix/fibre interface then the specific damping capacity developed by the composite can be very large indeed, but will be partly due to loss of stiffness. The basic lack of integrity inherent in an unbonded discontinuous fibre composite is sufficiently unattractive that it would seem best that a material developed for its damping/sound deadening properties should have a matrix which bonds well to the fibres and which has a dissipative

capacity increasing greatly with increase in shear strain and/or rate of deformation.

ACKNOWLEDGEMENTS

I would like to thank Professor J.D. Robson for affording me the opportunity of undertaking this work in the Department of Mechanics and Mechanism, University of Glasgow and for injecting a number of useful suggestions.

My thanks are also due to my supervisor Dr. John Hancock for numerous helpful discussions and showing great restraint in the face of severe provocation.

Dr. Colin Dodds helped with the supply and operation of some of the vibration equipment and Mr. Patrick Irwin provided useful advice and repairs when electronic things went wrong. Everything else that was required was produced by Mr. Neil Flaherty whose manifold skills did not cease to amaze me.

Finally I would thank Mrs. Margaret Earl for typing most of the manuscript.

D.J.N.

CONTENTS

NOTATION

Names in brackets refer to particular authors who were the source of some of the symbols.

a	fibre buckling amplitude (Rosen)
	amplitude of vibration
a_{max}	maximum amplitude (resonance)
a_n	maximum amplitude in a cycle of a decaying vibration
a_{res}	resonant amplitude
a_{st}	amplitude at zero frequency for same excitation force
	magnitude
A_c	cross-sectional area of composite
A_f	cross-sectional area of fibre
A_r	resonance amplification factor
c	half inter-fibre spacing (Rosen)
	viscous damping constant
c_{eq}	equivalent dashpot constant
C	constant of integration
e	$e_m - e_{max}$
e_c	composite strain
e_m	matrix strain
e_{max}	maximum matrix strain in cycle
e_{mc}	critical matrix strain
e_y	matrix strain (Rosen)
E	$E_f - E_m$
E_c	composite Young's modulus in fibre direction
E_{cs}	local Young's modulus during sliding

E_f	fibre Young's modulus
E_m	matrix Young's modulus
E_{SH}	strain-hardening modulus
E^*	complex Young's modulus
E'	storage modulus
E''	loss modulus
f	frequency
f_n	natural frequency
f_r	resonant frequency
F	force at mean amplitude (unbonded specimens)
	amplitude of exciting force
F_o	deviation from mean force at mean displacement (bonded specimens)
F_1	deviation from mean force at maximum displacement (bonded specimens)
G_m	matrix shear modulus
h	fibre thickness (Rosen)
	coefficient of hysteretic damping
h'	across flats dimension of fibre (Mileiko)
h''	inter-fibre spacing (Mileiko)
H	$\frac{2\pi G_m}{\log_e \frac{R}{r_f}}$ (Cox)
I	second moment of area
k	stiffness
k_{mean}	mean stiffness (bonded specimens)
k_x	stiffness at x

l	fibre length
l'	overlap length (Mileiko)
m	mass
p_i	interface pressure
P	load, force
P_c	critical fibre load
P_{fmax}	maximum fibre load due to constant $\tau_i = -\tau_{ic}$ along fibre length
r	radial co-ordinate
r_f	fibre radius
R	radius of cylinder of matrix round fibre
s	standard deviation
t	time
u	displacement in matrix (Cox and Rosen)
U_f	fibre strain energy (Rosen)
U_m	matrix strain energy (Rosen)
v	displacement in matrix (Cox and Rosen) magnitude of velocity
V	volume of matrix (Rosen)
V_f	volume fraction of fibres
w	displacement in matrix (Kelly)
W	matrix strain energy in a cycle
ΔW	energy lost per cycle work done by fibre load (Rosen)

x	co-ordinate along fibre
	displacement in oscillatory tests
x_m	maximum displacement in a cycle
x'	limit of sliding region
x'_r	limit of sliding region (reverse direction)
$\dot{x}$	velocity
$\ddot{x}$	acceleration
X	peak displacement amplitude
	resonant displacement amplitude
X_0	amplitude of vibration
X_1	displacement of driven mass (Adams)
y	co-ordinate in matrix
z	displacement in matrix
Z	mechanical impedance
α	proportion of bonded interface
β	$\left(\frac{H}{A_f E}\right)^{\frac{1}{2}}$ (Cox)
γ_{xy}	matrix shear strain (Rosen)
δ	logarithmic decrement
ε_0	strain amplitude
ζ	damping ratio
η	loss factor

μ	coefficient of interfacial friction
ν	relative displacement of fibres (Mileiko)
ν_m	matrix Poisson's ratio
σ_c	composite stress
σ_{cp}	composite stress due to Poisson's ratio effect
σ_f	direct fibre stress
$\sigma_{f(\frac{l}{2})}$	direct fibre stress at fibre centre
$\sigma_{fy(\frac{l}{2})}$	direct fibre stress at fibre centre on yielding
σ_y	matrix stress (Rosen)
τ_i	interface shear stress
τ_{ic}	critical interface shear stress
τ_{if}	sliding friction interface shear stress (pull-out test)
τ_{ip}	interface shear stress due to Poisson's ratio effect
$\tau_{i(0)}$	interface shear stress at fibre end
τ_m	matrix shear stress
τ_{po}	frictional interface shear stress at pull-out initiation
τ_{xy}	matrix shear stress (Rosen)
ψ	specific damping capacity
ω	circular frequency

CHAPTER ONE

1. Introduction

Damping is a general term referring to the dissipation of vibrational energy by any means. The word was apparently coined by Föppl in 1923 (von Heydekampf, 1931) and is a transliteration from the German "Dämpfung". The sources of damping in an engineering structure can be many and varied, e.g. (Adams, 1972) friction in joints, acoustical damping, various damping mechanisms in the material of the structure, the effect of applied damping treatments and the addition to the structure of a viscous damper or shock absorber.

The need for damping of a structure is usually quite simple and obvious. Frequently damping is required to minimise resonant amplitudes and thereby limit the possibility of high stresses which may lead to rapid fatigue and subsequent fracture. Some of the areas in which low damping is likely to create problems are given by Robertson and Yorgiadis, 1946 as in long transmission wires, aeroplane structures and propellers, turbine blades and engine crankshafts. The same authors also point out that high damping leads to heating of the material and is a disadvantage in problems concerning the whirling of shafts. Other damping requirements are of an environmental nature as in, for example, a road vehicle where the inclusion of shock absorbers in the suspension is a both adequate and simple solution to the problem.

It is not always possible to provide external damping through the use of viscous dampers attached to a structure and with the advent of welded construction, which does not use bolted or rivetted

joints, the major source of damping may be the material of which the structure is made. This realisation along with a belief that damping might be closely and predictably associated with fatigue prompted many investigators from the 1920 s onwards to attempt to measure damping as an engineering property of materials.

Primarily, these studies were intended to allow prediction of the damping inherent in a structure by summing the damping likely to occur in its component parts. Further to this, it was hoped that damping measurements might allow some assessment of a material particularly in relation to fatigue and consequently they were intended to be in the nature of an inspection procedure. A more recent suggested application of damping measurements as an inspection tool in the field of composite materials has been given by Adams et al. 1973.

By and large from the engineering point of view, it is probably only necessary to know whether materials have low or high damping. If the damping of the material of a structure is high, e.g. cast iron, then some reasonable damping of vibration may be expected. If on the other hand the damping is low, e.g. Duralumin, then some means of providing additional damping is likely to be required. Low damping, however, may also be inherently desirable in, for instance, the construction of instruments where a hysteresis loss may militate against accuracy.

The literature on damping is very extensive, if one includes in it, the work of metallurgists who have largely performed experiments at strains so low that they are not of engineering interest - see, for example, Zener 1948 and Entwhistle 1962. These

studies were, of course, directed at testing various theories about the structure of metals and were, therefore, not intended for engineering use.

Another area in the field of materials science which has yielded a substantial literature, e.g. Ferry 1970, is the study of polymers in which measurements of material moduli and loss factors as influenced in particular by temperature and frequency are designed to test theories related to the structure of polymers. This type of work is likely to gain in engineering significance with the growing interest in and use of fibrous composite materials which as Adams et al. 1973 put it "offer the possibility of both high strength (from the fibre) and high damping (from the matrix and from the matrix/fibre interface)". It must be pointed out, on the other hand, that gross interfacial sliding implies a significant loss in both strength and stiffness.

As is now known, Adams and Bacon 1973b, the damping produced in a continuous fibre composite material is fairly low - the maximum figures quoted by Adams and Bacon being all less than 1% specific damping capacity. This had already been theoretically predicted by Hashin 1970 who showed that for the case of continuous aligned fibres in a viscoelastic matrix the damping of the composite will be small.

The reason for this is that viscoelastic materials must undergo large deformations for any substantial energy dissipation to occur. Clearly in a composite material with aligned continuous high modulus fibres such as carbon fibres the stiffness in the fibre direction will be very great and the strain to failure consequently

small. The strain in the matrix will also be small.

Accordingly the production of a composite material of high damping almost certainly requires the use of discontinuous fibres such that the load will be continuously alternating between fibres and matrix along the loaded length of the material. This will occasion very much greater shear deformations in the matrix and a loss of stiffness in the composite relative to the continuous fibre case.

McLean and Read 1975, recognised that the shear strain amplification which occurs in a matrix reinforced by aligned discontinuous fibres could be an important source of damping. They predicted that a material in the configuration of their model would produce damping about two orders of magnitude greater than that of the matrix material alone. This is quite possible but because the reinforcement increases the stiffness of the material by an equivalent factor, the ratio of energy lost to maximum strain energy in a cycle of vibration (the specific damping capacity) does not change, if the fibres are relatively rigid.

The case of a material in which the matrix and fibre are not well bonded was also considered by McLean and Read. The analysis of such a system is complicated by the fact that sliding at the matrix fibre interface also occasions a loss in stiffness and, implicitly, inefficient use of the reinforcement. It seems likely in consequence that discontinuous fibre composite materials fabricated for their damping properties may find more ready application as spring/damper units rather than as predominantly structural materials.

The present work which deals with discontinuous fibre reinforced material models which have either good or poor interfacial bonding is split into three sections. In the first section (Chapters 2 - 6), the development of the material is described and its mechanics considered in detail using an extension of current theory. The second section (Chapter 7) deals with some slow strain cycle tests on the material and in the third section (Chapters 8 - 11), the measurement of damping is reviewed and the results for some dynamic tests analysed and compared with the results from Chapter 7 and linear theory.

In the twelfth and concluding chapter the entire work is reviewed and an attempt made to draw together its three different strands into a coherent whole or to show where necessary in which respects this is not really possible. Overall conclusions are also drawn in this chapter.

CHAPTER TWO

2. Theoretical Background

There have been a number of attempts to produce simple theories for load transfer between fibre and matrix some of which are reviewed by Holister and Thomas 1966. Although these theories are only concerned with an isolated fibre, consideration of them can still be instructive.

Cox 1952, for example, considered a fibre of length l in a matrix under a general strain e_m. He defined the displacements u and v at a point distance x from the end of the fibre as

u = displacement if fibre is present

v = displacement of same point if fibre is absent

The load transfer from matrix to fibre is then defined as

$$\frac{dP}{dx} = H(u - v) \qquad 2.1$$

where P is the load in the fibre and H a constant. The strain in the matrix is

$$e_m = \frac{dv}{dx} \qquad 2.2$$

and the strain in the fibre is $\frac{du}{dx}$ where

$$\frac{du}{dx} = \frac{P}{A_f E} \qquad 2.3$$

where A_f = the cross-sectional area of the fibre and $E = E_f - E_m$ is the difference between the fibre (E_f) and matrix (E_m) Young's moduli.

Differentiating 2.1 gives

$$\frac{d^2P}{dx^2} = H\left(\frac{du}{dx} - \frac{dv}{dx}\right) \qquad 2.4$$

and substituting 2.2 and 2.3 into 2.4 leads to

$$\frac{d^2P}{dx^2} = H\left(\frac{P}{A_f E} - e_m\right) \qquad 2.5$$

which has general solution

$$P = A_f E e_m + R\sinh\beta x + S\cosh\beta x \qquad 2.6$$

where

$$\beta = \left(\frac{H}{A_f E}\right)^{\frac{1}{2}} \qquad 2.7$$

Using the boundary conditions $P = 0$ at $x = 0$ and $x = l$ and a little additional manipulation gives

$$P = (E_f - E_m)A_f e_m\left[1 - \frac{\cosh\beta\left(\frac{l}{2} - x\right)}{\cosh\beta\frac{l}{2}}\right] \qquad 2.8$$

The stress in the fibre is thus

$$\sigma_f = (E_f - E_m)e_m\left[1 - \frac{\cosh\beta\left(\frac{l}{2} - x\right)}{\cosh\beta\frac{l}{2}}\right] \qquad 2.9$$

The shear stress τ_i at the fibre/matrix interface may be deduced from consideration of figure 1. whence

$$\frac{dP}{dx}\,dx = -2\pi r_f\,dx\,\tau_i$$

$$\tau_i = -\frac{1}{2\pi r_f}\,\frac{dP}{dx} \qquad 2.10$$

Differentiating 2.8 and substituting in 2.10 gives

$$\tau_i = -\frac{(E_f - E_m)A_f e_m \beta \sinh \beta\left(\frac{l}{2} - x\right)}{2\pi r_f \cosh \beta \frac{l}{2}} \qquad 2.11$$

No explanation is given by Cox for the form of the constant H but Kelly 1966 suggests the following. The composite is supposed to consist of a set of many parallel fibres of constant length l and of circular cross-section, radius, r_f . The mean centre to centre separation of the fibres normal to their length is $2R$. If $\tau_m(r)$ is the shear stress in the direction of the fibre axis on cylinders co-axial with the fibre then at the surface of the fibre $r = r_f$, $\tau_m(r_f) = \tau_i$ and

$$\frac{dP}{dx} = -2\pi r_f \tau_i$$

$$= H(u - v)$$

$$H = -\frac{2\pi r_f \tau_i}{u - v} \qquad 2.12$$

Let w be the actual displacement in the matrix close to the fibre. Then at the fibre matrix interface assuming no interfacial slip $w = u$. It is assumed that at the sufficiently large distance R from the fibre central axis $w = v$. Considering the equilibrium of the matrix between r_f and R and neglecting any change in the direct stress across the element gives

$$2\pi r \tau_m(r) = \text{constant} = 2\pi r_f \tau_i$$

And so the shear strain in the matrix is given by

$$\frac{dw}{dr} = \frac{\tau_m(r)}{G_m} = \frac{\tau_i r_f}{G_m r}$$

where G_m is the shear modulus of the matrix. Integrating from r_f to R

$$\Delta w = \frac{\tau_i r_f}{G_m} \log_e\left(\frac{R}{r_f}\right)$$

But $\Delta w = v - u$ so substituting in 2.12 gives

$$H = \frac{2\pi G_m}{\log_e\left(\frac{R}{r_f}\right)} \qquad 2.13$$

Non-dimensional plots of the fibre stress σ_f and the interface shear stress τ_i are shown in figures 2 and 3 using parameter values representative of the materials actually used. It will be noted that the shear stress distribution is very nearly linear and consequently the fibre stress distribution will be close to parabolic.

Another analysis, which may be adapted for elastic conditions, was presented by Mileiko 1970 as a model for creep. It is based on a rather ingenious model consisting of hexagonal cross-section fibres in a hexagonal array. This leads to consideration of diamond shaped elements (see figure 4). The incorporation of elastic rather than creep parameters in the model makes the analysis ccnsiderably simpler. Physically it is assumed that the resistance of the matrix to tensile stress is negligible - an assumption which implies that holes will open up in the matrix.

The interface shear stress is assumed constant. Using the same notation as before and that of figure 4

$$\tau_i = \frac{1}{2}\frac{h}{l'}\sigma_{f(\frac{l}{2})} \qquad 2.14$$

where $\sigma_{f(\frac{l}{2})}$ is the stress at the fibre centre, and l' (for equal overlaps) $= \frac{l}{2}$

From purely gecmetrical considerations, the shear stress in the matrix at position y (see figure 4) is

$$\tau_m(y) = \tau_i \frac{h'}{2y} \quad \text{for } \frac{h'}{2} \leq y \leq \frac{1}{2}(h'+h'')$$

and shear strain $\gamma_m(y) = \frac{\tau_i}{G_m}\frac{h'}{2y}$ 2.15

The relative displacement of the fibres is thus

$$\nu = 2\int_{\frac{1}{2}h'}^{\frac{1}{2}(h'+h'')} \frac{\tau_i}{G_m}\frac{h'}{2y}\,dy$$

$$\therefore \nu = \frac{\tau_i}{G_m} h' \log_e\left(\frac{h'+h''}{h'}\right) = \frac{\tau_i}{G_m} h' \log_e V_f^{-\frac{1}{2}} \qquad 2.16$$

On the assumption of equal overlaps the strained composite will appear as in figure 4 and the longitudinal strain will be

$$e_c = \frac{2\nu}{l} \qquad 2.17$$

Letting the general load $\sigma_c = \sigma_{f(\frac{l}{2})} V_f$, remembering $V_f = \left(\frac{h'}{h'+h''}\right)^2$ and substituting 2.14 and 2.16 into 2.17 gives

$$e_c = \frac{2}{l^2}\frac{\sigma_c}{G_m}\left(h'+h''\right)^2 \log_e V_f^{-\frac{1}{2}} \qquad 2.18$$

$$E_c = \frac{\sigma_c}{e_c} = \frac{G_m}{2}\frac{l^2}{(h'+h'')^2}\frac{1}{\log_e V_f^{-\frac{1}{2}}} \qquad 2.19$$

where E_c is the composite modulus in the fibre direction.

Outwater 1956 recognised that for polymers the bond between fibre and matrix might well be poor or non-existent which leads under sufficiently high loading to interfacial slip. However, his subsequent analysis is based on the improbable assumption that the matrix does not deflect in shear. In fact, the shear deflection of the matrix is important since the shear strains in a matrix reinforced as in fig. 4 will be very much greater than in a piece of unreinforced matrix at the same overall strain. This effect is described as shear strain amplification.

All these analyses deal with composites in tension. It will beccme clear that some analysis of composites or more particularly fibres in compression is required to explain the phenomena involved in this study. One such analysis is that due to Rosen 1965 which is however, more succinctly explained by Jones 1975.

It is supposed that when a composite is compressed that failure is due to fibre buckling. This in turn leads to the possibility of two modes of buckling failure - the extensional mode when the fibres buckle in anti-phase and the shear mode in which the fibres buckle in phase. These failure modes are shown in figure 5. The basic model is a two dimensional one with plates h thick embedded in a matrix at spacing $2c$. The plates, i.e. fibres, are very much stiffer than the matrix.

The method employed is an energy one described by Timoshenko and Gere 1961. The load per fibre P is supposed to do work during the buckling deformation which is equated to the change in strain energy of the fibre and surrcunding matrix. The calculated buckling load will be an upper bound on the true buckling load. It is likely that a fibre in the actual composites used will only buckle in the fundamental half-wavelength form so the analysis presented by Rosen has been simplified accordingly. Thus the buckling displacement perpendicular to the fibre direction is taken to be

$$v = a \sin \frac{\pi x}{l} \qquad 2.20$$

In the transverse mode the strain in the y direction is assumed independent of y i.e.

$$e_y = \frac{2v}{2c} \qquad 2.21$$

so that

$$\sigma_y = E_m \frac{v}{c} \qquad 2.22$$

The change in strain energy is assumed to be dominated by that due to the transverse stresses giving the change in strain energy of the matrix as

$$\Delta U_m = \frac{1}{2}\int_v \sigma_y e_y \, dV \qquad 2.23$$

$$\therefore \Delta U_m = \frac{E_m l}{2c} a^2 \qquad 2.24$$

From the analysis of Timoshenko and Gere the change in fibre strain energy is

$$\Delta U_f = \frac{\pi^4 E_f I}{4 l^3} a^2 \qquad 2.25$$

and the work done by the force on the fibre is

$$\Delta W = \frac{P \pi^2}{4 l} a^2 \qquad 2.26$$

It is assumed that

$$\Delta W = \Delta U_m + \Delta U_f \qquad 2.27$$

$$\therefore P \frac{\pi^2}{4l} a^2 = \frac{E_m l}{2C} a^2 + \frac{\pi^4 E_f I}{4 l^3} a^2$$

or

$$P = \frac{4l}{\pi^2}\left[\frac{E_m l}{2C} + \frac{\pi^4 E_f I}{4 l^3}\right] \qquad 2.28$$

Equation 2.28 gives the upper bound on the critical buckling load for the extension mode.

For the shear mode analysis the shear strains are presumed to be a function of the fibre direction co-ordinate alone

$$\gamma_{xy} = \frac{\partial v}{\partial x} + \frac{\partial u}{\partial y} \qquad 2.29$$

where v is the displacement in the y direction and u is the displacement in the x direction. Since the transverse displacement is independent of the transverse co-ordinate y

$$\left.\frac{dv}{dx}\right|_{matrix} = \left.\frac{dv}{dx}\right|_{fibre} \qquad 2.30$$

Since the shear strain is independent of y

$$\frac{\partial u}{\partial y} = \frac{1}{2C}\left[u(C) - u(-C)\right] \qquad 2.31$$

This relationship is shown in figure 6 from which it may also be deduced (ignoring fibre shear deformation) that

$$u(c) = \frac{h}{2}\left.\frac{dv}{dx}\right|_{fibre} \qquad 2.32$$

Thus

$$\frac{\partial u}{\partial y} = \frac{h}{2c}\left.\frac{dv}{dx}\right|_{fibre} \qquad 2.33$$

and

$$\gamma_{xy} = \left(1+\frac{h}{2c}\right)\left.\frac{dv}{dx}\right|_{fibre} \qquad 2.34$$

The change in strain energy of the matrix is this time dominated by shear

$$\Delta U_m = \frac{1}{2}\int_v \tau_{xy}\,\gamma_{xy}\,dV \qquad 2.35$$

$$\Delta U_m = G_m c\left(1+\frac{h}{2c}\right)^2 \frac{\pi^2}{2l} a^2 \qquad 2.36$$

Hence, since the work done and the buckled fibre strain energy are given by the same expressions as before,

$$P\frac{\pi^2}{4l}a^2 = G_m c\left(1+\frac{h}{2c}\right)^2\frac{\pi^2}{2l}a^2 + \frac{\pi^4 E_f I}{4l^3}a^2$$

$$P = 2G_m c\left(1+\frac{h}{2c}\right)^2 + \frac{\pi^2}{l^2}E_f I \qquad 2.37$$

Contrary to the view expressed by Jones the second term on the right hand side of equation 2.37 is not necessarily negligible. The apparent imbalance in the units of the first terms on the right hand side of equation 2.28 and 2.37 is due to the composite being taken one unit thick.

CHAPTER THREE

3. Material Development

Most investigators although making composites by well-tried methods e.g. Adams and Bacon 1973b, cannot be certain that there is a complete bond between the fibres and the matrix. It has been shown Adams et al 1973, that the type of fibre and surface treatment have measurable effects on damping and it is consequently assumed that the fibre-matrix interface is important. This being the case, a material was sought which could be made to bond or not bond as desired to fibrous materials.

It was found that "Silcoset 100" a proprietary silicone rubber produced by ICI and used for such purposes as encapsulation of delicate electronic equipment, satisfied this requirement. A good bond could be effected if the surface were cleaned and primed with a special primer supplied by ICI. In fact ICI claim that the bond should be stronger than the "Silcoset" itself (ICI 1972). If the primer were not used little if any bonding occurred.

Although the curing agent causes cross linking of the polymer chains in the basic material, "Silcoset" still exhibits some visco-elasticity so the production of a composite with damping in the matrix can also be effected with this material. "Silcoset" cannot be regarded as a practical composite material component but because it was relatively easy to work with, and was capable of producing the effects desired, it was decided to persevere with it. A fairly full description of the properties and uses of "Silcoset" is given in ICI 1972.

It had originally been hoped to use carbon or glass fibres in the experimental programme and early experiments were carried out with glass fibres largely because this material is relatively cheap. Apart from the problem of voids the greatestdifficulty experienced was in obtaining satisfactory penetration of the matrix into the glass fibre tows. There were two reasons for this, the first being that silicone rubber is more viscous than, for example, epoxy resins and the second that when the fibres were primed, which must be done at least half an hour before applying the matrix to allow the primer to dry, the fibres tended to become stuck together. Attempts to tease them apart again were largely unsuccessful. This led to a very uneven distribution of the reinforcement. There was also a tendency for the primed tows to twist which made fibre alignment difficult.

The silicone rubber used is basically a soft material of low modulus and it was found that it was not possible to clamp it or the composite specimens because the matrix tended to extrude from the clamps. Attempts were made to provide a surface sufficiently hard for clamping by paring away the ends of the specimen and encapsulating them in "Araldite" epoxy resin adhesive but this did not prove very satisfactory.

In view of the problems associated with the production of specimens which would be sufficiently close to what was desired using glass fibres, it was decided that it would probably be more useful to make the material conform more directly to the model. Experimentation with glass fibre was therefore abandoned. In order to have control over what happened during the manufacturing process, it seemed easier

to use fibres of such a size that they could be readily manipulated. Stub steel rods of 0.4mm diameter filled this requirement and all subsequent work was carried out using these. Although such material does not conform to the normal conception of fibres, this description will be retained for it.

This decision to change the material altered the nature of the problem completely. First attempts to make steel/"Silcoset" composites were made using 150mm lengths of fibre held in a square array by plastic netting of small gauge. The problem here was, that the fibres were not readily kept in alignment. In any case this approach did not seem likely to solve the problem and it in turn was abandoned.

Use was now made of another property of "Silcoset" - that it will bond to previously cured "Silcoset" while curing. A piece of steel plate was grooved on a shaping machine and some steel fibres laid in the grooves. Some of the silicone rubber was poured on top and once this had cured it proved possible to lift this lamina of matrix material bringing with it the array of steel fibres whether primed or unprimed, since they were sufficiently embedded in the matrix to remain in position. Thus an array of fibres set out on the steel plate could be transferred to the matrix. This suggested a method of preparing specimens in which the phase geometry could be fairly closely controlled.

A mould consisting principally of a steel plate 180mm long by 150mm broad was made. The central 100mm by 150mm section was grooved at a spacing of about 0.94mm - the grooves running in the direction of the 100mm length, the remaining 25mm at either end of

the grooves being machined away in a step of about 1mm. (see figure 7). An array of steel fibres overlapping in a "brickwork" pattern was set out in the grooves with longer fibres at the ends so that they overhung the step in the plate. Since the matrix does not bond directly to steel, these overhung fibres had to be primed along their full length in every case and as will be seen, eventually formed the part of the specimen to be gripped. The rest of the fibres could be primed or unprimed as desired. An example of a typical array is also shown in figure 7.

Once the fibre array had been set out with the overhung fibres supported by thin strips of "Plasticene", a quantity of matrix which had been degassed was carefully poured on to the array so as not to disturb it. The lid of the mould was then put on and the composite left to cure in air. After curing, by removing the lamina produced carefully from the mould and cutting it into 6mm wide strips, the basic units from which the composite was made were ready.

The primer was cleaned from the fibres protruding from the ends of these strips. By using several of the strips and some additional "Silcoset", a rod specimen approximately 100mm long by 6.25mm square could be built up in an open ended mould like that shown in figure 8. Once the matrix had cured a specimen of 150mm overall length was obtained - the central 100mm section containing the desired fibre array set in the matrix and the remaining 25mm at either end containing only fibres. The specimen ends were completed by encapsulating these fibres in "Araldite" epoxy resin adhesive which is, of course, much harder than "Silcoset". The specimens were now ready for testing. Specimens could also be made incorporating only the end fibres for gripping. This allowed the properties of the matrix alone to be tested.

During the development process, it was found that cleaning the fibres in trichloroethylene did not seem to allow proper application of the primer although this later proved to be erroneous. However, at this stage some of the fibres were not only cleaned but etched in very dilute nitric acid. It was later shown that etched unprimed fibres as opposed to unetched unprimed fibres had a marked effect on the characteristics of the composite. For this reason three different types of specimen were made viz, with the fibres primed to effect a good bond and with the fibres unprimed both etched and unetched to investigate the interface effects.

To aid in the investigation of the interface characteristics pull-out specimens consisting of 50mm long cylinders of matrix with one fibre running up the centre of the cylinder were made. These specimens were moulded in cylindrical brass tubing with end caps which had small central holes. The holes were initially plugged up with "Plasticene" to locate the fibre and prevent spillage of the matrix. Two holes were drilled at either end of the brass mould with centres on the same generator - one larger hole for injecting the matrix material and the other smaller hole to let air escape. Once the rubber had set the end caps were removed.

CHAPTER FOUR

4. Pull-out Tests

Pull-out tests are intended to establish the properties of the interface between the fibre and matrix. It is assumed that the stresses created by the shrinkage of a polymer on to the fibre create a friction shear stress when an attempt is made to pull the fibre out. For the matrix material used, ICI 1972 give the linear shrinkage as 0.2% which allied to the low modulus of the material would produce very little effect.

In fact, shrinkage stress does not seem to be a factor in the present study. The pull-out test results, however, highlight the difference between etched and unetched interfaces. It is presumed that the lack of quantitative agreement between the pull-out specimens and the composite specimens is due to the significant difference in stress states in the two cases.

4.1 Method

An Instron tensile testing machine was used to test the pull-out specimens. To perform the pull-out tests a truncated female cone was passed over the fibre, the fibre was then passed through the hole in the crosshead of the Instron and the end of it gripped in the machine jaws. The cone was required because the hole in the Instron crosshead was larger than the specimen diameter and it was deemed desirable to leave the end of the cylinder of matrix as a free surface. The arrangement is shown schematically in figure 9.

The pull-out test could be carried out by using downward motion of the Instron crosshead. Since the matrix, the brass cylinder and the cone constituted part of the load, the load cell of the machine had to be zeroed before the specimen was put in position,

4.2 Results

Several different diameters of cylinder were used in making the pull-out specimens but there did not seem to be any correlation between this and the load at the start of pull-out. Consequently all the results were treated together regardless of the cylinder diameter. The assumption behind the making of pull-out specimens of different diameter was that there might be different amounts of shrinkage depending upon the specimen size. It seems, however, that "Silcoset" does not shrink much on curing as previously suggested.

The major difference between the etched and unetched pull-out tests was the shape of the load-displacement plot produced. Figure 10 shows the difference at its most obvious. It would be misleading, however, to suggest that all pull-out tests showed such a marked difference. Figure 11 shows unetched and etched specimens whose characteristics were much more similar. It would also be misleading to suggest that etched fibres were in all cases capable of sustaining higher loads before pull-out began than unetched ones. Indeed in both cases there were instances in which the cylinder and cone slid off the fibre under their own weight. This was possibly due to lack of cleanliness of the fibre or rough handling of the specimen before test.

However although there was a wide spread in the loads to the initiation of pull-out, the average for the etched fibres was more than one and a half times the average for the unetched, 7.87N compared to 4.82N. The range of loads to initiate pull out was quite wide being from 1.47N to 22.1N in the case of the etched fibres and 0.78N to 11.4N for the unetched.

Clearly since there was such a wide variation in the results of the pull-out tests there was likely to be a fairly wide variation in the results from the composite specimens although this variation would be reduced by the fact that the presence of many fibres in the composite specimens has an averaging effect.

Another area in which the pull-out test can provide some insight is the magnitude of the frictional shear stress. If it is assumed that the friction shear stress, τ_{iF} is constant along the length of the fibre once sliding has started, the incremental load dP over fibre length, dx will be

$$dP = -2\pi r_f \tau_{iF} dx$$

or

$$\frac{dP}{dx} = -2\pi r_f \tau_{iF} \qquad 4.1$$

or

$$\tau_{iF} = -\frac{1}{2\pi r_f}\frac{dP}{dx}. \qquad 4.2$$

where $\frac{dP}{dx}$ is the slope of the load displacement curve of the pull out test as the fibre end is pulled through the cylinder.

The variation in interfacial shear stress during sliding is, perhaps not surprisingly, quite wide in the unetched specimens. τ_{if} varies from -0.037 N/mm^2 to -0.068 N/mm^2 with an average of -0.054 N/mm^2.

The etched specimens which do not exhibit the same characteristics as the unetched ones as already noted show much lower values of frictional shear stress round about -0.016 N/mm^2.

To summarise then, the etched specimens show a higher resistance to the initiation of pull-out than the unetched ones but a lower resistance once pull-out has begun.

One other type of pull out test was carried out. Specimens with double lengths of fibre were made so that they could be pulled in either direction. This was done because it was thought that the interface might have directional properties.

Figure 12 summarises the results of one of these tests in terms of load to start pull-out. It will be noted that the load to initiate sliding drops to about one third of its initial value after several reversals and does not appear to depend much on direction. Figure 13 shows two sample charts of initiation of pull-out, one in each direction. There is obviously not much difference between them.

The load to initiate pull-out is given by integrating equation 4.1 such that

$$P = -2\pi r_f l \tau_{po} \qquad 4.3$$

where τ_{po} is the frictional shear stress at the initiation of pull-out. The average and range of values of τ_{po} are tabulated below

Table 1

		Average	Range
τ_{po}	Etched	-0.125	-0.023 to -0.351
N/mm^2	Unetched	-0.077	-0.012 to -0.181

CHAPTER FIVE

5. Matrix and Composite Specimen Tests

5.1 Method

The "Silcoset" and composite specimens were tested by a typical tensile test procedure. No evidence of slipping in the grips was noticed for the low loads which are required to test these materials. To obtain hysteresis loops an Instron G-51-15M strain gauge extensometer of 25mm gauge length was attached to the central 25mm of the specimen. This extensometer allows for elongations of up to 100%. For some tests a similar extensometer G-51-11M allowing only 10% elongation was also used. It was necessary to support the weight of the extensometer by means of a counterweight over a pulley to avoid any bending load on the specimen.

The extensometer was plugged into the strain gauge amplifier section of the machine via a D69-57 socket which reverses the motion of the chart drive sc that the elongation occurred on the x positive axis of the chart for load along the y positive axis. The chart was calibrated using Coventry Gauge matrix blocks and the load cell was calibrated using the calibration weights supplied by Instron.

5.2 Results

As can be seen from figure 14 the silicone rubber does show some hysteresis particularly at high strains. The load-displacement relationship is also quite clearly non-linear. Fracture in these specimens occurred at the ends of the fibres used as part of the grips presumably because these constitute stress raisers. It is apparent from figure 14 that the modulus of the matrix is very low.*

*See Addenda after Figure 89.

The mean Young's modulus of the matrix is plotted against maximum strain in the cycle in figure 15, data coming from the load displacement charts exampled in figure 14. There does not seem to be any particular trend so the average value of 3.17 N/mm^2 was used in calculations.

It is hardly surprising after examination of the difference between etched and unetched fibres in the pull-out test results that there should also be a marked difference in the characteristics of the etched and unetched composite specimens. This initial difference is best illustrated by reference to figure 16 which shows typical examples of the first tests on etched and unetched specimens. In the case of the etched specimen there was a very clear yielding* at a load of about 78.5N, the load then dropping to 45.6N before recovery began. In contrast the unetched specimen showed a distinct yield point at about 25.0N but there was only a small load drop as the strain was increased beyond this point. In several of the unetched specimens there is no drop at all.

Clearly there is likely to be some spread in the results for the yield points as is illustrated in the following table.

Table 2

Yield Load (N)	Average	Minimum	Maximum	Average Load drop after yield	No. of Specimens
Etched	69.6	58.9	85.3	29.6	7
Unetched	18.6	8.6	30.4	0.6	12

*See Addenda after Figure 89.

The proportionate variation is very much less than in the pull-out tests as might be expected because of the averaging effect already mentioned.

After yielding, the modulus of the composite was very much reduced. If the strain were increased, then, in the case of the etched specimens, further yielding occurred while, in the case of the unetched specimens, the load increased steadily. When the direction of straining was reversed the load and strain returned to zero in the case of the etched specimens but in the case of the unetched specimens, a permanent set was usually left.

On reloading after the initial yielding cycle all the unbonded specimens showed a distinct breakaway in the load-strain curve. However, on average the breakaway point occurred at a lower load in the etched specimens than the unetched as the table below shows.

Table 3

Breakaway Load (N)	Average	Minimum	Maximum	Standard Deviation
Etched	14.2	9.8	23.1	2.2
Unetched	20.4	11.8	27.5	4.5

It is noticeable that the breakaway loads on subsequent testing of the unetched specimens were very close to the original yield loads and on average in excess of them. On the otherhand the breakaway loads in the etched specimens are very much less than the yield loads - being only about 20% of them on average. This is perhaps predictable from the pull-out tests in which the load drop once the initial bond was broken was generally very much less for the unetched specimens compared to the etched ones.

In both etched and unetched specimens after the breakaway point there is, in general, a curved portion in the load-displacement relationship followed by a portion which is usually close to linear. Analysis of these linear portions shows that the stiffness of the composite at this stage is generally somewhat greater than that of the silicone rubber alone. Typical loops are shown in figure 17.

In the case of the early loops from etched specimens, the strain-hardening modulus of the specimen may be very much greater than the modulus of the matrix. It is supposed that this is due to the fact that not all the interfaces have broken, a supposition confirmed by the fact that additional yielding may occur on subsequent cycles. The unetched specimens exhibit a strain-hardening modulus much closer to that of the matrix but here again any additional stiffness may be due to residual bonding.

Clearly the whole shape of the hysteresis loop will be critically dependent upon the breakaway load and the subsequent slope of the load-displacement curve. The first part of the cycle might reasonably be approximated by a bilinear spring model with a friction element such as that shown with its load-displacement curve in figure 18. However, there is a distinct departure from this simple bilinear behaviour on the unloading part of the cycle.

On unloading the modulus of the composite is initially similar to the modulus on loading up to the breakaway point. There is then what may be described as a reverse breakaway point which occurs after a load drop which is generally greater than the original breakaway load in the cycle but less than twiccas large. The load drop

to the reverse breakaway point will be designated the reverse breakaway load. The expectation in a simple bilinear model would be that the reverse breakaway load would be twice the original breakaway load. Figure 19 shows the reverse breakaway load against breakaway load in the same cycle for both etched and unetched specimens. It is clear from this figure that there is a difference between etched and unetched specimens in this respect.

The behaviour of the etched specimens is particularly interesting. Although the reverse breakaway loads were up to three times the breakaway load in the cycle, the loops consistently closed at zero load and displacement. The likely reasons for this behaviour and the connection between it and the behaviour of the unetched specimens will be discussed later.

Some primed fibre, i.e. bonded, specimens were also tested and these exhibited somehysteresis at small strains. It must be remembered that small composite strains imply much larger shear strains in the matrix. The bonded specimens also exhibited non-linear stiffness which is almost certainly due to the non-linear nature of the matrix load-displacement relationship. A typical result for a primed specimen is shown in figure 20.

CHAPTER SIX

6. Interpretation of Results

6.1 Bonded fibre specimens

The volume fraction of fibres (V_f) in the composites under consideration is about 7.5%. It is assumed that this is a sufficiently dilute concentration for the theory of Cox to apply. The fact that the matrix exhibits non-linear stiffness presents an additional problem since H defined in equation 2.13 will not be constant. As noted previously an average value of the matrix Young's modulus = 3.17 N/mm^2 has been used in calculations. It is also assumed that the matrix is incompressible i.e. that the matrix shear modulus $G_m \simeq \frac{1}{3}E_m \simeq 1.06\ N/mm^2$

The value of H depends upon $\log_e \frac{R}{r_f}$ which may be interpreted more generally as $\log_e V_f^{-\frac{1}{2}}$. This implies an assumption of an average value for the fibre centre to centre spacing 2R. In this instance we have $\log_e V_f^{-\frac{1}{2}} \simeq 1.295$ implying R = 0.73mm, H = 5.14 N/mm^2 and $\beta = 1.394 \times 10^{-2}\ mm^{-1}$

According to Kelly 1966, the Young's modulus of the composite using Cox's theory will be

$$E_c = E_f V_f \left(1 - \frac{\tanh \frac{\beta l}{2}}{\frac{\beta l}{2}}\right) + E_m (1 - V_f) \qquad 6.1$$

With $\frac{\beta l}{2} = 0.1743$, $\tanh \frac{\beta l}{2} = 0.1725$, $V_f = 0.075$, $E_f = 210000\ N/mm^2$

$$E_c = 160.4\ N/mm^2$$

An alternative interpretation of the results may be made using the theory of Mileiko with elastic parameters. Equation 2.19

gives the composite modulus as

$$E_c = \frac{G_m}{2} \frac{\ell^2}{(h' + h'')^2} \quad \frac{1}{\log_e V_f^{-\frac{1}{2}}} \qquad 6.2$$

For the purposes of the composite under consideration we already have $\log_e V_f^{-\frac{1}{2}} = 1.295$, $\ell = 25\text{mm}$ and $G_m = 1.06\ \text{N/mm}^2$. As an approximation we can take $h' = 2r_f = 0.4\text{mm}$ and estimate h'' from

$$V_f = \left(\frac{h'}{h' + h''}\right)^2 \qquad 6.3$$

With $V_f = 0.075$ this gives $h'' = 1.06\text{mm}$ and hence $E_c = 120.0\ \text{N/mm}^2$.

In both the Cox and Mileiko analyses, the modulus is very heavily dependent on the inter-fibre spacing. The justification for taking a mean is that although the inter-fibre spacing is known in one direction (the pitch of the grooves in the plate mould) the array is basically rectangular and the pitch in the orthogonal directions may differ. Using an average figure based on the volume fraction seems a reasonable compromise. If anything this procedure underestimates the Young's modulus of the composite, since the stiffness measured experimentally on primed fibre specimens was of the order of $200\ \text{N/mm}^2$, a result which tends to favour the Cox analysis. Probably the more reasonable conclusion is that taking the volume fraction based average fibre spacing has a more severe effect on the Mileiko analysis.

6.2 The yield point in unbonded specimens

As is clear from figures 16 and 20 the unprimed specimens both etched and unetched have very different characteristics from the primed specimens. The difference arises due to slippage at the matrix fibre interface which gives rise in the first instance to yield. This is very much more marked in the etched than the unetched specimens as might be expected (at least qualitatively) from the pull-out test results already discussed.

It might be supposed that this yielding would occur when the shear stress at the matrix/fibre interface exceeded some critical value, τ_{ic} . Unfortunately, the critical value cannot be quantified exactly because, as is evident from the pull-out tests, friction and yielding at the interface can vary very significantly from one interface to another. It is possible, however, to look at average properties.

The average yield load for an etched specimen is 69.6N. Since (considering the cross sections through the fibre centres and remembering the brickwork layout) there are essentially twelve fibres supporting this load at their centres $(x = \frac{l}{2})$, the stress at the fibre centre at yield $\sigma_{fy(\frac{l}{2})}$ is

$$\sigma_{fy(\frac{l}{2})} = 46\ N/mm^2$$

On Cox's theory this implies a certain maximum interface shear stress at $x = 0$

Equation 2.11 may be rewritten as

$$\frac{\tau_i}{(E_f - E_m)e_m} = -\left(\frac{G_m}{2E\log_e \frac{R}{r_f}}\right)^{\frac{1}{2}} \frac{\sinh \beta(\frac{l}{2} - x)}{\cosh \beta \frac{l}{2}}$$

At $x = 0$

$$\frac{\tau_{i(0)}}{(E_f - E_m)e_m} = -1.396 \times 10^{-3} \tanh \frac{\beta l}{2}$$

$$= -0.241 \times 10^{-3}$$

while from equation 2.9 at $x = \frac{l}{2}$

$$\frac{\sigma_{f(\frac{l}{2})}}{(E_f - E_m)e_m} = 1 - \frac{1}{\cosh \frac{\beta l}{2}}$$

$$= 0.0150$$

$$\therefore \frac{\tau_{i(0)}}{\sigma_{f(\frac{l}{2})}} = -0.0161 \qquad 6.4$$

For the Cox theory to fit the average yield point data a maximum shear stress $\tau_{i(0)} = -0.740$ N/mm^2 would be necessary. This must be compared with an average of -0.133 N/mm^2 for the interface shear stress at the start of pull-out in the etched specimens. It is, indeed, more than twice as great as the maximum shear stress recorded at pull-out initiation which is the equivalent of yield.

The Mileiko theory assumes a constant shear stress (equation 2.14). In the present case the interface shear stress will be

$$\tau_i = \frac{r_f}{l} \sigma_{f(\frac{l}{2})} \qquad 6.5$$

$$= 0.368 \text{ N/mm}^2$$

This is closer to but still higher than the results from pull-out tests. It seems likely that pull-out tests do not adequately reflect the stress state in the composite. It might be noted, however, that the equivalent calculations for the unetched composite yield $\sigma_{fy(\frac{l}{2})} = 12.3$ N/mm^2, $\tau_{i(o)} = -0.198$ N/mm^2 (Cox) and $\tau_i = -0.098$ N/mm^2 (Mileiko). The average value of interface shear stress at yield from the pull-out tests was -0.077 N/mm^2.

Yielding in the etched specimens may be explained with reference to the pull-out test results. It may be supposed that the interface shear stress builds up round a particular fibre until the yielding shear stress for that interface is reached. The interface is now ready to break but will not do so if there is another route by which load can be transferred. Yielding will occur when the interfaces at a particular cross-section cannot sustain any further load increase. Since, as is evidenced by the pull-out test results, the load cannot be sustained by the interface once sliding has begun, there must be a substantial load drop until equilibrium is restored between the total external load and the sum of the individual fibre loads. The external load can now increase again but the stiffness is very much reduced because some of the interfaces have slipped. As figure 21 shows, further yielding may take place in the same or a subsequent loop.*

6.3 Breakaway behaviour in unbonded specimens using a modification of Cox's Theory.

The breakaway behaviour exhibited in the hysteresis loops of fig. 17 may be explained starting from the theory of Cox and proceeding as follows

* See Addenda after Figure 89.

We suppose a rigid fibre in a compliant matrix and that the load transfer relationship is given by

$$\frac{dP}{dx} = H(u - z) \qquad 6.6$$

where P is load in the fibre

x is the co-ordinate along the fibre

u is the displacement at x in the matrix in the presence of a fibre

z is the displacement at x in the matrix in the absence of a fibre

H is a constant

This is, of course, simply Cox's approach and if there is no sliding then the rigid fibre gives $u = 0$

For no sliding

$$\frac{dP}{dx} = -Hz \qquad 6.7$$

Differentiating 6.7

$$\frac{d^2P}{dx^2} = -He_m \qquad 6.8$$

since $$e_m = \frac{dz}{dx}$$

Integrating 6.8

$$\frac{dP}{dx} = -He_m x + A$$

$$\frac{dP}{dx}=0 \text{ at } x=\frac{\ell}{2} \quad \therefore 0=-He_m\frac{\ell}{2}+A$$

$$\therefore A=He_m\frac{\ell}{2}$$

$$\therefore \frac{dP}{dx}=He_m\left(-x+\frac{\ell}{2}\right) \qquad 6.9$$

In the region of sliding it is assumed that there can be no increase in the interface shear stress so $\frac{d^2P}{dx^2}=0$ and differentiating 6.6

$$\frac{du}{dx}=\frac{dz}{dx}=e_m$$

whence $$z=e_m x+C$$

Say $x=x'$ is the limit of the sliding region where $Z=0$ and the constant of integration, $C=-e_m x'$

$$\therefore Z=e_m(x-x') \qquad 6.10$$

We also have from equation 2.10 that

$$\frac{dP}{dx}=-2\pi r_f \tau_i$$

We can assume that there is some critical $\tau_i=-\tau_{ic}$ which when exceeded allows sliding to occur.

Combining this with equation 6.9 gives

$$2\pi r_f \tau_{ic}=He_m\left(-x'+\frac{\ell}{2}\right) \qquad 6.11$$

We use x' because for equation 6.11 to apply there must be a sliding region. Further there is a minimum value of $e_m = e_{mc}$, say, for x' to exist. This is found by putting $x' = 0$ in equation 6.11 giving

$$e_{mc} = \frac{4\pi r_f \tau_{ic}}{H\ell} \qquad 6.12$$

If there is no sliding then equation 6.9 applies and

$$P = \int_0^{\frac{\ell}{2}} H e_m \left(-x + \frac{\ell}{2}\right) dx$$

$$\therefore P = H e_m \frac{\ell^2}{8} \qquad 6.13$$

There will be some critical load P_c at the strain e_{mc} for which the interface or parts of it are on the verge of sliding i.e.

$$P_c = H e_{mc} \frac{\ell^2}{8} \qquad 6.14$$

$$\text{or} \quad e_{mc} = \frac{8 P_c}{H\ell} \qquad 6.15$$

Equating this with the value from equation 6.12 gives

$$P_c = \frac{1}{2}\left(2\pi r_f \tau_{ic} \frac{\ell}{2}\right) \qquad 6.16$$

$2\pi r_f \tau_{ic} \frac{l}{2}$ is the load at the fibre centre if a constant interface shear stress, $-\tau_{ic}$ is assumed over the fibre half length $0 < x < \frac{l}{2}$. Calling this force P_{Fmax} i.e. the maximum friction load in the fibre

$$P_{Fmax} = 2\pi r_f \tau_{ic} \frac{l}{2} \qquad 6.17$$

$$P_c = \frac{1}{2} P_{Fmax} \qquad 6.18$$

The load at the fibre centre when there is sliding over $0 < x < x'$ and no sliding $x' < x < \frac{l}{2}$ is

$$P_{(\frac{l}{2})} = \int_0^{x'} 2\pi r_f \tau_{ic}\, dx + \int_{x'}^{\frac{l}{2}} He_m \left(-x + \frac{l}{2}\right) dx$$

$$= 2\pi r_f \tau_{ic} x' + \frac{1}{2} He_m \left(\frac{l^2}{4} + x'^2 - l x'\right)$$

From equation 6.11

$$x' = \frac{l}{2} - \frac{2\pi r_f \tau_{ic}}{He_m} \qquad 6.19$$

Hence

$$P_{(\frac{l}{2})} = 2\pi r_f \tau_{ic} \frac{l}{2} - \frac{\left(2\pi r_f \tau_{ic} \frac{l}{2}\right)^2}{4 He_m \frac{l^2}{8}} \qquad 6.20$$

Using equation 6.14 and 6.17 in 6.20 gives

$$P_{(\frac{l}{2})} = P_{Fmax} - \frac{P_{Fmax}^2}{4 \frac{e_m}{e_{mc}} P_c}$$

and finally using equation 6.18 gives

$$P_{(\frac{l}{2})} = P_{Fmax}\left(1 - \frac{e_{mc}}{2\,e_m}\right) \qquad 6.21$$

Equation 6.21 applies when $e_m \geq e_{mc}$. When $e_m < e_{mc}$ then equation 6.13 applies.

Equations 6.13 and 6.21 may now be used with a number of further modifications to fit the hysteresis loops.

Clearly as e_m becomes large $P_{(\frac{l}{2})}$ tends to P_{Fmax} which as can be seen from equation 6.17 depends solely on the value of τ_{ic} for a given fibre length and radius. A typical value of the composite stress, σ_c at breakaway is 0.43 N/mm^2. We consider all this load to be borne by the fibres so that the total load on the fibres is $\sigma_c A_c = 17.2$ N where A_c is composite cross-sectional area Hence load per fibre

$$P_{Fmax} = \frac{17.2}{12} = 1.433 \text{ N}$$

From this critical shear stress τ_{ic} may be calculated

$$\tau_{ic} = \frac{P_{Fmax}}{\pi r_f l}$$

$$= 0.091 \text{ N/mm}^2$$

This gives a value for e_{mc} of

$$e_{mc} = \frac{4\pi r_f \tau_{ic}}{Hl}$$

$$= 0.00178$$

Equations 6.13 and 6.21 are plotted using these numbers in figure 22. Also plotted in figure 22 is a portion from a typical hysteresis loop for an etched specimen. The reason for the great discrepancy between the portions of the curves after breakaway is that the matrix is not taken into account in equation 6.21.

After the breakaway point the matrix is loaded directly without the load also passing through the fibres. It would be expected that the matrix modulus would account for a significant portion of the strain-hardening part of the loop. If no other effect were operating, the strain-hardening modulus would be $E_m(1-V_f) = 2.93\ N/mm^2$. This has been superimposed on the Cox analysis in figure 23.

Figure 23 shows that the addition of the effect of the matrix still does not account for the strain-hardening modulus. There are at least two possible explanations for this. One is that, as already noted, not all the interfaces will be broken by the first yielding and hence some of the fibres are still capable of contributing to the composite stiffness. The other is that there may be a Poisson's ratio effect which by increasing the interface shear stress as the longitudinal strain is increased allows further load transfer to the fibres to occur even during sliding. These propositions are examined in the next section,

6.4 Strain-hardening modulus

Measured strain-hardening moduli well in excess of the matrix modulus indicate that not all the interfaces have slipped. A rough estimate of the proportion of interfaces at which slip has occurred may be obtained from consideration of the strain-hardening moduli. Suppose in length l there is a proportion of interfaces α which is still bonded - that is a proportion α still has the bonded composite modulus, E_c - while the proportion $(1-\alpha)$ in series with it has the modulus of the matrix, E_m then the strain-hardening modulus E_{SH} will be.

$$E_{SH} = \frac{\alpha}{E_c} + \frac{(1-\alpha)}{E_m} \qquad 6.22$$

and

$$\alpha = \frac{E_c}{E_c - E_m}\left(1 - \frac{E_m}{E_{SH}}\right) \qquad 6.23$$

This means for example, that evenwhen the strain-hardening modulus is only 10% greater than the matrix modulus, there may still be about 9% of the total interfaces unbroken. Equation 6.23 formally constitutes the upper bound on the proportion of unslipped interfaces. The lower bound is obtained by considering a cross section in which proportion α of the bonds are unbroken and the proportion $(1-\alpha)$ in parallel with it are broken bonds. This leads to

$$E_{SH} = \alpha E_c + (1-\alpha)E_m \qquad 6.24$$

and $$\alpha = \frac{E_{SH} - E_m}{E_c - E_m} \qquad 6.25$$

In this case $E_{SH} = 1.1E_m$ gives $\alpha = 0.2\%$. It seems reasonable to suggest that α is likely to have a value closer to the upper bound than the lower bound on the grounds that the initial yielding is likely to take place across a particular complete cross-section. It is also likely that the above analysis has more relevance to the etched specimens than the unetched as will become clear in the discussion of the unloading part of the cycle.

From consideration of the curves in figure 23, an additional strain-hardening modulus of about 1.15 N/mm^2 is required to bring the modified Cox analysis plus matrix into line with the experimental result. This makes the bounds on α from equations 6.23 and 6.25 $0.7\% < \alpha \leq 28.7\%$. The effect of increasing the strain-hardening modulus is shown in figure 24.

The space occupied by a fibre may be considered as a hole in the matrix. If the matrix is strained in the direction of the fibre then due to Poisson's ratio effects the hole will decrease in radius. This is, of course, not possible due to the presence of the fibre so the situation is analogous to a shrink fit. It is supposed that the shrink fit analysis presented by, for example, Durelli and Riley 1965 may be superimposed on the existing stress state. From consideration of this analysis it may be concluded that for a rigid cylindrical inclusion in an incompressible matrix, the longitudinal strain of the

matrix e_m and the interface pressure p_i are related by

$$\frac{e_m}{2} = \frac{1}{E_m}\left\{\frac{1}{\left(\frac{R^2}{r_f^2}-1\right)}\left(\frac{R^2}{r_f^2}(1+\nu_m)+(1-\nu_m)\right)\right\}p_i \qquad 6.26$$

where Poisson's ratio $\nu_m = \frac{1}{2}$

Using $\frac{R}{r_f} = 3.65$ and $E_m = 3.17\ N/mm^2$ as before it is found that

$$p_i = 0.953\, e_m \qquad 6.27$$

Also $$\tau_{ip} = \mu p_i \qquad 6.28$$

where μ is the coefficient of friction between fibre and matrix and τ_{ip} is the interface shear stress due to the Poisson effect.

So $$\tau_{ip} = 0.953\, \mu e_m \qquad 6.29$$

The usual method for establishing the coefficient of friction between rubber and steel is not applicable here. It is possible, however, to obtain an estimate for μ and p_i by considering the curves in figure 23 and that the additional composite stress due to the Poisson's ratio effect σ_{cp} is given by

$$\sigma_{cp} = \frac{l}{R^2} r_f \tau_{ip} \qquad 6.30$$

Considering, for example, the situation at a strain of e_m = 0.136, the composite stress in the sample is 0.981 N/mm^2 while the modified Cox analysis gives 0.426 N/mm^2 as the fibre contribution to the composite stress. The difference is thus 0.555 N/mm^2 of which 0.399 N/mm^2 comes from the matrix so it is assumed that (at most) 0.156 N/mm^2 comes from the Poisson effect.

Say $$\sigma_{cp} = 0.156 \text{ N/mm}^2$$

$$\therefore \tau_{ip} = \frac{0.156 R^2}{l r_f}$$

$$= 0.0166 \text{ N/mm}^2$$

From equation 6.29

$$\mu = \frac{\tau_{ip}}{0.953 e_m}$$

$$= 0.128$$

and from equation 6.27

$$p_i = 0.953 e_m \quad = 0.13 \text{ N/mm}^2$$

The additional effect of the foregoing supposition is shown in figure 24 which is, of course, through choice of numbers identical for the presumed Poisson effect and the residual bonding effect. In fact, it is likely that there will be a combination of factors involved and some of the strain-hardening modulus will arise from each of these effects and possibly other effects which have not been considered like local variations in friction.

6.5 Breakaway behaviour of unbonded specimens using a modification of Mileiko's theory.

Another possible explanation of breakaway behaviour may be deduced from the theory of Mileiko. In the etched specimens when the interfaces had once been broken, it was clear that there was a greater readiness to slide at the interfaces on subsequent loading. However, for the breakaway not to be abrupt it might be concluded that sliding started to occur at the interfaces at different strains. This suggested that a statistical model incorporating a distribution of strains and implicitly of critical shear stresses at which the interfaces start to slide was likely to describe the observed material behaviour.

Before any sliding occurs it is assumed that the composite has a modulus as calculated in section 6.1. After sliding has occurred it is assumed that the strain-hardening modulus of the composite is reduced to the modulus of the matrix and the contribution of, say the residual bonding effect discussed in section 6.4. It may be noted that if all the interfaces slipped at the same strain, then the model would be reduced to the simple bilinear one illustrated in figure 18.

Let $f(e_c)$ be the distribution of strains at which sliding occurs. For a piece of composite at strain e_c the Young's modulus E_{cs} will be

$$E_{cs} = E_{SH}\int_0^{e_c} f(e_c)de_c + E_c\int_{e_c}^{\infty} f(e_c)\,de_c \qquad 6.31$$

where E_{cs} is the Young's modulus when sliding is taking place, E_{SH}

is the strain-hardening modulus and E_c is the composite Young's modulus when there is no sliding.

For a Gaussian distribution

$$f(e_c) = \frac{1}{S\sqrt{2\pi}} \exp - \frac{(e_c - \bar{e}_c)^2}{2S^2} \qquad 6.32$$

where $\bar{e}_c$ is the mean strain at which sliding occurs, e_c is strain and S is the standard deviation.

The cumulative distribution is

$$F(e_c) = \int_0^{e_c} f(e_c)\, de_c \qquad 6.33$$

which is tabulated for the normalised Gaussian distribution . Thus since

$$\int_0^{\infty} f(e_c)\, de_c = 1$$

$$E_{cs} = E_{SH} F(e_c) + E_c(1 - F(e_c)) \qquad 6.34$$

Returning to the analysis given in chapter 2 and combining equations 2.16 and 2.17 gives

$$e_c = \frac{2\tau_i}{G_m} \frac{h'}{l} \log_e V_f^{-\frac{1}{2}} \qquad 6.35$$

Making appropriate substitutions gives

$$e_c = 0.039\, \tau_i$$

This equation may be regarded as the average condition, so

$$\overline{e}_c = 0.039\overline{\tau}_i$$

In this case to maintain a parallel with the modified Cox analysis let $\overline{\tau}_i = \tau_{ic} = 0.091$ N/mm^2. Thus

$$\overline{e}_c = 0.00356$$

The standard deviation is not a known quantity but the effect that standard deviation has will be on the slope of the curve - that is the sharpness of the breakaway. Arbitrarily the standard deviation has been taken as two thirds of the mean and the result plotted in figure 25 along with a portion of a sample experimental result.

The relationship used is

$$\sigma_c = \sum \delta\sigma_c = \sum E_{cs}\delta e_c \qquad 6.36$$

where E_{cs} has been evaluated at the mean of the interval δe_c which was taken, again arbitrarily, as half of the standard deviation,

6.6 The Modified Cox Analysis Applied to the Unloading Part of the Cycle.

If the unbonded material could be characterised by a classic bilinear hysteresis model (illustrated in figure 18) then the reverse breakaway would occur at a load equal to the maximum load in the cycle less twice the breakaway load. In fact the characteristic reverse breakaway load observed varies between one to

three times the breakaway load - the unetched specimens being nearer the former and the etched ones the latter (see figure 19). It is clear that something rather more complicated than a simple bilinear hysteresis model governs the behaviour.

One possible explanation is provided by the modified Cox analysis which can be applied (further extended) to the unloading situation. Figure 26 shows the non-dimensional interface shear stress distribution and the fibre stress distribution predicted by Cox on the loading part of the cycle at the onset of sliding. The assumed distributions when sliding is well developed are shown in figure 27.

By superposing the Cox definition of load transfer on the constant shear stress of figure 27, the interface shear stress expressions for unloading become

for $0 < x < \frac{l}{2}$

$$-2\pi r_f \tau_i = 2\pi r_f \tau_{ic} + He\left(\frac{l}{2} - x\right) \qquad 6.37$$

and for $\frac{l}{2} < x < l$

$$-2\pi r_f \tau_i = -2\pi r_f \tau_{ic} + He\left(\frac{l}{2} - x\right) \qquad 6.38$$

in which $$e = e_m - e_{max} \qquad 6.39$$

where e_{max} is the maximum strain in the cycle

When $e = -e_{mc}$ and using equation 6.12, 6.37 and 6.38 become

$$\tau_i = -\frac{2\tau_{ic} x}{l} \quad \left(0 < x < \frac{l}{2}\right) \qquad 6.40$$

and $$\tau_i = 2\tau_{ic}\left(1-\frac{x}{l}\right) \qquad \left(\frac{l}{2}<x<l\right) \qquad 6.41$$

The corresponding fibre stress expressions are

$$\sigma_f = \frac{2}{\tau_f l}\tau_{ic}x^2 \qquad \left(0<x<\frac{l}{2}\right) \qquad 6.42$$

$$\sigma_f = \frac{2}{\tau_f l}\tau_{ic}(l-x)^2 \qquad \left(\frac{l}{2}<x<l\right) \qquad 6.43$$

The distributions of equations 6.40 to 6.43 are plotted non-dimensionally in figure 28.

A further reduction in the strain to $e=-2e_{mc}$ yields the fibre stress distributions of figure 29. The relevant equations are

$$\tau_i = \tau_{ic}\left(1-\frac{4x}{l}\right) \qquad \left(0<x<\frac{l}{2}\right) \qquad 6.44$$

$$\tau_i = \tau_{ic}\left(3-\frac{4x}{l}\right) \qquad \left(\frac{l}{2}<x<l\right) \qquad 6.45$$

and $$\sigma_f = \frac{2\tau_{ic}}{\tau_f l}x(2x-l) \qquad \left(0<x<\frac{l}{2}\right) \qquad 6.46$$

$$\sigma_f = \frac{2\tau_{ic}}{\tau_f l}(x-l)(2x-l) \qquad \left(\frac{l}{2}<x<l\right) \qquad 6.47$$

The distribution described by equations 6.46 and 6.47 is interesting in that each half of the fibre is in compression but the direct stress at the fibre centre is zero. A further reduction in

strain is required ($e<-2e_{mc}$) before any compressive stress is transmitted across the fibre centre. Also since the critical shear stress has again been reached at the fibre ends sliding will now occur there.

Figure 30 shows the stress distributions at $e=-\frac{3}{2}e_{mc}$ i.e. an intermediate point between those of figures 28 and 29. It will be noted that although the fibre ends are subject to compressive stresses the fibre centre is still in tension.

For $e<-2e_{mc}$, as already noted, sliding will occur at the fibre ends over a length say, x_r' . Equation 6.37 may be amended by analogy with equation 6.11 to give

$$-2\pi r_f \tau_{ic} = 2\pi r_f \tau_{ic} + He\left(\frac{l}{2} - x_r'\right) \qquad 6.48$$

such that

$$x_r' = \frac{l}{2} + \frac{4\pi r_f \tau_{ic}}{He} \qquad 6.49$$

The load at the fibre centre becomes

$$P_{(\frac{l}{2})} = -2\pi r_f \tau_{ic} x_r' \qquad 6.50$$

which on substituting 6.49 and using 6.12 and 6.17 gives

$$P_{(\frac{l}{2})} = -P_{Fmax}\left(1+\frac{2e_{mc}}{e}\right) \qquad 6.51$$

It will be noted that this gives correctly $P_{(\frac{l}{2})} = 0$ for $e=-2e_{mc}$

The load at the fibre centre which will be compressive may now be calculated and added to the tensile load in the matrix to give the net load in the composite. The resulting composite stress is illustrated in figure 31 which is essentially a continuation of figure 24.

Clearly if there is a Poisson's ratio effect then sliding will not occur quite so soon as predicted since the interface shear stress at the maximum load point will be greater than the critical shear stress at which sliding first occurred. Accordingly a greater reduction in strain than that predicted above will be required to reach the sliding point on the unloading part of the cycle. In any case, however, the agreement between the experimental and theoretical results is not good on the last part of the unloading curve.

Thereis some evidence to suggest that the criterion for reverse sliding presented above is correct - that is sliding occurs when the critical shear stress is reached at the fibre ends as predicted by the extension of the Cox analysis. By taking the maximum strain in a cycle and multiplying by the average matrix Young's modulus and the area of the matrix an estimate of the load carried directly by the matrix was obtained. Subtracting this from the maximum load in the cycle gave an estimate of the maximum load carried by the fibres. According to the extension of the Cox analysis (above) the reverse breakaway load should be equal to or greater than the load in the fibres. As figure 32 shows, this is indeed generally the case for both etched and unetched specimens.

It is clear that sliding in the reverse direction does not follow the path suggested by the theoretical analysis. It is not difficult to see why the stress distribution predicted by the extended Cox analysis may break down near the reverse breakaway point. Consider the stresses indicated in figure 29 at $x = \frac{l}{2}$ and $x = \frac{l}{4}$. There is no direct stress at $x = \frac{l}{2}$ and a compressive stress at $x = \frac{l}{4}$ Due to the regularity of the phase geometry of the composite no load at the fibre centres implies that all the load at that cross-section is carried by the matrix which is, of course, in tension. At $x = \frac{l}{4}$ the load in the fibre is compressive which requires for equilibrium that the tensile load in the matrix be greater at this cross-section than it is at the cross-section containing the fibre centres. It is supposed that this state of affairs cannot be sustained and that there is localised action which allows the fibre to shed its compressive load while the matrix sheds some of its tensile load.

6.7 The Mileiko Theory and the Possibility of Buckling on Unloading

As has just been noted, a stage in the cycle is reached at which all the fibres with slipped interfaces are in compression. This raised the possibility that the sliding in the reverse direction might be the result of high shear stresses caused by fibre buckling. The reason why this idea may be plausibly linked to the Mileiko theory is explained below.

In section 6.5, it was suggested that a Mileiko model of a discontinuous fibre composite incorporating a statistical distribution of sliding strains could be used to interpret the experimental results. This approach is more descriptive than explanatory. In particular, it would be necessary to provide some criterion derived from the mechanics of the composite to account for the reverse breakaway behaviour. It seemed possible that such a criterion might be deduced from the analysis of compressive failure of composites presented in section 2.

The main difficulty arising is that this analysis deals with uniaxially loaded continuous fibre composites - the model being a plate one and hence only two dimensional. It is thus not immediately obvious what substitutions may sensibly be made in the buckling load formulae (equations 2.28 and 2.37). It would appear that almost any reasonable values of the parameters in the extension mode equation 2.28, give rise to answers that are at least two orders of magnitude too large when compared with the experimental results.

One way of viewing the composite is shown in figure 33. This retains the correct volume fraction, $V_f = 0.075$ while also incorporating the correct flexural rigidity of the fibre which is the controlling influence. Substituting in 2.37 with $G_m = 1.06\ N/mm^2$, $C = 0.64$ mm, $l = 25$ mm, $E_f = 210{,}000\ N/mm^2$, $I = 0.00126\ mm^4$ and interpreting $(1 + \frac{h}{2c})^2$ as $(1-V_f)^{-2}$ gives

$$P = 5.77\ N$$

This is the upper bound on the critical buckling load for one fibre assumed loaded axially at its ends. So the critical buckling load for the composite as a whole would be at most 70 N. This is still an order of magnitude too large.

It is perhaps not surprising that the analysis is inadequate since it is based on a model in which the fibres are loaded up independently of the matrix and in turn the matrix, which is loaded by the fibres, is controlled by their stiffness. In contrast, the load transfer to the fibres in the composite under investigation must be through the matrix. Further, at the point of interest the matrix is still in tension and accordingly its flexual stiffness will have been increased.

This being the case, if there is any tendency to buckle on the part of the fibres, then it is likely that the action of the matrix in opposing the attempted buckling deformation of the fibre will give rise to an increase in the interface shear stresses and a consequent reduction in the net tensile load in the composite. This mechanism would lead to interface sliding fairly rapidly but it seems likely that the interface shear stress would have to be so high to initiate buckling that sliding would probably occur first in any case.

Although the Mileiko analysis may be used to describe the initial breakaway behaviour, unless there is some mechanism involved which has not been considered, it does not seem likely that the Mileiko assumption of constant interface shear stress for a given strain is valid. The alternative proposition would have to be that for some unexplained reason the critical shear stress in the

unloading direction must be substantially lower than in the loading direction. This is not substantiated by the reverse pull-out tests although the mechanics involved will be somewhat different.

6.8 Other Features of the Results

The existence of unbroken bonds, as suggested in section 6.4 goes some way to accounting for the difference between the etched and unetched specimen loops. The etched specimen loops show in general higher strain-hardening moduli implying that in traversing the cycle those fibres which have intact interfaces will always be in tension and the stress distributions described in section 6 are not relevant to them. It seems likely that the rather anomalous behaviour of the etched specimens in which there can be an increase in load while the strain is reducing (vide figure 21) is due to local interactions between the fibres in tension and those in compression.

In the unetched specimens it is supposed that the mechanism suggested above for etched fibres is inoperative for the lack of bonded interfaces. The typical characteristic of the unetched specimens is that they tend to show a permanent set which is caused by the compressive load induced in the fibres balancing the tensile load in the matrix. It was noted in a series of tests on the unetched specimens that the breakaway load increased with increase in permanent set. This is not surprising since before tensile load can be applied to the fibres in the succeeding cycle, the compressive load associated with the permanent set must be removed from them.

As can be seen from figure 17, the composites exhibited some load recovery and, if the test were stopped at the maximum point in the cycle, stress relaxation. This is due to the properties of the matrix and has for the present been ignored as a relatively small effect.

Another interesting feature of the results is the relationship between the shapes of a matrix only hysteresis loop and that from a primed specimen. Examples of these are shown in figure 34.

CHAPTER SEVEN

7. Hysteresis in the Discontinuous Fibre Composite Specimens

In the preceding chapters the mechanics of discontinuous fibre composites with and without interfacial slip have been considered and it is clear from the results quoted that there was considerable hysteresis loss during loading and unloading at very low strain rates. In the present chapter this hysteresis loss is quantified and results of some slow cycle tests on the various composite specimens are reported and compared with each other.

7.1 Hysteresis in low strain rate tests

Samples of the hysteresis loops obtained at low strain rates are shown in figure 17. The strain rate used for these tests was about 0.07%/s, so a complete cycle might take several minutes. It is clear that the hysteresis in a cycle is considerable but energy lost at such low rates of strain does not necessarily indicate a capacity for damping vibrations or absorbing shocks.

Further, the maximum strains in the cycles are large being from about 2% to 20%. It is unlikely in most vibrating systems that such large strains would occur without some considerable danger of fracture of other components. It will also be noted that the tests reported did not involve any compressive loading of the specimens. This was intentional since even a very low compressive load produced gross buckling of the specimen.

One of the most widely used measures of hysteresis or damping in vibrating systems is specific damping capacity (ψ) which is defined as the ratio of the energy lost in a cycle (ΔW) to the

maximum strain energy in the cycle (W) in the case of a system oscillating about a zero mean. Alternatively, in the case of a system oscillating about a non-zero mean W is taken to be the change in strain energy between the mean position and the maximum amplitude of vibration. Since the tests presently under discussion were non-oscillatory, the use of the term specific damping capacity is really meaningless but for the sake of describing the results, the definition $\frac{\Delta W}{W}$ may be borrowed and this ratio is plotted in figure 35 against maximum strain in the cycle in the case of the etched specimens and cumulative maximum strain in the case of unetched specimens. The reason for this is the unetched specimens usually exhibited a permanent set. It will be noted that there is not much difference between the etched and unetched specimen results although the unetched specimens show a slightly decreasing trend with increasing strain.

The equivalent plot for a bonded specimen is shown in figure 36. It will be observed that the ratio $\frac{\Delta W}{W}$ is smaller than for the unbonded specimens but also the maximum strains in each cycle are much closer to what is practically feasible in a vibrating system.

7.2 Low-frequency sinusoidal testing

An extensive literature exists on the sinusoidal straining of polymers and rubbers e.g. Ferry 1970, Payne and Scott 1960. For many of the methods described the authors have constructed their own apparatus much of which seems to be designed for the deformation of shear or compression specimens. The essence of nearly all the methods is that force and displacement be measured either explicitly or in the form of a hysteresis loop.

Modern equipment allows the recording of hysteresis loops at low frequency and constant amplitude without much difficulty. The machine used for the tests described here was an hydraulically driven Instron TT-KM tensile tester with facilities for load or displacement control of the crosshead. The hydraulic pump imposes limitations on the combinations of frequency and amplitude which may be used. The tests were conducted at 50 cycles/min. or 0.83 Hz. Displacement control of the crosshead was achieved through the use of a strain gauge extensometer attached to two steel rods which were fixed to the crosshead and base using magnetic blocks.

The standard pen recorder which employs paper motion for one axis is incapable of responding with sufficient speed at the highest rates which the machine can achieve. For this reason a Bryans Southern Instruments 26000 X - Y plotter was substituted for it. This proved very satisfactory.

The use of crosshead control means that any deformation due to lack of rigidity in, for instance, the load cell would reduce the apparent modulus of the specimen. In fact, the load cell has a stiffness between one and two orders of magnitude greater than that of the specimens so it is necessary to make an allowance for this in presenting the results.

Equally, any source of energy loss in the system will tend to increase the area of the hysteresis loop and thereby cause an overestimate of the damping in the specimen. The fact that the specimens must necessarily be tested with a preload (because of the low resistance to buckling) reduces some of the problems of backlash but obviously will not eliminate all extraneous losses. By testing

a steel rod of stiffness very much greater than the composite specimens estimates of the system stiffness and energy loss per cycle were obtained. The energy lost as represented by hysteresis loops turned out to be almost insignificantly small. The correction curves used for the bonded specimens are shown in figure 37.

The different natures of the bonded and unbonded specimens required slightly different experimental treatment. The bonded specimens were tested with a mean load of about 50 N while the unbonded specimens were tested with a mean displacement of 7.5 mm.

7.3 Results of low-frequency testing

The results for the bonded and unbonded specimens are quite distinct in nature and will be considered separately before being compared.

(a) The bonded specimens

Even at low amplitudes the loops obtained from the bonded specimens exhibit a lack of symmetry (see figure 38). This is seen even further developed in figure 39 in which it will be noted that the co-ordinates of the point indicating the mean of force and displacement lie outside the hysteresis loop. This has important consequences for the average stiffness of the hysteresis loop which are discussed below.

It was also observed that the mean force changed with change in the amplitude of oscillation. This variation is shown in figure 40. The non-linear non-elliptical nature of the hysteresis loop as exampled in figure 39 indicates implicitly distortion of the force signal from the basic sinusoidal form of the input. The change in

the mean force level is another of the consequences of this. A sample of the force output and some calculated points for a true sine wave are shown in figure 41 in which the particular nature of the distortion may be seen.

The energy lost per cycle was established by measuring the areas of the hysteresis loops with a planimeter. Results obtained at amplitudes of less than 0.1 mm (rms) must be treated with caution since the area to be measured becomes comparable with the thickness of the pen line tracing the loop. At higher amplitudes the error should not be more than 5% and falls to less than 1% for the largest loops. A typical plot of energy lost per cycle versus the root mean square amplitude of oscillation is shown in figure 42. The energy lost per cycle clearly increases with the amplitude of the oscillation and a log-log plot shows the variation to be approximately to the power 1.7.

It is, as has already been noted, a common practice to quote specific damping capacity as the measure of damping since this takes into account the strain energy involved in the vibration. In the present case the evident variation in the stiffness of the specimen during any given cycle means that the term must be redefined - most plausibly in terms of an average stiffness. In estimating this average stiffness for the whole cycle it was clear that the line O - A in figure 43 was likely to constitute an over-estimate, so a method was sought which would give a more reasonable estimate of the average stiffness of the cycle.

Using the mean force and displacement point as the origin of co-ordinates, it is possible to approximate the mean line through the hysteresis loop by a Lagrange polynomial $P(x)$, which is force

as a function of displacement. The stiffness at any point is then approximately

$$k_x = \frac{dP(x)}{dx} \qquad 7.1$$

and the average stiffness is

$$k_{mean} = \frac{1}{2x_m}\int_{-x_m}^{x_m} k_x\,dx = \frac{1}{2x_m}\left[P(x)\right]_{-x_m}^{x_m} \qquad 7.2$$

where x_m is the maximum displacement in the cycle.

Using a five node approximation with the notation indicated in figure 43, k_{mean} turns out to be

$$k_{mean} = \frac{F_1}{x_m} \qquad 7.3$$

It thus transpires that the mean stiffness is necessarily given by the slope of the line OA, no matter what the order of the polynomial. Other methods of averaging such as taking a mean strain energy also lead to the same conclusion.

Accordingly, all the stiffnesses for this type of specimen were calculated on the basis of equation 7.3 and then corrected for machine stiffness from figure 37. It should be noted that correcting for stiffness implies that the oscillatory amplitude of the specimen was less than that recorded in the loops. A simple linear allowance was made for this reducing the peak amplitude by the ratio of the stiffness as calculated to the corrected stiffness. An example of the results thus obtained is shown in figure 44.

Initially the stiffness falls with increasing amplitude but there is a turning point at about 0.25 mm (rms) and the stiffness increases again because the hysteresis loops become even more concave about the origin at the higher force end of the loop. This feature is a reflection of the nature of the static load-displacement loop.

It should be noted that the points plotted in figure 44 are not representative of the specimen in general but are only relevant to oscillations in which there is a mean load of about 50 N. For example increasing the mean load to about 62.5 N increases the stiffness by from 12 to 25% depending on amplitude. There is no corresponding change in the energy lost per cycle which remains similar to that lost at the lower mean load for the same oscillatory amplitude.

Specific damping capacity may be calculated using the stiffness already derived. The strain energy is taken to be $(\frac{1}{2} k_{mean} x_m^2)$ in which both k_{mean} and x_m have been corrected for machine stiffness. The result is plotted in figure 45. As will also be noted from the figure a higher mean load causes a drop in specific damping capacity which is entirely due to the increase in stiffness already mentioned. This perhaps highlights the weakness of quoting specific damping capacity in isolation in that although it takes into account the stiffness of the material, the actual value of the stiffness must be given independently. In other words, a high specific damping capacity may be of little use if the material stiffness is not of engineering interest.

(b) The unbonded specimens

The hysteresis loops from the unbonded specimens both etched and unetched give the appearance of being almost elliptical

(figure 46). As the amplitude is increased, however, the shape of the loops changes as indicated by figure 47. This change is due to the onset of gross sliding at the matrix/fibre interfaces. The loops increase markedly in area because of this sliding as the amplitude is further increased (figure 48). The sliding occasions a loss in stiffness which is plotted against the root mean square amplitude of oscillation in figure 49. In this case there is no need for a complicated definition of stiffness since the decreasing force leg of the loop is nearly an exact reversal of the force increasing portion. This is shown in figure 50 for a sample etched specimen loop. The stiffness of the specimen at any particular amplitude is therefore taken to be the slope of the diagonal of the rectangle defined by the maxima and minima of force and displacement in the loop and modified suitably to take into account machine stiffness.

Sliding or the possibility of sliding also has a marked effect on the mean force about which the loops are described. As indicated previously an overall displacement of 7.5 mm was first imposed on the specimens. In all cases such a displacement would take the specimens well into the sliding region of the static loops like those in figure 17 since a strain of greater than 10% is implied. The superposition of a sinusoidal motion on the static displacement causes a fall in the mean force. The reason is that the stiffness on unloading from a particular point is very much higher than the stiffness if the load is increased from that point. When low amplitude cyclic motion is begun, the mean force position changes immediately to a lower value such that the higher force end of the loop does not cross the force-displacement curve of the static loop. Indeed, the mean force may well fall by an amount greater than that required to fulfil

this condition. The change in mean force against rms amplitude of oscillation during progressive cycling at 0.83 Hz is shown in figure 51 for an etched and an unetched specimen.

In both cases the amplitude of oscillation was increased until the lower part of the loop almost crossed the zero load line and in both cases, it will be noted, the mean force remained virtually unchanged when the amplitude of oscillation was reduced again. This is a contributing factor to the nature of the result shown in figure 49 in which the stiffness of the unbonded specimens (particularly the etched one) is different, when the amplitude was being reduced, from the values when the amplitude was being increased.

Since there is no countervailing reason for the mean load to increase while the amplitude is reduced, reducing the amplitude has the effect of altering the shapes of the loops compared with when the amplitude was increasing. The effect is shown in figure 52 for an etched specimen for which the loop becomes significantly longer and thinner as the amplitude is reduced than when it was being increased. The effect on the unetched specimens is less marked but the loops do increase slightly in slope and become smaller in area.

If the experiment is repeated immediately, i.e. if the amplitude of oscillation is increased again, it is clear that different circumstances are involved compared with the first loading sequence since significant mean load changes have already occurred. It was found that on repeating the experiment the mean load retraced the path of the initial amplitude reduced mean load (figure 51) when the amplitude was increased again. A further slight fall in mean load occurred when the amplitude was reduced.

The stiffness results showed features similar to those already described for the first amplitude increased/decreased sequence but the variation especially for an etched specimen was much smaller. In particular the amplitude increased results on the second loading sequence were very close to the amplitude reduced results of the first loading sequence. This implies that the amplitude reduced portions of the results presented are more representative of steady state material properties than the initial loading results.

From the foregoing it is clear that the effect of loading history is very important in these specimens. Different results will be obtained depending on how large the initial mean displacement is made. It is expected, however, that the results would all be of a similar nature except in the case where the initial mean displacement is so small that gross sliding at the interfaces does not occur and the loops remain small and nearly elliptical.

It is interesting to note that very similar stiffness results can be obtained from quite differently shaped loops. This is particularly clear in figures 47 and 48. The difference between the etched and unetched specimens of similar stiffness shows up more clearly in the measurement of energy loss per cycle which is shown in figure 53. When the amplitude is being increased, the energy lost per cycle in the etched specimens is up to twice as much as that lost in the unetched ones for the same amplitude of oscillation. When the amplitude is reduced the difference becomes less obvious due to the effect already noted in figure 52.

Calculating specific damping capacity for these specimens highlights the effects just discussed. When the amplitude is being

increased there is an increase in energy lost per cycle and a decrease in stiffness. This implies a very rapid rise in specific damping capacity. When the amplitude is being reduced the rate of decrease in the area of the loop and the rate of increase of its stiffness are higher than the corresponding rates when the amplitude was increased. This conversely implies a very rapid reduction in specific damping capacity. The net result is specific damping capacity curves in the form of loops which are shown in figure 54.

For the bonded specimens, it was found that there was significant distortion of the force response to the sinusoidal displacement input. In the case of the unbonded specimens the distortion (which must be present since the loops are not elliptical) cannot be distinguished by the naked eye.

The results recorded so far are for specimens in which it is believed that there is a complete bond at the matrix/fibre interface or no bond at all. It was not intended that the third possibility of an incomplete bond between fibre and matrix be discussed. However, figure 55 shows a sample hysteresis loop from a specimen which was intended to be bonded but which does not seem to have been completely successful in manufacture. In comparisons in the ensuing discussion, results from this specimen will be shown, to demonstrate their intermediate nature between bonded and unbonded specimens.

7.4 Discussion of results

The illustrative results have all been plotted against displacement without relating this to strain. As indicated, the mean displacement of 7.5 mm represents a mean strain of about 11% so the

maximum amplitude of oscillation of about 0.5 mm peak represents<1% strain. The relationship of these results to the static results reported in Chapter 5 and exampled in figure 17 may be deduced. The oscillatory loops are, in fact, only a fairly small fraction of the size of the static loops. It should also be noted that the imposition of an oscillatory motion on the etched specimens has some effect on the interfacial properties. This is evidenced by the fact that after sinusoidal straining the etched specimens produce static hysteresis loops more closely resembling the unetched loop in figure 17 than the etched loop in the same figure.

However, these slow sinusoidal tests clearly indicate that a significant difference still exists between the properties of the etched and unetched specimens - a difference which has already been demonstrated by figures 47 and 48. Equally clearly, the etched and unetched unbonded specimens are very significantly different from the bonded specimens. Since all three different types of specimen are of a non-linear nature, characterisation of their properties is not a simple procedure. The following discussion is intended only as an introduction to that task.

In much of the literature on rubber, attempts are made to analyse results on the basis of a Voigt or Kelvin element which implies that the material under test is composed of a linear stiffness element and a viscous damping element in parallel. This implies that the experimental results should consist of a series of ellipses with an axis of a particular slope such that the area of the ellipse gives the energy lost in a cycle and the slope of its axis the material stiffness. In practice, the hysteresis loops are not elliptical and the slope of the axis of the loops is not a constant.

This is also true of the materials presently under discussion.

The use of linear analysis involves calculation of an equivalent dashpot constant C_{eq} for the hysteresis loops on the basis that the equivalent ellipse would have area $\pi C_{eq} \omega X^2$ where ω is the frequency of the oscillation and X its amplitude. The unetched specimen results seem most suited to this approach since they appear to be nearly elliptical. Figure 56 implies that even if the loops are elliptical, the way in which they increase in size is not governed by a simple linear law. Since it has already been established that the stiffness of the specimens is not constant with amplitude this observation is not unexpected.

It is clear that this kind of approach must be treated with caution. For example, the result of calculating C_{eq} for a bonded specimen is also shown in figure 56 and the variation is very much less than for the unbonded specimens although the bonded specimen hysteresis loops look very much less like ellipses than the unbonded ones. It could, of course, be argued that the bonded specimen loops are basically elliptical but are distorted by the nature of the specimen stiffness.

Some simple comparison with linearity for each loop seems to be desirable. One plausible possibility for this is to calculate the area of the ellipse which has the same principal axis dimensions as the experimental loop and to compare this area with the actual area of the hysteresis loop as measured with the planimeter. The necessary measurements are the force, F at the mean amplitude and the amplitude of the loop, X. The area of the relevant ellipse is then

$$\Delta W = \pi F X \qquad 7.4$$

There would of course be little point in this procedure if the loops did not look plausibly elliptical.

For the unetched specimens, the calculated areas are at most 15% greater than the measured areas while for the etched specimens, the difference is as much as 24%. In both types of specimen, the difference shows a fairly marked dependency on the amplitude of the loops. This is due to the way in which the width of the loop changes at the mean displacement position with change in loop amplitude.

If the bonded and intermediate specimen loops are indeed distorted ellipses then the equivalent calculation may be carried out for them also. To obtain some comparison among the specimens, the percentage differences have been averaged for sample specimens and are tabulated below.

Table 4

Type of specimen	Mean $\left(\frac{\Delta W_{calculated} - \Delta W_{measured}}{\Delta W_{measured}}\right)\%$	Standard deviation %
Unbonded etched	15.2	8.0
Unbonded unetched	6.0	4.5
Bonded	1.0	5.8
Intermediate	3.6	2.3

Zero mean percentage difference and standard deviation would imply a material whose damping was close to linear although not necessarily viscous. The bonded specimen has the lowest mean but quite a large standard deviation while the intermediate specimen has a slightly higher mean but a low standard deviation. In both

cases the deviation from linearity may be traced to lack of symmetry on either side of the mean position, i.e. the loops are slightly wider on the higher force side of the mean displacement.

As has been implied the unbonded unetched loops which looked nearly elliptical must deviate quite significantly from that form. Just as the unetched specimen loops appeared plausibly elliptical, so the etched loops looked as though they might be modelled by a bilinear hysteresis loop (figure 18). This proposition was investigated using the largest loop from one of the etched specimens as the basis. Clearly some criteria are required for the comparison. The most obvious are (a) the same stiffness (slope of the diagonal) (b) the same energy loss per cycle (area of the parallelogram) and (c) the same amplitude of oscillation.

Use of the diagonal of the experimental loop defines (a) and (c) so for the same damping it is only necessary to take half the area of the experimental loop and equate it to the area of the triangle which has the loop diagonal as base. There is, of course, an infinite number of triangles having the same base and height and hence giving the same area. Some additional criteria are required. Two such criteria are that the slope of neither leg may be negative which means that the maximum slope of the stiffer leg is infinite and the minimum slope of the other leg is zero. This reduces substantially the number of possibilities for the position of the third vertex of the triangle. There is a further implication to choice of stiffness for the stiffer leg in that this stiffness allied to the locus of the height of the triangle defines the loop collapse amplitude of oscillation, i.e. the amplitude at which the less stiff leg disappears altogether.

It may be noted here that any plausible mechanical arrangement to produce a bilinear hysteresis loop must describe steady state oscillations about a constant mean load. This means that matching the initial loading loops to a bilinear model is not likely to be possible since there are significant changes in the mean load. It was found, however, that even in the case of results from a second loading sequence in which the mean load changes only marginally, it was impossible to match up the stiffnesses at lower amplitudes while retaining the same energy loss per cycle at the higher amplitudes. Conversely, if the damping is kept the same at the higher amplitudes the stiffness at lower amplitudes is too great. This occurs because although the experimental results look as though they might be approximated by straight lines, it transpires that the slope of the less stiff leg changes from one loop to another. It was accordingly concluded that attempting to characterise the etched specimen hysteresis loops by a bilinear model was neither readily possible nore likely to be productive.

It is possible to characterise the bonded specimen results empirically since the properties do not vary too much as a function of stress history. The characterisation of the unbonded specimens cannot readily be achieved empirically because there are so many factors including interface properties which must be taken into account. Some direct comparison of the results is still useful.

Figure 57 shows the stiffnesses of a bonded specimen, the intermediate specimen and an unetched specimen which is the less stiff of the two types of unbonded specimen. The intermediate specimen shows a clear loss in stiffness with respect to the bonded

specimen although the general character of the bonded result is retained. The results obtained from this specimen when the amplitude is increased and reduced again are very close to each other over the whole range of amplitude. Generally, the stiffness falls slightly as the amplitude is reduced compared to the amplitude increasing results. There is no tendency on the part of the bonded or intermediate specimens to show the figure of eight pattern which is a feature of the unbonded specimens. The reason for this is the difference in the nature of the change in mean force which is due in turn to the bonded or unbonded state of the interface.

An etched unbonded specimen has been chosen for the comparison of the energy lost per cycle with a bonded and the intermediate specimen in figure 58. The close relation between the intermediate and bonded specimen results again suggests that the intermediate specimen is essentially bonded in character (as indeed it should be). Figure 59 shows the comparative relationship among the same three specimens of specific damping capacity and in some ways highlights the limitations of this parameter as a measure of damping. The apparent superiority of the etched unbonded specimen as a spring/damper conceals the fact that the stiffness of this specimen is very much less than the other two and a very large initial displacement is required to achieve the behaviour illustrated.

There are a number of other features of the results which require comment. One is that there is no simple relationship between loss of stiffness and increase in damping in the unbonded specimens. The nature of the relationship between specific damping capacity and displacement testifies to this. A related feature is that there is no clear point at which sliding begins. This is

perhaps not surprising since considerable sliding has already occurred in reaching the mean position and the change in mean force once oscillation is begun indicates that there is some internal rearrangement of the load distribution accommodated presumably by sliding. The particular non-linear nature of the matrix stiffness would in any case be likely to obscure the existence of an explicit incipient sliding strain amplitude.

It is, nonetheless, instructive to consider the energy lost through friction in the unbonded composites. McLean and Read 1975 deduced the energy lost per cycle per fibre as (using the notation of Chapter 6) $2\pi r_f \tau_{ic} e_m l^2$, where r_f is the fibre radius, τ_{ic} the friction shear stress at the interface during sliding, e_m is the overall matrix strain and l is the length of the fibre. This conclusion was also reached by McMeeking 1972 but consideration of the experimental results presented here shows that the energy loss per cycle is not as predicted linear with strain.

The formulation above implies that there is complete sliding at the interface at all strains. As has already been shown, this is not the case even when there is virtually no bond between the fibre and the matrix. A modification may be made to the calculation by introducing x', the distance along the fibre over which sliding is taking place. This distance was derived theoretically (equation 6.19) in relation to the quasi-static loops and may be used here to give a better estimate of the energy lost per cycle.

Using this parameter and the same argument as McLean and Read for the reduced sliding length, the energy lost per cycle per fibre is given by $8\pi r_f \tau_{ic} e_m x'^2$. There is an additional uncertainty in

this calculation since the strain in the matrix is not known precisely because of end effects near the bonded fibres which form part of the grips. However, using the value of $\tau_{ic} = 0.091$ N/mm^2 as used in Chapter 6, and taking the effective length of the specimen as 66.7 mm, the energy loss per cycle has been calculated and is shown in figure 60. The experimental points for an etched specimen are also shown in this figure. It is not intended to imply that this calculation is in any way exact. It does seem, however, that the introduction of the notion of progressive sliding yields approximately the correct form for the energy loss although it must be remembered that the energy lost in the matrix has not been taken into account and would make the prediction slightly larger.

There is one final feature of the results of considerable importance and that is the relationship between the bonded composite specimens and specimens made from the matrix only. In simple linear viscoelastic theory, the storage and loss moduli of the composite should be greater than those of the matrix alone by the same factor - the magnitude of which would depend on the nature and disposition of the reinforcement. This being the case, the specific damping capacities for the bonded specimen and matrix only specimen should be the same (if the fibres are considered to be rigid).

In the present case as figure 61 indicates there is a difference between the composite and matrix only specific damping capacities of about 2 - 3 times. At least part of this may be accounted for by the non-linear nature of the matrix material which, as previously noted, has a very marked effect on the properties of the composite. This is evidenced by the fact that there is a great difference in the factor by which the energy loss per cycle and stiffness change

such that although there is a fairly constant stiffness amplification by a factor of about 30, the amplification of energy loss per cycle varies by a factor of between 50 and 80.

CHAPTER EIGHT

8. Measures of and Methods of Measuring Damping

Some of the measures of and methods of measuring damping have already been mentioned in the last chapter. The following chapters relate to dynamic test methods in general and, in particular, the testing of the discontinuous fibre composite specimens as part of a one degree of freedom system. The bulk of the present chapter is concerned with reviewing the relevant literature on damping. By way of introduction the linear measures of damping and their relationship to each other are first considered.

8.1 Measures of damping

Plunkett 1959 lists some of the measures of damping. Those relevant to the present work are

(a) logarithmic decrement

(b) amplification factor

(c) complex modulus and loss factor

(d) bandwidth

to which may be added

(e) specific damping capacity.

All these various measures of damping may be converted one between the other although there are some limitations on the accuracy of the process.

(a) Logarithmic decrement, δ may be defined as

$$\delta = \ln \frac{a_n}{a_{n+1}}$$

in other words as the natural logarithm of the ratio of the maximum amplitude of a cycle of a freely decaying oscillation to the maximum

amplitude in the succeeding cycle. Ideally logarithmic decrement measurements should be confined to linear systems, i.e. ones in which energy lost per cycle is proportional to the square of the amplitude or the dissipative force is proportional to velocity (viscous damping). In these cases the value of δ obtained is constant regardless of the initial amplitude.

(b) Amplification factor A_r is defined as

$$A_r = \frac{a_{res}}{a_{st}}$$

where a_{res} is the resonant amplitude of a system for a given applied sinusoidal force and a_{st} is the amplitude at zero frequency for the same force amplitude. Again, for A_r to be constant, the damping in the system must be linear.

(c) The Complex Modulus representation of damping assumes that material moduli, e.g. Young's modulus may be represented by a complex number $E^* = E' + iE''$ where E' is the storage modulus and E'' is the loss modulus.

This may be represented as

$$E^* = E'(1 + i\eta) = E' + i\eta E'$$

Hence $$\eta E' = E''$$

and $$\eta = \frac{E''}{E'} = \text{loss factor}$$

This representation is only suitable for the description of the steady state response to a forced sinusoidal input.

(d) Bandwidth is based upon the difference in the two frequencies at which the amplitude is the same when the exciting force is the same (Plunkett 1959). It may be shown for a viscously damped system in which $\zeta^2 << \left\{\left(\frac{a_{max}}{a}\right)^2 - 1\right\}$

that

$$2\zeta = \frac{\Delta f}{f_n}\sqrt{\frac{a^2}{a_{max}^2 - a^2}}$$

where ζ is the damping ratio, Δf is the difference in frequencies at which the amplitude is a, f_n is the resonant frequency of the system, and a_{max} is the maximum amplitude.

The most commonly used criterion is $a_{max} = \sqrt{2}\, a$ such that

$$2\zeta = \left(\frac{\Delta f}{f_n}\right)_{3dB}$$

(e) Probably the most universally useful measure of damping is specific damping capacity ψ defined as

$$\psi = \frac{\Delta W}{W}$$

where ΔW is the energy lost per cycle and W is the maximum strain energy stored during the cycle.

Although specific damping capacity may be inferred from, for example, decay measurements, to be of maximum practical value, specimens should ideally be resonating in direct tension-compression.

8.2. Relationships between the measures of damping

The relationships are probably best illustrated with reference to specific damping capacity as defined above, viz.

$$\psi = \frac{\Delta W}{W}$$

(a) Logarithmic decrement

Let $$\delta = \ln\left(\frac{a + \Delta a}{a}\right)$$

$$= \ln\left(1 + \frac{\Delta a}{a}\right) = \frac{\Delta a}{a} - \frac{1}{2}\left(\frac{\Delta a}{a}\right)^2 + \ldots\ldots$$

$$\simeq \frac{\Delta a}{a} \quad \text{to first order}$$

If the stored energy is proportional to the square of the

amplitude, i.e.

$$W = k(a+\Delta a)^2$$

then the energy dissipated in one cycle

$$\Delta W = k(a+\Delta a)^2 - ka^2$$
$$= k(2a\Delta a + (\Delta a)^2)$$
$$\simeq 2ka\Delta a$$
$$\therefore \psi = \frac{\Delta W}{W} \simeq \frac{2ka\Delta a}{ka^2} = 2\frac{\Delta a}{a} \simeq 2\delta$$

(b) Amplification factor

For a resonant system of one degree of freedom with viscous damping, the resonant amplitude

$$a_{res} = \frac{F/k}{2\zeta}$$

where F is the exciting force amplitude, k is the spring stiffness, ζ is the damping ratio and $a_{st} = F/k$. Therefore,

$$A_r = \frac{a_{res}}{a_{st}} = \frac{1}{2\zeta}$$

For the same system decaying freely, it can be shown(Myklestad 1956)that

$$\delta = \frac{2\pi\zeta}{(1-\zeta^2)^{1/2}} \simeq 2\pi\zeta \text{ for } \zeta \text{ small}$$

so

$$\zeta \simeq \frac{\delta}{2\pi}$$

$$\therefore A_r \simeq \frac{\pi}{\delta} \simeq \frac{2\pi}{\psi}$$

or

$$\psi \simeq \frac{2\pi}{A_r}$$

(c) Complex modulus

The energy lost per unit volume per cycle in a material with complex modulus $E^* = E' + iE''$ undergoing forced sinusoidal oscillations of strain amplitude ε_0 is

$$\pi\varepsilon_0^2 E'' = \pi\varepsilon_0^2 \eta E'$$

and the maximum strain energy is $\frac{1}{2}\varepsilon_0^2 E'$.

Therefore, $$\psi = \frac{2\pi\varepsilon_0^2\eta E'}{\varepsilon_0^2 E'} = 2\pi\eta$$

(d) Bandwidth

$$2\zeta = \left(\frac{\Delta f}{f_n}\right)_{3db}$$

$$\therefore \psi \simeq 2\pi\left(\frac{\Delta f}{f_n}\right)_{3db}.$$

Thus $$\psi = \frac{\Delta W}{W} = 2\pi\eta \simeq 2\delta \simeq \frac{2\pi}{A_r} \simeq 2\pi\left(\frac{\Delta f}{f_n}\right)_{3dB}.$$

8.3. Methods of measuring damping

There have been many investigators of material damping in the past and they have used a wide variety of methods of which some have proved considerably more popular than others.

Some of the methods are listed below.

(a) Static tests

(b) Temperature methods

(c) Free decay in (i) torsion (ii) bending

(d) Rotating-bending tests

(e) Bandwidth measurements

(f) Energy input in (i) torsion (ii) bending (iii) direct tension-compression

(g) Resonance amplification factor measurements

(h) Complex modulus

Many of the methods overlap in some way in the sense that the testing system used is capable of producing results which can be analysed in different ways to give the damping in more than one of the measures of damping described in section 8.2.

(a) Static tests

In principle the simplest way to obtain the energy lost in a cycle of strain is to perform a static test. Hopkinson and Williams 1912 tried this in direct tension-compression but could only obtain an estimate of the width of the hysteresis loop at zero stress with the crude equipment at their disposal.

To obtain more easily measureable deflections, Rowett 1913 used thin-walled torque tubes and was able to plot a hysteresis loop from his measurements in torsion. Although the use of thin-walled tubes is an improvement on solid torsion specimens, the stress is not constant across the sections under test.

About twenty years after Rowett, Dorey 1932 tested solid torsion specimens in an apparatus which he admitted to be similar to Rowett's. In the discussion of Dorey, Lewis raised the objection to the tests that the specimens being solid had a large variation of stress in them from zero at the centre to a maximum at the outside. He also suggested a method of correlating results from solid specimens with those from tubular specimens but this idea does not seem to have been pursued. In defence of Dorey's method, it might be said that his tests were explicitly on crankshaft steels and from the practical point of view, a solid torsional specimen more nearly approximates to part of a crankshaft than a tubular one.

As has already been seen, it is currently possible to measure the area of a hysteresis loop for a high damping material using a standard modern tensile testing machine.

(b) Temperature methods

Hopkinson and Williams 1912 seem to have been the first to

try to utilise the increase in temperature which occurs due to the dissipation of mechanical energy as a measure of damping. Their apparatus was originally constructed for fatigue testing (Hopkinson 1911) and consisted of a specimen supporting a large mass in a one degree of freedom arrangement which was caused to resonate by a magnetic driving system. The temperature measurements were made at the centre and ends of the specimen and the system calibrated to give the energy loss by a method which is less than clear.

Other investigators most notably in Germany used fatigue testing machines for the measurement of damping. Von Heydekampf 1931, reviewing methods of measuring damping, describes them as the starting up test in which the temperature rise in unit time is measured and the energy converted into heat deduced, and the equilibrium temperature method in which the damping energy is found from the steady state temperature of the specimen and the slope of the cooling curve when the machine is switched off.

Much more recently Adams and Percival 1969 have conducted experiments, based on an idea similar to that of Hopkinson and Williams, in which a free-free bar specimen was set into longitudinal resonance by a magnetostrictive transducer and the temperature measured at various points along its length. The advantage of the system is that energy losses at various stress levels may be inferred simultaneously from one test but due to the nature of the driving system only one (rather high) frequency could be used.

Robertson and Yorgiadis 1946 criticised methods employing the measurement of temperature on the ground that damping varies with temperature. If this is a valid cause for objection then any method

which employs a resonant specimen is likely to be unsuitable because it will involve a temperature rise in the specimen whether this is measured or not.

(c) Measurements of freely decaying vibrations

(i) In torsion

The apparent ease with which a system may be constructed to measure the free decay of torsional oscillations made this method of measuring damping popular for a considerable time. All that seemed to be necessary was a frame (latterly freely suspended), clamps for the specimen, an inertia bar, some means of holding and releasing this bar at preset positions and a method of recording the subsequent decay.

Rowett 1913 extended his static investigation by employing such a system and concluded inter alia that the damping of his steel specimens was independent of frequency. A widely used apparatus for measurements of this type was the Föppl-Pertz machine which was advocated by Föppl 1936 for its simplicity. The original Föppl-Pertz instrument used a pen on wax paper recording system which Contractor and Thompson 1940 abandoned in favour of an optical system since they found that the friction of the pen on the paper caused significant losses. They also made other modifications designed to reduce the losses inherent in the machine.

Hatfield, Stanfield and Rotherham 1942 used a proprietary machine - the Cambridge Instruments Torsional Damping Recorder - but found it unsatisfactory and so designed their own apparatus which was basically an inverted Föppl-Pertz arrangement. They expanded their measurements in a second paper, Hatfield, Rotherham and Harvey

1944 but only to the extent of answering criticisms of their original experimental programme and apparently no improvement to the design of their apparatus was sought. Both these papers contain extensive bibliographies on damping studies of all sorts prior to this time.

Using very large torsional compound pendulum specimens and very low stresses, Frommer and Murray 1944 measured damping at vanishing oscillatory amplitudes and produced results which indicated very much smaller values of damping at low stresses than had been indicated at much higher stresses using apparatus of the Föppl-Pertz type.

This possibly anomalous situation was investigated by Cottell, Entwhistle and Thompson 1948 in a classic study. Quite apart from criticisms of free decay measurements such as that of Robertson and Yorgiadis 1946 that at high rates of decay, the decrement cannot be associated with any specific stress or strain amplitude or of Russell in his discussion of Contractor and Thompson 1940 that the stress distribution in solid torsional specimens precludes the damping being associated with any particular stress level, Cottell, Entwhistle and Thompson concluded that the design of machines of the Föppl-Pertz type was open to serious criticism. By successive improvement to the design of a Föppl-Pertz instrument, these investigators reduced the apparent specific damping capacity of the same specimen by between two and three orders of magnitude. This seems to have marked the end of experimentation with the Föppl-Pertz machine.

However, some time later, Cochardt 1954, 1955 performed some experiments in free decay in torsion. His specimens were wires in which were induced static mean stresses by hanging weights on the

specimens as well as an inertia bar. To prevent lateral motion, the end of the rod carrying the weights was dipped in an oil bath but no mention is made of what effect this arrangement may have had on the results.

(ii) In bending

Freely decaying steel cantilever beams were used by Ockleston 1938 to study damping in flexure. This fixed-free arrangement is criticised by Adams and Bacon 1973a on the grounds that a complex stress field is induced at the fixed end and there is necessarily a high force and moment transfer there also. Adams and Bacon also criticise Shabtach and Fehr 1944 for their tuning fork specimens which these authors defend on the ground that their specific interest was in steam turbine blades which are, like the tines of a tuning fork, at least approximately cantilevers.

Person and Lazan 1956 adapted what had been a rotating cantilever arrangment to perform free decay tests in bending on hollow tubular specimens to which were applied a static mean stress using a lever arm and weight. In this arrangement it was necessary to provide a steady bar to keep the vibrating system in one plane.

Using more conventional rectangular solid section specimens, Nagel and Clark 1957 employed a fixed-fixed beam arrangement in which the specimen ends were in massive suspended blocks. This set-up allows a static tension to be applied by lowering one block below the level of the other. A lot of the experimental details in this system, however, are not made clear.

Perhaps the first reported damping measurements on composite

materials were made by Schultz and Tsai 1968 who employed double cantilever specimens clamped to the table of an electrodynamic shaker. The system was caused to resonate and then the free decay of the system found with the shaker switched off. Adams and Bacon 1973a criticised this system extensively starting with the fact that the shaker itself will act as a damper. There are also problems with the mode shape of the beams unless the central mass is very much greater than the beam mass and, of course, if this is the case, the driving point amplitude is likely to be low. However, Schultz and Tsai were sufficiently confident in their results to conclude that their specimens were anisotropic linear viscoelastic.

Dudek 1970 used the proprietary Brüel and Kjaer type 3930 Complex Modulus apparatus to measure damping during the free decay of the cantilever beam specimens which are required by this equipment. He concluded that it was necessary to employ Timoshenko beam theory in data reduction since the shear term excluded from Bernouilli-Euler theory becomes significant for a composite material. The same criticisms apply to this apparatus as were levelled at that of Ockleston.

To test free-free composite material beam specimens, Wright 1972 sought to reduce any possible interference with his specimens by exciting them using air coupling and measuring the decay with an optical device. Apart from the fact that only low stress levels can be achieved due to the inefficiency of the air coupling, the work of Adams and Bacon 1973b suggests that aerodynamic damping is likely to be significant. Of necessity Wright's apparatus cannot be operated in vacuo.

(d) Rotating-bending tests

When an overhung rod supported by bearings and loaded at its end is caused to rotate, the deflection is not only downwards due to the load but also lateral due entirely, it is claimed to "internal friction" in the material of the rod (Kimball and Lovell 1926). Mason 1923 seems to have been the first to propose this arrangement - the loading he suggested being a couple. Kimball and Lovell claim to have thought of the idea independently of Mason and indeed their work probably had more influence since they proposed a coefficient of internal friction which was alleged to be constant and concluded that damping energy was proportional to the square of stress. The most curious part of their work seems to have been the arrangement which held the rod end steady while readings were taken. Since this device was in essence a damper, knowledge of the effect it had on the results would be intriguing but is not disclosed since its removal would presumably preclude the gathering of any data at all.

Lazan and Wu 1951 revived the use of rotating cantilevers for the measurement of damping. Their specimens were slightly tapered tubes and the loading, produced by a weight on a moment arm, could be varied by altering the orientation of the apparatus in the gravitational field. Again it was necessary to introduce a damper to take readings due to excessive whip of the loading arm.

(e) Bandwidth measurements in flexure

In general bandwidth measurements do not seem to be a very popular way of measuring damping. Gemant 1940 deduced the damping properties of some soft materials by testing steel tubes filled with the material of interest and inferring the results from bandwidth

measurement on an apparatus similar to that of Förster and Köster 1939. The arrangement involves having the specimen suspended in loops of wire situated very close to the nodes and exciting the specimen in flexure down one suspension wire while picking up the response at the other. Necessarily the stresses induced in the specimen are very small.

Schultz and Tsai 1968 also took bandwidth measurements at the 3dB points for the higher modes of their double cantilver beams and relied entirely on bandwidth measurements in some additional experiments reported in Schultz and Tsai 1969.

(f) Energy input methods

Ideally damping measurements are best made at maintained stress levels thus obviating at least one of the objections to decay and bandwidth methods. The most usual way of achieving this is to employ a resonant system of which the specimen is usually only a part. However, results from resonant systems either in torsion or in bending are still open to the objection that the stress is not constantly distributed throughout the specimen. The measurement of energy input at resonance has been attempted in torsional, flexural and direct tension-compression resonant systems.

(i) Torsional

Canfield 1928 tested tubular specimens in torsion with a magnetic system driving an inertia bar. He did not seem very confident in his results which, perhaps not surprisingly, differed in form from those of Kimball and Lovell 1926.

A very painstaking approach to the problem was taken by

Hanstock and Murray 1946 who concluded that "the experience obtained throughout this investigation demonstrates that methods of measuring damping capacity based on the vibration of a composite system of which the specimen forms only a part are fundamentally unsound - the joints in such a system being the sources of considerable dissipation of energy". For this reason they chose a compound torsional pendulum specimen suspended from a steel wire and excited electromagnetically. Their pessimism on the subject of the removal of extraneous losses in composite testing systems is probably largely due to the fact that some of the aluminium alloys which they tested have exceedingly low damping capacities as has been confirmed by other investigators, e.g. Cottell, Entwhistle and Thompson 1948.

Sumner and Entwhistle 1958 although admitting to some influence from Hanstock and Murray used what was essentially a resonant Föppl-Pertz apparatus while Adams et al. 1969 returned to the simple inertia bar arrangement with a dummy Duralumin specimen to prevent bending. In fact, Adams et al. 1973, Adams and Bacon 1973b and Adams and Short 1973 have used this latter apparatus extensively - partly to develop non-destructive tests for composite materials. However, not all the experimental details have been made clear.

(ii) Flexural

Canfield 1928 could also induce bending resonances in his system by the simple expedient of turning the driving system through 90^{o} so that the force produced acted in the plane of the specimen. Adams et al. 1969 also used a flexural apparatus for testing composite materials in which a beam was driven in its fundamental

free-free mode by a coil-magnet pair - the beam being supported on polyurethane knife edges. This apparatus was improved by Adams and Bacon 1973a - mainly by changing the supports to threads and changing the displacement measuring system - and used by them Adams and Bacon 1973b and by Adams and Short 1973 for investigations into the dynamic properties of composite materials.

(iii) Direct tension-compression

In principle, the best method of measuring damping is in direct tension-compression resonance with an arrangement such that the stress in the specimen is constant along its length. This allows variation in damping with stress to be measured directly as long as extraneous losses are sufficiently small.

Robertson and Yorgiadis 1946 tried this with equipment developed by Lazan 1943. The arrangement consisted of a specimen mounted between two large masses which rested on polished rollers on hardened steel rails. Essentially, the system had one degree of freedom and was driven by an electric motor with eccentric weights. The authors admit that their results were obtained only within 5 or 10 degrees of resonance which is probably not a sufficiently accurate criterion, particularly for materials with low damping.

Adams and Fox 1972 revived this basic system but with many modifications. The masses they used were supported on air bearings which have extremely low friction and the specimens were connected to the masses by an interference fit which could be ingeniously released by oil pressure. The system was driven by a standard electrodynamic shaker which was modified only to the extent of introducing a beryllium-copper spider for lateral constraint in

place of the standard "Tufnol" piece. The apparatus was intended for the measurement of high damping cast iron specimens which could not be tested using, for example, the apparatus described by Adams and Percival 1969 because of the non-linear stress-strain characteristic of cast iron.

(g) Resonance amplification factor

As pointed out previously many of the systems described can be used to provide damping data in more than one form. Lazan 1943 used the same apparatus as Robertson and Yorgiadis 1946 to report damping data in terms of resonance amplification factor. He also used a machine of his own invention called the hypocyclic oscillator to drive specimens in torsion, bending and direct-tension compression. By suspending this driving device from the specimen and altering the orientation of the eccentric weights that provided the force, it was possible to produce resonance in the mode desired. These tests were also reported in terms of resonance amplification factor.

(h) Complex modulus

Measurements of complex modulus are commonly made in the field of viscoelasticity. An example of such experiments is the work of Norris and Young 1970 who drove their specimens in longitudinal resonance and deduced the material properties from the outputs of accelerometers at either end of the specimen.

McConnell 1969 proposed a one degree of freedom system for the testing of viscoelastic materials but Ruzicka criticised the system in the discussion of the paper on the grounds that a Kelvin element model for the specimen was too simplistic and accordingly the proposal would be unlikely to work as the author had envisaged. This system is discussed further in the following chapter.

CHAPTER NINE

9. Dynamic Tests

9.1 General considerations

It will be clear from the foregoing review that dynamic tests to establish the mechanical properties of materials are both many and varied. When considering which method was most suitable for the testing of the particular composite developed in this study, it was obvious that some methods might be discounted immediately. For instance, temperature measuring methods were inappropriate due to the inhomogeneous nature of the material. Quasi-static tests although employed here for other purposes, as has already been reported, are not necessarily suited to the prediction of the dynamic characteristics of a material.

Another important feature to be considered is the nature of the deformation undergone by the specimen. Quite apart from considerations of variation of stress in the specimen, torsion, for instance, is not an appropriate means of testing these materials since the shear strain amplification desired will not occur. It is interesting to note that Adams et al 1969 and Adams and Bacon 1973b report consistently higher specific damping capacities in torsion than in bending for continuous fibre composites. This is quite reasonable since the shear modulus in the longitudinal direction will be relatively small for these materials and much higher shear strains will be obtained in torsion than in bending when testing continuous fibre specimens.

Perhaps the major consideration in devising a testing system

was the desire to keep the composite specimens in tension. The reason for this was that it was early established when experimenting with glass fibre composites that local buckling of the composite could occur if the material were compressed due to the lack of restraint provided by the compliant matrix. So, although some shear strain amplification should occur in bending specimens, it was felt that it would be preferrable to try to confine the loading to the longitudinal direction which, apart from being the mode in which the greatest shear strain amplification occurs, is also the mode which should be most easily related to static tests. This is particularly important in view of the non-linear nature of the materials.

The problem of compression remains. However, since the loads required for quite sizeable deformations of the specimen are small, it is relatively easy to add a mass to the specimen so that the configuration is that of a single degree of freedom system. Overall compression of the specimen may then be avoided if the amplitude of vibration is suitably limited.

Damping tests are frequently carried out at resonance - this certainly being the case for many of the tests described in section 8.3. The major disadvantage is that the range of test frequencies available will usually be fairly limited. The advantages are that at resonance vibration amplitudes are relatively large and in principle at least the only input is that required to overcome damping energy losses in the test material.

The definition of resonance can itself be a problem. Adams and Fox 1972, for instance, presuppose that there is nearly enough a 90^{o} phase difference between force and displacement at displacement

resonance and that the damping energy will be $\pi F X_1$, where F is the amplitude of the force input and X_1, the displacement of the driven mass in their system. Resonance is defined as occurring at the maximum displacement amplitude for a given driving force. The results quoted in the paper show a maximum specific damping capacity of $\psi = 25\%$ which is very roughly equivalent to a damping ratio, of 0.02 which amply justifies the initial supposition.

Adams and Bacon 1973a state that "at displacement resonance, providing the damping is not large, the exciting force and the resulting displacement are 90° out of phase" and then proceed to use the same formula as the one quoted above for damping energy although in this case the displacement is of the centre point of a beam (the tests being in flexure). It is implicit in their work that the damping under consideration is of a hysteretic nature. They also state that "for non-hysteretic materials, the phase angle is slightly less than 90° but providing the damping is not large (i.e. greater than 50% specific damping capacity) the error involved is negligible".

Jacobsen 1930 suggested the criterion of equal work dissipated per cycle to derive equivalent dashpot "constants" for analysis of systems in which the damping mechanism is not viscous and Sperry 1964 has applied this method in a survey of theoretical rheological models. It seems to be reasonable to conclude from these analyses that provided the damping is small, the dissipative mechanism may be disregarded and the assumption made that the displacement resonance will nearly enough coincide with the velocity and acceleration resonances so that the damping energy per cycle may be taken as $\pi F X$ where F is the amplitude of the exciting force and

X the resonant displacement amplitude.

An even greater problem in defining resonance arises when the damping is not small. In the case of a simple one degree of freedom system with viscous damping, it is well known that if the damping factor ζ is sufficiently large then the frequencies at which the maximum amplitudes of displacement velocity and acceleration occur become quite distinct. In this case, the maximum energy dissipation occurs when the phase angle between force and displacement is 90^{o} and there is a maximum in velocity. Establishing either the 90^{o} phase difference or the velocity maximum is sufficient to define resonance for damping measurements.

However, simple viscously damped one degree of freedom systems do not occur often in practice and Ruzicka in the discussion of McConnell 1969 is critical of the suggestion in that paper that a 90^{o} phase shift between force and displacement be used as the criterion of resonance. Bert 1973 describes a Kelvin element as a first approximation to the behaviour of a viscoelastic solid and McConnell is essentially using this type of element as the model of his supposed test material. Ruzicka's criticism is that it is not a very good model for a viscoelastic material if there is any significant degree of damping - his major objection being that if a model with more than the two elements of the simple one proposed is used the phase angle is no longer 90^{o} at resonance.

In practical terms, McConnell's criterion of a 90^{o} phase difference between force and acceleration would be unlikely to be realised directly since there will almost certainly be a phase shift through the pre-amplifiers usually required with impedance

heads. This means that the criterion for resonance would not be simply established even if the model were an accurate one.

Once it was resolved that a one degree of freedom system represented the best arrangement for trying to establish the dynamic properties of the composites, there remained the problem of an appropriate means of extracting relevant data. When the system had been set up and some initial attempts made to measure resonance curves, it became clear from the results particularly for the unbonded specimens that it would be difficult if not impossible to know which if any of the measures of damping listed in the last chapter would be suitable for describing the damping in the system.

In spite of the fact that the composites seemed to be significantly non-linear, it was decided to try to obtain mechanical impedance (ratio of force to velocity) data for the system. The reason for choosing mechanical impedance measurements was that potentially a large amount of information about the system under test is provided at each point on the resonance curve. The way in which this was achieved is described in the following sections.

9.2. The Apparatus

The rig in which the vibration tests were carried out is illustrated in figure 62 and consisted principally of a massive rectangular steel frame manufactured from hollow 200 x 100 mm section which was subsequently filled with concrete. The frame stood upright on welded steel feet mounted on rubber pads. The internal dimensions of the rectangle were 610 x 305 mm with a plate welded across the 305 mm dimension of the frame to provide the backing for the upper grip on the specimen.

Hixson 1961 points out that in mechanical impedance tests the vibrator should be suspended independently from the structure under test. A Ling Dynamic Systems series 400 vibrator was bolted to a piece of concrete-filled rectangular steel section and using two support blocks this arrangement was made to form a bridge over the lower bar of the rectangular frame. The support blocks were also mounted on rubber sheeting such that the driving arrangement had a fundamental resonance at about 150 Hz - well in excess of any of the test frequencies. The driving arrangement was also well isolated from the main frame.

Force was measured using a Brüel and Kjaer (Band K) type 8200 force transducer screwed directly into the vibrator table via a short grub screw. A cylindrical mass was then screwed on top of the force transducer. This mass had a plate welded to its top side in which a number of holes had been drilled and tapped 5/16" diameter BSF on a 73 mm P.C.D. The other part of the mass consisted of a plate with four slots on the same P.C.D. as the holes and of width sufficient to allow clearance for 5/16" diameter screws. A block, which formed the backing for the lower specimen clamp, was welded on to the top plate. It was necessary to have the mass split in this way since the connection to the force gauge was a screwed one and some means of allowing the mass to load the specimen was required.

The difficulty experienced with gripping the specimens at all has been described in chapter 3. It was recognised from the review of the literature of damping that any simple method of gripping the specimen was likely to be a source of considerable energy dissipation. However, the friction grips used in the slow cycle tests did not produce a very large loss in relation to the energy lost in the

specimen itself. If the specimens had had an extremely low damping capacity this would not have been the case.

Since the specimen ends could not be machined in any way there was little alternative to the use of some sort of friction grips. After some experimentation, these were constructed as indicated in figure 63. Two small blocks for lateral location were screwed on to the backing plate by means of four 2BA screws such that the specimen could be entered between them. The clamping force was provided by two OBA screws which were screwed through a bridge piece straddling the lateral location blocks and which bore on a small clamping block. This block was serrated so that it would bite into the epoxy resin which formed the specimen grips. The bridge piece was secured to the back plate by four OBA screws. In order to ensure that the mass preloaded the specimens small spacer blocks were introduced between the two parts of the mass while the clamps were being tightened. Lock nuts, were provided on the clamping screws to ensure that they did not work loose during the experiment. Finally the two parts of the mass were drawn together by tightening the 5/16" set screws. At various times two different sizes of mass were used in the experimental system - one just greater than 3 kg and one just less than 5 kg.

The vibrator under the mass was driven by a B and K type 1017 beat frequency oscillator (BFO) through a Henelec type MU 442 power amplifier which had been selected for its good sinusoidal performance at low frequencies. It is desirable to maintain a constant force input into a system on which mechanical impedance tests are being conducted. For this reason, the force signal was fed into the input of the BFO compressor (feedback) circuit via a B and K type 2628 low frequency charge amplifier. This had the effect of keeping the

system force input very nearly constant (usually within 5% total range).

A B and K type 4334 accelerometer was screwed on to the clamping backing block on the mass. It was assumed that for the low test frequencies involved, there would be no appreciable deformation in the mass between one end and the other. Although mechanical impedance is defined as the ratio of force to velocity the motion was measured as acceleration because the integrating networks of the B and K type 2625 vibration pick-up pre-amplifier through which the acceleration signal was passed attenuate the signal very appreciably. There was an additional reason for wishing to keep the motion signal as large as possible which is explained below.

Apart from measuring a signal proportional to the force and one proportional to the motion, it was necessary to obtain the phase angle between the two. A Solartron JM 1600A transfer function analyser with associated JX 1606 mechanical reference synchroniser was used for this purpose. This combined instrument accepts a periodic signal as a reference to which other signals may be related. The force signal was fed in as the reference and the acceleration as the signal to be compared with it. One limitation of the mechanical reference synchroniser is that it requires a signal of at least one volt to operate so it was necessary to pass the pre-amplified acceleration signal through a B and K type 2409 electronic voltmeter which is also an amplifier in order to obtain signals of sufficient magnitude. This last procedure has the additional advantage of removing the 13 volt DC bias from the pre-amplifier output. Although the BFO provides reasonably accurate increments of frequency its design is such that it is sensitive to temperature

changes. Set frequencies were found to alter by as much as 1 Hz as the instrument warmed up. Even after a warm-up period of two hours there was still a tendency for the set frequency to drift. This meant that a frequency counter was required for accurate frequency measurement and a Racal type SA 520 digital frequency meter was used for this purpose at the power amplifier output.

See Addenda after Figure 89.

A schematic view of the apparatus is shown in figure 64.

9.3 Measurements

Clearly in any system which appears to be non-linear care must be exercised in obtaining and interpreting data. One of the most likely areas in which inaccuracy may arise is that many non-linear systems tend to generate harmonics of the excitation frequency. It has also been noted already that some difficulty had been experienced in obtaining a power amplifier which would operate in the frequency range desired without significant signal distortion occurring. It therefore seemed important to make some study of the harmonic content of the signals to be measured.

Although the basic measuring system yields data on the fundamentals of force and acceleration, the mechanical reference synchroniser has the additional facility of allowing the measurement of their harmonics. The apparatus was checked for harmonic content of the signals over the relevant frequency range using initially a small mass screwed on top of the force gauge as the system loading the vibrator and thereby providing a force feedback signal. The power amplifier output under these circumstances showed a maximum 2nd harmonic of 3.3% of the fundamental and typically figures for the 2nd to 4th harmonics of between 1 and 2%. When an unbonded

specimen loaded by a mass was introduced as the system, there was no significant alteration in the harmonic content of the power amplifier output.

Readings of force and acceleration were also taken with the vibrator loaded by a mass only and again the largest harmonic content was found to be a second harmonic less than 4% of the fundamental. Introducing a bonded specimen and mass did not significantly increase the harmonic content of the force and acceleration signals although at frequencies near resonance of the system the 2nd harmonic of the acceleration signal was in fact doubled but the resulting figure was still $<$ 5% of the fundamental. When it is recalled that an acceleration at twice the fundamental frequency implies a displacement of one quarter the fundamental displacement for the same magnitude of acceleration signal, it seems reasonable to conclude that the harmonic content of the signals, whether introduced by the system under test or extraneously, will not seriously detract from an assumption of point for point linearity in analysing the results.

The basic measurements made were the fundamental root mean square voltages representing force and acceleration. The reference sensitivity of the accelerometer was 56 mV/g but rather than check this directly it seemed much more useful to calibrate the acceleration signal using the measuring system for the actual experiment. To this end the accelerometer was screwed to the vibrating table of a B and K type 4292 calibrator using a B and K type 2606 measuring amplifier as the power source for the calibrator and the resulting acceleration signal at 80 Hz was passed through the pre-amplifier and amplifier/ voltmeter to the transfer function analyser. 1g (peak) was established

by observing the distortion of the acceleration trace on an oscilloscope when the ball in the calibrator just began to rattle. This seemed to be a fairly sensitive and repeatable point so the manufacturer's statement that calibration accuracy better than 10% can be achieved seems unduly pessimistic - the variation in the result from this procedure being at most $\pm$ 1%.

Displacement resonance curves were calculated on the assumption that the motion was near enough sinusoidal i.e. by dividing the acceleration by the square of frequency. Since the typical variation in the frequency readings is $\pm$ 0.25% the overall error in this procedure should not be greater than $\pm$ 1.5%. Since the material under test is only a model rather than a practical material, it was not considered essential to try to achieve the highest standards of accuracy but obviously it is still necessary to have a reasonable estimate of the accuracy of the measurements.

The force gauge is calibrated by the manufacturer such that its sensitivity in picoCoulombs per Newton may be dialled up on the Type 2628 charge amplifier. The output of this instrument on the range used in the experiments was 1 volt per Newton. This magnitude of signal was, as has been noted, essential as an input to the mechanical reference synchoniser which effectively set the minimum exciting force for the system at 1 N. The upper limit on the excitation was set by the output characteristics of the type 2628 at about 7N (rms) since at forces greater than this amplifier overload occurred. Use of the next range on the instrument required employment of a minimum excitation force of 10 N (rms) which was higher than was necessary or desirable.

Checking the calibration of the force gauge is neither simple nor really necessary since it is the overall performance of the force gauge, accelerometer and frequency meter in measuring mechanical impedance that is required. An estimate of this could be obtained by the same method as for the harmonics - loading the vibrator with a mass of known size and taking readings of force and acceleration over the experimental frequency range.* The mean value obtained for the mass size was within 1% of the value by weighing and the overall variation was about 6%. Taking into account errors in frequency measurement, the magnitude of mechanical impedance should not be in error by more than $\pm$ 3.5%.

The other important measurement to be made was that of phase.* It transpired that the phase measurement obtained was heavily distorted from what might be expected. The amount of distortion could be checked with the same arrangement used for estimating errors in the magnitude of impedance just described. The force and acceleration for a mass alone should be in phase but were found to be apparently in anti-phase - the distortion being around 170^{o}, varying by usually 2^{o} or 3^{o} over the frequency range and increasing with frequency. According to B and K, the phase distortion in the force transducer and pre-amplifier is small so most of the distortion must come from the accelerometer and its pre-amplifier.* Applying a phase distortion correction as obtained above to the phase difference readings in the experimental results has in any case the effect of correcting for both errors. It has been supposed from the near sinusoidal nature of the results that the velocity lags the acceleration by 90^{o}.

The accuracy of the transfer function analyser phase measure-

*
See Addenda after Figure 89

ment is given as ± 10 minutes of arc at full scale amplitude down to ± 1° at 0.1 full scale amplitude. In general the readings were repeatable within 20 minutes of arc but at lower amplitudes the variation was certainly greater. Less credence has been placed on these results which were more important as part of the resonance curve than for mechanical impedance data. Additionally the phase distortion correction will introduce a further error of up to 30 minutes of arc so it is likely that even at the higher amplitudes, the phase measurement will still only be within about ± 1°. This, of course, has a significant but varying effect on the calculation when the mechanical impedance data are split into real and imaginary parts.

9.4 Sample results and their analysis.

The repeatability of the resonance curve results was checked using a bonded specimen which is less stress history sensitive than the unbonded specimens. There was no significant difference between two separate runs nor was there any significant difference in the results obtained from measuring the resonance curve in the frequency increasing and decreasing directions. Figure 65 shows a typical resonance curve for a bonded specimen and also one for an unbonded specimen. It is clear, and not unexpected, that the differences between the bonded and unbonded specimens are also reflected in the results of this experiment.

Before proceeding to the method of analysis, it is important to give some consideration to what it implies. Timoshenko et. al. 1974 treat the case of a prismatic bar made from a homogeneous isotropic material loaded by a mass at one end. If the mass is

sufficiently large with respect to the mass of the bar, it is shown that for longitudinal vibration, the static axial stiffness of the bar may be taken as the spring constant of the system which thereby reduces to one with a single degree of freedom. A further consequence of this is that the strain in the bar is constant over its length. Neither of these conditions can be fulfilled in the case of specimens which exhibit stiffness characteristics which have some dependence on the rate of deformation, but it is implicitly supposed in what follows that even in these non-homogeneous anisotropic specimens, the dynamic strain is sufficiently uniform that the overall stiffness and damping of the specimen are directly representative of the material properties.

The other conditions which appertain to the homogeneous isotropic case - that plane sections remain plane and that particles in every cross section move only in the axial direction of the bar* - are not fulfilled in the present case either but at least the length of the longitudinal waves in the composite will be much greater than the lateral dimensions of the bar.

In classical linear theory a forced viscously damped one degree of freedom system is governed by the equation

$$m\ddot{x} + c\dot{x} + kx = Fe^{i\omega t} \qquad 9.1$$

where m is the mass, c the viscous damping constant, k the spring stiffness, x the displacement, F the exciting force and ω the exciting frequency. Translated into mechanical impedance terms this equation becomes

$$Z = \frac{F}{v} = c + i\left(\omega m - \frac{k}{\omega}\right) \qquad 9.2$$

*See Addenda after Figure 89.

where v is the amplitude of velocity.

If the results taken from a one degree of freedom system by splitting the mechanical impedance into real and imaginary parts do not produce a constant real part then it may be concluded that the damping is not linearly viscous or the system is non-linear or is composed of more than the two elements (spring and damper) supposed in the simple analysis.

Comparing the material impedance (having removed the effect of the mass) with the forms of impedance curves given by Hixson 1961 indicated that the material is non-linear rather than a more complicated arrangement of linear elements. This being the case, the results were analysed on the basis that the mechanical impedance for each measured point could be split into real and imaginary parts and that the real part would reasonably describe the dissipative element while the imaginary part could (once the impedance of the mass had been subtracted from it) yield a significant representation of the specimen stiffness. This, of course, ignores the other possibility that the specimen is composed of more than two non-linear elements. However, as the analysis of the results in the following chapters shows, the assumption made does not seem to be an unreasonable one.

The analysis is essentially then one which assumes linearity point for point on the resonance curve - an assumption partly justified by the low incidence of harmonics in the measured signals. The real part of the impedance is not, however, a constant and does not depend on velocity so it is convenient to change the notation in equation 9.2 to

$$Z = \frac{h}{\omega} + i\left(\omega m - \frac{k}{\omega}\right) \qquad 9.3$$

where h is the coefficient of hysteretic damping.

This is not a rigorous alteration even in linear theory but rather a device used to indicate that the damping is displacement rather than velocity dependent. Bishop 1955 gives the basic hysteretic damping theory and some of the difficulties are discussed in Scanlan and Mendelson 1963. In linear theory h would be a constant but in the present non-linear case, it is variable with amplitude. In fact, the real part of impedance is not an important quantity in itself but may be used to estimate the damping energy lost per cycle (ΔW) through the equation

$$\Delta W = \pi h X^2 \qquad 9.4$$

where X is the peak displacement amplitude of the vibration for the given frequency.

Samples of the calculated stiffnesses taken from the same results as the resonance curves of figure 65 are shown in figure 66. Estimates of the likely error in deriving the stiffness show that the result should be within 0.5 - 1% of the true value. Accordingly the fact that the unbonded specimen stiffness results show a variation of up to nearly 3% probably indicates a material characteristic rather than an experimental error. Similarly samples of the energy lost per cycle results are shown in figure 67. In this case, the accumulation of possible error could produce a total range of 6 - 15% round the true figure so as with the stiffness results, the variations in the energy lost per cycle results for the unbonded specimen are taken to be at least in part characteristic of the material. These points will be discussed in greater detail in the following chapters.

It will have been noted that no mention has been made of the energy lost in the vibrating system other than that lost in the specimen. It was recognised that this energy loss would be quite substantial and some means of estimating it was sought. Since the method used involves reference to the results from the bonded specimens, discussion of it may conveniently be left until the next chapter.

CHAPTER TEN

10. Bonded Specimen Results

Since the bonded and unbonded specimen results are quite distinct, they will be discussed separately. In this chapter, the bonded specimen results are dealt with from the point of view of both analysis and synthesis. Firstly, however, the energy lost in the system must be considered.

10.1 Energy losses in the experimental system

In many instances, e.g. Adams and Fox 1972, Duralumin has been used in experimental systems to estimate the background damping present. (Duralumin is used because it has been found to possess an extremely low specific damping capacity.) This procedure is quite satisfactory in circumstances in which the actual experiment is to be carried out on materials with stiffnesses similar to Duralumin since the energy lost in the system may then be estimated at similar frequencies and displacement amplitudes. In the present case, however, any aluminium alloy specimen of the appropriate stiffness would be required to be about $1mm^2$ in cross-sectional area. In spite of this, attempts were made to use aluminium specimens of this sort but the small lateral dimensions caused these specimens to be either extremely fragile or so prone to bending that it was impossible to work with them.

Another plausible possibility for estimating the system damping was to use a steel coil spring which, it was thought, would be more readily made of a suitable stiffness than an aluminium bar specimen and also have fairly low damping. In fact, it proved very

difficult to make a spring of the correct order of stiffness and fit it into the rig. One of the main problems was non-linearity of the spring stiffness. When a spring of an appropriate stiffness had been obtained, it was set up in the system loaded by a mass. It was found that a relatively small input caused the system to resonate violently but there was also gross distortion of the input waveform. The smallness of the input in any case created measurement problems because the feedback signal to the oscillator compressor circuit was not large enough for the proper operation of that instrument and the force signal was not sufficiently large to be measured using the transfer function analyser. This made the extraction of any relevant data from the spring/mass system virtually impossible.

Before proper tests had been conducted, it seemed possible that the matrix and consequently the bonded specimens would have relatively small damping and indeed the first bonded specimens were made with this possibility in view. It transpired, as has already been seen, that the bonded specimens have quite substantial damping but it was also found in the type of test reported in Chapter 7 that the properties of the bonded specimen were insensitive to change of rate - both the stiffness and damping being very similar for frequencies an order of magnitude apart (0.83 Hz and 0.083 Hz).

It has therefore been assumed for the purposes of estimating the energy losses extraneous to the specimen that the damping in the bonded specimens is rate insensitive and that the damping as reported in Chapter 7 is more nearly representative of the specimen damping than that calculated from the one degree of freedom system experiment. Since the static test loops for the specimens are also

very similar in shape and width to the loops at 0.083 and 0.83 Hz, this does not seem an unreasonable extrapolation. Results typical of the one degree of freedom system and the 0.83 Hz tests are shown in figure 68. The difference between the lines drawn through the experimental points is taken to be a reasonable estimate of the energy lost per cycle in the rest of the system.

10.2 Stiffness results from vibration experiment

An example of the stiffness results from a bonded specimen has already been given in the last chapter. A number of the experimental points were omitted from the graph because on the scale used the points lie so close together that plotting them all contributes little to clarity. In replotting these results on a larger scale in figure 69, only the envelope which contains all the points from the vibration test and in which the points are fairly evenly distributed, has been shown. An approximate mean line is drawn through the results which will be used in the subsequent synthesis of resonance curves. Also shown in figure 69 are some typical results from the 0.83 Hz tests reported in Chapter 7.

Since these two methods of estimating the stiffness are completely independent, the close agreement between the results lends support to the simple quasi-linear analysis of the one degree of freedom test results. Such disparity as does exist between the two sets of results may readily be accounted for in terms of differences between the two test methods and subsequent treatment of the results. In particular, a specimen underwent many more cycles of oscillation in the course of the one degree of freedom system test than in a test at 0.83 Hz. This probably had some effect on the evidence of

stress history dependency of the results although this characteristic of the specimens is still shown in the 3.5% spread of the results from the vibration test.

The nature of the averaging (since the stiffness results constitute an average stiffness over the whole cycle) is also likely to have some effect. In contrast to the assumption about the damping, it is assumed that the stiffness results provided by the vibration experiment give a sufficiently reliable estimate of the specimen stiffness about a mean load of $\sim$ 50 N.

10.3 Synthesis of a better estimate of the resonance curves for bonded specimens

The existence of non-linear characteristics in the specimens makes the analytical description of the experimental results more difficult than in the linear case. The difficulty is not eased by the fact that the stiffness and damping are necessarily plotted against loop amplitude rather than the analytically more desirable instantaneous value of displacement.

Non-linear damping (which is not so great as to affect seriously the sinusoidal nature of the result) with linear stiffness is in some ways more tractable than non-linear stiffness with linear damping since resonant frequencies are not affected in the former case. In the case of constant stiffness and small non-linear damping, the establishment of the resonant frequency of a one degree of freedom system for one input implies knowledge of the resonant frequency for all other inputs. It is upon this fact that the approach proposed by Jacobsen 1930 is founded. This involves an attempt to linearise the damping in terms of equivalent damping

coefficients based on a criterion of equal energy dissipated at resonance in the actual and linearised systems. However, when the stiffness is non-linear and the mean stiffness is dependent upon the vibration amplitude, the amount and nature of damping in the system can have an important effect on the resonant frequency and therefore such an approach will be inadequate.

Since the stiffness and damping are both non-linear in the present case it seems unlikely that a simple linearised formulation i.e. constant values of stiffness and damping will adequately describe the specimen characteristics. The requirement is for a means of constructing resonance curves from the information contained in, for example, figures 68 and 69. This may be done by a method which is essentially an inversion of the analysis procedure. Cooper 1959 described this method which involves plotting curves of force, F against frequency for a constant displacement amplitude, X. Adopting the notation of the last chapter for hysteretic (frequency independent) damping, the force equation from Cooper's paper (in which there is an error) is

$$F = X\left(h^2 + (k - m\omega^2)^2\right)^{\frac{1}{2}} \qquad 10.1$$

It must be remembered that h and k are not constant but depend on the amplitude X and it must be emphasised again that the plot of stiffness against amplitude in figure 69 is only applicable to the situation where the mean load is of the order of 50 N. Any significant change in the mean load will have a marked effect upon the mean stiffness which will be reduced for a smaller load and increased for a larger one (assuming the same displacement amplitude).

Before demonstrating the use of the method, the curves of

figure 68 may be converted into h values by assuming that the energy lost per cycle results derive from ellipses as implied by equation 9.4 so that

$$h = \frac{\Delta W}{\pi X^2} \qquad 10.2$$

The result of this procedure is shown in figure 70.

The method may now be demonstrated and is perhaps best illustrated by reconstructing the resonance curves as measured before proceeding to estimate what the resonance curves would look like if there were no extraneous damping. Using the h values for the vibration test result from figure 70 and the mean stiffness values from figure 69, equation 10.1 yields calculated force curves of constant displacement amplitude. Some typical curves are shown in figure 71. F is really the driving force amplitude so any line parallel to the frequency axis constitutes a constant amplitude force input and the resulting resonance curve may be deduced from the intercepts of such a line and the calculated curves. A comparison of two resonance curves measured directly and some points deduced from the above procedure is shown in figure 72. The calculated points and the curves are not, of course, independent and if the stiffness and damping results all lay on single lines then all the points would lie on the resonance curves. Figure 72 is presented to show that taking average values of stiffness and damping (at any given displacement amplitude) yields a reasonable approximation to measured resonance curves for particular force amplitudes. By implication, the method will give reasonable predictions of resonance curves at any other force amplitude less than the greatest amplitude used in the experiment.

Since the driving force in the experiment is not exactly

constant, the particular value chosen for the reconstruction of a resonance curve is to some extent arbitrary. As figure 72 shows, the variation is not so great that use of the mean force gives a misleading result. The overestimate or underestimate of the resonant amplitudes is due to the fact that the mean force was greater or less than the actual force at resonance.

Having established that Cooper's method gives a reasonable estimate of the measured resonance curves, attention may be turned to what effect there is on the result when the damping figures from the 0.83 Hz test (figures 68 and 70) are used in place of the values deduced from the vibration experiment. It is intuitively obvious that lowering the damping estimate for the same stiffnesses will have the effect of reducing the minima of the curves of figure 71. As seen in figure 73 this in turn has the effect of reducing the width of the resonance peak and producing the same resonant amplitude with a smaller exciting force. It is apparent, however, that the nature of the resonance is not too seriously masked by the extraneous damping.

10.4 Comparison of the estimated non-linear results with linearity

One obvious way of comparing the non-linear result with linearity is to note that in the linear system equivalent of figure 71 all the curves would have a minimum at the same (resonant) frequency. Additionally curves calculated for equal increments of displacement would be equispaced along the resonant frequency line. This is not, however, a very helpful comparison since it is not usual practice to plot curves of constant displacement to represent the characteristics of a one degree of freedom system.

A more readily comprehensible comparison is shown in figure 74 in which the estimated non-linear resonance curve is compared with a linear resonance curve calculated for a system having the same mass, driving force, resonant frequency and amplitude as in the non-linear case. The damping was chosen to be hysteretic although calculations supposing viscous damping show that there is very little difference between the viscous and hysteretic results in the narrow frequency range under consideration. The quantities used in calculating the linear curve were stiffness, $k = 77530$ N/m and hysteretic damping constant, $h = 4640$ N/m.

With reference to the 1.8 N (rms) driving force curves, the fact that the linear system shows higher amplitudes than the non-linear system on the low frequency side of resonance in spite of having lower damping is due to the greater stiffness at low amplitudes in the non-linear case. On the high frequency side of resonance the results are more nearly coincident due in part to the increasing importance of the mass in determining the amplitude. The increasing stiffness of the bonded specimen as the amplitude falls eventually causes the non-linear system displacement to be greater than that of the linear system - i.e. the non-linear stiffness has the opposite effect to what it had on the low frequency side.

Also shown in figure 74 are the resonance curves for the same linear and non-linear systems at a driving force of 1 N (rms). The disparity between the two systems is much more evident since the increased stiffness at lower displacements in the non-linear system causes the resonant frequency to increase. The damping also increases with reduction in amplitude so that the resonant amplitude is significantly reduced in comparison with the linear prediction.

If the comparison of linear and non-linear systems had been carried out on the criterion of matching a linear system to, for example, the resonant peak of the 1 N (rms) non-linear curve then the linear predictions for higher driving forces would give too low a resonant amplitude at too high a frequency.

Another characteristic which yields important information about a resonant system is the phase angle between force and displacement. Figure 75 shows the phase angles for the linear and non-linear systems. A linear system has a unique phase angle/frequency relationship independent of the driving force whereas the non-linear system has a different phase angle/frequency relationship for each resonance curve. The phase angles for the linear system and the non-linear system at 1.8 N (rms) driving force seem to be in reasonable agreement over much of the range but the difference at other driving forces of the non-linear system is quite marked. This is not simply due to the change in resonant frequency because the difference is still notable when the frequencies are normalised by dividing by the resonant frequency. The lack of agreement is even more obvious if the comparison is made with phase angles from the second linear system based on the 1 N (rms) resonance mentioned above. As will be seen below, however, it transpires that the 1 N (rms) peak represents an extreme condition.

Finally, in figure 76 is plotted the estimated specific damping capacity for a typical bonded specimen. For each point this has the form

$$\psi = \frac{2\pi h}{k} \qquad 10.3$$

Also shown are the specific damping capacities for the linear systems

which it will be noted intersect the non-linear curve at the 1 N (rms) and 1.8 N (rms) driving force resonant amplitudes - the source of their derivation. It will also be noted that the specimen specific damping capacity has a maximum at the 1 N (rms) peak.

CHAPTER ELEVEN

11. The Unbonded Specimen Results

The treatment of the results of the unbonded specimens is very similar to that of the bonded specimens presented in the last chapter. The distinction between the etched and unetched specimens became less clear in the results of the one degree of freedom system tests, although the etched specimens remained somewhat stiffer than the unetched. This fact occasioned the manufacture and use of the smaller (3 kg) mass when testing the unetched specimens so that the resonant frequencies were raised above the frequency region in which gross electrical distortion of the signals might occur. In this chapter some results from the unbonded specimens are presented and compared with the results from the 0.83 Hz tests, an approximate solution to the bilinear hysteresis one degree of freedom system problem, and linear theory.

11.1 Experimental results

As might be expected from the variation in the results for the unbonded specimens from the 0.83 Hz tests, there is also a considerable spread in the results from the one degree of freedom system tests. The variation recorded is greater than would be expected as the result of experimental error alone and is probably due to stress history effects. It seems likely in this instance, however, that the mean position of oscillation will change rather than the mean load as in the case of the earlier tests.

Typical envelopes of the stiffness and energy loss per cycle results are shown in figures 77 and 78. Also shown in these figures are examples of the individual results taken from particular resonance

curves. It is clear from the examples shown and the overall shape of the envelopes that the results from each resonance test are distinct. In the case of the bonded specimens, due to the even spread of the results, the mean line through the envelope described them well enough to allow the successful application of Cooper's method of reconstructing the resonance curves. In the present case in order to be able to reconstruct the resonance curves with reasonable accuracy a "best line" passing through the results taken from the points close to resonance of the various resonance curves must be used. As will become evident, the results from the different resonance curves are not so disparate that a reasonable approximation to the original resonance curves cannot be reconstructed using single line representations of the results such as those indicated in figures 77 and 78.

The stiffnesses as calculated from the experiment may vary by up to 12% total range about the best line as defined above while the energy loss per cycle has a total variation of as much as 35% about the best line at the intermediate amplitudes. In spite of these variations, as indicated above, the resonance curves may be reconstructed using Cooper's method as in the case of the bonded specimens. An example of this is given in figure 79.

Because the correction for extraneous energy loss is much smaller relative to the damping in the unbonded specimens it does not have so much effect on the resonance curves as in the bonded specimen case. Indeed the spread of the energy lost per cycle results is greater than the estimated extraneous energy lost per cycle. The correction for the extraneous energy loss has the greatest effect in the middle of the range of amplitudes at which the tests were conducted. Figures 80 and 81 show comparisons of a typical worst case. In

figure 80, the measured resonance curve, points for the reconstructed curve, and for the reconstructed curve with extraneous energy loss correction are shown, while figure 81 shows the phase angle for the same three cases. It will be noted that there is not a great difference between the measured results and the two sets of reconstructed results. It is proposed therefore to use the results as measured and as calculated from the best line in the experimental results as being reasonably representative of the properties of the specimen under the given experimental conditions.

11.2 Comparison of vibration and 0.83 Hz test results

As might be expected from what is already known about the bonded and unbonded specimens from the 0.83 Hz test, the relationship between the one degree of freedom system and 0.83 Hz test results for the unbonded specimens is quite different from that for the bonded specimens. It will be recalled that for the bonded specimens, the stiffness results from the two tests were very similar but that the energy lost per cycle results from the 0.83 Hz tests were less than those from the vibration test and that the former were taken to be representative of the specimen properties.

In the case of the unbonded specimens, the damping as measured in the vibration experiment was less than the damping in the 0.83 Hz test in spite of the extraneous energy loss in the vibrating system. Additionally, the stiffness was increased by a factor of up to 50%. These effects are shown in figures 82 and 83.

It is not difficult to see the reason for these effects once it is known that the critical interface shear stress increases with increase in the rate of deformation. Referring again to the bilinear

hysteresis loop in figure 18, it is clearly possible that if the load to initiate sliding, P_c , (and by analogy the critical interface shear stress) is increased, then for the same loop amplitude, the area of the loop may decrease while the mean stiffness will increase. This effect of increased critical interface shear stress in relation to energy lost per cycle may also be illustrated by performing a calculation similar to that in Chapter 7. Figure 84 shows the effect of doubling the critical interface shear stress by comparison with the original calculation. Again, no great rigour is claimed for this argument but the qualitative effect is clear.

The rate sensitivity of the critical interface shear stress in the unbonded specimens could be one of the reasons for the range of stiffnesses at any one amplitude exhibited in the experimental results. Clearly there is an order of magnitude (of velocity) effect indicated by figures 82 and 83 but there may also be effects due to the changes in velocity for a given displacement within the frequency range of the experiment. This would be likely to be a small effect but could contribute to the spread of the results.

11.3 Comparison of etched specimen results with a bilinear hysteresis one degree of freedom system

Although it has already been observed in Chapter 7 that the bilinear hysteresis model is not a very good one for the etched specimens, it is still instructive to compare the experimental results with results from an analysis of the bilinear hysteresis one degree of freedom system. This type of system has received quite extensive treatment - see for example Iwan 1965 who shows that an exact solution to the problem is little different from an approximate analysis developed by Caughey 1960. Caughey's work is based on the

work of Kryloff and Bogoliuboff which is also known as the method of slowly varying parameters.

In spite of the fact that calculations based on the solution due to Caughey will yield slightly high resonant amplitudes at resonant frequencies which are too low (Iwan 1965), the comparison has been based on the Caughey analysis because in the limit, the Caughey and Iwan analyses make an identical prediction about the nature of the bilinear hysteresis one degree of freedom system response which is seriously at odds with the experimental observation.

Some criteria for a comparison are again required but in this instance due to the implicit nature of the relationships involved, it is not an entirely simple matter to satisfy even approximate criteria of equivalence. An attempt was made to match as closely as possible the 1N (rms) (nominal) driving force resonance curves for an etched specimen and a bilinear hysteretic system loaded by the same mass and excited by the same force. The stiffnesses of the legs of the bilinear hysteresis system were chosen so the same resonant amplitude was achieved at (almost) the same frequency as the experimental result. The implicit nature of the relationships makes it difficult to assess what effect changing the parameters will have so the result shown in figure 85 was actually achieved by trial and error.

Also shown in the figure are the results for the same systems at twice the original driving force. Obviously these results diverge very significantly. This divergence increases with increase in the excitation force and in fact, both the Iwan and Caughey analyses predict that at less than 4N (rms) driving force this particular bilinear

hysteretic system will go into an unbounded resonance. The experimental result for an excitation of 5N (rms) is also shown in figure 85 and this indicates that far from allowing an unbounded resonance to occur, the damping in the etched specimens continues to increase with the amplitude of vibration and to limit severely the resonant amplitudes for each increment of excitation.

11.4 Comparison with linear system

In spite of the fact that it is implicit in the foregoing that linear modelling of the system will be unsatisfactory, it is still relevant to establish in what respects the characteristics of the unbonded specimens differ from those of a linear system. Again, the comparison presented here is with a hysteretically damped linear system in which the same resonant amplitude at the same resonant frequency is used as the criterion of equivalence.

Since the unbonded specimens uniformly exhibit softening resonances in which the damping increases markedly with the excitation, if the specimens are modelled linearly at low excitations then the linear predictions for the higher excitations yield amplitudes which are much too large and at too high a frequency. If, conversely, the specimens are modelled linearly at higher excitations the predictions for the lower excitations are too low in amplitude at too low a frequency. This latter effect is shown in figures 86 and 87.

As for the bonded specimens, the reason for the nature of part of the difference between the linear system and the specimens is that the stiffness of the specimens falls with increase in amplitude of vibration. The decrease in stiffness is greater than for the bonded

specimens and is due more to the mechanics of the composite than the nature of the mechanical properties of the matrix. In contrast to the bonded specimens, the damping in the unbonded specimens increases greatly with amplitude - approximately to the power 3. This has, of course, the effect of curtailing the resonant peaks which can be difficult to discern at the higher excitations. The increase in damping coupled with the decline in stiffness as the amplitude increases causes a great increase in specific damping capacity as shown in figure 88. This figure has been drawn from the best line results.

CHAPTER TWELVE

12. Summary and Conclusions

In this concluding chapter, an attempt is made to place the work in its wider context before proceeding to the summary and conclusions.

12.1 The wider context

The basis of engineering analysis (and more importantly synthesis) usually incorporates a range of assumptions included among which is, that material properties are either known or predictable over the required range of operating conditions. For reasonably homogeneous metals such as steel, the determination of Young's modulus implies a capacity to carry out the very large range of engineering calculations for which this property is the only one required. It is particularly important and a great computational convenience that the Young's modulus of metals is broadly speaking rate insensitive so that predictions may be made about dynamic behaviour of structures from a single static determination of the material property.

It will already be clear that the properties of the composite materials under consideration are amplitude dependent and rate sensitive e.g. figures 82 and 83. It is, therefore, of more than usual importance to determine whether there are any simplifying assumptions which can be made to assist in the prediction of dynamic response from a static test. In this respect there seems to be more promise in the results from the bonded specimens than from the unbonded.

Although there are some stress history effects, it is fairly clear particularly in the case of the bonded specimens that the variation during the vibration tests is not sufficiently great for stress history to be considered a predominant influence. However, the existence of these effects in addition to the non-linearity in stiffness raises the question of how accurate it is possible to be in predicting the resonant frequencies and amplitudes. Since the stiffness of the bonded specimens seems to reduce to a limiting value, linear predictions for higher amplitudes will not be much in error. A greater difficulty arises with the smaller excitations which are, however, less important (figure 74).

In the case of the unbonded specimens, it was not intended that the study should involve any consideration of fatigue but it is likely to be an important aspect of any material which incorporates friction elements that there will be wear between the sliding surfaces which in this case will lead to loss of stiffness and possibly a greater tendency to fracture. The lower limiting frequency will depend upon the properties of the matrix. It is not clear what may happen to the damping after a very large number of cycles but it seems likely that the degradation of the material will lead to a long flat resonance curve at low frequency. If this is the case then caution must be exercised concerning the prediction of long term dynamic behaviour from relatively short term results.

Another problem concerning the prediction of dynamic behaviour is that of generality. There are variations between specimens of any one type even if the overall characteristics for the type are similar. However, statistically speaking the specimens under discussion do not contain very many fibres and it is quite possible

that the large number of fibres present in a more practical material would reduce the variation rather than increase it. A more significant limitation to generality in composite materials with a non-linear matrix is the importance of the initial loading or displacement in determining the average stiffness of the material. The quality and nature of the fibre surface treatment whether with the intent of obtaining bonds or not is also likely to be very important.

One of the important uses of engineering calculations is the prediction of the behaviour of a system when it is subjected to some loading other than those which have been tested experimentally. As has already been noted, it is most convenient if predictions can be made from the results of a static test. In the present case this is not really possible as is explained below.

It has already been reported in Chapter 10 that there seems to be some relationship between the static results and the results at 0.83 Hz for the bonded specimen - at least as far as the overall shape of the loops is concerned. It has also been seen that the stiffnesses calculated from the 0.83 Hz test and one degree of freedom system test are in broad agreement (figure 69). The question arises as to whether it is possible to make reasonable predictions concerning the one degree of freedom test results using information derived from a single static loop.

An attempt was made to estimate the stiffness from a static loop at various supposed vibration amplitudes using the mean load applied by the mass in the one degree of freedom test as the mean point. The result of this procedure is shown in figure 89. It is clear that any calculation based on these figures with say typical

damping figures from the 0.83 Hz test would yield resonance curves at frequencies near those found experimentally but of a different shape.

The discrepancy found between the static results and the 0.83 Hz or one degree of freedom system test results seems to be typical of rubbers. For example, the effect noted here is also described by Payne and Scott 1960 with reference to filled rubbers.

The same type of effect is also shown by the unbonded specimens although at least in part, for different reasons. It has already been noted that the rate of loading has an effect on the stiffness of the unbonded specimens because of the increase in the critical interface shear stress with rate of loading. It would therefore be expected that cycling at the higher rates would yield greater stiffnesses than a static test. The difference in this case is so great (factor of two) that it is not possible to make useful predictions. Even the 0.83 Hz tests would not provide a very good estimate of the vibration test results because the stiffness is too low and the damping too high (figures 82 and 83). Where possible it is usually considered desirable to formulate an analytical interpretation of experimental results. If this can be derived from the fundamental parameters in an experiment then a substantial advance may be made. In the present case this is not readily possible because, for example, the relationship between the behaviour of the interface and the overall properties of the specimens when the amplitude of oscillation is changed is not sufficiently well understood.

In vibration studies, the analytical treatment of non-

linearity is frequently confined to the relatively simple cases such as the cubic non-linearity in restoring force of Duffing's equation. In these cases, the spring stiffness is assumed to depend on the instantaneous value of displacement which is an inadequate description for the composite specimens. The composite material properties must be defined in terms of the amplitude of displacement rather than the instantaneous value. This also seems to be a common feature of filled rubbers (Gehman 1957).

Gehman also states that, "However, at any one amplitude, under conditions such as shear for which the stress-strain curve is linear, the response to a sinusoidal driving force is sinusoidal without any evidence of harmonic content such as would be expected if non-linearity is present. The non-linearity only becomes evident when the amplitude is changed. It causes distortion of the resonance curve." Although the first of these statements is rather too sweeping in the context of the present work, these observations are broadly speaking supported by the evidence from the silicone rubber composites used whether with bonded or unbonded interfaces.

It would appear to be the case that when a material has properties which are dependent upon the amplitude of oscillation, at least under the conditions of the one degree of freedom system test, there will be no significant distortion of a sinusoidal input. Unlike the case of the cubic restoring force spring, it seems to be possible for a resonance curve from the one degree of freedom system test to be comprised of points each of which could be supposed to derive from a different linear system. The relationship between one point and another on the resonance curve is not readily predictable in other than the empirical sense. This is particularly so for the

unbonded composites since the relationship depends on detailed changes in interfacial behaviour. It seems possible that the small distortion evident in the results will increase with amplitude. However, to allow the use of larger amplitudes a larger mass would be required which would in turn reduce the resonant frequency and thus create other experimental difficulties. It is not readily possible to state under what conditions it remains plausible to treat these non-linear results in a quasi-linear fashion. This point will be considered further later.

The treatment of the experimental results has shown that synthesis of resonance curves is possible using a graphical method. The same effect may be achieved by means of an empirical method in which it is necessary to describe the results by polynomials and calculate the frequencies at which particular amplitudes occur for a given excitation. Stiffness, $k(X_0)$, and damping, $h(X_0)$, are taken to be functions of X_0, the amplitude of vibration. The equation of motion approximately describing the system is

$$m\ddot{x} + [k(X_0) + i\,h(X_0)]x = F e^{i\omega t} \qquad 12.1$$

Equation 12.1 is presumed (nearly enough) to have the solution $x = X_0 e^{i\omega t}$ which on substitution and after appropriate manipulation gives

$$\omega^2 = \frac{k(X_0)}{m} \pm \sqrt{\left(\frac{F}{X_0}\right)^2 - h^2(X_0)} \qquad 12.2$$

Resonance occurs when

$$F = h(X_0)\,X_0 \qquad 12.3$$

and the resonant frequency f_r is given by

$$f_r = \frac{1}{2\pi}\sqrt{\frac{k(X_0)}{m}} \qquad 12.4$$

in which $k(X_o)$ has been evaluated for the maximum value of X_o found from equation 12.3.

There are no particular advantages in this formulation compared with the graphical presentation used in the preceding chapters. The resonant amplitude and frequency may be obtained fairly rapidly for a given input. However, this is only possible once appropriate and sufficiently accurate polynomials have been fitted to the results. The calculation of even a single resonance curve involves considerable computational effort which depends on the powers of the polynomials used.

Non-linearity in vibration is often associated with jump phenomena. This is not surprising when, for example, the rapid changes in mean restoring force implied by a cubic variation with amplitude are considered. The range of instability of such systems is much reduced by increasing damping which has the effect of raising the level of excitation required for the onset of instability. The only non-linear jump phenomena noted in the present work occurred when an overall compression was applied to a specimen in the one degree of freedom test. This resulted in a lateral instability of the specimen due to the very low flexural stiffness of the composites.

It is interesting to note, however, the possible implications of predicting the response of a system which has not been tested experimentally. If the specific damping capacity reduces with amplitude as is the case here for the bonded specimens, then it does not require much additional non-linearity in stiffness for the force curves of constant displacement amplitude (figure 71) to coalesce - as indeed they do in Cooper 1959. This implies the existence of a jump phenomenon. There is a wide variety of combinations of stiff-

ness and damping for which this might happen. The question arises (although it is not intended to pursue it here) as to whether this would be a valid prediction. It may be the case that a system in which a jump almost occurs is the limiting case which may be treated in the quasi-linear fashion.

All the tests were intentionally conducted at fairly low frequencies which most readily allow higher displacement amplitudes at limited values of acceleration. This has been more than justified by the primary dependency on the amplitude of vibration of the properties of the composites tested. It is important, however, to consider the effects likely to be found in practical materials. One of the greatest differences is that a practical material would require to be very much stiffer than those used in the experiments. An estimate of the ratio of the Young's modulus of the composite to the Young's modulus of the matrix is found from equation 6.2 as

$$\frac{E_c}{E_m} = \frac{1}{6}\frac{\ell^2}{(h'+h'')^2}\frac{1}{\log_e V_f^{-\frac{1}{2}}} \qquad 12.5$$

(assuming $E_m = 3G_m$). The factors which increase this ratio are increasing the length of the fibres, ℓ, reducing the fibre centre to centre spacing, $(h' + h'')$ or increasing the volume fraction of fibres, V_f (although these last two are not completely independent). Clearly it should be possible to obtain a bonded fibre composite material with a practical Young's modulus by suitable selection of the properties and disposition of its components - the limiting factor being the shear strength of the interface or of the matrix itself. It may be reiterated here that the shear properties of the matrix and matrix/fibre interface are almost certain to be the dominant factors in these composites.

The interrelation between stiffness and damping in a discontinuous fibre composite is rather complex. Some of the more important aspects for both bonded and unbonded types are discussed below. In the case of the bonded type, assuming that the stress levels are such that problems of interface or matrix failure (or for that matter fibre failure) may be ignored, increasing the volume fraction of fibres has the effect of producing a stiffer composite because the shear strain amplification is increased. For the same cycle of stress, the overall strains produced will be reduced and the shear strain energy of the composite (essentially the matrix) will fall. In the simplest case in which the specific damping capacity of the matrix is assumed constant with shear strain, and that of the fibres negligible, the specific damping capacity per unit volume of matrix will not change but the specific damping capacity of the composite will be reduced because there is now less matrix per unit volume. It may seem in this respect that something has been lost rather than gained by the introduction of additional reinforcement to the matrix but the important comparison to be made is not so much with other combinations of the same matrix and fibres but with alternative materials having the same stiffness.

It should be possible in a practical case in which the relevant parameters are known to optimise the amount of damping and stiffness for a particular application. It is most unlikely that a practical material would have the regular layout of the Mileiko model so such calculations would be rather speculative until some experimental experience has been gained with a more practical material. If an unbonded discontinuous fibre composite material of high volume fraction is considered, the extended Cox theory (Chapter 6) would

predict that sliding would occur at very low strains because of the great shear strain amplification rapidly creating the required critical interface shear stress. It should be noted, however, that predictions for high volume fraction composites derived from Cox's theory must be treated with caution since the theory was originally developed for an isolated fibre. The close proximity of the fibres in practical composites is likely to have a significant influence on the local stress distribution.

In the static experiments it has been seen that when an increasing strain was imposed on the etched unbonded composites, significant yielding occurred (figure 16). Ultimate fracture of the unbonded composites always occurred at a cross-section containing the fibre centres and ends because the matrix which was at high strain could no longer sustain the increasing direct load upon it. In the experimental case, the critical shear stress at the interface was very low because very little if any lateral shrinkage on curing of the matrix took place. If, however, the matrix shrank on to the fibres creating a high critical interface shear stress, sliding at the interface might precipitate immediate fracture of the composite through tensile failure of the matrix. Against this it may be said that it would be unlikely for a practical material to have the completely regular layout of the model which seems to contribute to this type of failure.

It may be emphasised again that in general the damping provided by the matrix and sliding at the interface are competing sources. If interface sliding occurs then this precludes any significant increase in the matrix shear strain and occasions a loss in stiffness relative to the bonded case. The full utilisation of interfacial slip as a source of damping probably demands relatively

high amplitudes and an application in which loss of stiffness does not have serious consequences. Shock absorption may be the most likely application of this type of material. Application for the bonded composites might be found in the construction of sound deadening panels for use in the audio frequency range in which amplitudes (despite shear strain amplification)are likely to be low For the best use of the bonded composites, a matrix with damping properties which increase rapidly with shear or deformation rate seems desirable.

12.2 Summary

After introducing the subject (Chapter 1), there is a general review of some of the theory (Chapter 2) which forms the background to later chapters of the study. The development of the uni-directional discontinuous fibre composite material models on which the experiments were conducted is described in Chapter 3. A model material was chosen because working with continuous glass fibres was not found to be easy and it was thought that control of the disposition of discontinuous reinforcement would have been extremely difficult. The specimens were accordingly manufactured from stub steel rod and a proprietary silicone rubber since the phase geometry could be readily controlled although volume fractions were low. It proved exceedingly difficult to grip these specimens because of the softness of the matrix material so an epoxy resin adhesive was eventually used for the gripping area. Some of the specimens had bonded fibre/matrix interfaces while others were not bonded and some of the unbonded specimens had etched fibres while others did not.

Unbonded fibre pull-out specimens were also made and tested

(Chapter 4). The diameter of the cylinder of matrix from which the fibre was pulled did not seem to make much difference to the results and the pull-out tests were most valuable for pointing up qualitatively the different nature of the interface due to etched and unetched fibre surfaces.

The composite specimens of Chapter 3 were tested at low strain rates using a typical tensile test procedure (Chapter 5). The bonded specimens exhibited non-linear properties which reflected those of the matrix (figure 34) while the unbonded specimens exhibited yielding behaviour due to interfacial sliding - the etched specimens also showing a large load drop on initial loading beyond yield (figure 16). On unloading the unetched specimens tended to show a permanent set while the etched specimens exhibited the unusual characteristic for a system containing friction of returning to the zero load and displacement point when the load was removed (figure 17).

The phenomena related to these tests are discussed in considerable detail in Chapter 6 and a possible explanation for the behaviour, developed as an extension of current theory, is presented. Particular attention was paid to the distribution of shear stress at the interface and direct stress in the fibre (figures 26 - 30).

The specimens were also tested using imposed slow (0.83 Hz) sinusoidal displacement cycles (Chapter 7). The tests demonstrated that at these low strain rates, the bonded composite stiffness decreased with increase in displacement amplitude while the energy lost per cycle increased at less than the linear (power 2) rate. In the unbonded composites, the stiffness also declined with increase in amplitude but the damping increased with amplitude approximately

to the power 3 and was thus shown to be at variance with simple theoretical predictions for the unbonded case.

Some typical linear measures of damping and a wide variety of methods of measuring damping are reviewed in Chapter 8. Chapter 9 is concerned with the particular difficulties involved in testing for the mechanical properties of the discontinuous fibre composites. The one degree of freedom system chosen to perform these tests is described and some sample results given. The bonded specimen results are considered in greater detail in Chapter 10 and seen to be similar to the results of Chapter 7. In Chapter 11 the results from the vibration tests for the unbonded specimens are presented and seen to differ from the results in Chapter 7 due to a rate effect.

12.3 Conclusions

There is a fairly large number of conclusions which may be drawn. These will be dealt with broadly speaking in the order in which they have arisen in the text.

The first conclusions arrived at concerned the manufacture of discontinuous fibre composite materials. As was indicated in Chapter 3, great difficulty was experienced in working with continuous carbon or glass fibres which led to the use of the model material for the experimental programme. Although no local expertise in the manufacture of discontinuous fibre composites was available and although it is recognised that various types of discontinuous fibre composites are manufactured commercially, it seems likely that it will not be a simple task to manufacture a genuinely fibrous composite material with the geometry desirable for utilising shear strain

amplification to its maximum advantage. It should still be possible to manufacture a material in which there is significant shear strain amplification. In any case as was noted previously the optimisation of the shear strain amplification may be undesirable through the increased possibility of fracture.

If a discontinuous fibre composite material is to be used structurally, then it is even more important to obtain adequate bonding at the interface than in continuous fibre composites where the matrix is principally a binding rather than load carrying agent. Should a uni-directional discontinuous fibre reinforced composite prove inadequate structurally (where joining will also be a problem) it would still be worthwhile to consider the material in the role of a surface treatment.

Pull-out tests, it has already been noted, did not provide very much useful quantitive information. The important qualitative difference between the etched and unetched interfaces which aided in the interpretation of the static composite test results was, however, well illustrated by these tests.

One of the most important conclusions from the static tests is the great influence exercised by the fibre treatment on specimens which were otherwise identical. Yield behaviour (both initial and secondary), breakaway on subsequent loading, and reverse breakaway on unloading were all affected to a large extent by the fibre surface being etched or unetched.

The results of the experiments on the unbonded discontinuous fibre composites were not readily predictable - in particular the initial behaviour of the etched specimens which returned to the zero

load and displacement position even after gross interfacial sliding had occurred. It was, however, possible to offer some explanation of the observed behaviour through an extension of the theory of Cox 1952 for an isolated fibre. Use of a model based on the work of Mileiko 1970 with elastic parameters was less successful in interpreting the behaviour of the unbonded composites. It may be mentioned in passing that the objection to Mileiko's model, raised by McLean 1972, that holes will open up in the matrix seems invalid since pulling a sample of a bonded discontinuous fibre lamina in the longitudinal fibre direction showed that the matrix readily broke away from the fibre ends (forming holes). It may also be noted here that fracture always occurred in the unbonded specimens at the cross-section containing the fibre centres and ends.

Both Cox and Mileiko models gave reasonable, if slightly low, predictions of composite modulus for the bonded specimens. A more rigorous examination of the plausibility of these theories would be provided by testing a discontinuous fibre composite in which the matrix was linear elastic.

The static tests also yielded the conclusion that stress history was important since the unetched specimens, exhibited a permanent set. It may be noted here that, in this instance, permanent set is something of a relative term since it was possible to restore the specimens to their original length by hand. It was not possible to do this by machine because of the low buckling loads for these specimens and, of course, it was not possible to tell what residual stresses might be left once the operation had been performed.

The results in Chapter 7 indicated that the difference between

the etched and unetched specimens was not a passing phenomenon although it was noted that once the etched specimens had been subjected to an oscillatory type of test they also showed permanent set on unloading during a subsequent static test. There is also for both types of unbonded specimen a clear rate effect which caused hysteresis loops at 0.83 Hz to show greater stiffness than those from static tests. The bonded specimens showed much less rate sensitivity but the oscillatory nature of the loading had an important influence at small amplitudes.

Under imposed sinusoidal displacement conditions, both bonded and unbonded specimens exhibited changes in the mean load. In the case of the unbonded specimens this was due to internal changes in equilibrium allowed by sliding while in the case of the bonded specimens it was due to non-linearity of the matrix.

It has been shown that the materials tested were not readily modelled by linear elements and that the simplest prediction of frictional energy lost per cycle (McLean and Read 1975 and McMeeking 1972) was inaccurate. An estimate using the simple theory of Chapter 6 gave a remarkably good prediction.

The accurate measurement of the damping properties of materials is extremely difficult. In this instance the production of useful results depended entirely upon the fact that the damping in the specimens under test was quite high. The low incidence of harmonics in the results led to the conclusion that quasi-linear analysis of the mechanical impedance results obtained was reasonable.

The results from the one degree of freedom system test added to the evidence that the bonded specimens were relatively rate insensitive. It was concluded that the stiffness results from the

one degree of freedom test and the damping results from the 0.83 Hz test gave the best representation of the properties of the bonded specimens. It was possible to synthesise resonance curves by a procedure which is essentially an inversion of the analysis of the results.

The unbonded specimens showed further evidence of rate effects in the one degree of freedom system test results such that the stiffness was greater and the damping less than in the 0.83 Hz test. It was concluded that the extraneous damping was not sufficiently great that it masked the real nature of the resonance curves. The unbonded specimens were no easier to model as part of the one degree of freedom system than they had been in the 0.83 Hz test. It was concluded that this was because the behaviour of the specimens was to an important extent dependent upon detailed changes at the matrix/fibre interface. Again with these specimens empirical construction of resonance curves was possible. It may be concluded finally that the discontinuous reinforcement of a matrix material such that shear strain in the matrix is amplified can be an important source of damping and stiffening. If there is little or no bonding at the matrix/fibre interface then the specific damping capacity developed by the composite can be very large indeed but will be partly due to loss of stiffness. The basic lack of integrity inherent in an unbonded discontinuous fibre composite is sufficiently unattractive (both theoretically and practically) that it would seem best that a material developed for its damping/sound deadening properties should have a matrix which bonds well to the fibres and which has a dissipative capacity increasing greatly with increase in shear strain and/or rate of deformation.

REFERENCES

Adams and Percival 1969 — Measurement of strain dependent damping of metals in axial vibration. J. Phys. D; Appl. Phys. 2 (1969) p 1693

Adams et al 1969 — The dynamic properties of unidirectional carbon and glass fibre reinforced plastics in torsion and flexure. J. Comp. Mater. 3 (1969) p 594

Adams 1972 — The damping characteristics of certain steels, castirons and other metals. J. Sound. Vib. 23(2) (1972) p199.

Adams and Fox 1972 — Measurement of the damping capacity and dynamic modulus of high damping metals under direct cyclic stress. J. Phys. D; Appl. Phys. 7 (1972) p 1274.

Adams and Bacon 1973a — Measurement of the flexural damping capacity and dynamic Young's modulus of metals and reinforced plastics. J. Phys. D: Appl. Phys. 6 (1973) p27.

Adams and Bacon 1973b — The dynamic properties of unidirectional fibre reinforced composites in flexure and torsion. J. Comp. Mater. 7 (1973) p53.

Adams and Short 1973 — The effect of fibre diameter on the dynamic properties of glass fibre reinforced polyester resin. J. Phys. ^ 6 (1973) p1032. D: Appl. Phys.

Adams et al 1973 — Effects of shear damage on the torsional behaviour of carbon fibre reinforced plastics. J. Comp. Mater. 7 (1973) p68.

Bert 1973 — Material damping: an introductory review of mathematical models, measures and experimental techniques. J. Sound Vib. 29(2) (1973) p129.

Bishop 1955 — The treatment of damping forces in vibration theory. J. Roy. Aero. Soc. 59 (1955) p738.

Canfield 1928 — Internal friction in metals. Phys. Rev. 32, 2nd series (1928) p520.

Caughey 1960 — Sinusoidal excitation of a system with bilinear hysteresis. J. Appl. Mech. 27 (1960) p640.

Cochardt 1954 — Some new magneto mechanical torsion experiments. J. Appl. Phys. 25 (1954) p670.

Cochardt 1955 — Effect of static stress on the damping of some engineering alloys. Trans. ASM 47 (1955) p440.

Contractor and Thompson 1940 — The damping capacity of steel and its measurement. J.I.S.I. 141 (1940) p157.

Cooper 1959 — Method of applying the results of dynamic testing to rubber anti-vibration systems. Trans. Inst. Rubber Ind. 35 (1959) p166.

Cottell, Entwhistle, and Thomspon 1948 — The measurement of the damping capacity of metals in torsional vibration. J. Inst. Metals 74 (1948) p373.

Cox 1952 — The elasticity and strength of paper and other fibrous materials. Brit. J. Appl. Phys. 3 (1952) p72.

Dorey 1932 — Elastic hysteresis in crankshaft steels. Proc. I. Mech. E. 123 (1932) p479.

Dudek 1970 — Young's and shear moduli of unidirectional composites by a resonant beam method. J. Comp. Mater. 4 (1970) p232.

Durelli and Riley 1965 — Introduction to Photo-mechanics. Prentice Hall Inc. 1965 p68.

Entwhistle 1962 — The internal friction of metals. Metallurgical Rev. 7 (1962) p175.

Ferry 1970 — The Viscoelastic Properties of Polymers. 2nd ed. John Wiley and Son 1970.

Föppl 1936 — The practical importance of the damping capacity of metals especially steels. J.I.S.I. 134 (1936) p393

Förster and Köster 1939 — Modulus of elasticity and damping in relation to the state of the material. J.I.E.E. 84 (1939) p558.

Frommer and Murray 1944 — Damping capacity at low stresses in light alloys and carbon steel with some examples of N.D.T. J. Inst. Metals 70 (1944) pl.

Gehman 1957 — Dynamic properties of elastomers. Rubber Chem. and Tech. XXX (1957) p1202.

Gemant 1940 — The measurement of solid friction of plastics. J. Appl. Phys. 11 (1940) p647.

Hagel and Clark 1957 — The specific damping energy of fixed-fixed beam specimens. J. Appl. Mech. 24 (1957) p 426.

Hanstock and Murray 1946 — Damping capacity and the fatigue of metals. J. Inst. Metals 72 (1946) p97.

Hashin 1970 — Complex moduli of visco-elastic composites - II fibre reinforced materials. Int. J. Solids Structures 6 (1970) p797.

Hatfield, Stanfield and Rotherham 1942 — The damping capacity of engineering materials. Trans. N.E. Coast Inst. Eng. Shipbuilders 58 (1942) p273.

Hatfield, Rotherham and Harvey 1944 — Further experiments on the damping capacity of engineering materials. Trans. N.E. Coast Inst. Eng. Shipbuilders 60 (1944) p227.

Hixson 1961 — Mechanical impedance and mobility. Chapter 10 of Harris and Crede, Shock and Vibration Handbook Vol. 1 McGraw Hill 1961.

Holister and Thomas 1966 — Fibre Reinforced Materials Elsevier 1966 p14.

Hopkinson 1911 — A high speed fatigue tester and the endurance of metals under alternating stress of high frequency. Proc. Roy. Soc. A86 (1911-12) p131.

Hopkinson and Williams 1912 — The elastic hysteresis of steel. Proc. Roy. Soc. A87 (1912) p502.

ICI 1972 — ICI Silicones. 6th ed. August 1972.

Iwan 1965 — The dynamic response of the one degree of freedom bilinear hysteretic system. Proc. 3rd World Conf. on Earthquake Engineering 1965 Vol. II p783.

Jacobsen 1930 — Steady forced vibration as influenced by damping. Trans. ASME 52 (1930) p169.

Jones 1975 — Mechanics of Composite Materials. McGraw Hill 1975 p134.

Kelly 1966 — Strong Solids. OUP 1966 p125.

Kimball and Lovell 1926 — Internal friction in solids. Trans. ASME 48 (1926) p479.

Lazan 1943 — Some mechanical properties of plastics and metals under sustained vibrations. Trans ASME 65 (1943) p87.

Lazan and Wu 1951 — Damping, fatigue and dynamic stress-strain properties of mild steel. Proc. ASTM 51 (1951) p649.

Mason 1923 — The mechanics of the Wöhler rotating bar fatigue test. Engineering 115(1) (1923) p698.

McConnell 1969 — A proposed experimental method for accurate measurement of the dynamic properties of visco-elastic materials. Shock and Vibration Bulletin 39 part 4 (1969) p11.

McLean 1972 — Viscous flow of aligned composites. J. Mater. Sci 7 (1972) p98.

McLean and Read 1975 — Storage and loss moduli in discontinuous composites. J. Mater. Sci. 10 (1975) p481.

McMeeking 1972 — Damping of Fibrous Composite Materials.University of Glasgow Department of Mechanical Engineering Honours Project Report 1972.

Mileiko 1970 — Steady state creep of a fibrous composite. J. Mater. Sci. 5 (1970) p254.

Myklestad 1956 — Fundamentals of Vibration Analysis. McGraw Hill 1956 p75.

Norris and Young 1970 — Complex modulus measurement by longitudinal vibration testing. Experimental Mechanics 10 (1970) p93.

Ockleston 1938 — The damping of the lateral vibration of a mild steel bar. Phil. Mag. 26, 7th series (1938) p 705.

Outwater 1956 — The mechanics of plastics reinforcement in tension, 22 (1956) p158. Modern Plastics.

Payne and Scott 1960 — Engineering Design with Rubber. MacLaren and Sons Ltd. London 1960 p18.

Person and Lazan 1956 — The effect of static mean stress on the damping properties of materials. Proc. ASTM 56 (1956) p1399.

Plunkett 1959 — Measurement of damping. Section 5 of Structural Damping (ed. J.E. Ruzicka) ASME 1959.

Robertson and Yorgiadis 1946 — Internal friction in engineering materials. J. Appl. Mech. 13 (1946) pA173.

Rosen 1965 — Mechanics of composite strengthening. Chapter 3 of Fibre Composite Materials ASM 1965.

Rowett 1913 — Elastic hysteresis in steel. Proc. Roy. Soc. A89 (1913-14) p528.

Scanlan and Mendelson 1963 — Structural damping. J. AIAA 1 (1963) p938.

Schabtach and Fehr 1944 — Measurement of the damping of engineering materials during flexural vibration at elevated temperatures. J. Appl. Mech. 11 (1944) pA86.

Schultz and Tsai 1968 — Dynamic moduli and damping ratios in fibre-reinforced composites. J. Comp. Mater. 2 (1968) p368.

Schultz and Tsai 1969 — Measurements of complex dynamic moduli for laminated fibre-reinforced composites J. Comp. Mater. 3 (1969) p434.

Sperry 1964 — Rheological - model concept. J. ASA 36(1) 1964 p.376.

Sumner and Entwhistle 1958 — The measurement of the strain-dependent damping of metals vibrating torsionally. Brit. J. Appl. Phys. 9 (1958) p434.

Timoshenko and Gere 1961 — Theory of Elastic Stability. 2nd ed. McGraw Hill 1961 p24.

Timoshenko et al 1974 — Vibration Problems in Engineering. 4th ed. John Wiley and Sons 1974 p387.

von Heydekampf 1931 — Damping capacity of materials. Proc. ASTM 31 (1931) p157.

Wright 1972 — The dynamic properties of glass and carbon fibre reinforced plastic beams. J. Sound Vib. 21 (2) (1972) p205.

Zener 1948 — Elasticity and Anelasticity. University of Chicago Press 1948.

FIG. 1

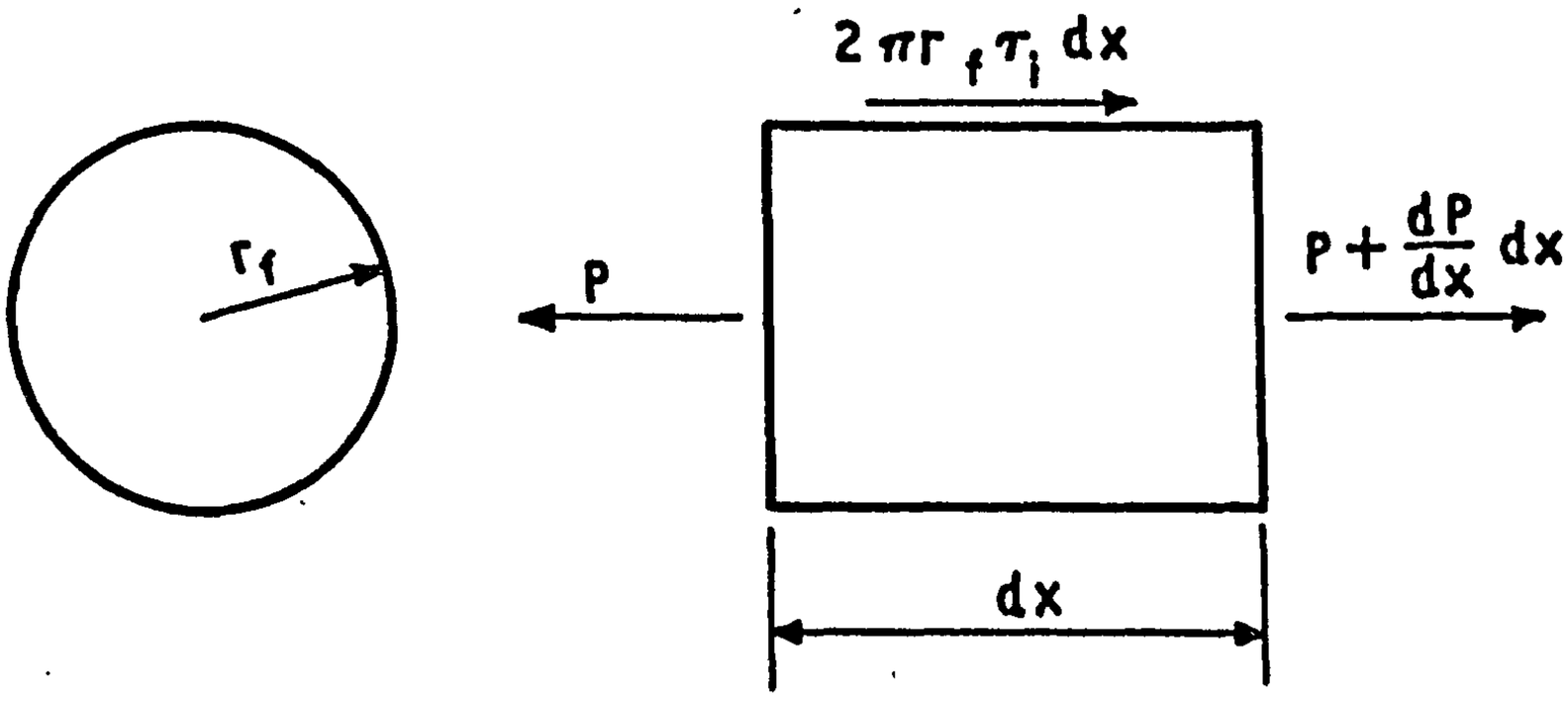

WHENCE $\frac{dP}{dx} = -2\pi r_f \tau_i$

COX'S MODEL

LOAD TRANSFER

FIG. 2

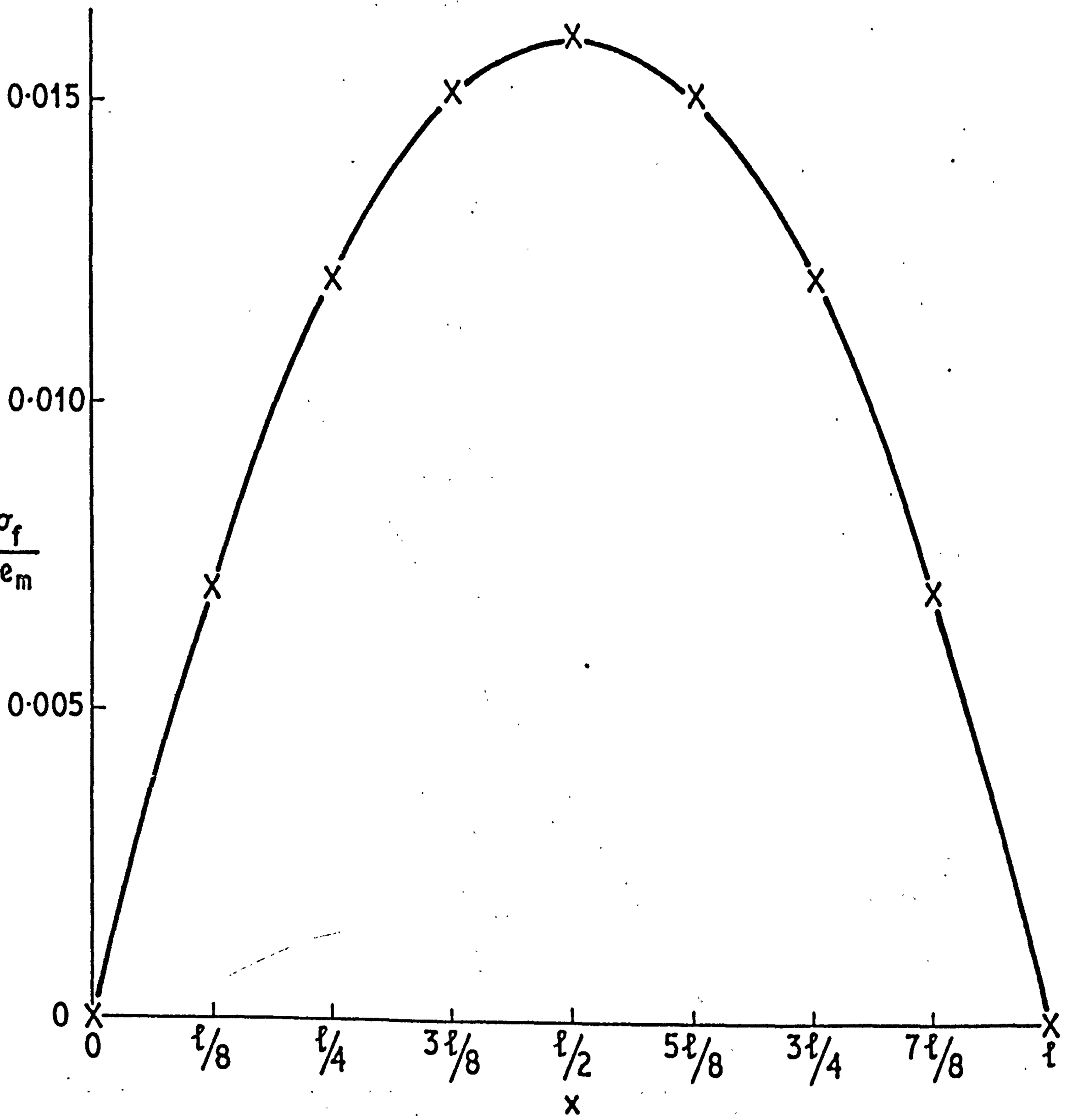

COX THEORY :
NON-DIMENSIONAL FIBRE STRESS
AGAINST DISTANCE ALONG FIBRE

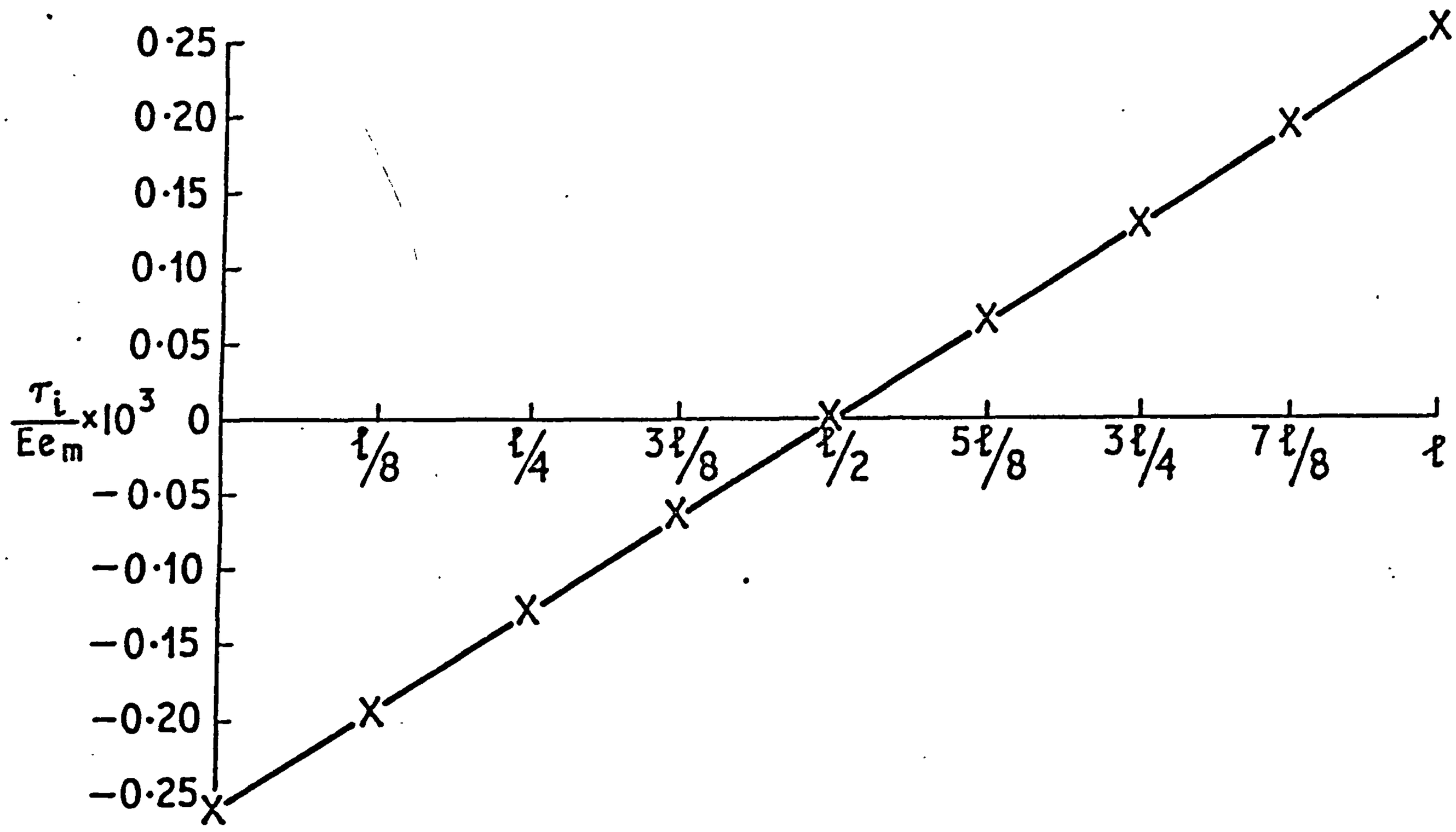

FIG. 3

COX THEORY :
NON-DIMENSIONAL INTERFACE SHEAR STRESS
AGAINST DISTANCE ALONG FIBRE

FIG. 4

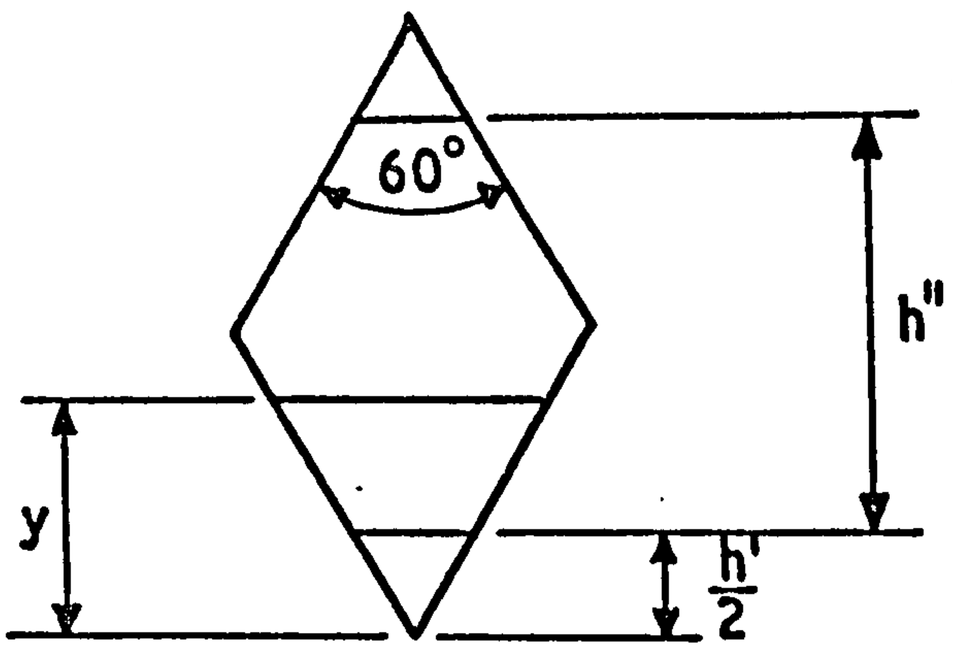

SECTION THROUGH SHEAR CELL
FOR HEXAGONAL FIBRES IN
HEXAGONAL DISTRIBUTION

LONGITUDINAL SECTION THROUGH COMPOSITE
IN UNSTRAINED CONDITION

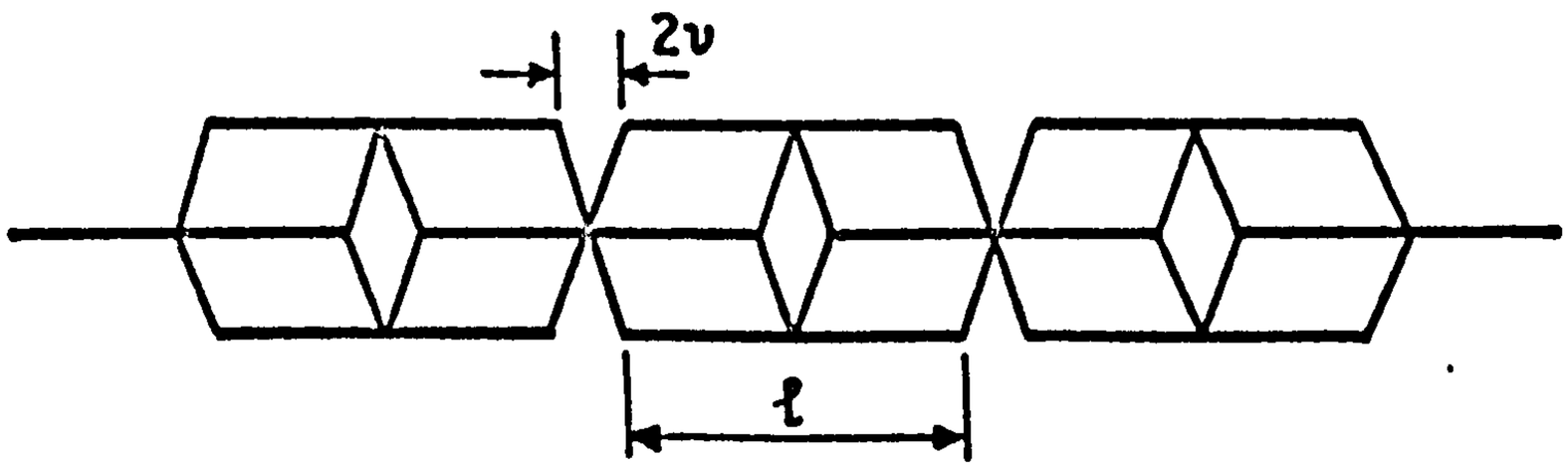

LONGITUDINAL SECTION IN STRAINED CONDITION
STRAIN $e = \frac{2v}{l}$

MILEIKO MODEL ELEMENT

FIG. 5

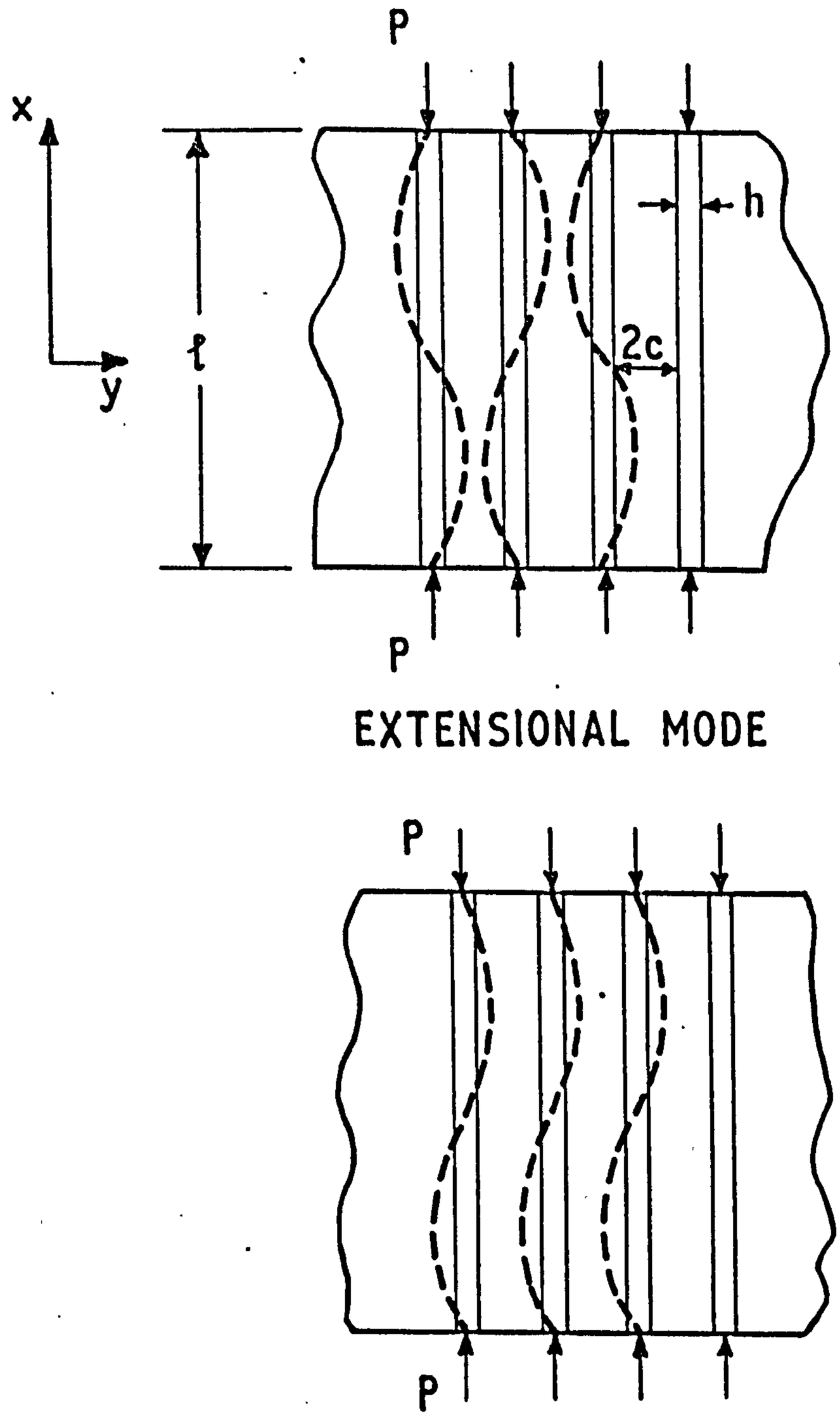

BUCKLING MODES IN COMPRESSION
(AFTER ROSEN)

FIG. 6

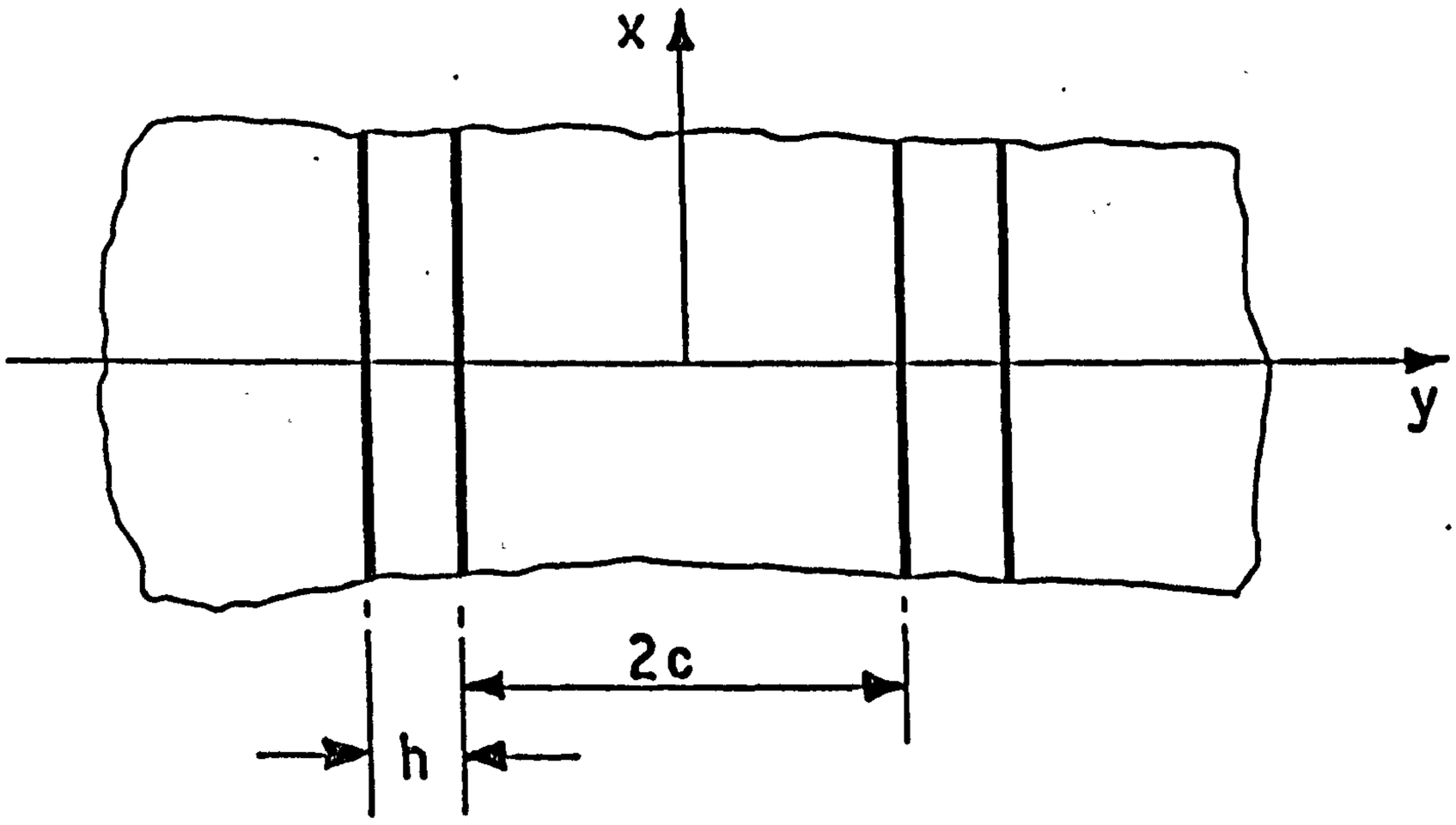

BEFORE BUCKLING

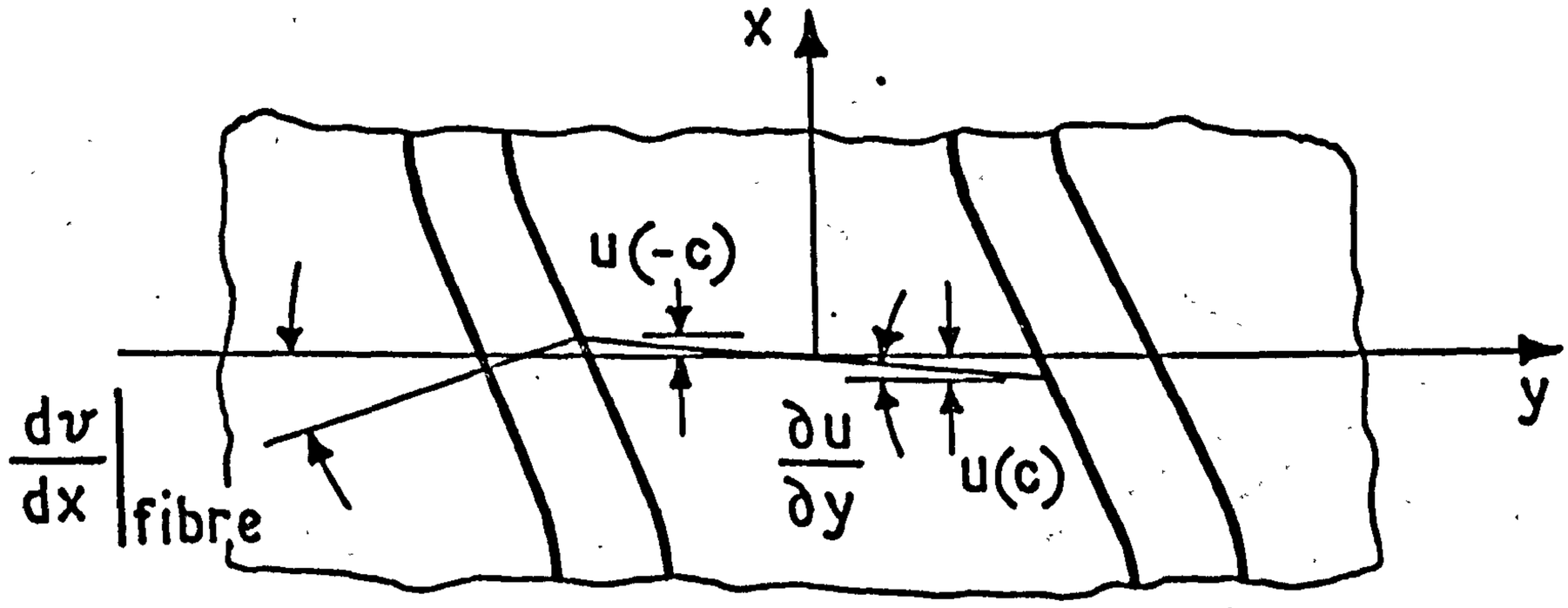

AFTER BUCKLING

FIBRE DEFORMATION IN SHEAR BUCKLING MODE
(AFTER JONES)

FIG. 7

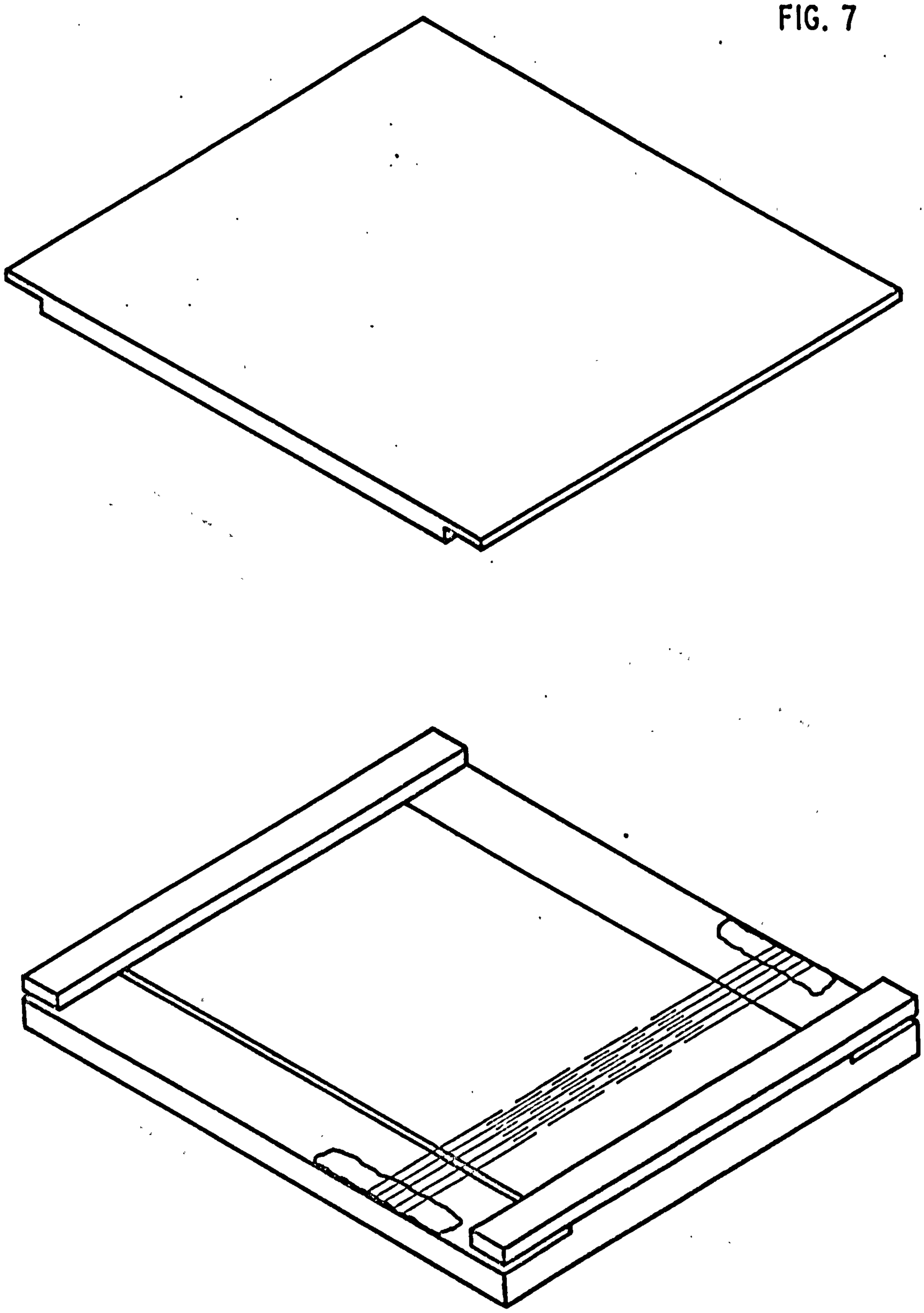

MOULD USED FOR PREPARING STEEL /'SILCOSET' LAMINAE

SHOWING AN EXAMPLE OF A STEEL FIBRE ARRAY

SCALE 1 : 2 MATERIAL : STEEL

FIG. 8

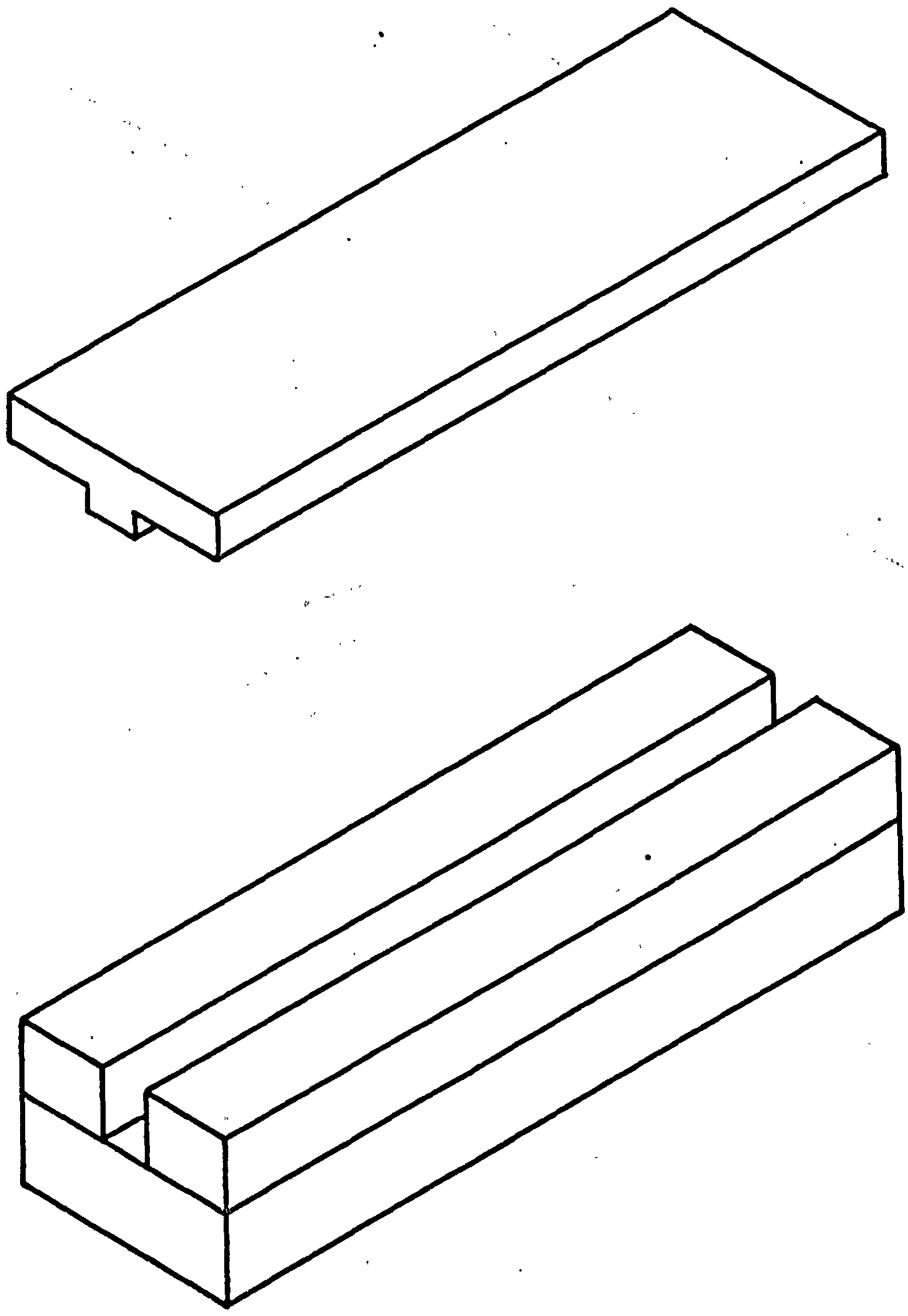

MOULD USED FOR PREPARING STEEL / 'SILCOSET' SPECIMENS

SCALE : FULL SIZE MATERIAL : PERSPEX

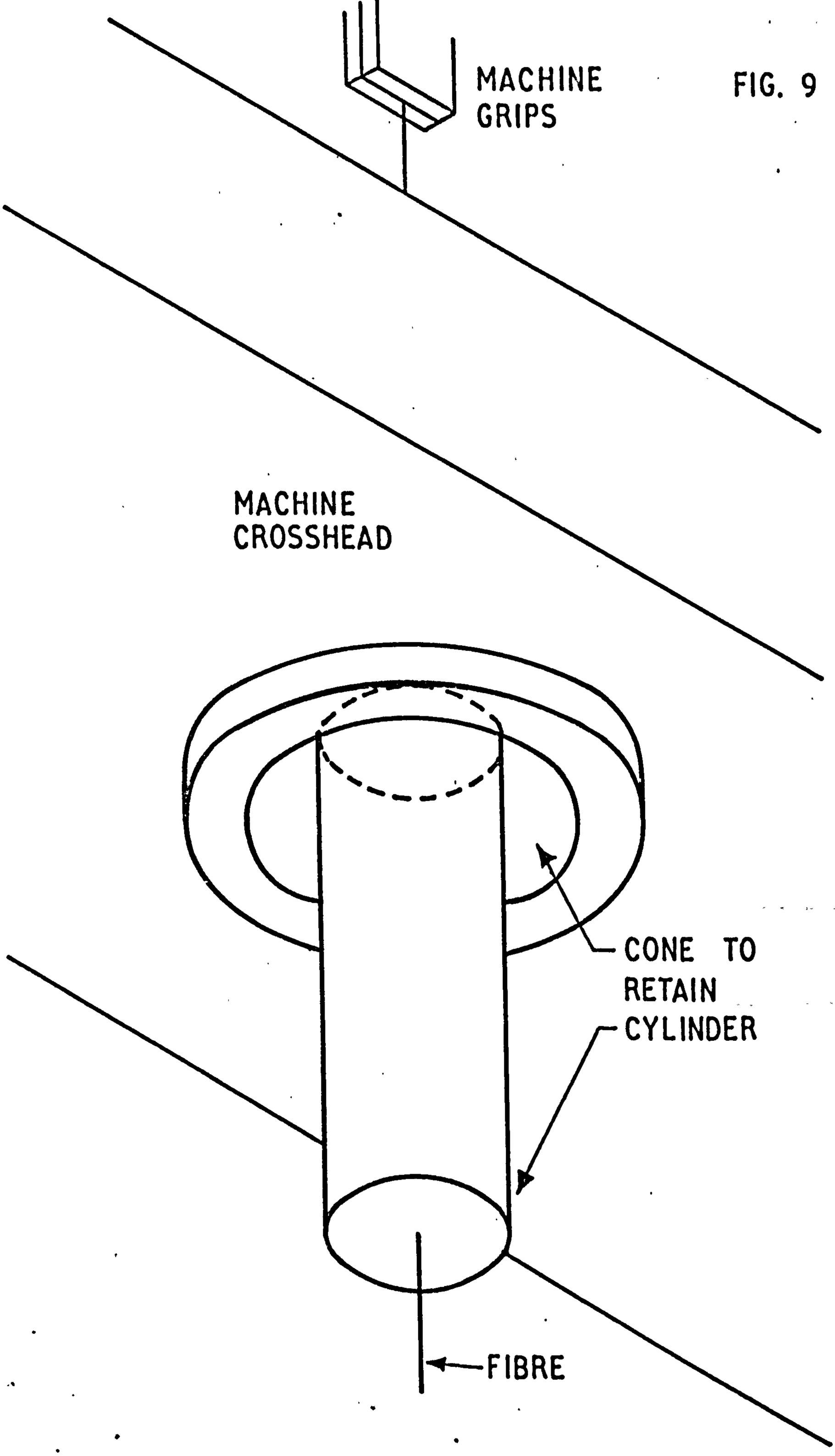

FIG. 9

PULL-OUT TEST ARRANGEMENT

NOT TO SCALE

FIG. 10

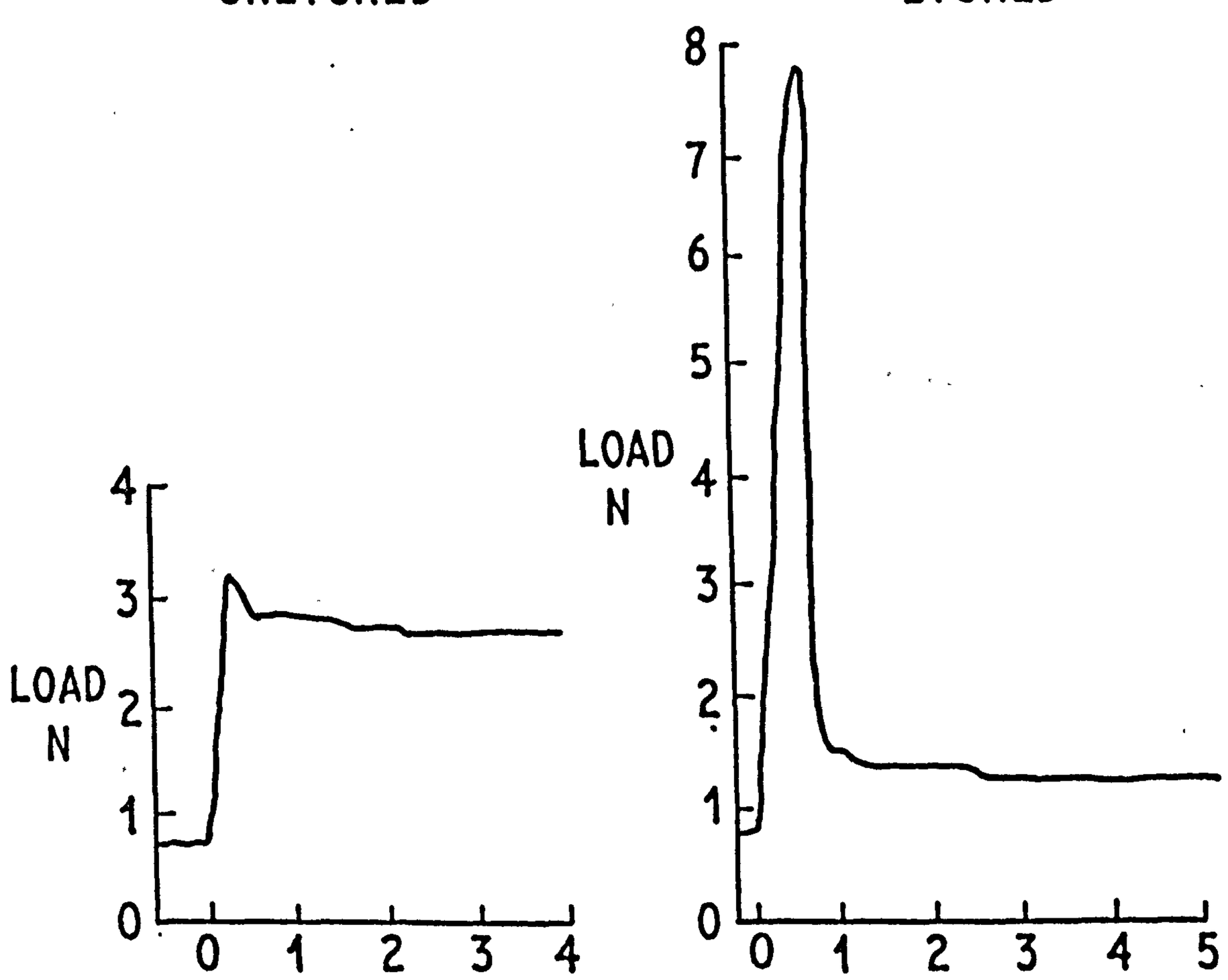

UNETCHED AND ETCHED SPECIMEN
PULL-OUT TEST RESULTS OF
OBVIOUSLY DIFFERENT CHARACTER

FIG. 11

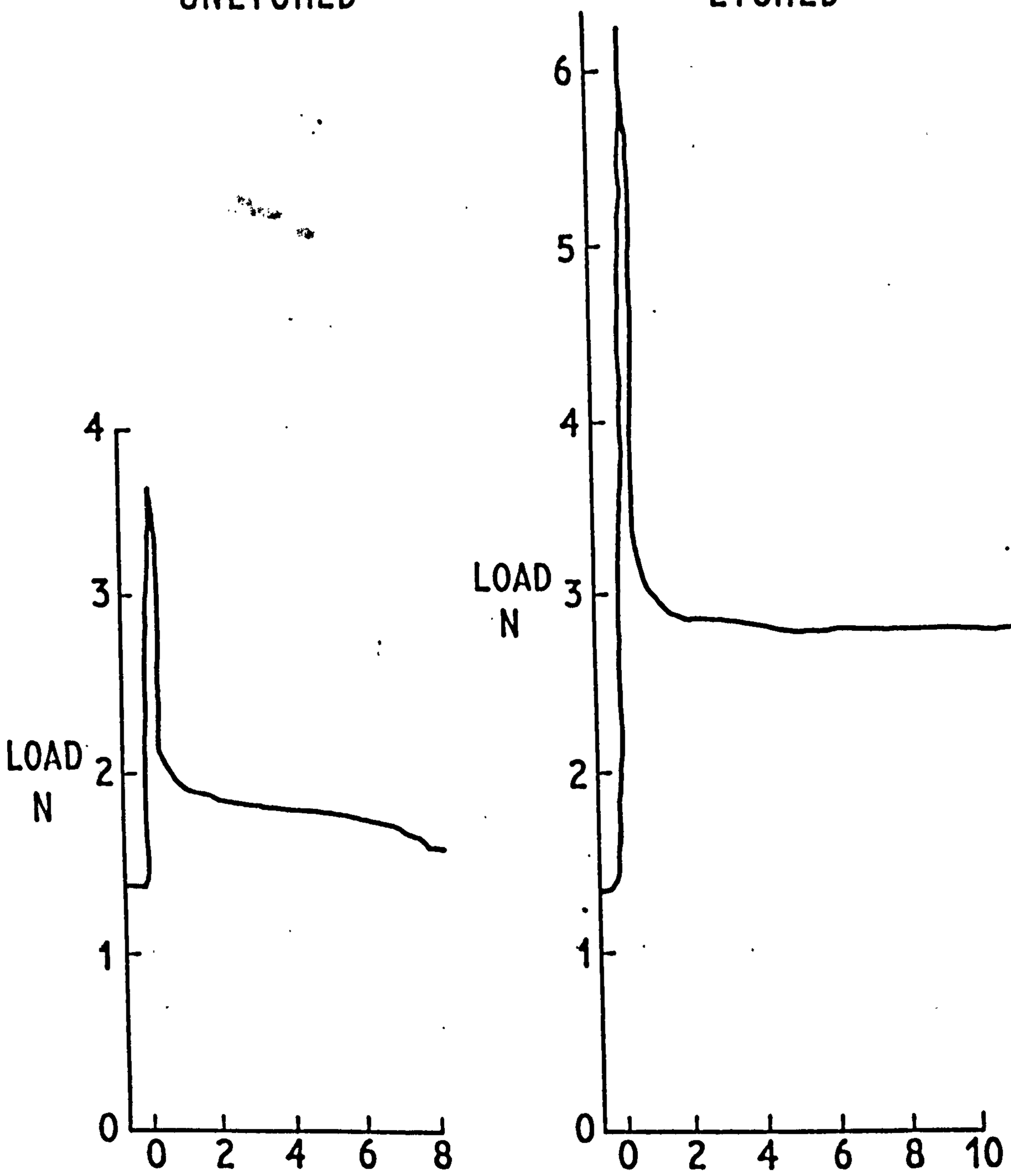

UNETCHED AND ETCHED SPECIMEN

PULL-OUT TEST RESULTS OF SIMILAR CHARACTER

FIG. 12

O = ORIGINAL DIRECTION
R = REVERSE DIRECTION

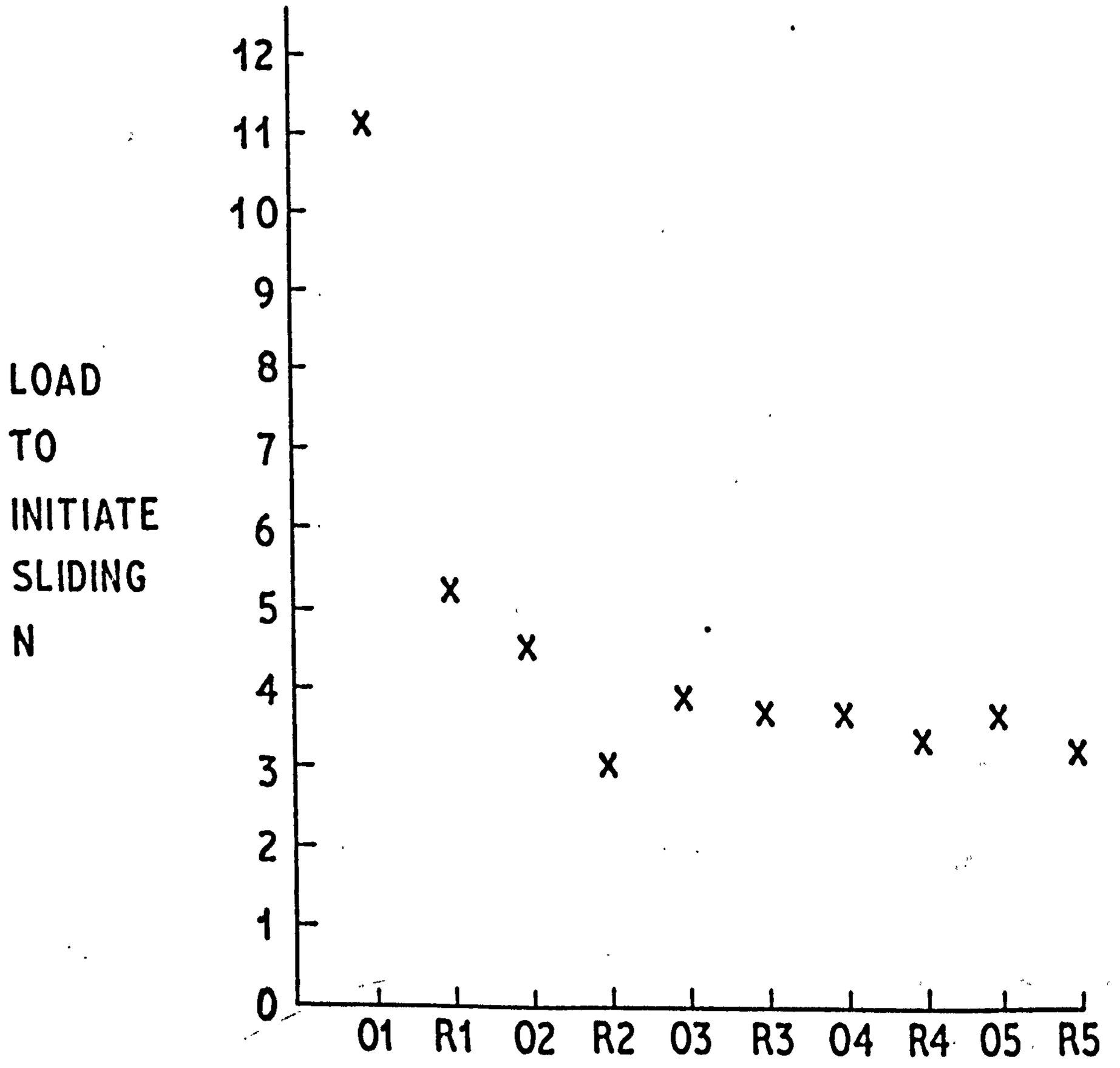

LOADS TO INITIATE SLIDING IN REVERSIBLE PULL OUT SPECIMEN AGAINST DIRECTION OF PULL

FIG. 13

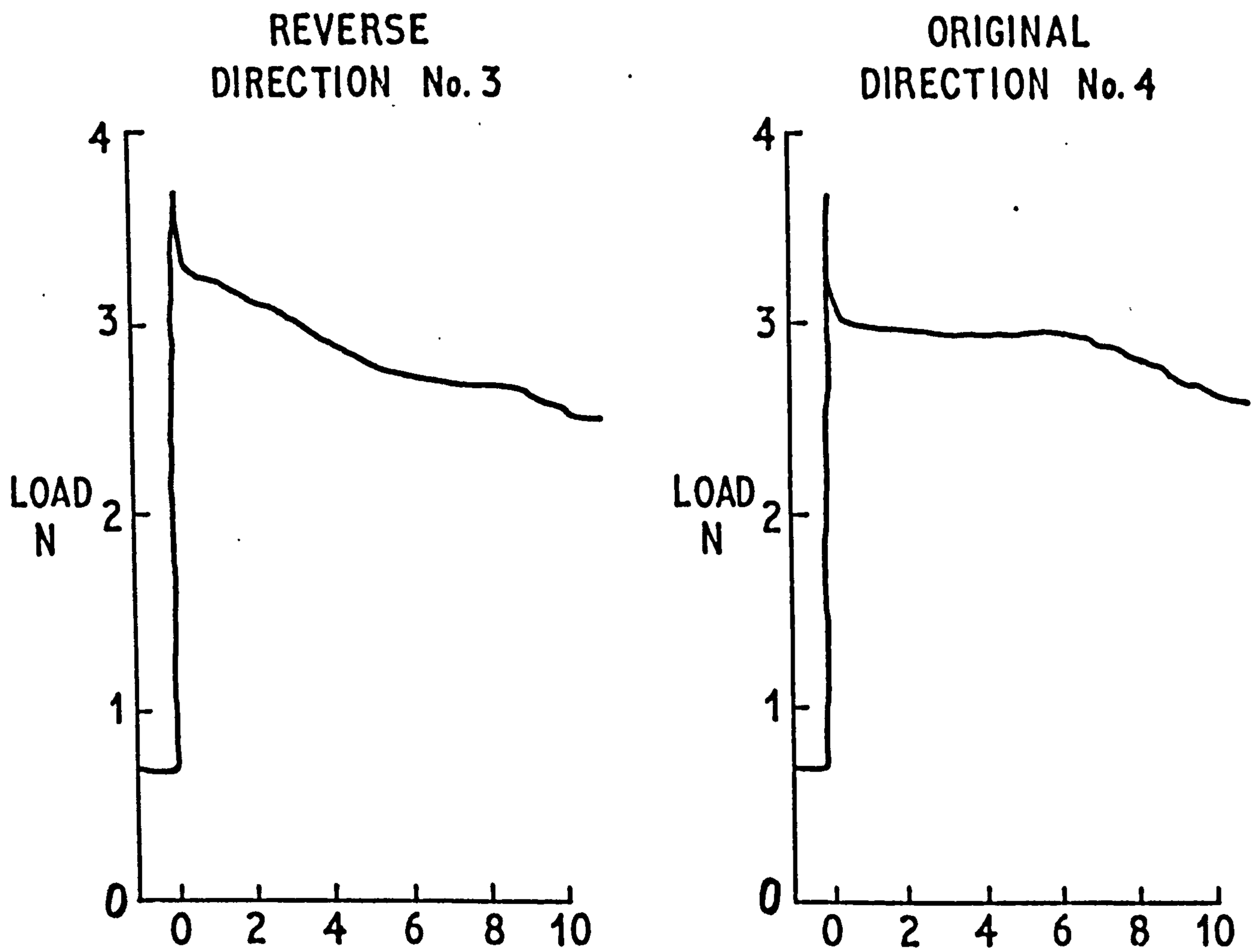

SAMPLES OF PULL-OUT RESULTS FROM A DOUBLE LENGTH UNETCHED SPECIMEN SHOWING SIMILAR CHARACTERISTICS IN EITHER DIRECTION

FIG. 14

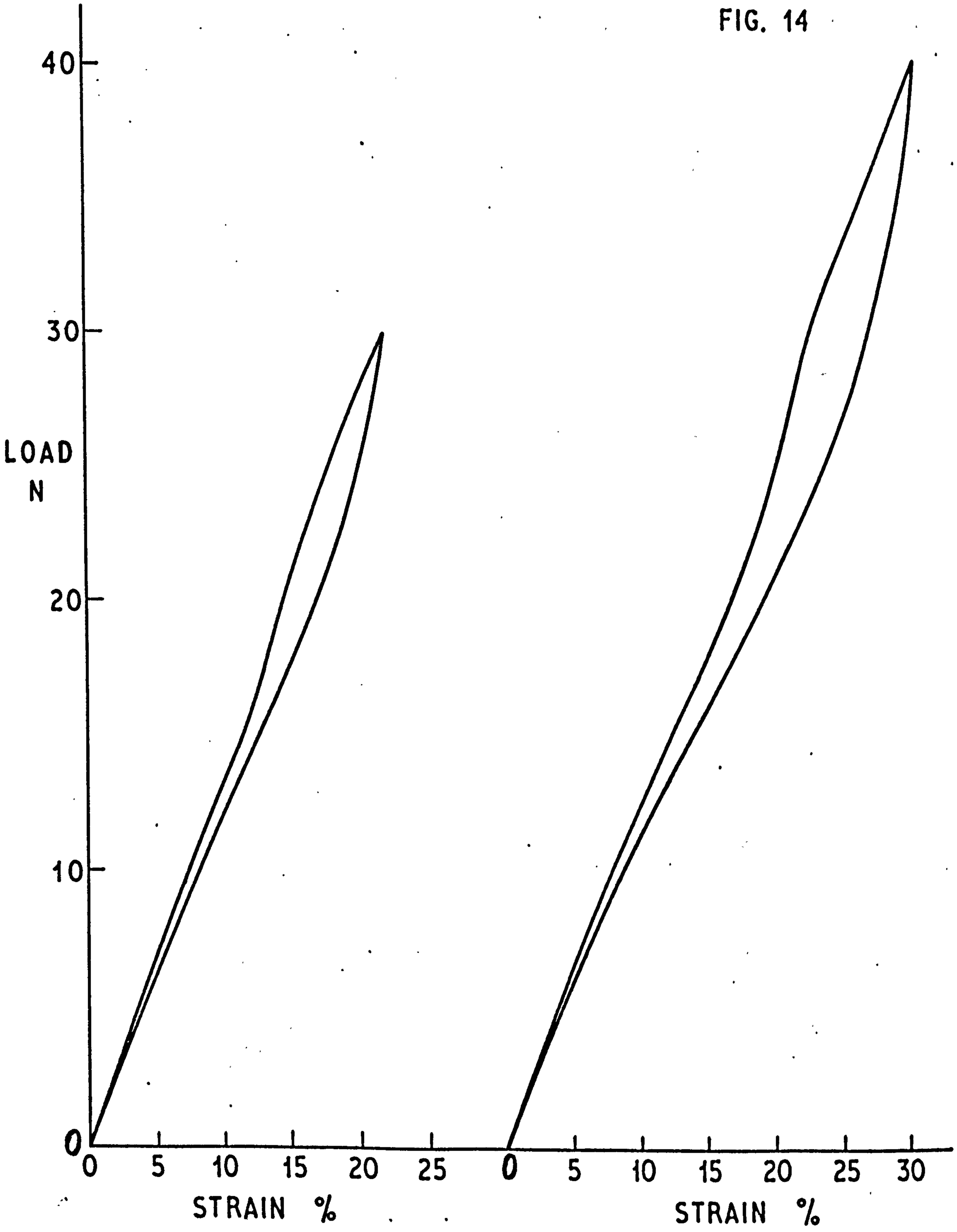

TYPICAL 'SILCOSET' HYSTERESIS LOOPS

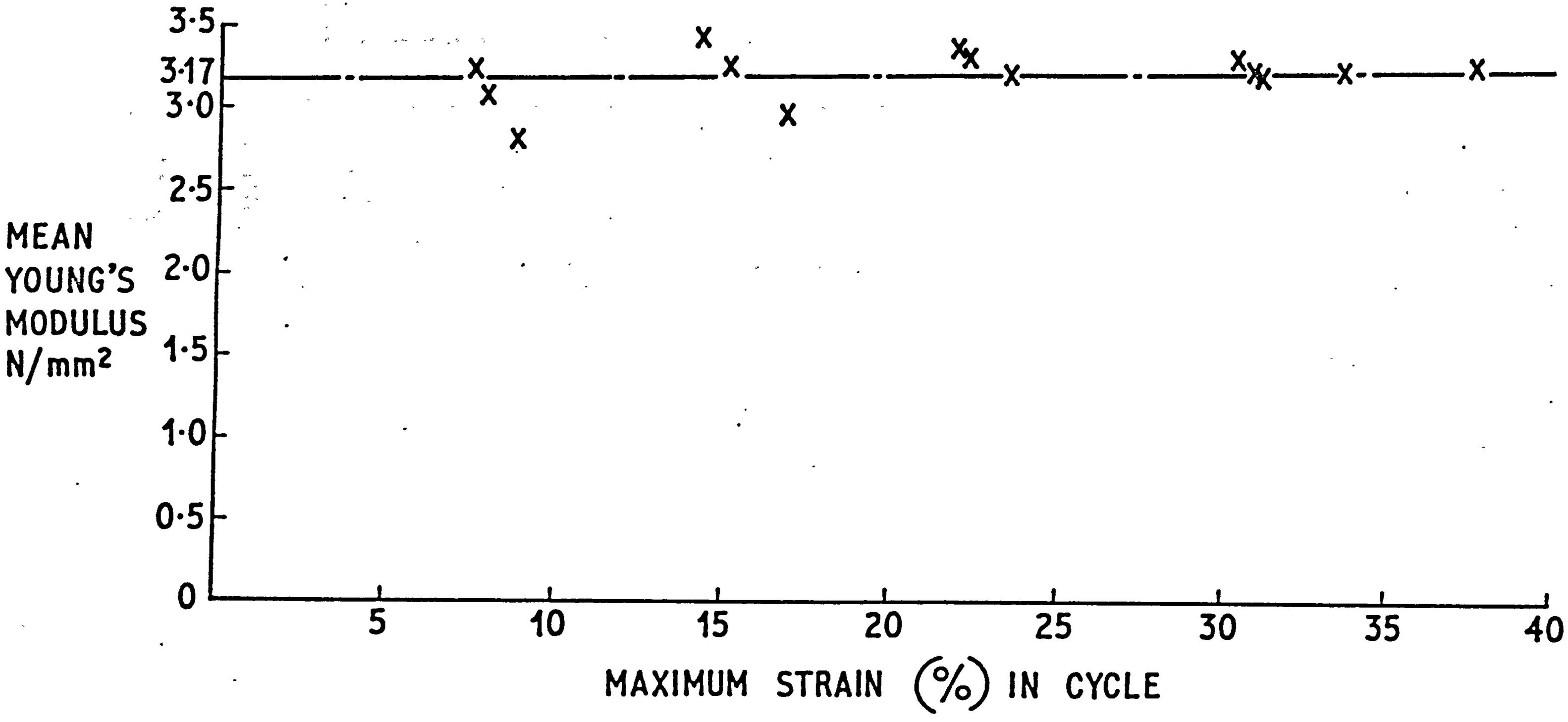

MEAN "SILCOSET" YOUNG'S MODULUS VERSUS MAXIMUM STRAIN IN CYCLE

FIG. 15

FIG.16

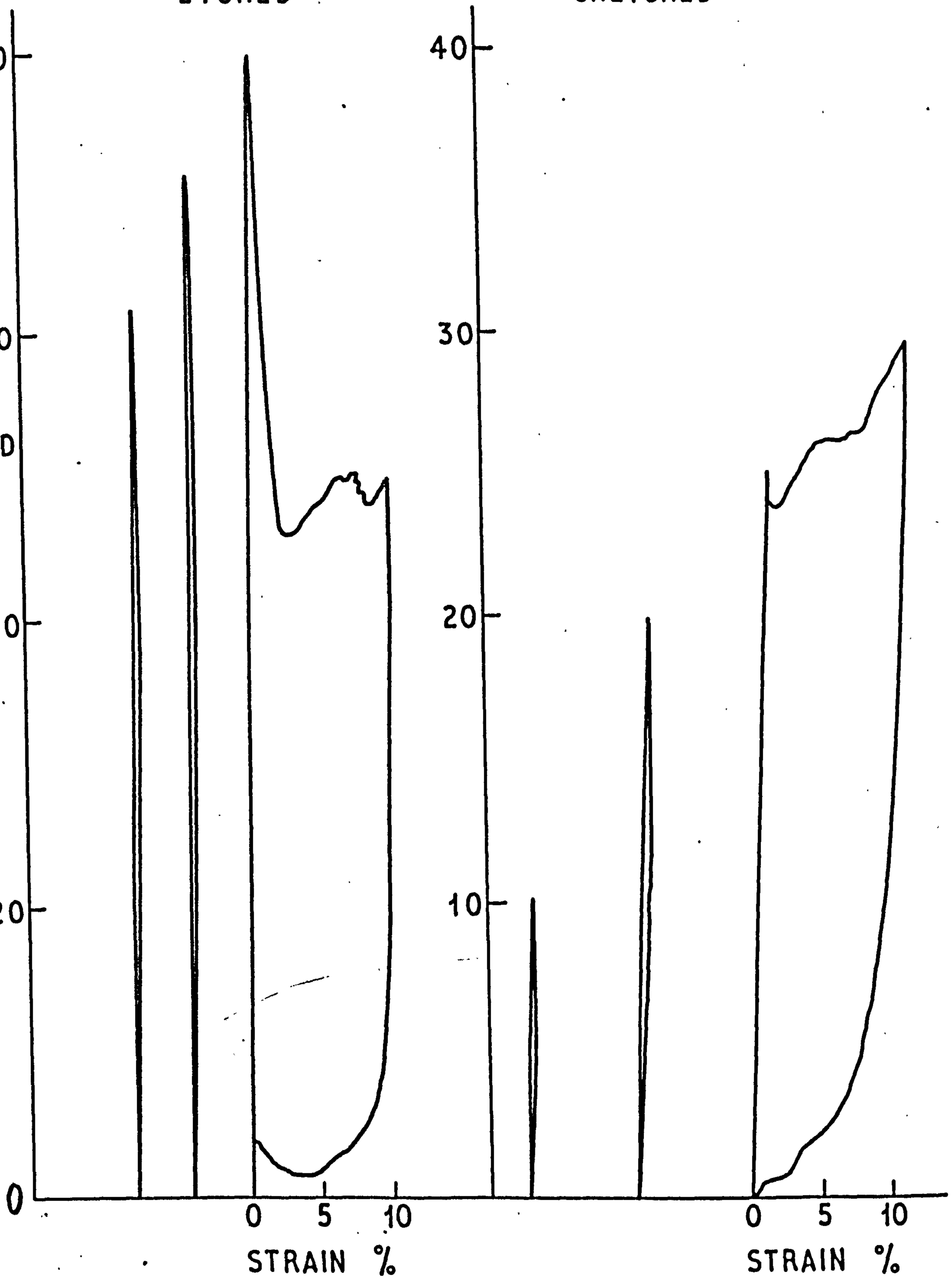

EXAMPLES OF INITIAL YIELDING

FIG. 17

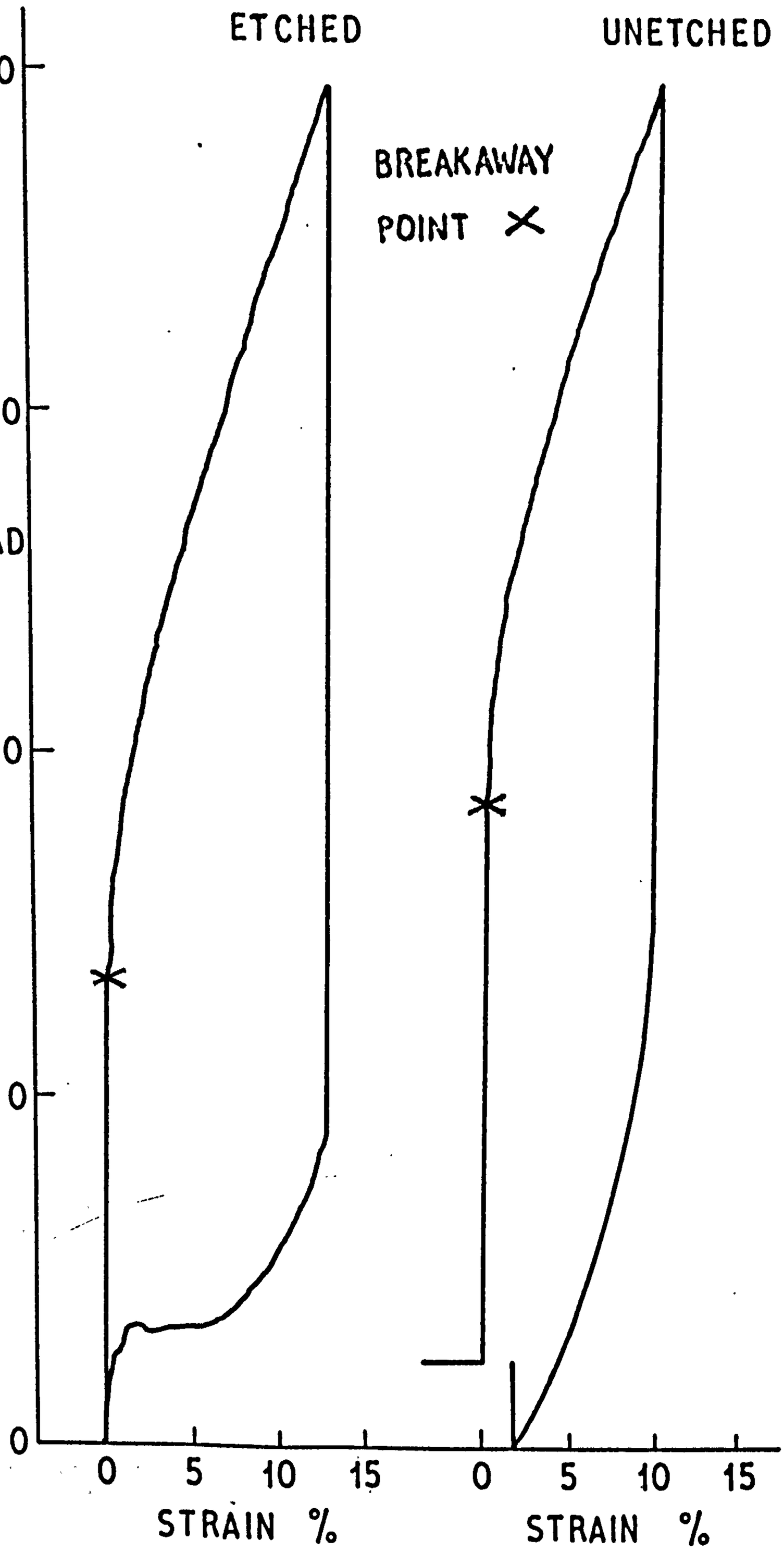

EXAMPLES OF TYPICAL HYSTERESIS LOOPS

FIG. 18

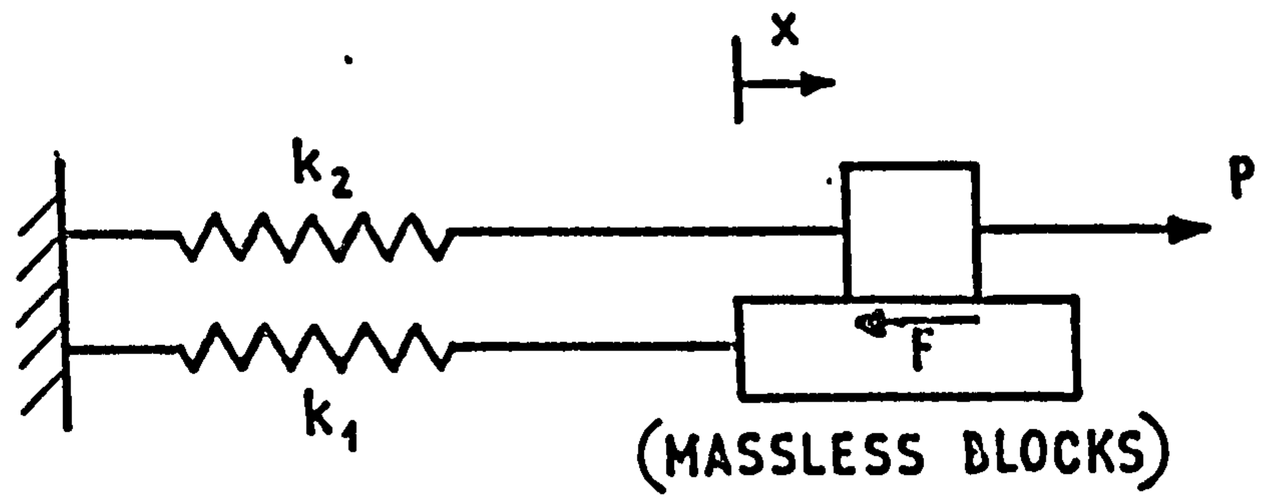

$P = (k_1 + k_2)x$ BEFORE SLIDING

$F = k_1 x_c$
$P_c = F + k_2 x_c$
} AT POINT OF SLIDING

$P = P_c + k_2 (x - x_c)$ DURING SLIDING

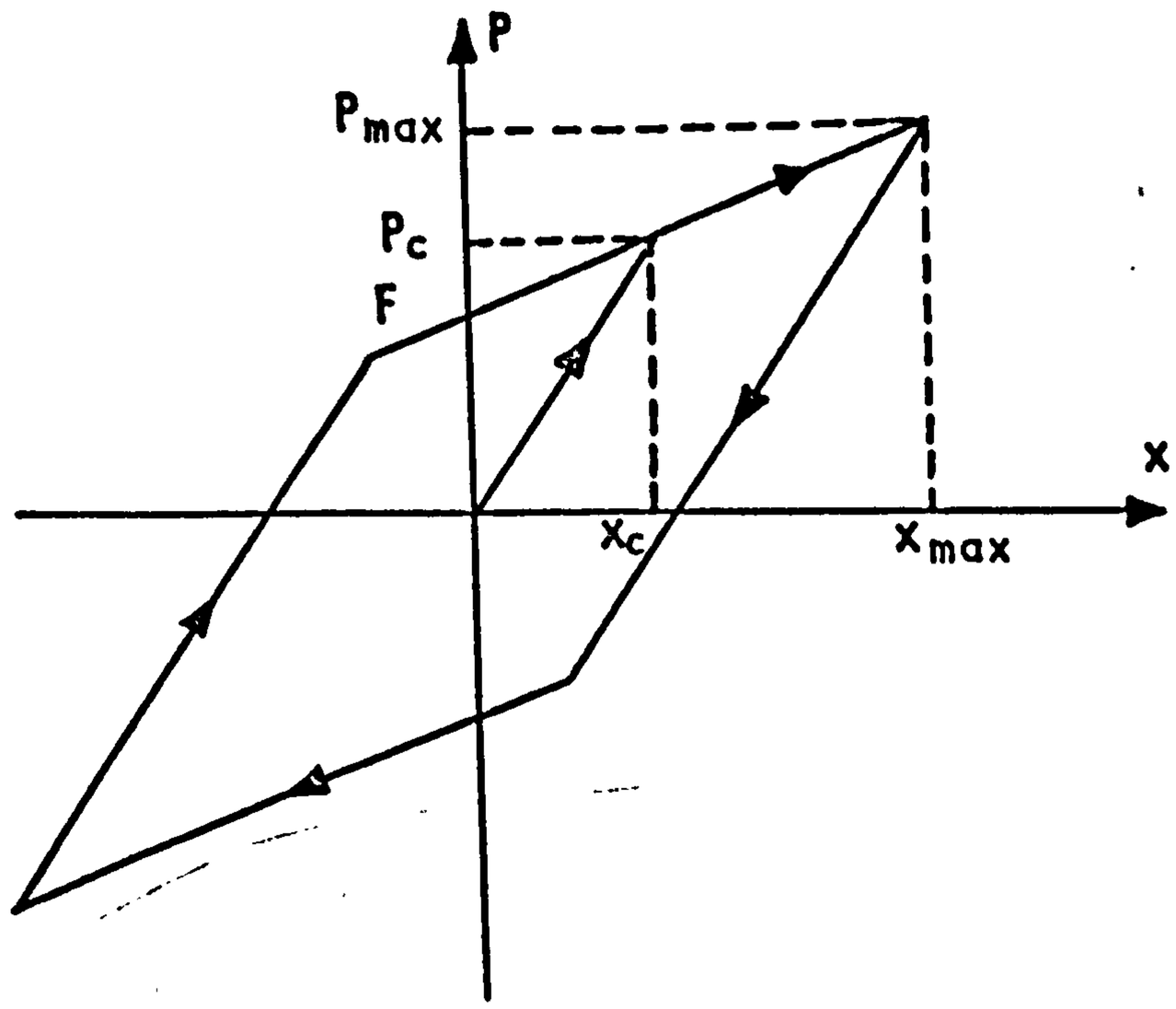

LOOP CHARACTERISTIC

BILINEAR HYSTERESIS MODEL

FIG. 19

ETCHED SPECIMENS X

UNETCHED SPECIMENS O

- - - - - - - LINE SHOWING AVERAGE ETCHED SPECIMEN BREAKAWAY LOAD

—— —— LINE THROUGH ORIGIN AND AVERAGE BREAKAWAY, REVERSE BREAKAWAY POINT (20.4 , 22.1) UNETCHED SPECIMENS

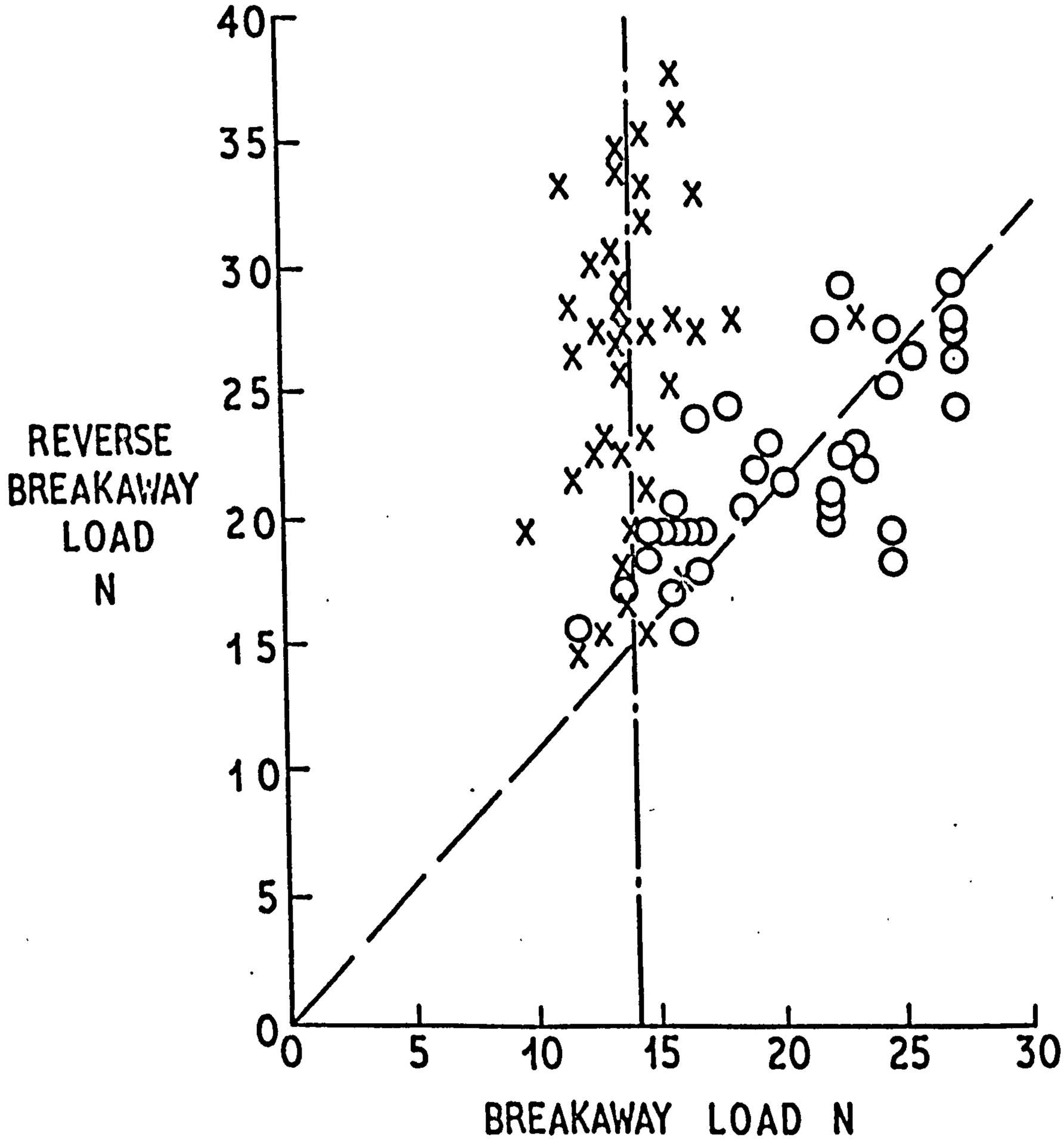

REVERSE BREAKAWAY LOAD VERSUS BREAKAWAY LOAD

FIG. 20

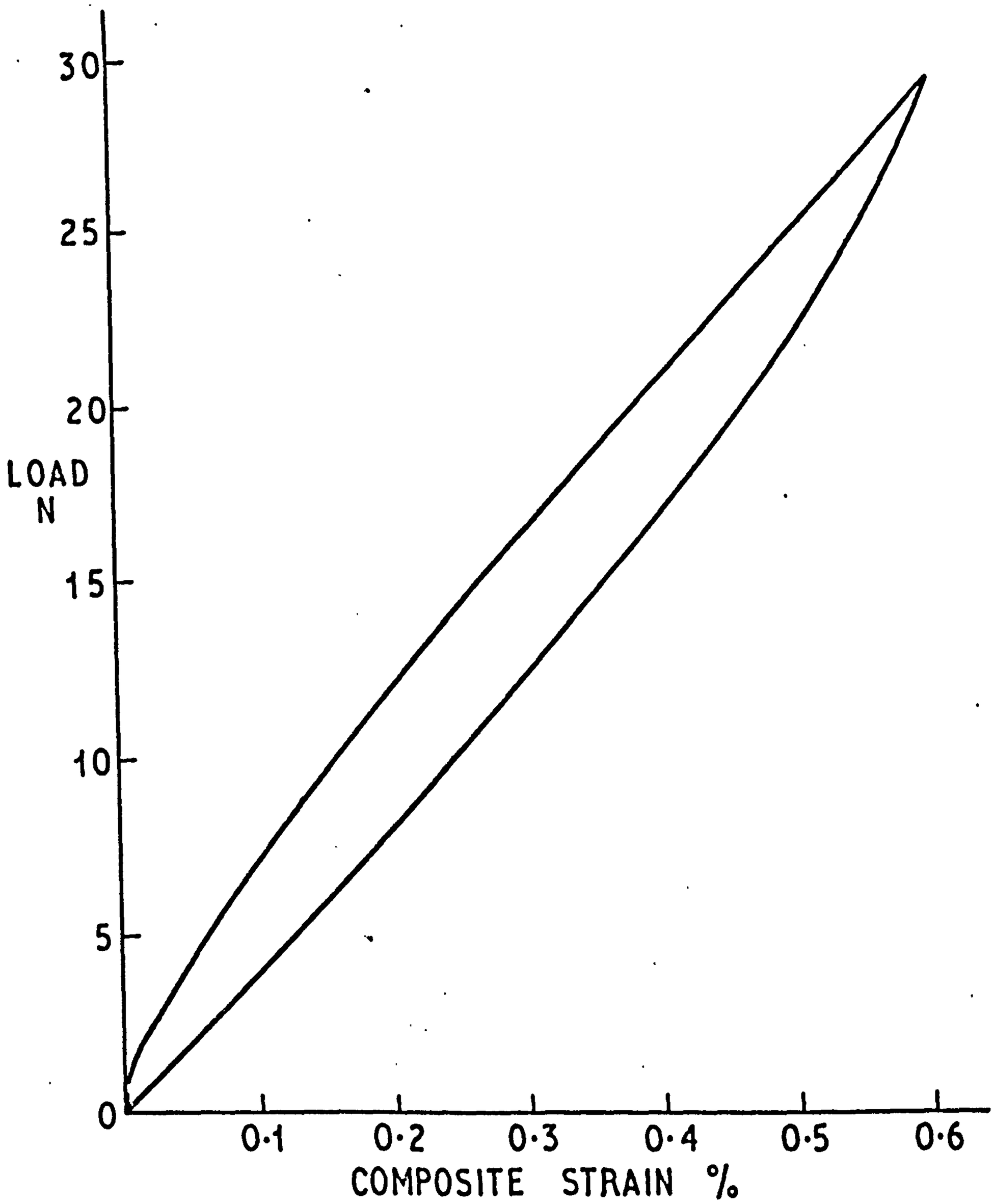

TYPICAL PRIMED SPECIMEN
HYSTERESIS LOOP

FIG. 21

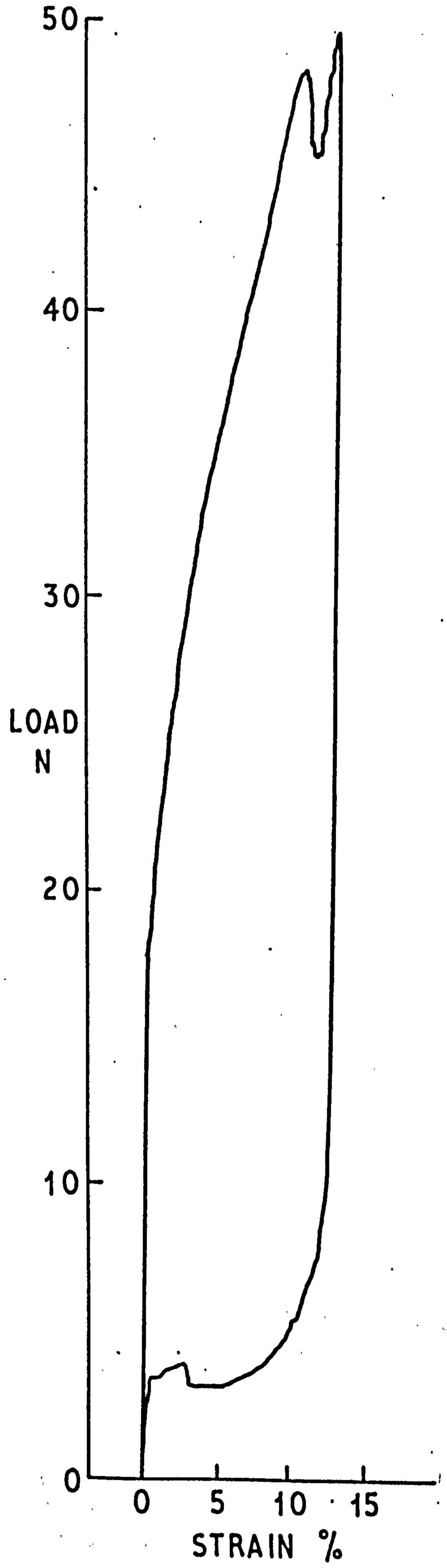

EXAMPLE OF SECONDARY YIELDING

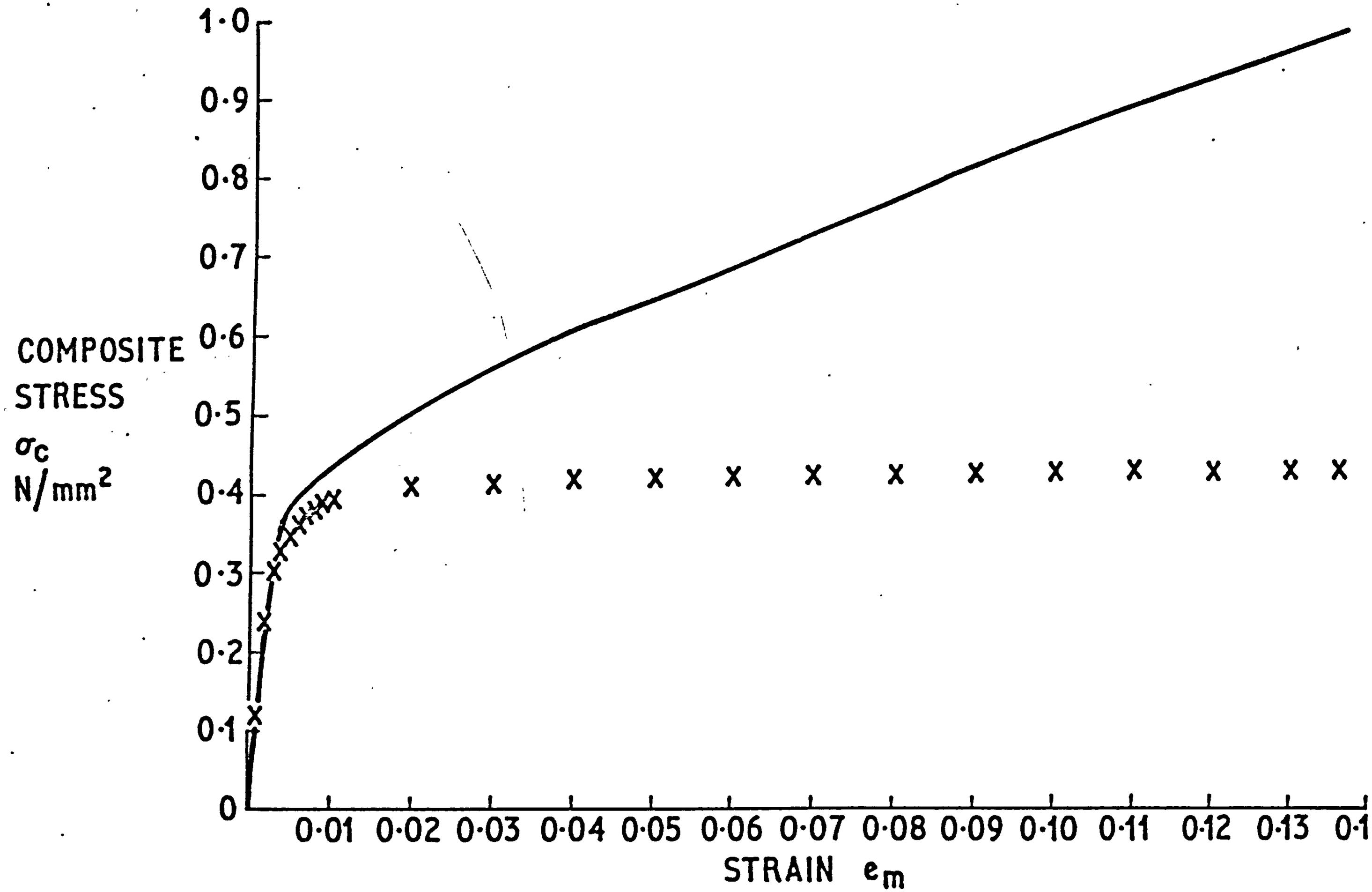

FIG. 22

PORTION OF ETCHED SPECIMEN HYSTERESIS LOOP & FIBRE LOAD ACCORDING TO MODIFIED COX THEORY EXPRESSED AS COMPOSITE STRESS x VERSUS STRAIN

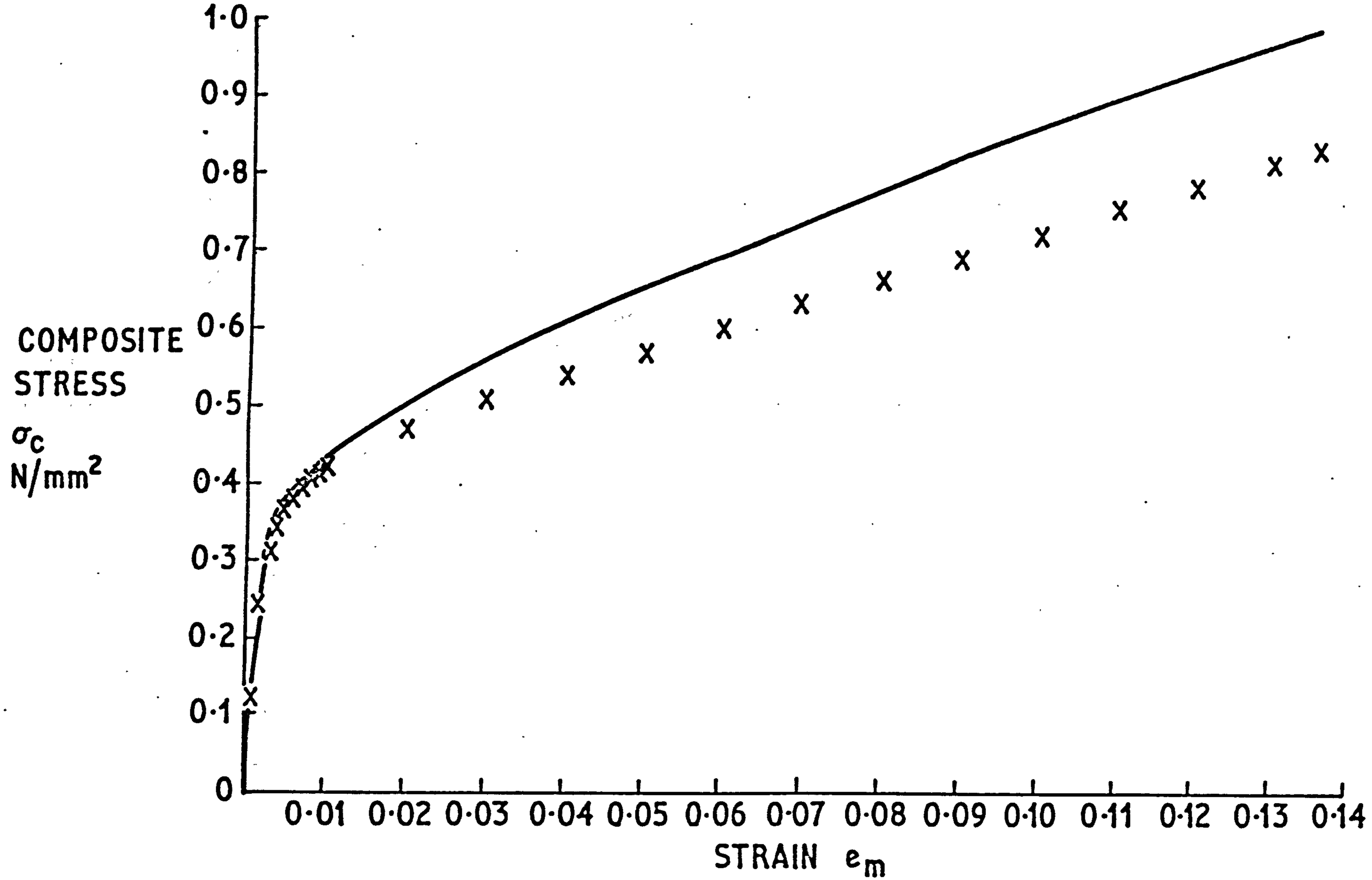

FIG. 23

PORTION OF ETCHED SPECIMEN HYSTERESIS LOOP & FIBRE LOAD ACCORDING TO MODIFIED COX THEORY PLUS MATRIX LOAD EXPRESSED AS COMPOSITE STRESS x VERSUS STRAIN

FIG. 24

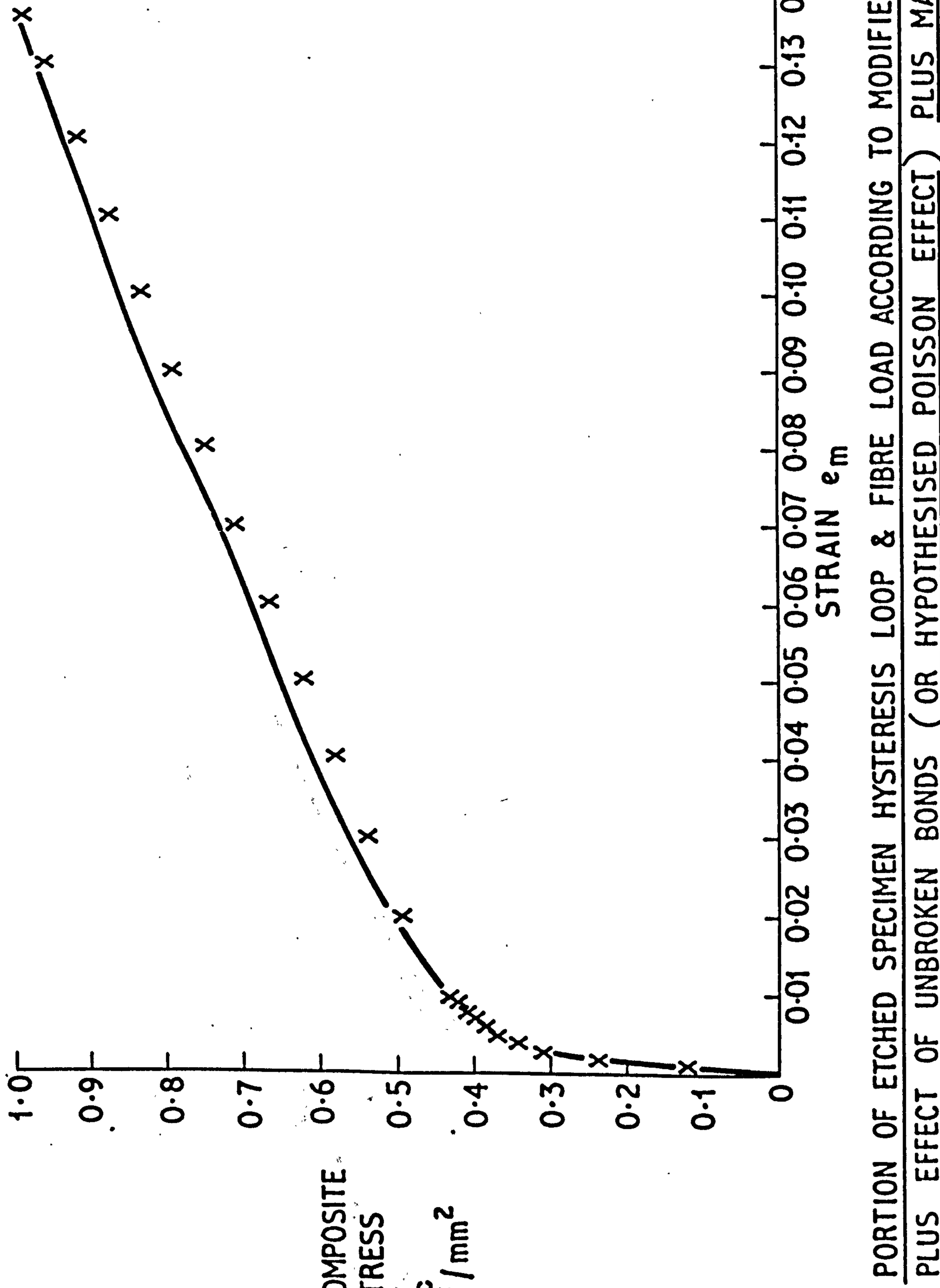
PORTION OF ETCHED SPECIMEN HYSTERESIS LOOP & FIBRE LOAD ACCORDING TO MODIFIED COX THEORY
PLUS EFFECT OF UNBROKEN BONDS (OR HYPOTHESISED POISSON EFFECT) PLUS MATRIX LOAD
EXPRESSED AS COMPOSITE STRESS X VERSUS STRAIN
COMPOSITE STRESS σ_c N/mm^2
1·0
0·9
0·8
0·7
0·6
0·5
0·4
0·3
0·2
0·1
0
0·01 0·02 0·03 0·04 0·05 0·06 0·07 0·08 0·09 0·10 0·11 0·12 0·13 0·14
STRAIN e_m

FIG. 25

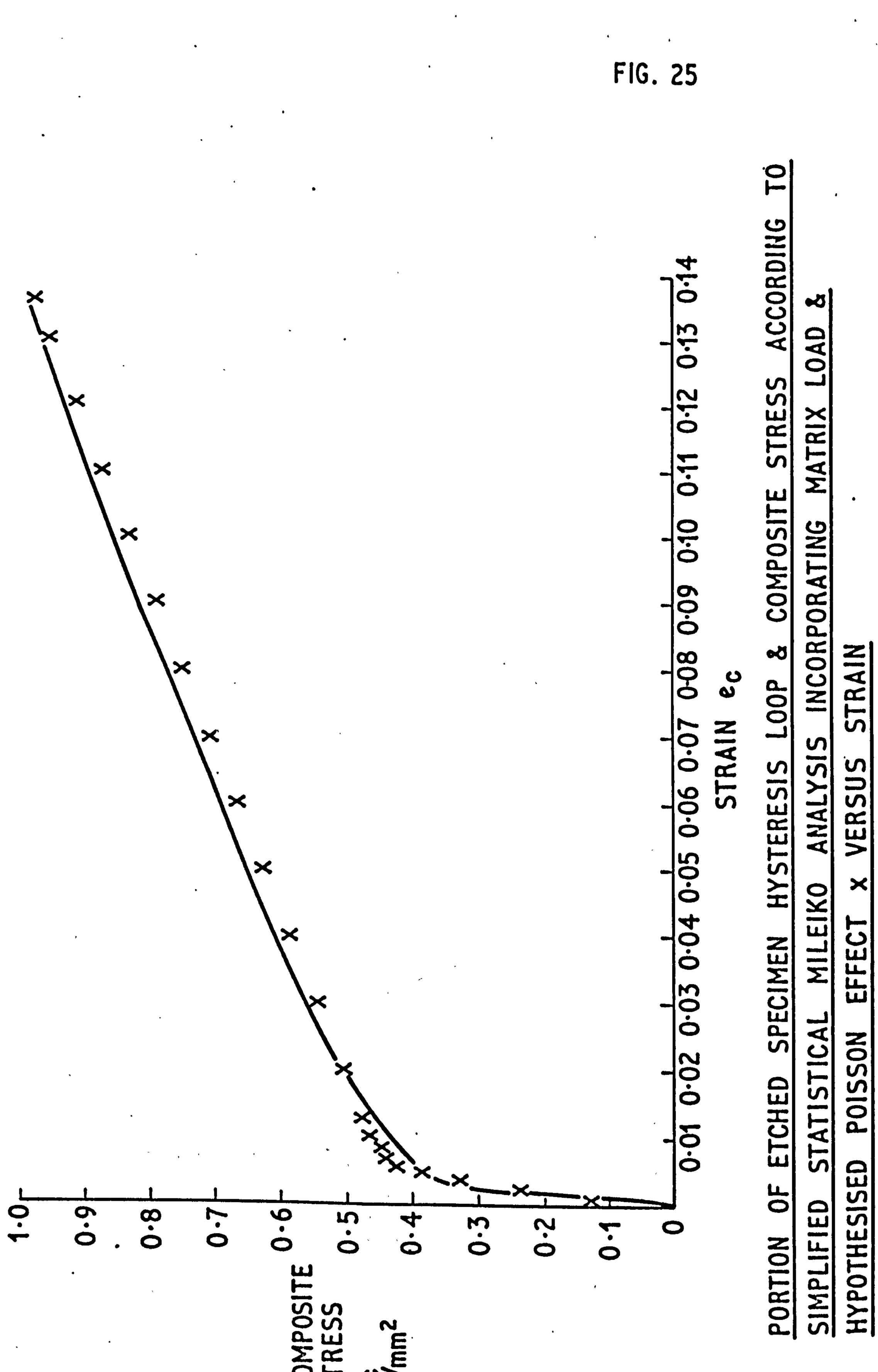
PORTION OF ETCHED SPECIMEN HYSTERESIS LOOP & COMPOSITE STRESS ACCORDING TO
SIMPLIFIED STATISTICAL MILEIKO ANALYSIS INCORPORATING MATRIX LOAD &
HYPOTHESISED POISSON EFFECT x VERSUS STRAIN
COMPOSITE STRESS σ_c N/mm^2
1·0
0·9
0·8
0·7
0·6
0·5
0·4
0·3
0·2
0·1
0
0·01 0·02 0·03 0·04 0·05 0·06 0·07 0·08 0·09 0·10 0·11 0·12 0·13 0·14
STRAIN e_c

FIG. 26

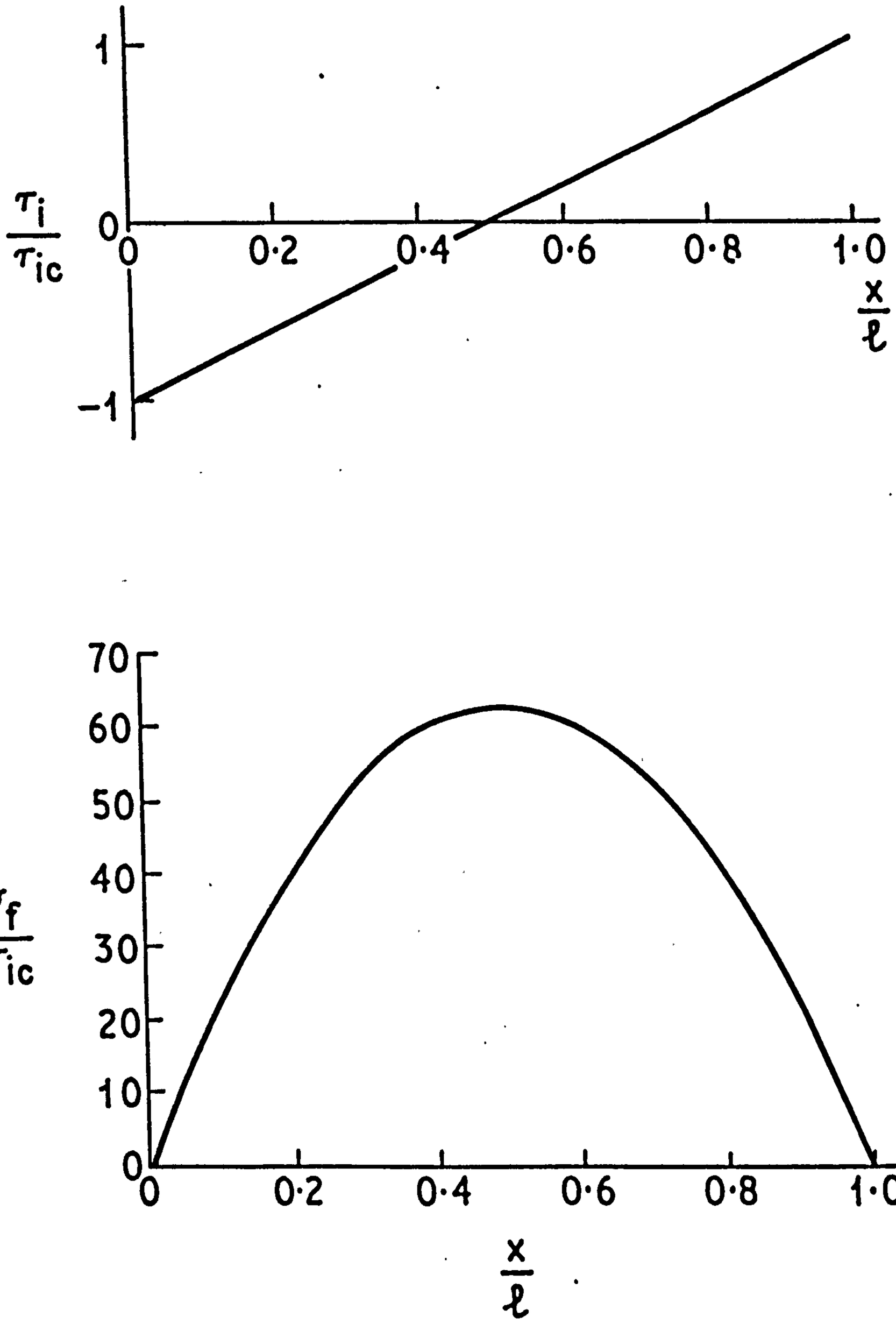

NON-DIMENSIONAL INTERFACE SHEAR STRESS AND FIBRE STRESS AGAINST DISTANCE ALONG FIBRE WHEN $e_m = e_{mc}$ (MODIFIED COX THEORY)

FIG.27

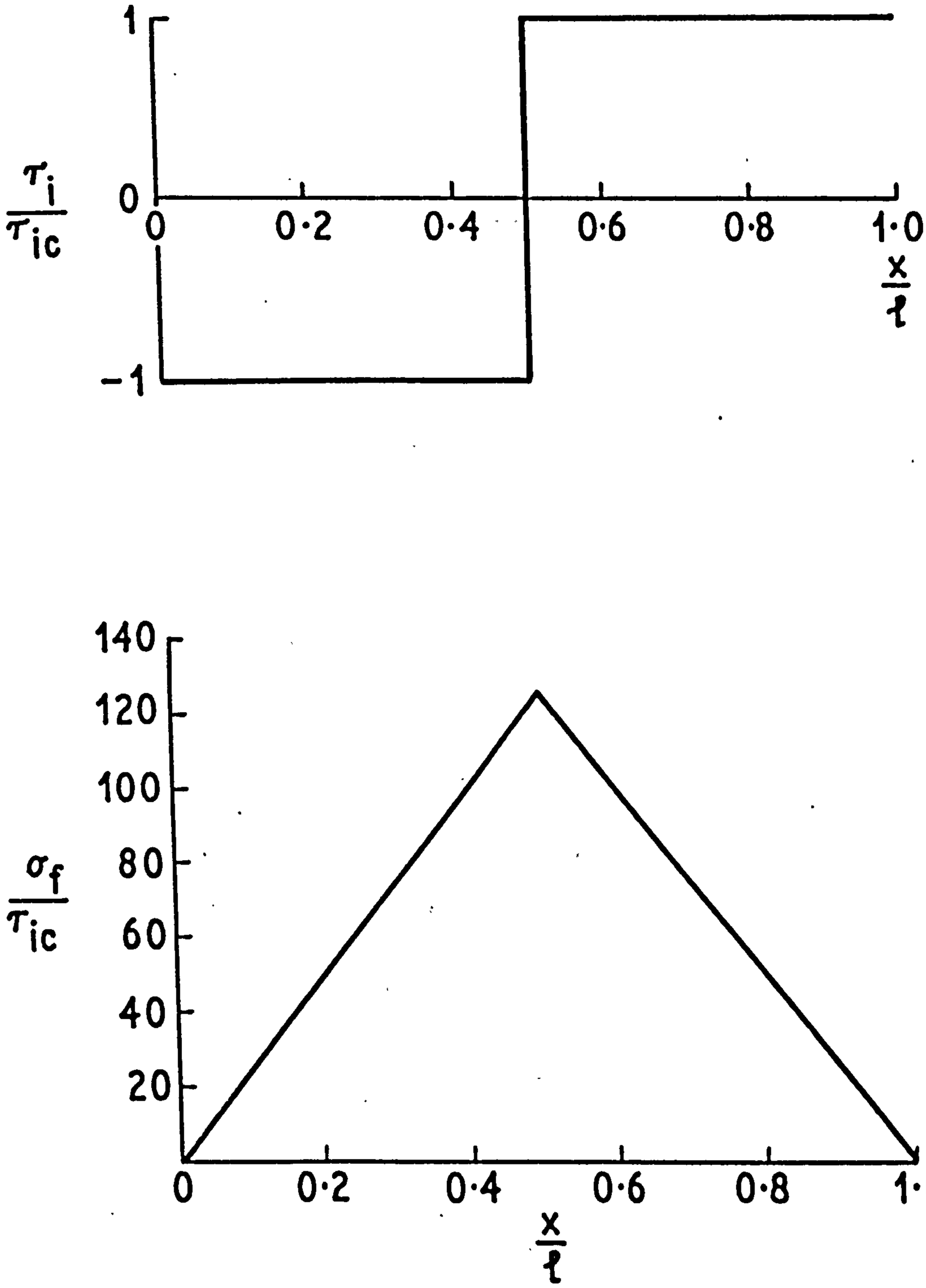

NON-DIMENSIONAL INTERFACE SHEAR STRESS AND FIBRE STRESS AGAINST DISTANCE ALONG FIBRE WHEN $e_m >> e_{mc}$ (MODIFIED COX THEORY)

FIG. 28

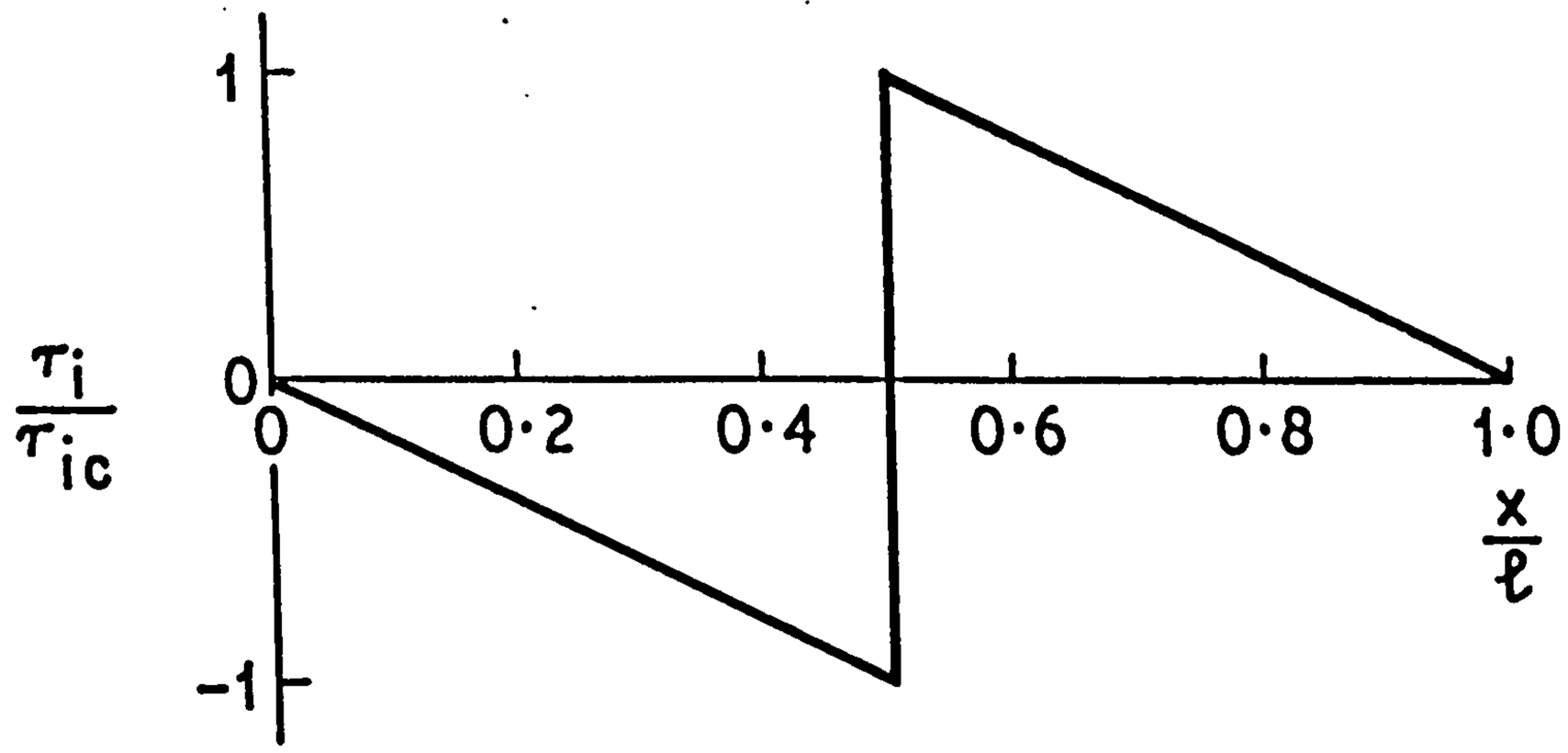

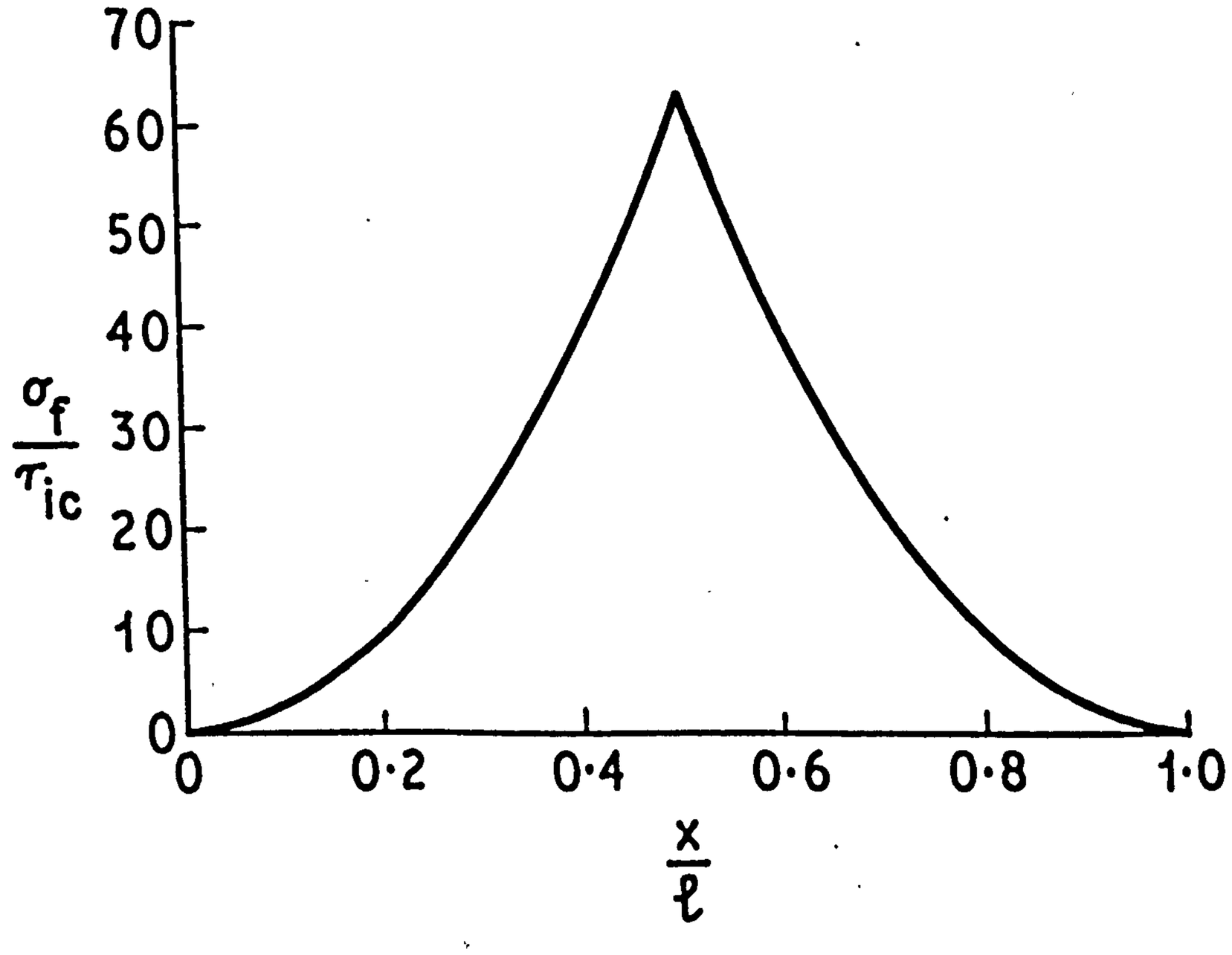

NON-DIMENSIONAL INTERFACE SHEAR STRESS AND FIBRE STRESS AGAINST DISTANCE ALONG FIBRE WHEN $e=-e_{mc}$ (MODIFIED COX THEORY)

FIG. 29

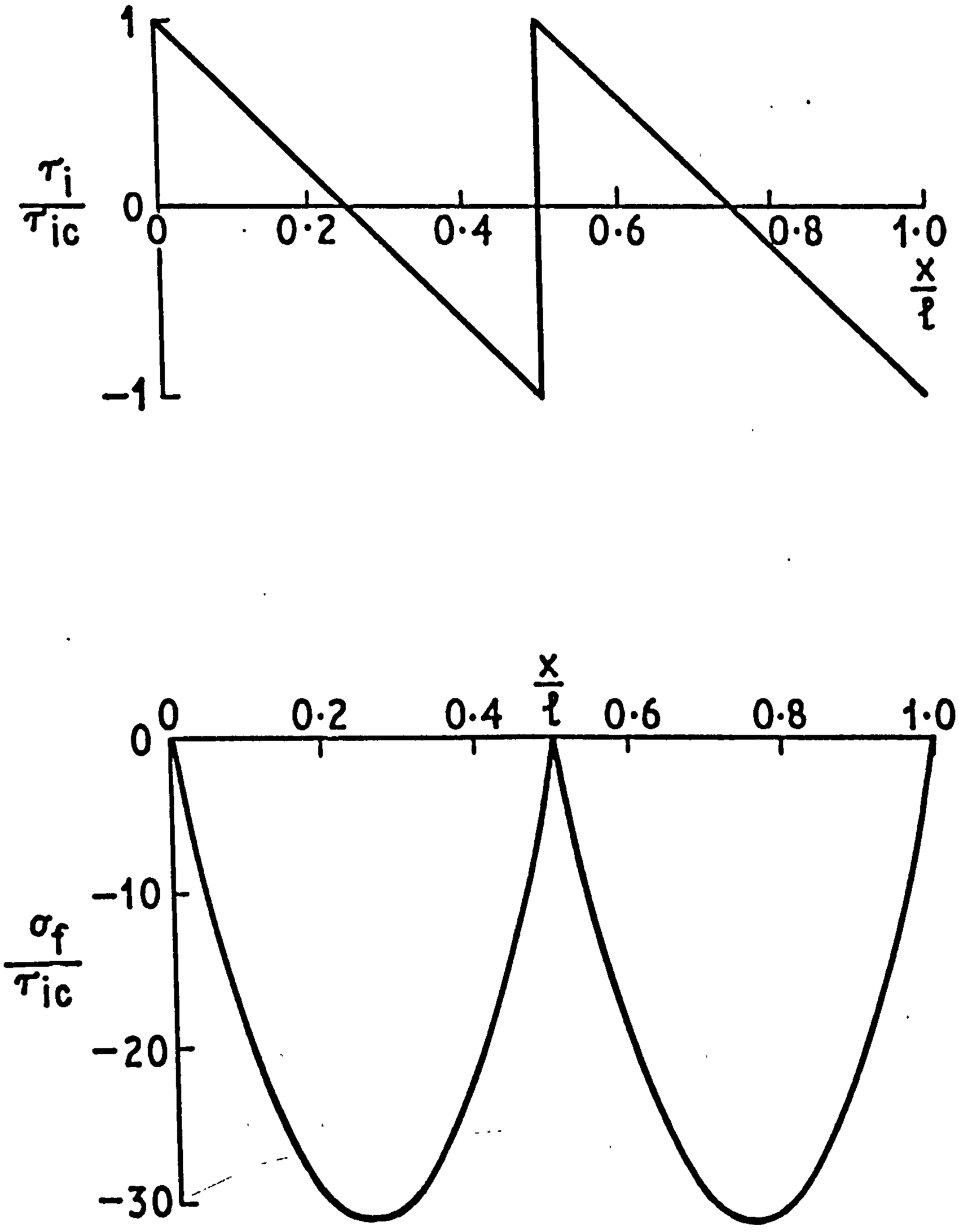

NON-DIMENSIONAL INTERFACE SHEAR STRESS AND FIBRE STRESS AGAINST DISTANCE ALONG FIBRE WHEN $e = -2e_{mc}$ (MODIFIED COX THEORY)

FIG. 30

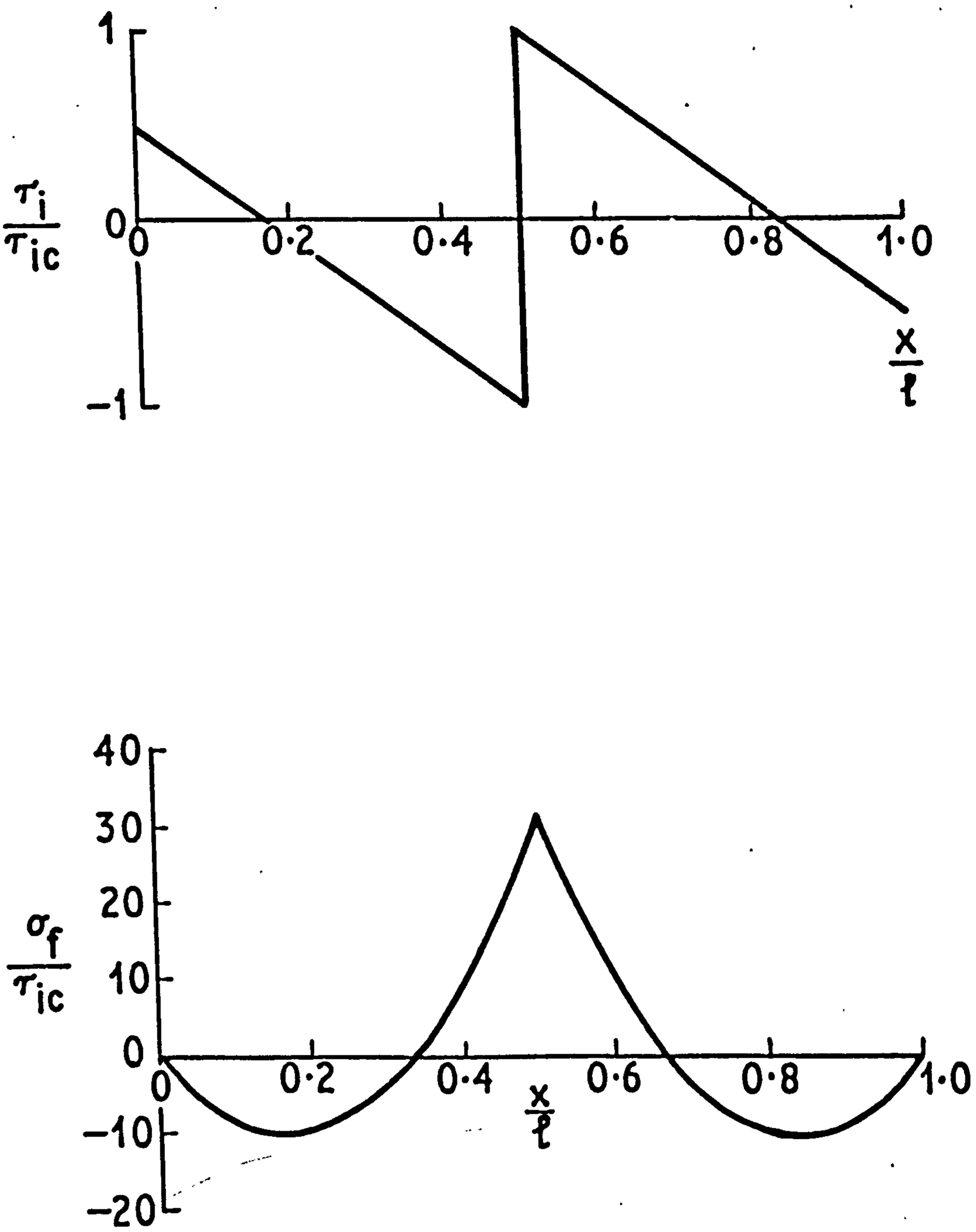

NON-DIMENSIONAL INTERFACE SHEAR STRESS AND FIBRE STRESS AGAINST DISTANCE ALONG FIBRE WHEN $e = -3/2\ e_{mc}$ (MODIFIED COX THEORY)

FIG. 31

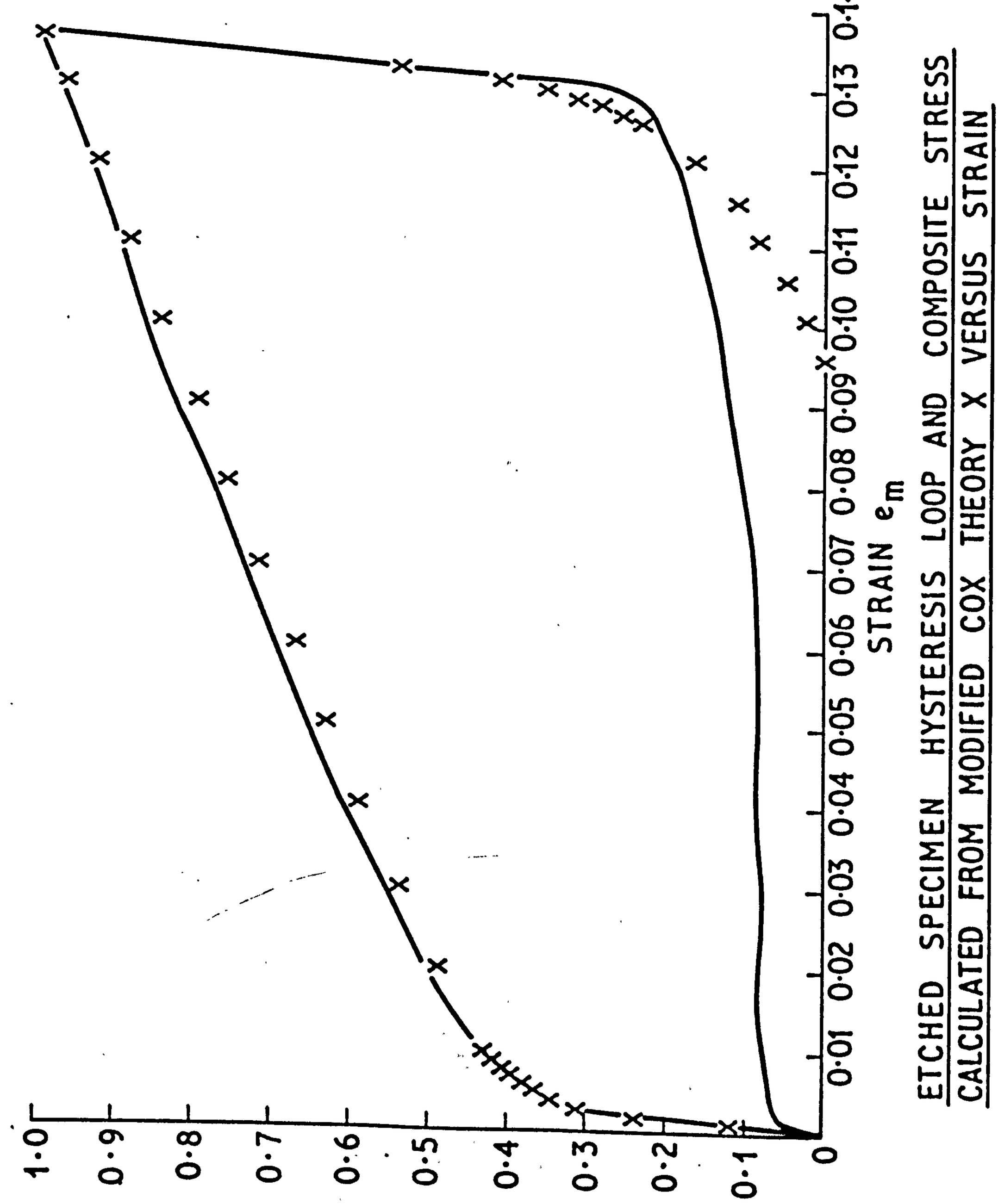
ETCHED SPECIMEN HYSTERESIS LOOP AND COMPOSITE
CALCULATED FROM MODIFIED COX THEORY X VERSUS STRESS
STRAIN e_m
0·01 0·02 0·03 0·04 0·05 0·06 0·07 0·08 0·09 0·10 0·11 0·12 0·13 0·14
COMPOSITE STRESS σ_c N/mm²
0 0·1 0·2 0·3 0·4 0·5 0·6 0·7 0·8 0·9 1·0

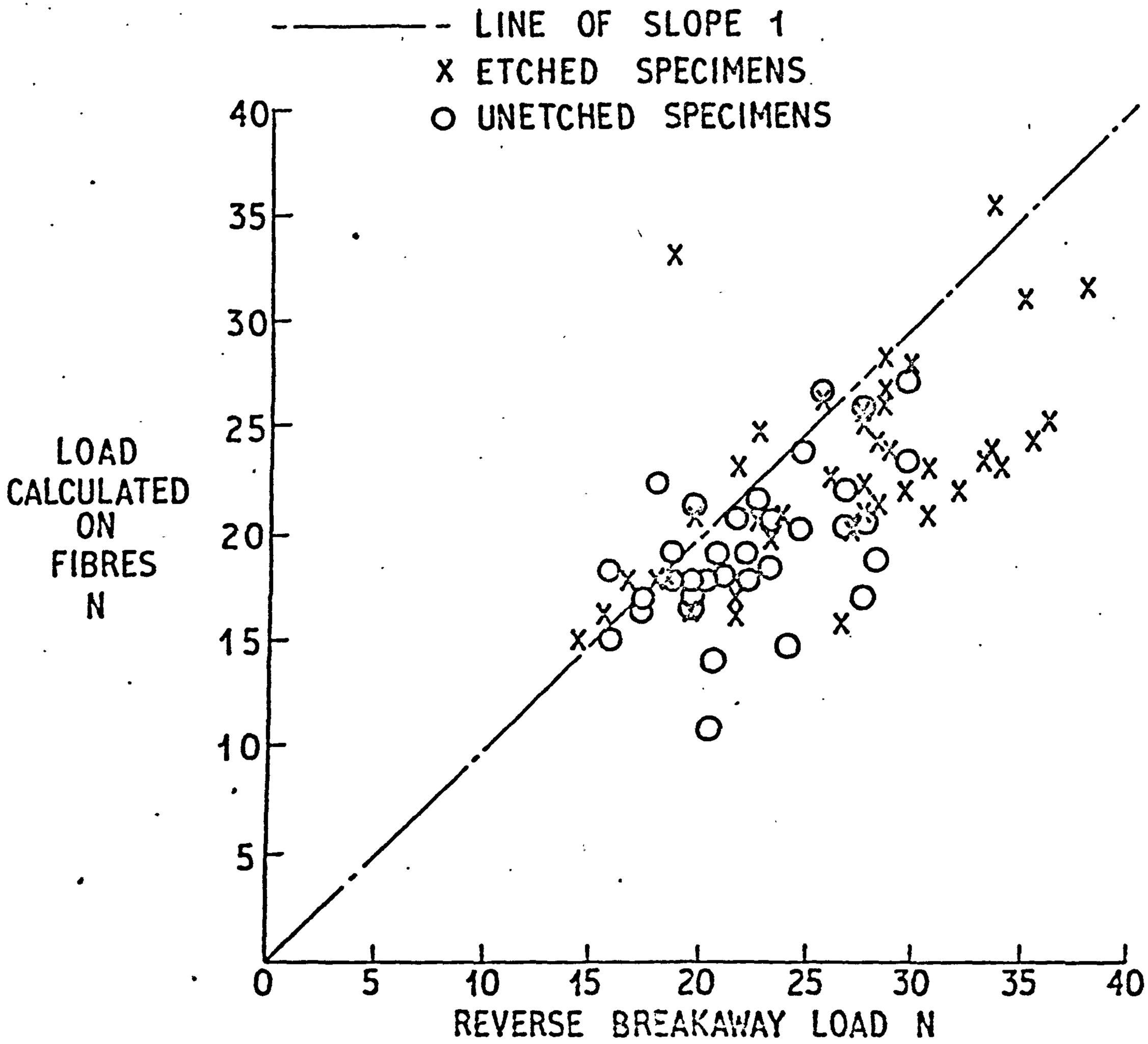

FIG. 32

LOAD CALCULATED ON FIBRES VERSUS REVERSE BREAKAWAY LOAD

FIG. 33

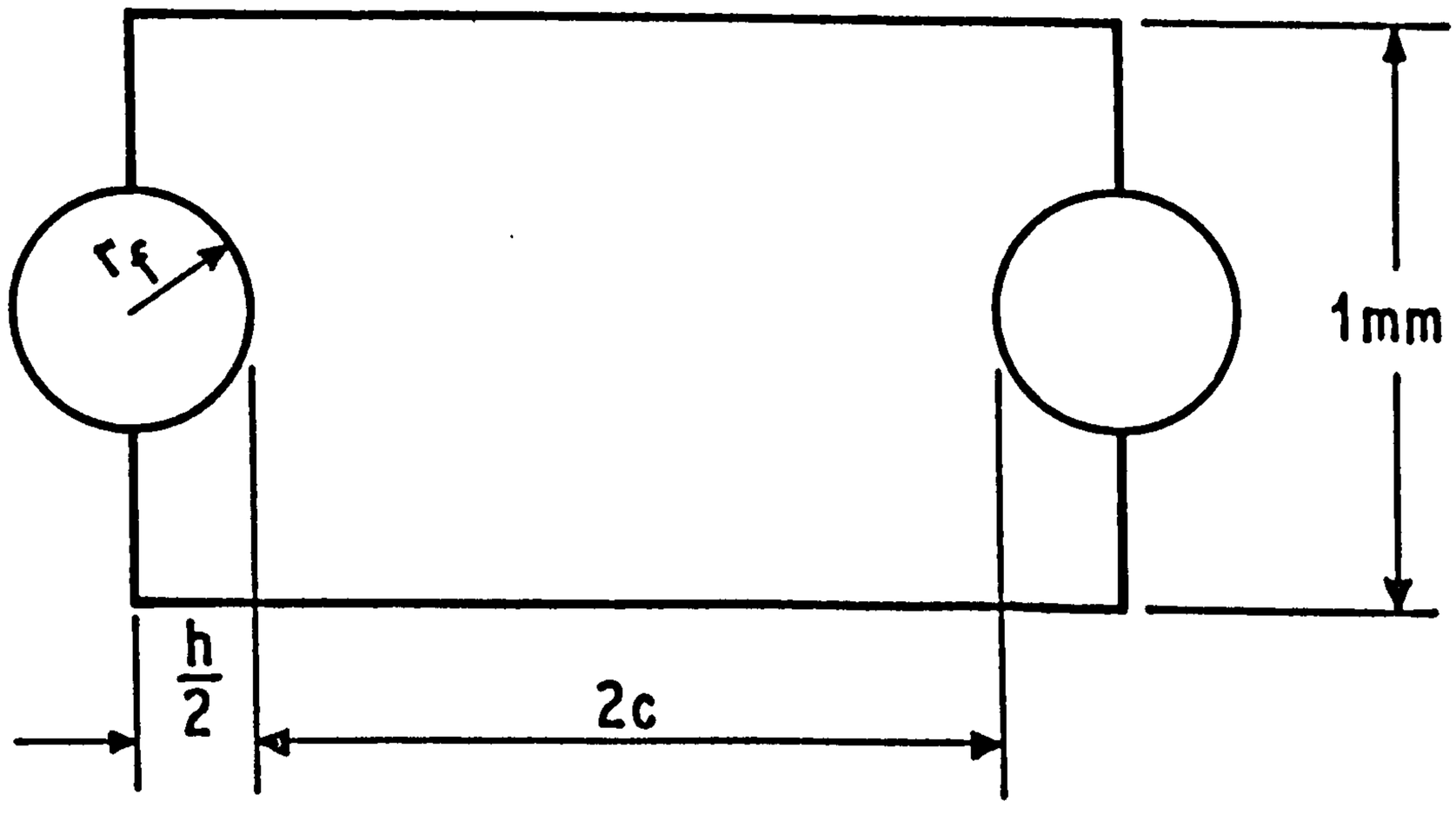

SUPPOSED GEOMETRY OF COMPOSITE FOR CALCULATION OF BUCKLING LOADS RETAINING VOLUME FRACTION $V_f = 0{\cdot}075$ AND WITH $\frac{h}{2} = r_f$

FIG. 34

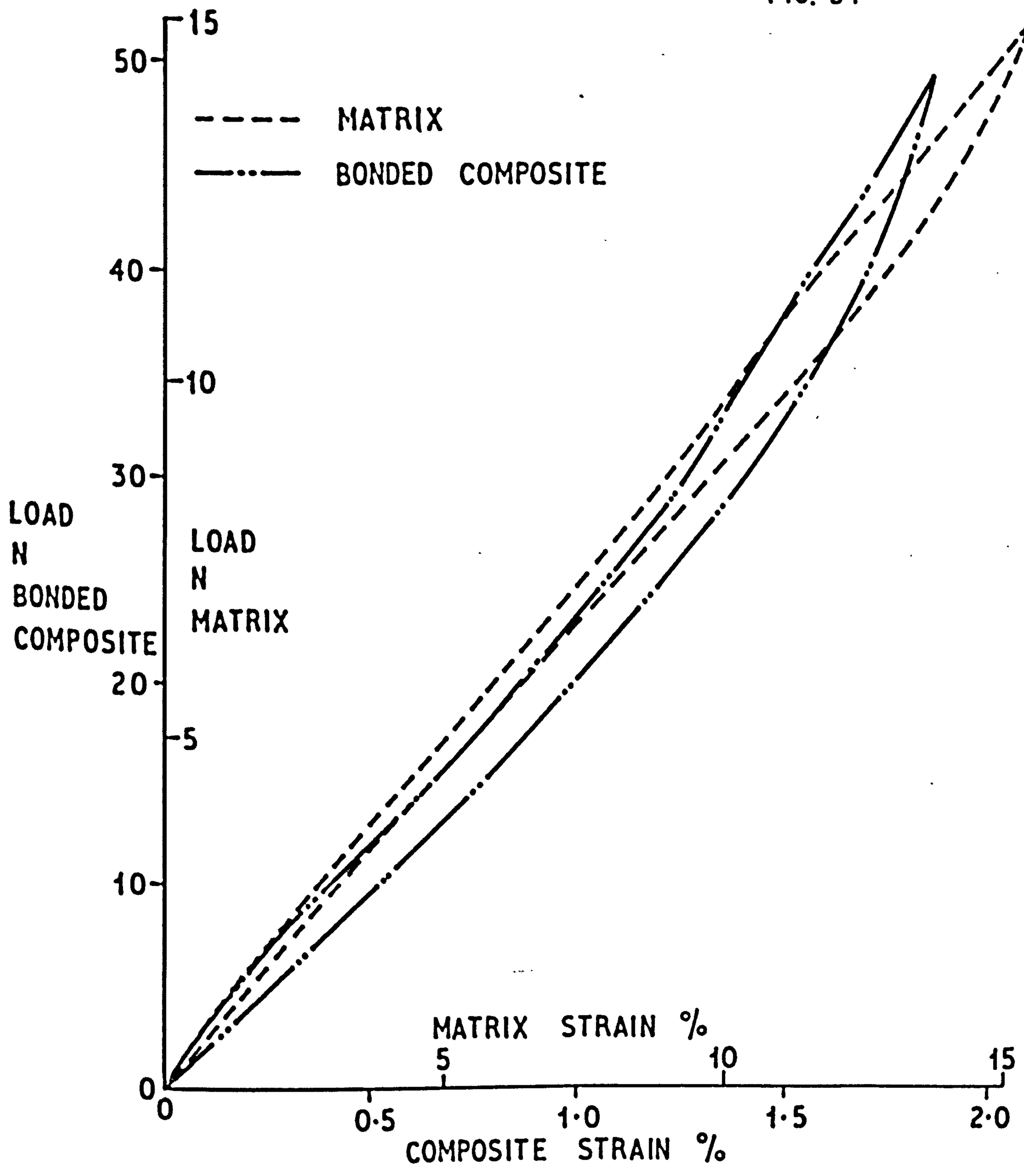

ALL – MATRIX SPECIMEN AND BONDED FIBRE COMPOSITE SPECIMEN ON REDUCED CO-ORDINATES

FIG. 35

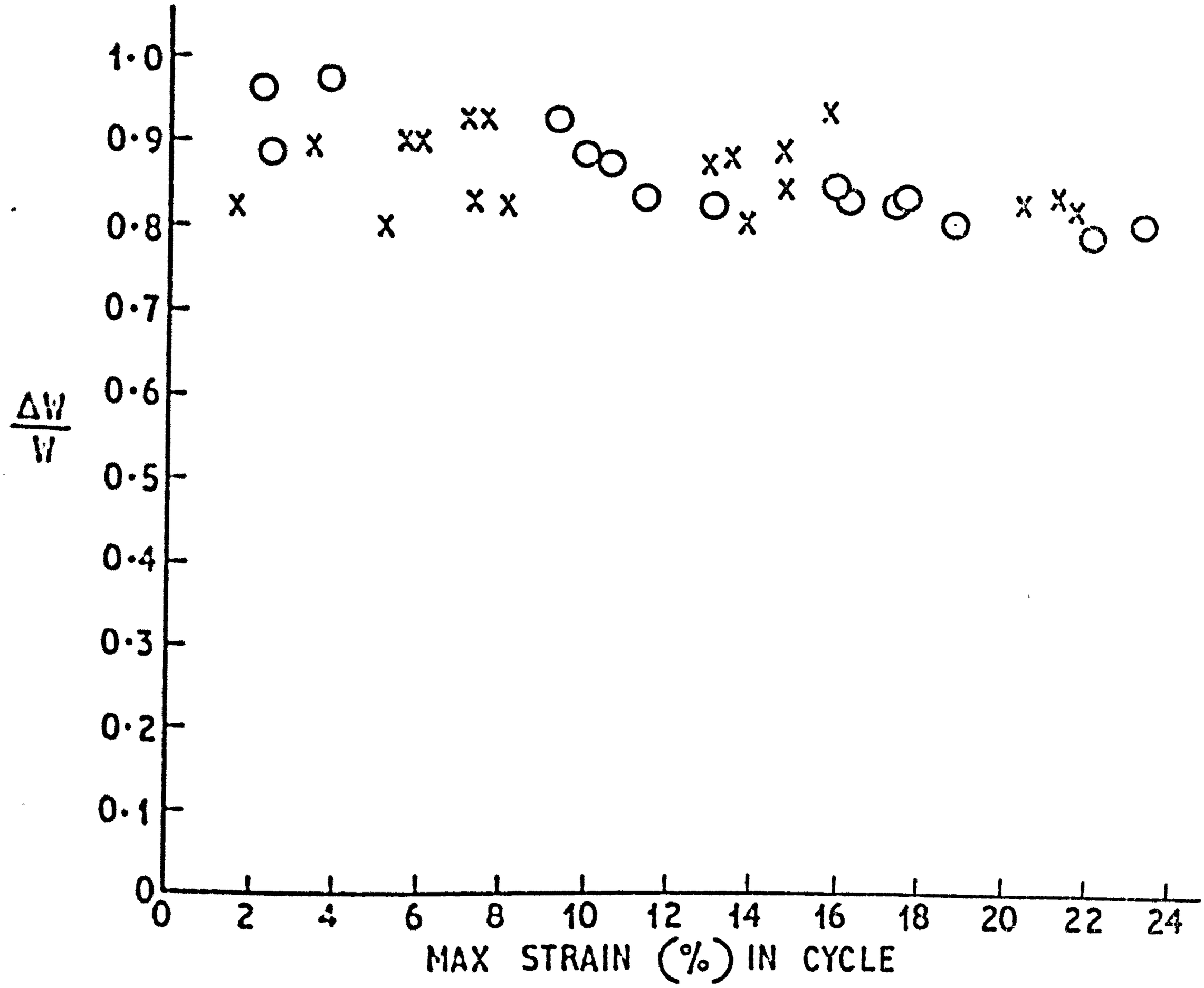

ENERGY LOST IN CYCLE OVER MAX STRAIN ENERGY IN CYCLE VERSUS STRAIN (UNBONDED SPECIMENS)

FIG. 36

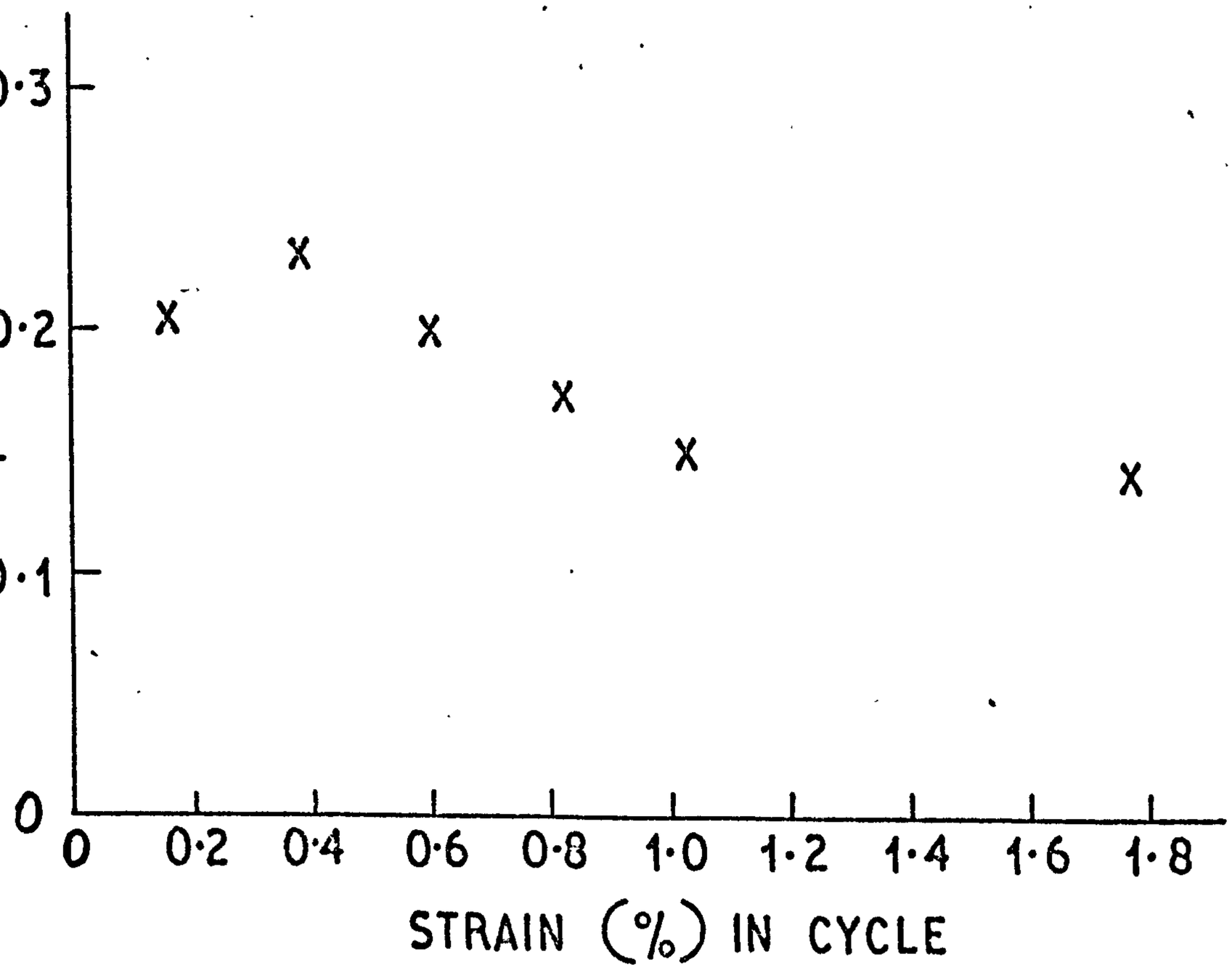

ENERGY LOST IN CYCLE OVER MAX STRAIN ENERGY IN CYCLE VERSUS STRAIN (BONDED SPECIMEN)

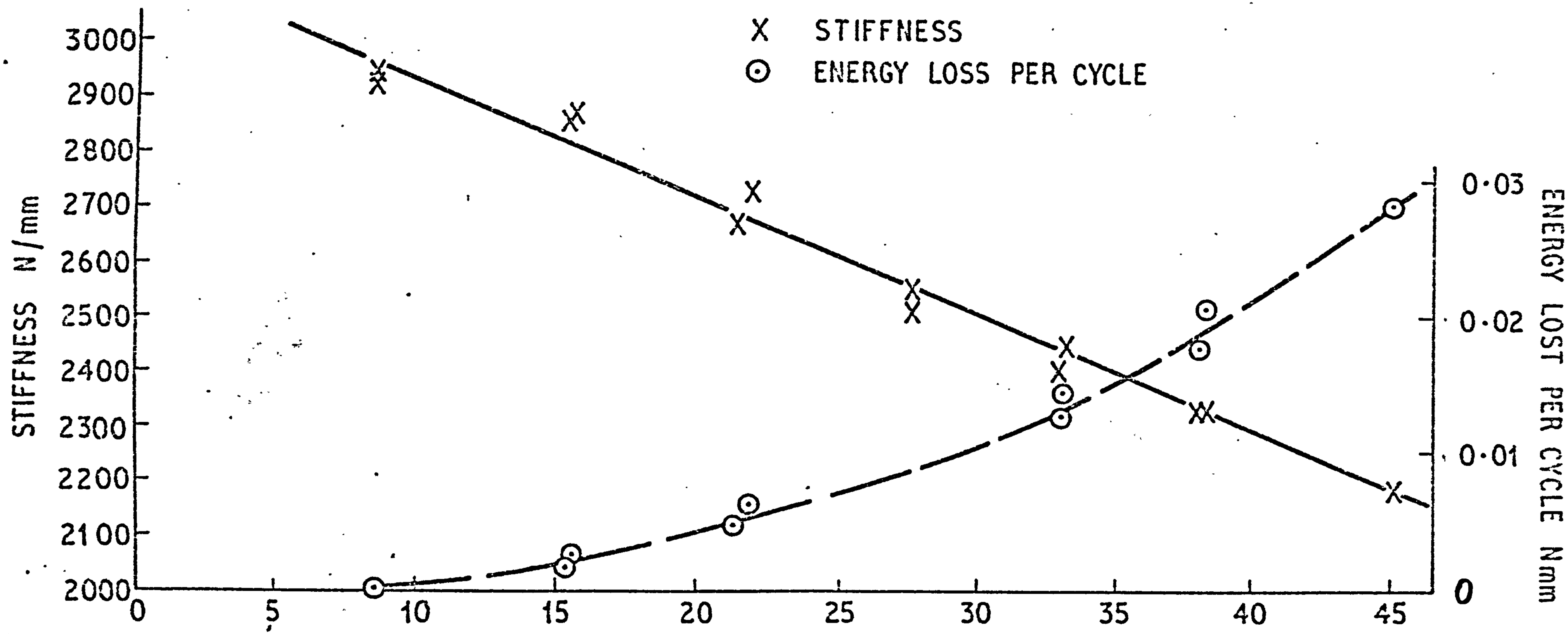

CORRECTION CURVES FOR STIFFNESS OF LOAD CELL AND ENERGY LOSS PER CYCLE IN LOAD CELL AND GRIPS (BONDED SPECIMEN TESTS)

FIG. 37

FIG. 38

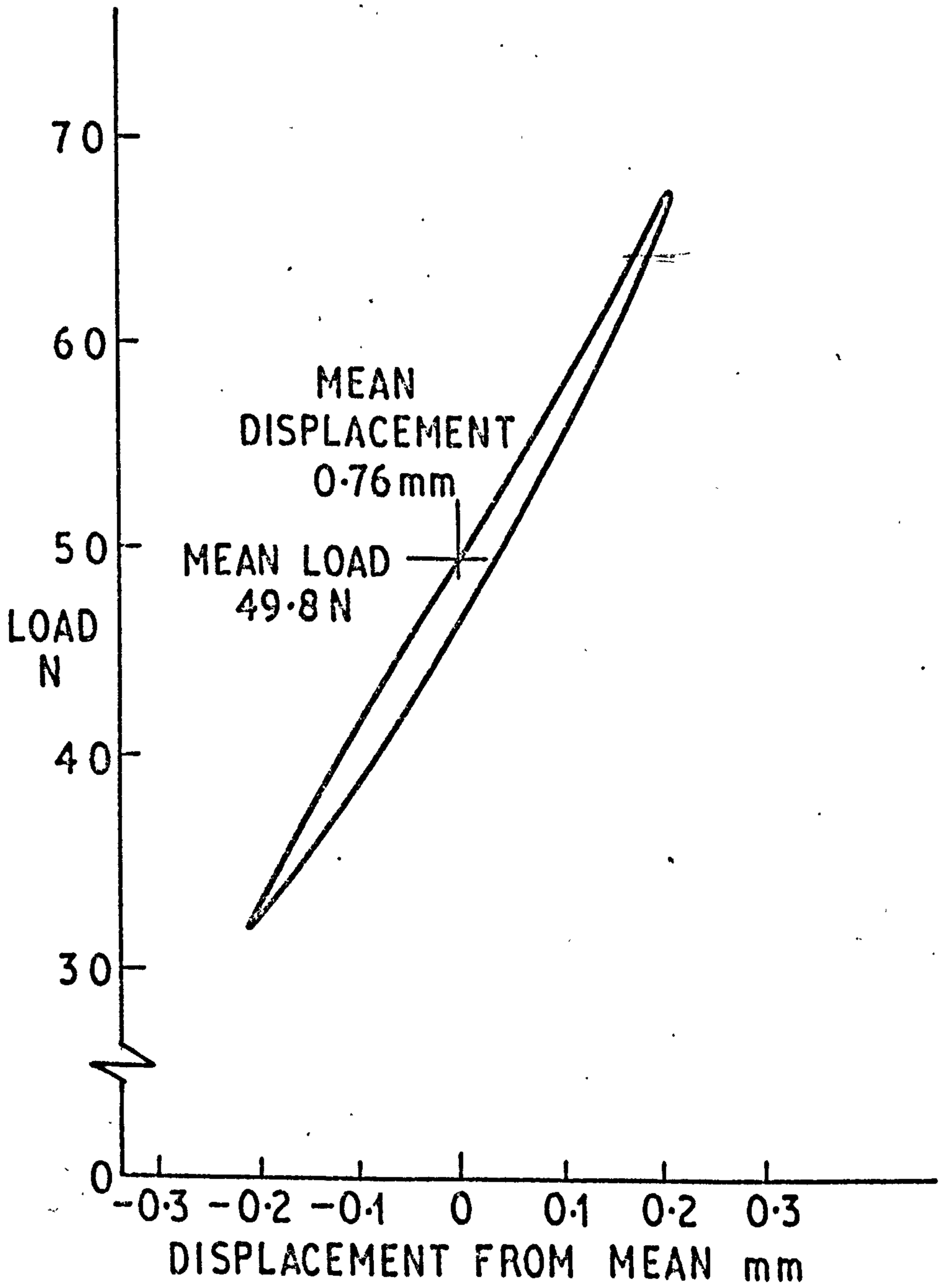

TYPICAL BONDED SPECIMEN HYSTERESIS LOOP
AT LOW AMPLITUDE OF OSCILLATION

FIG. 39

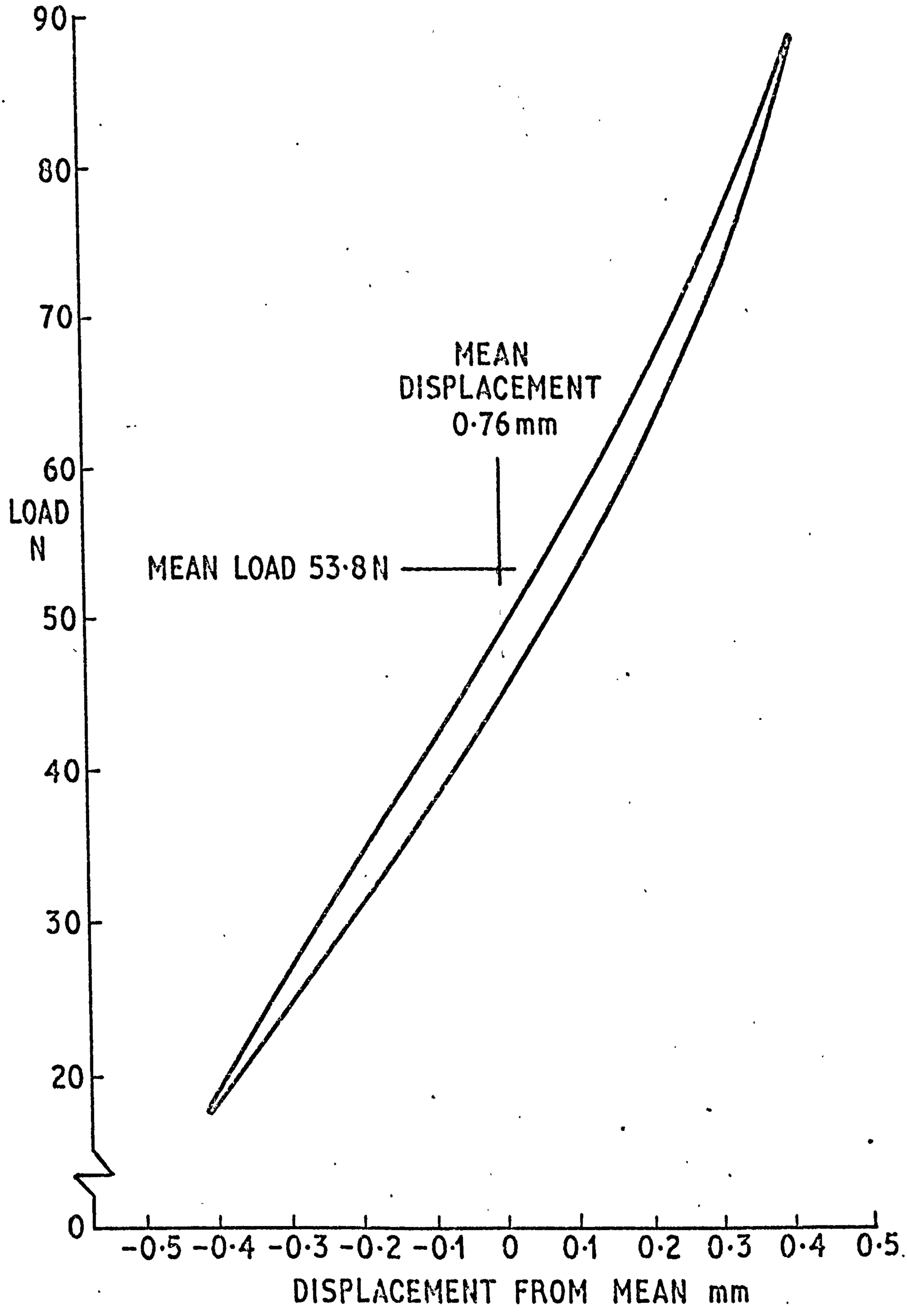

TYPICAL BONDED SPECIMEN HYSTERESIS LOOP
AT HIGHER AMPLITUDE OF OSCILLATION

FIG. 40

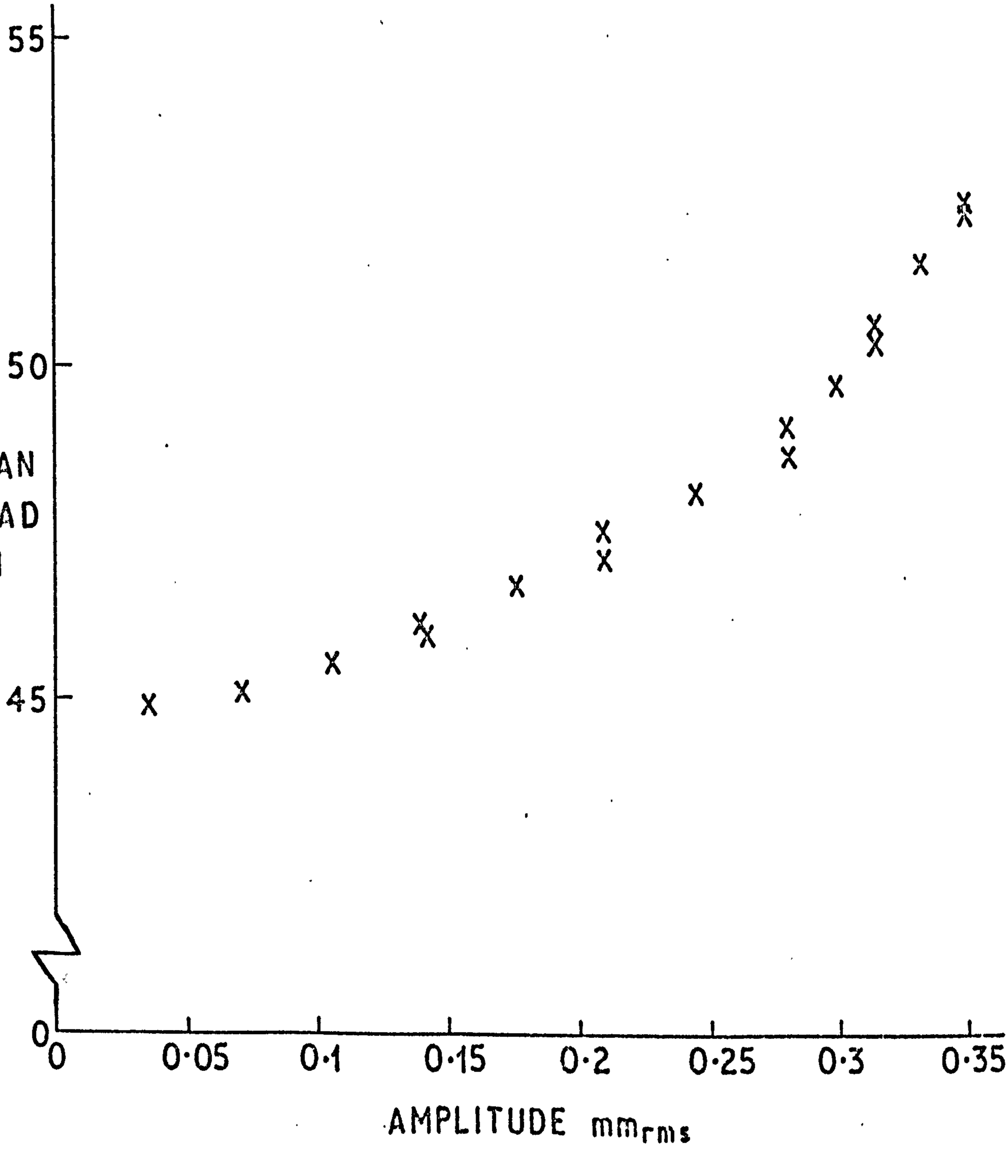

VARIATION IN MEAN LOAD WITH AMPLITUDE OF OSCILLATION (BONDED SPECIMEN)

FIG. 41

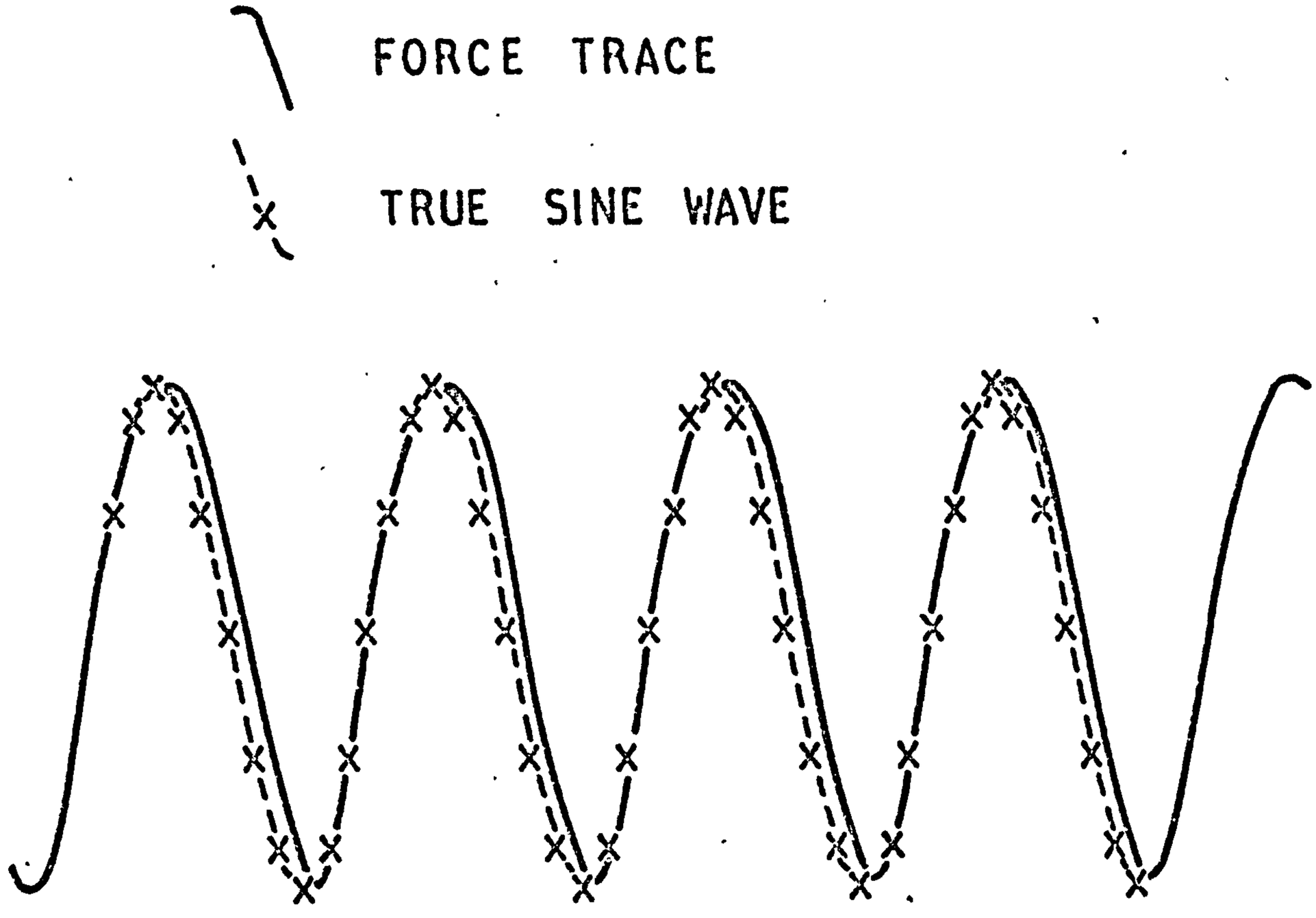

COMPARISON OF FORCE TRACE FROM
BONDED SPECIMEN HYSTERESIS LOOP AND
TRUE SINE WAVE

FIG. 42

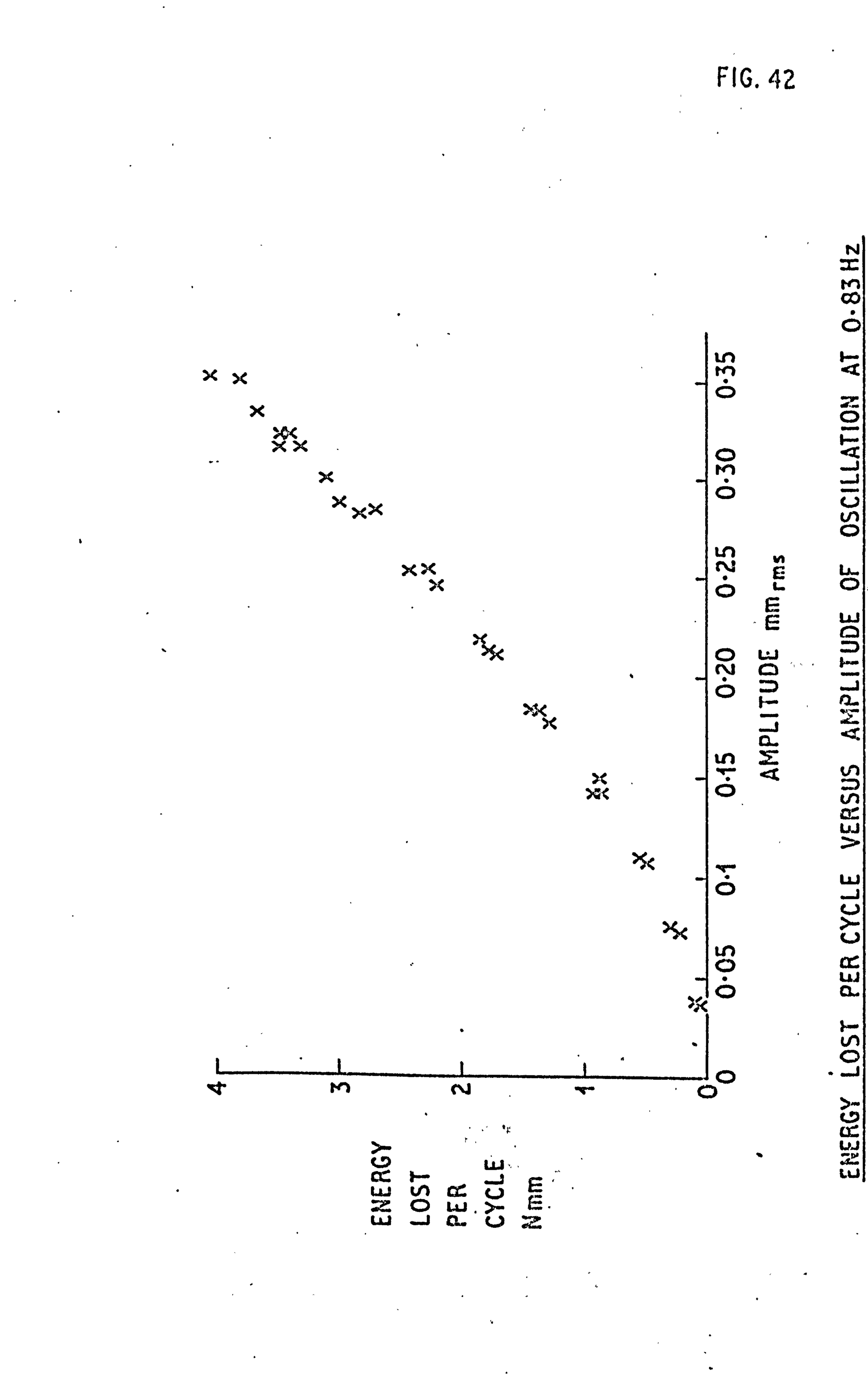
ENERGY LOST PER CYCLE VERSUS AMPLITUDE OF OSCILLATION AT 0·83 Hz
(BONDED SPECIMEN)
ENERGY LOST PER CYCLE Nmm
0
1
2
3
4
0·05
0·1
0·15
0·20
0·25
0·30
0·35
AMPLITUDE mm rms

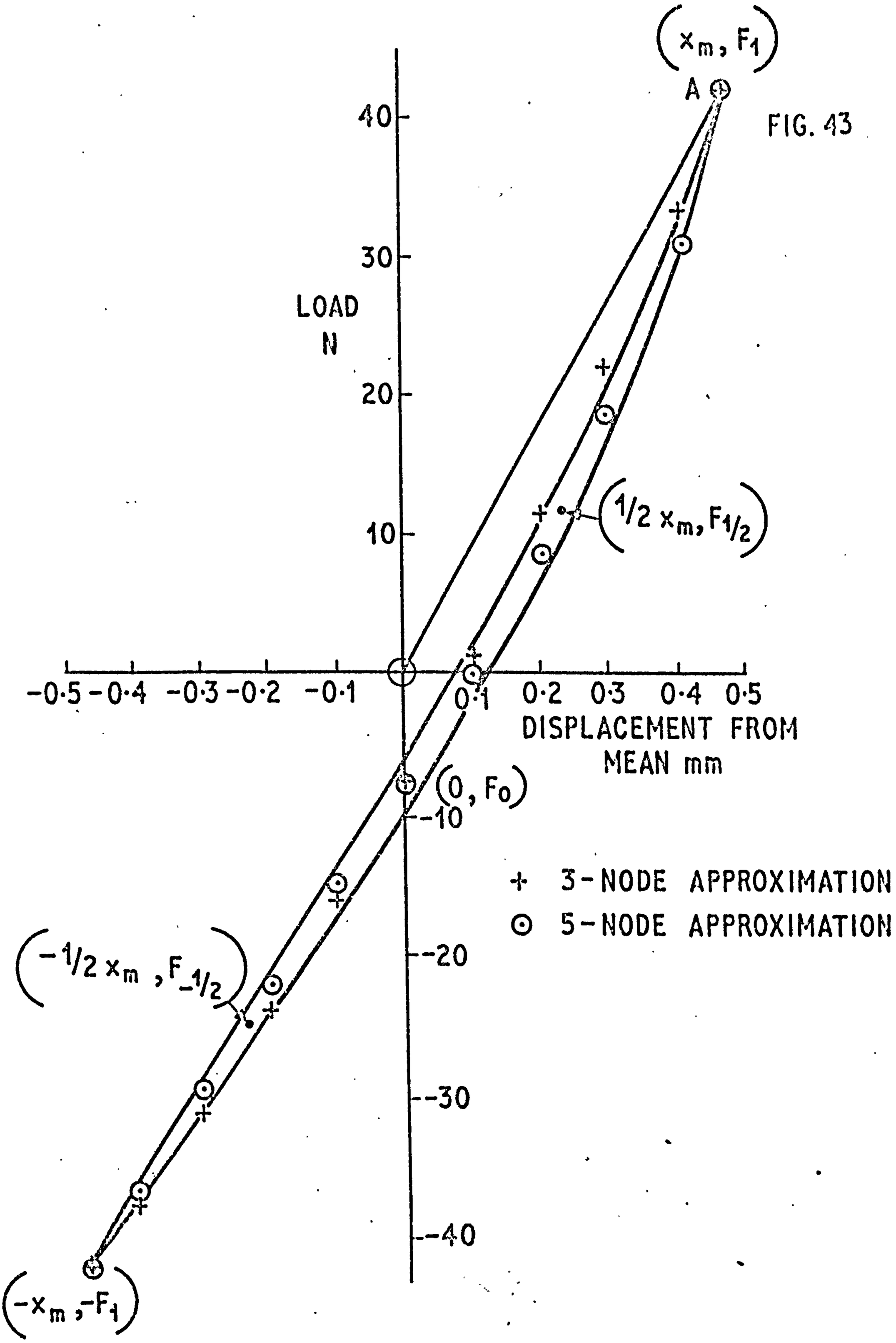

FIG. 43

SAMPLE BONDED SPECIMEN HYSTERESIS LOOP WITH POINTS CALCULATED FROM APPROXIMATING POLYNOMIALS

FIG. 44

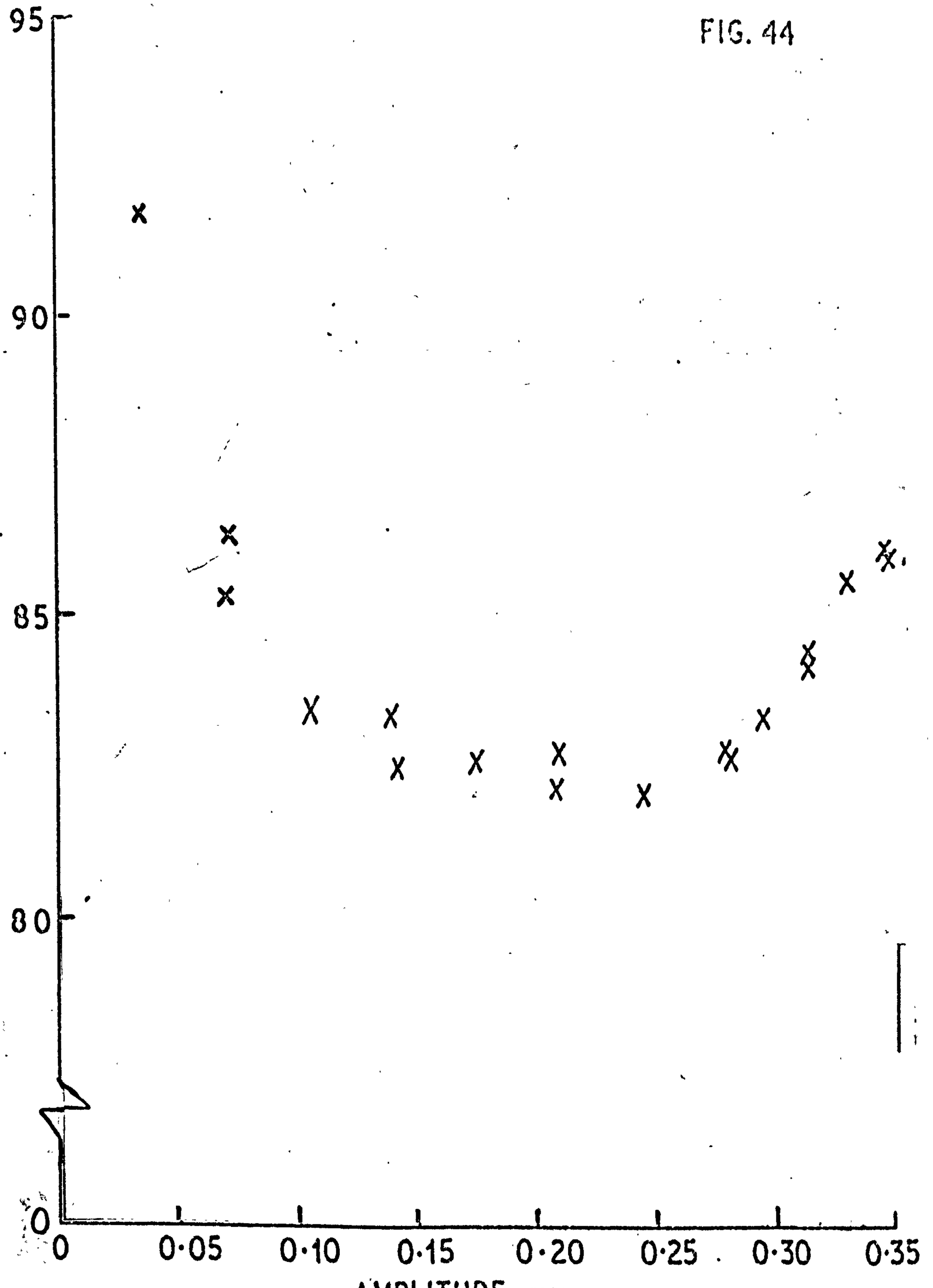

AVERAGE STIFFNESS (K_{mean}) VERSUS AMPLITUDE OF OSCILLATION AT 0·83 Hz (BONDED SPECIMEN)

FIG. 45

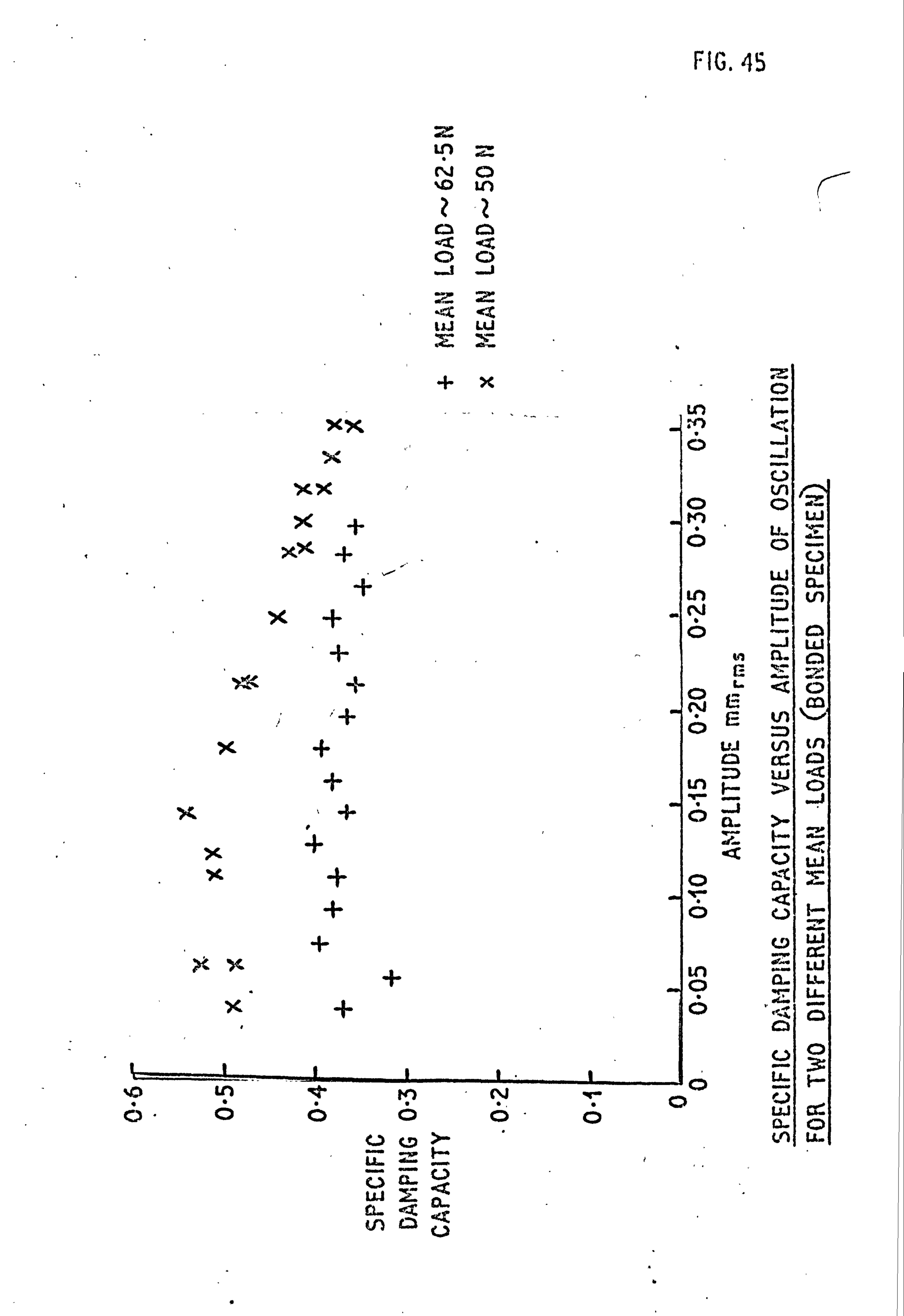
SPECIFIC DAMPING CAPACITY VERSUS AMPLITUDE OF OSCILLATION FOR TWO DIFFERENT MEAN LOADS (BONDED SPECIMEN)
SPECIFIC DAMPING CAPACITY
0
0·1
0·2
0·3
0·4
0·5
0·6
AMPLITUDE mm rms
0·05
0·10
0·15
0·20
0·25
0·30
0·35
+ MEAN LOAD ~ 62·5 N
× MEAN LOAD ~ 50 N

FIG. 46

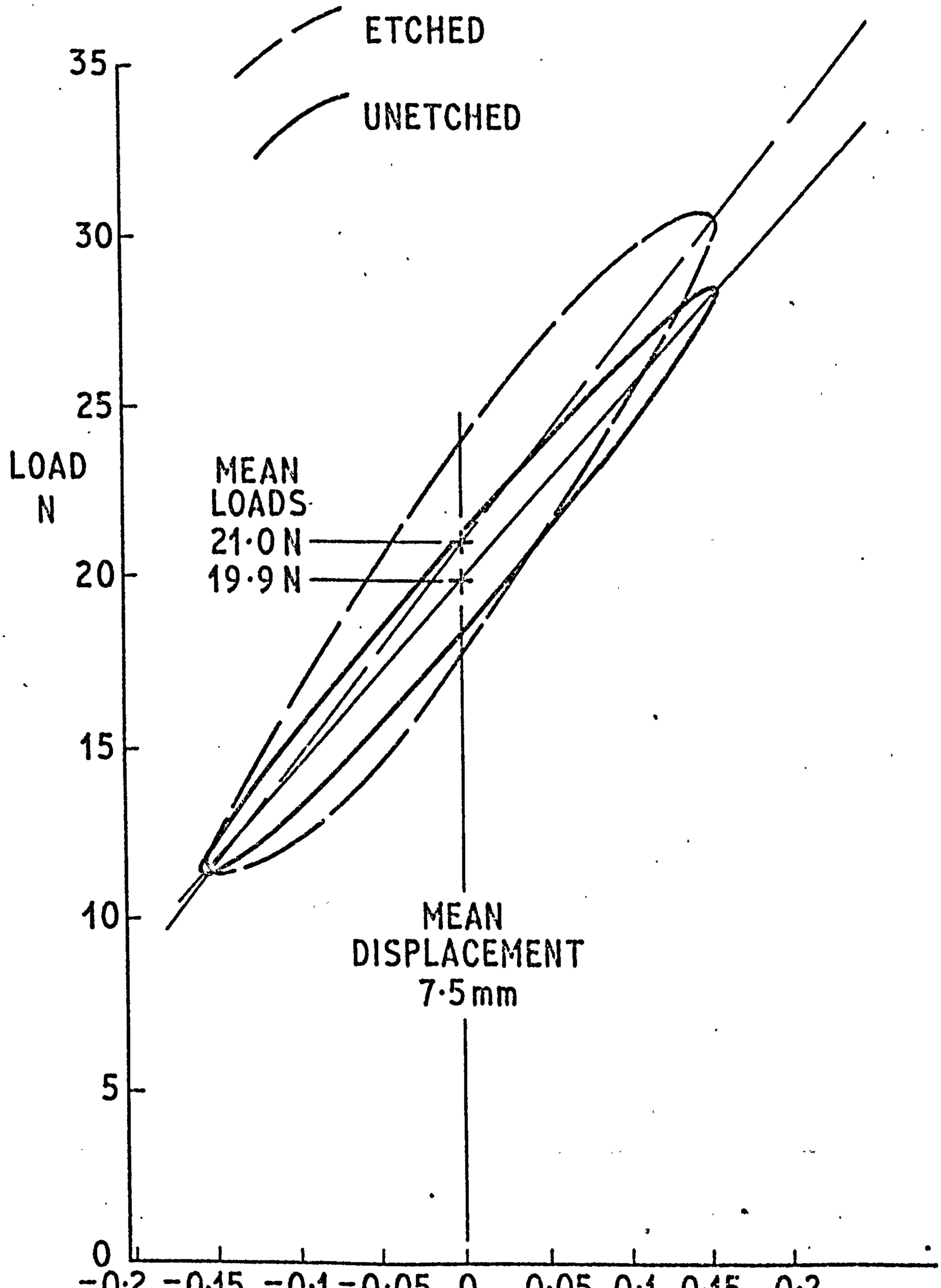

COMPARISON OF TYPICAL UNBONDED SPECIMEN
HYSTERESIS LOOPS AT LOW AMPLITUDE OF OSCILLATION

FIG. 47

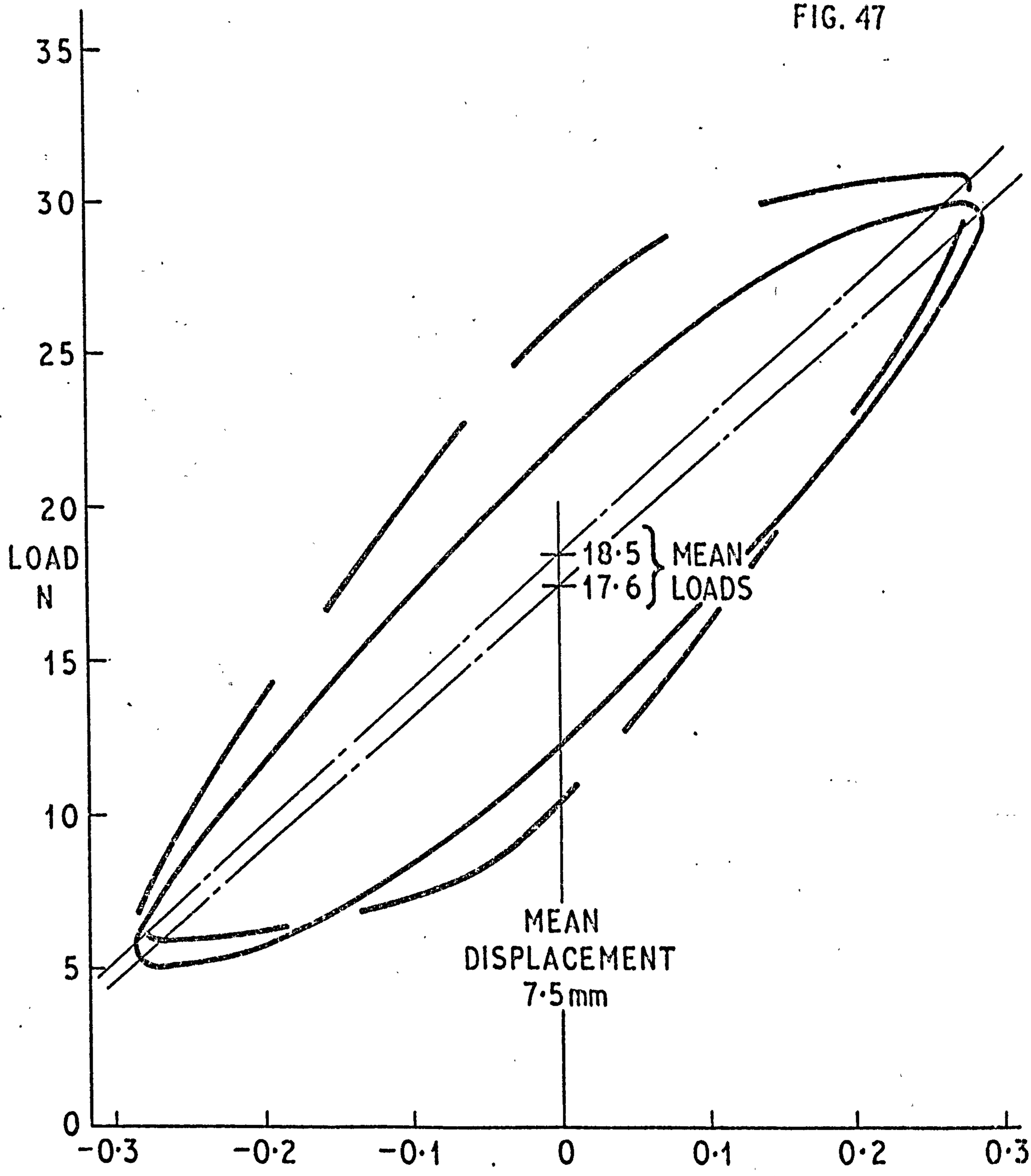

COMPARISON OF TYPICAL UNBONDED SPECIMEN LOOPS AT INTERMEDIATE AMPLITUDE OF OSCILLATION

FIG. 48

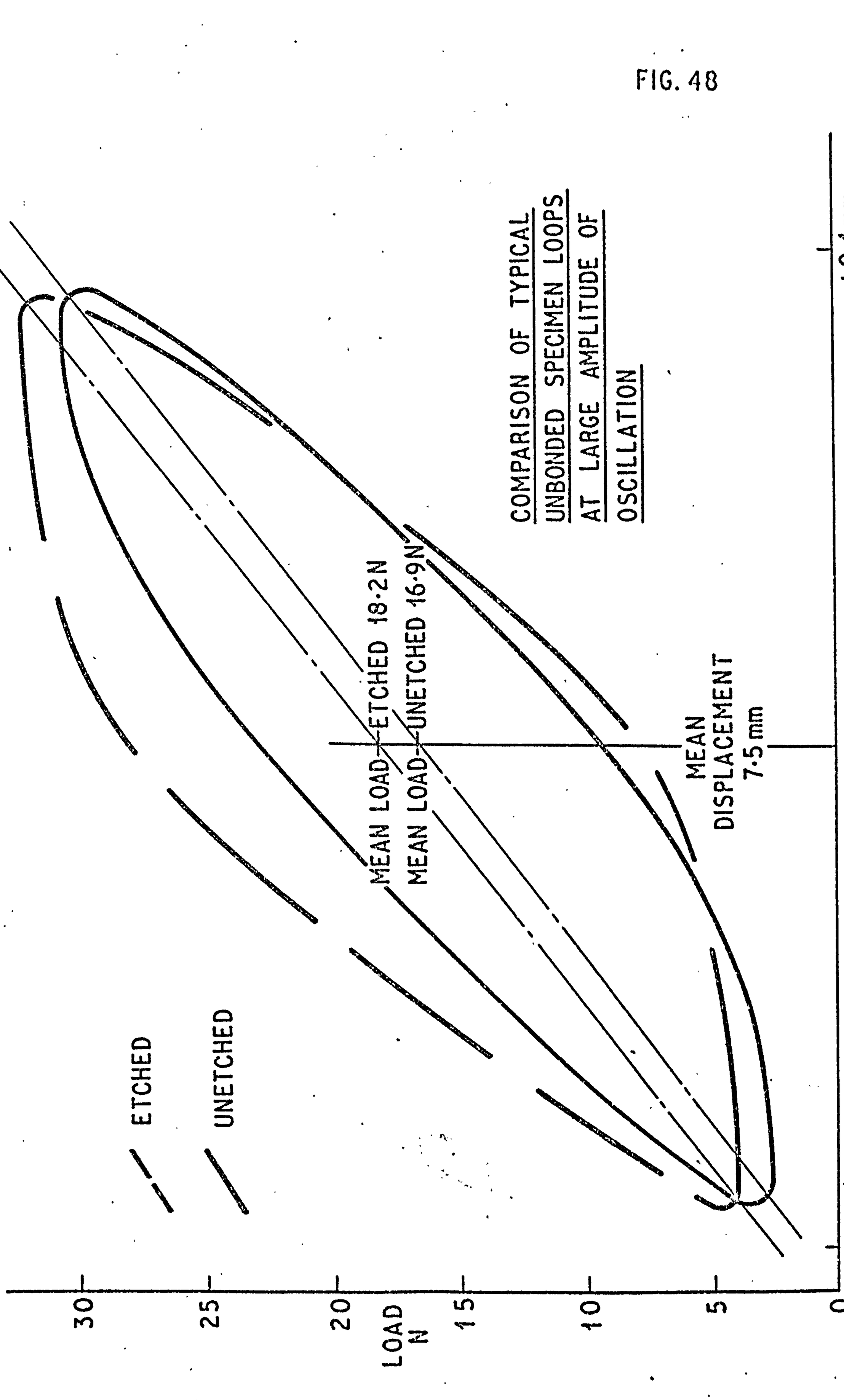
COMPARISON OF TYPICAL
UNBONDED SPECIMEN LOOPS
AT LARGE AMPLITUDE OF
OSCILLATION
+0·4 mm
MEAN
DISPLACEMENT
7·5 mm
−0·4 mm
ETCHED 18·2N
UNETCHED 16·9N
MEAN LOAD — ETCHED
MEAN LOAD — UNETCHED
ETCHED
UNETCHED
LOAD
N
0
5
10
15
20
25
30

FIG. 49

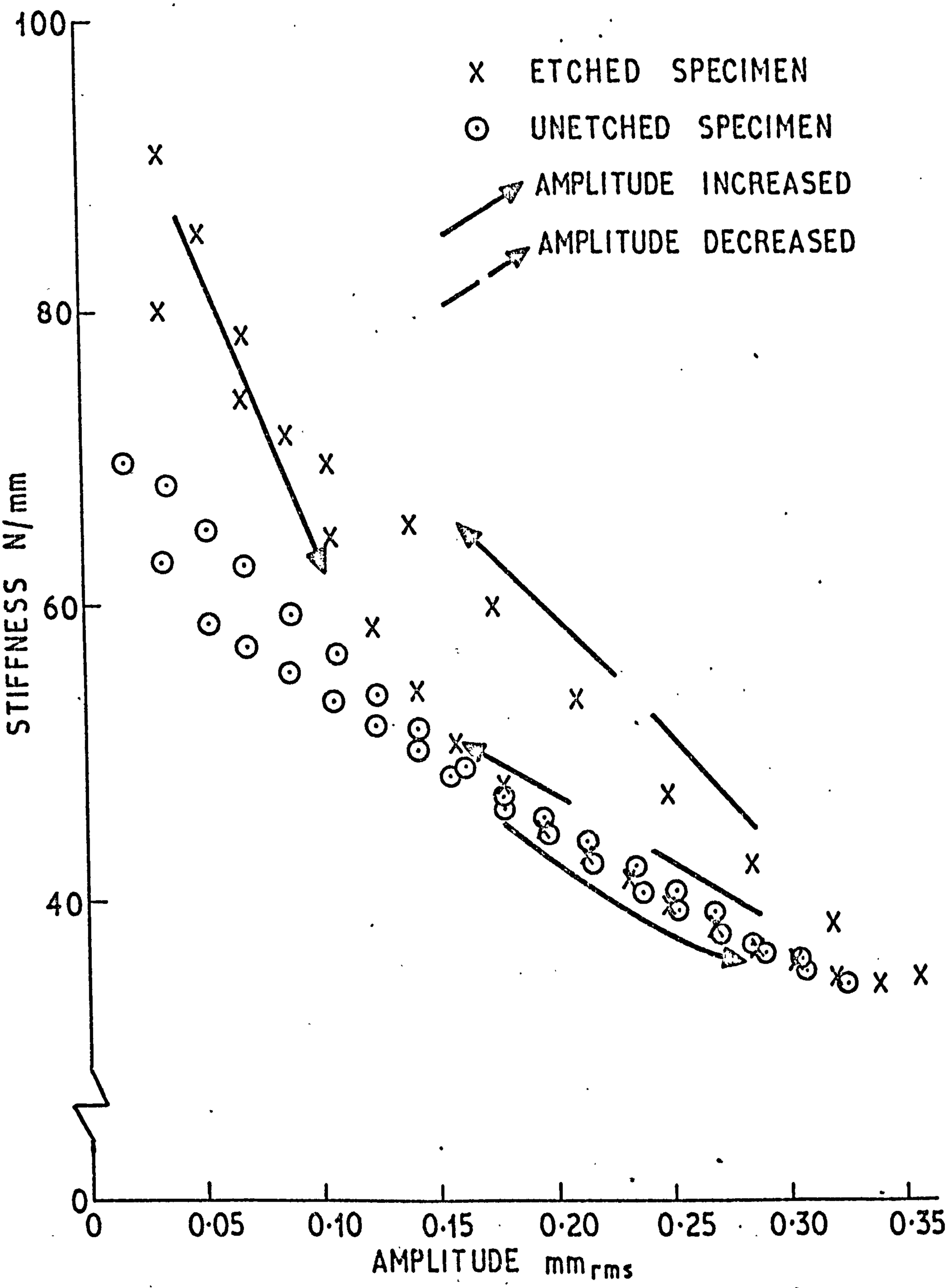

STIFFNESS VERSUS AMPLITUDE OF OSCILLATION AT 0·83 Hz (UNBONDED SPECIMENS)

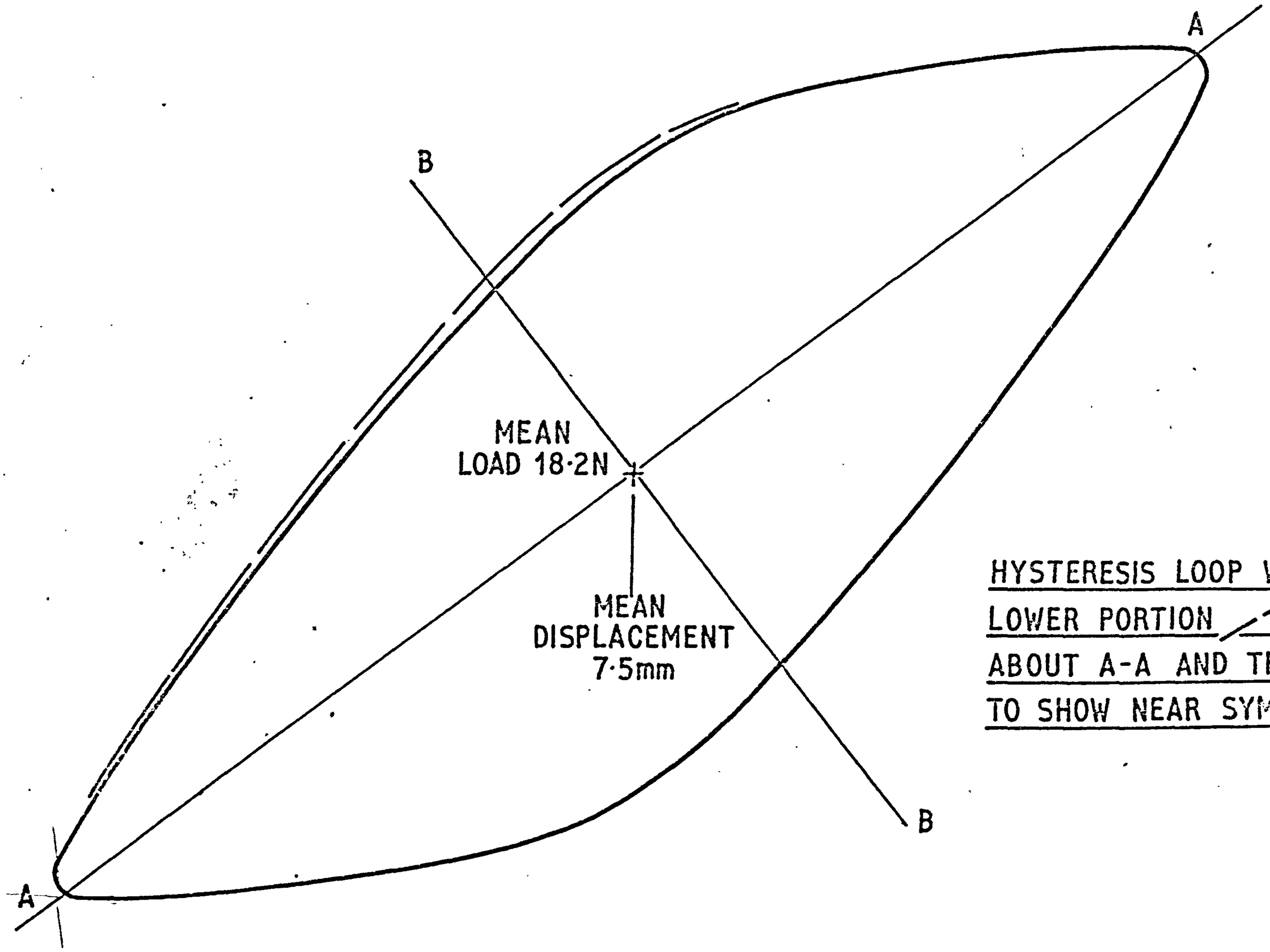

HYSTERESIS LOOP WITH LOWER PORTION ROTATED ABOUT A-A AND THEN B-B TO SHOW NEAR SYMMETRY

FIG. 50

FIG. 51

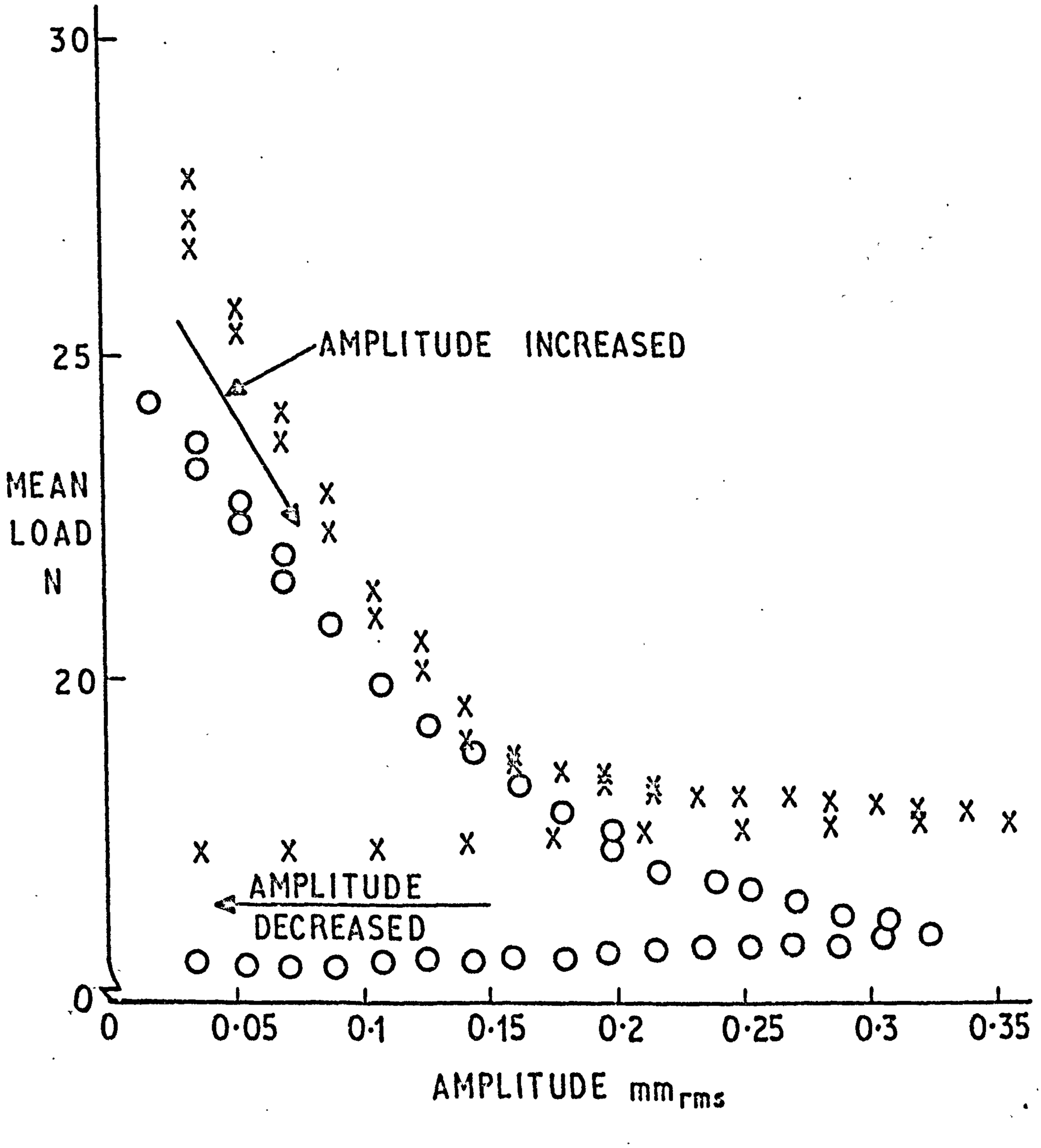

VARIATION IN MEAN LOAD WITH AMPLITUDE OF OSCILLATION (UNBONDED SPECIMENS)

FIG. 52

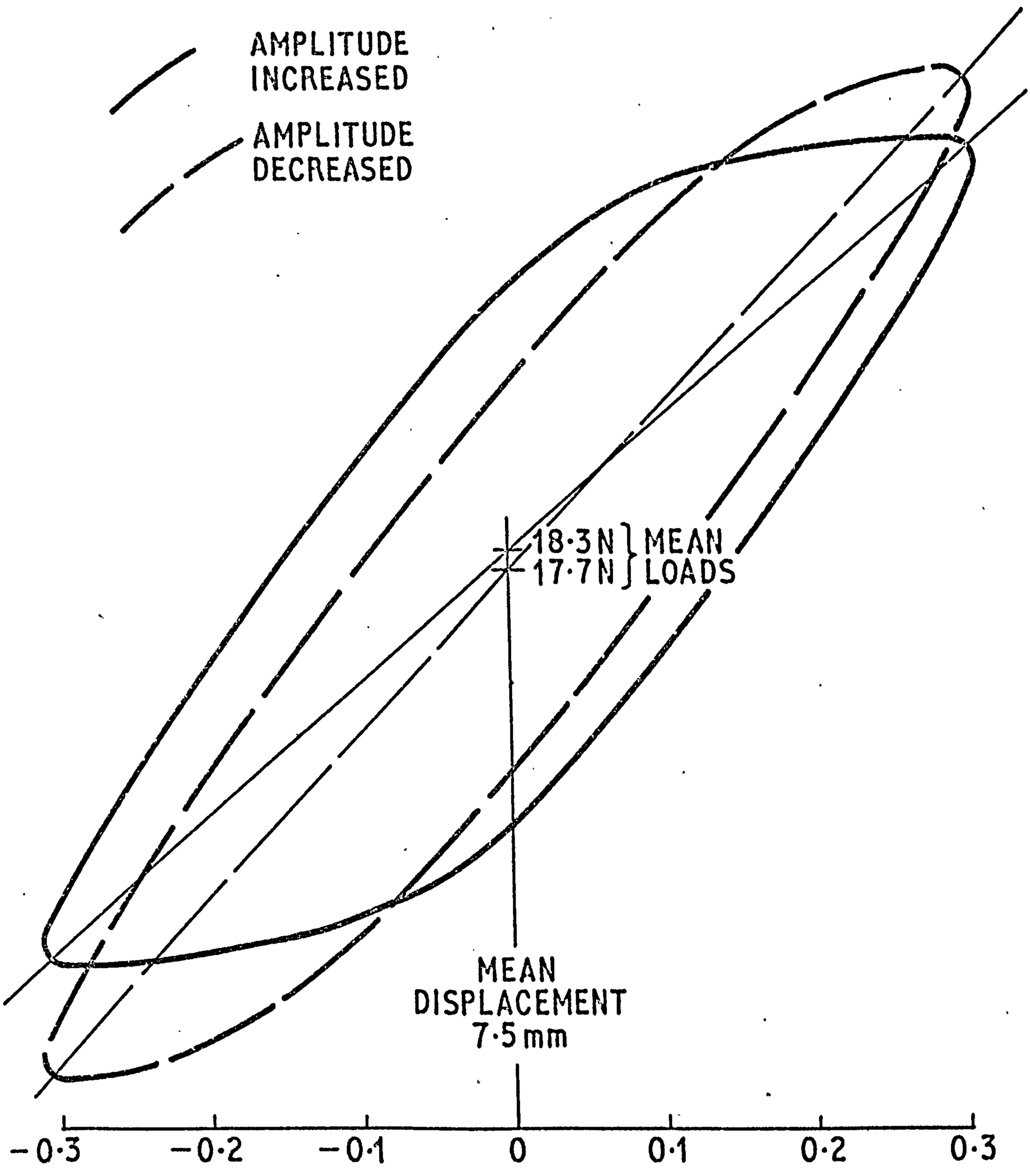

COMPARISON OF ETCHED SPECIMEN LOOPS WHEN AMPLITUDE WAS INCREASED AND DECREASED

FIG. 53

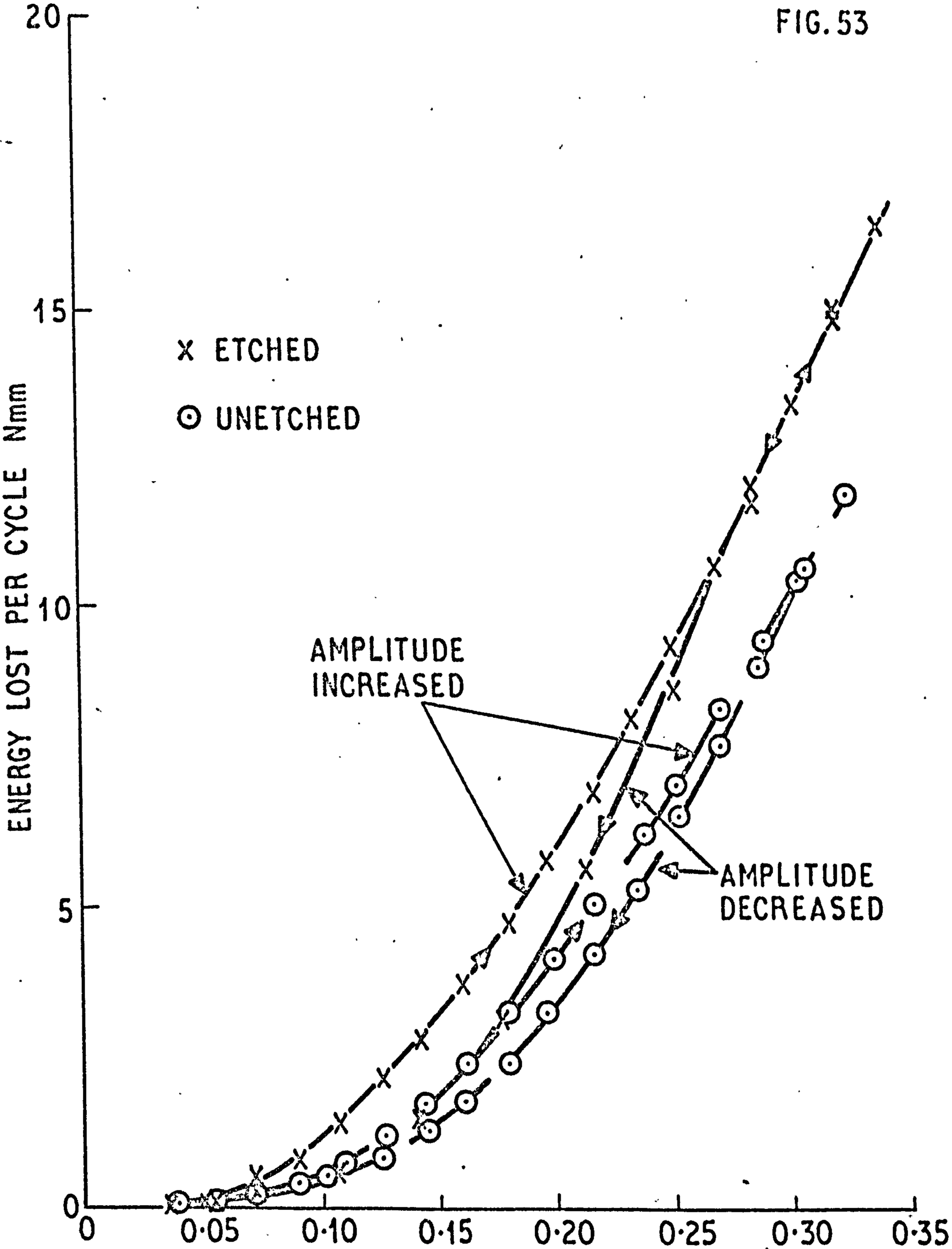

ENERGY LOST PER CYCLE VERSUS AMPLITUDE
OF OSCILLATION AT 0·83 Hz (UNBONDED SPECIMENS)

FIG. 54

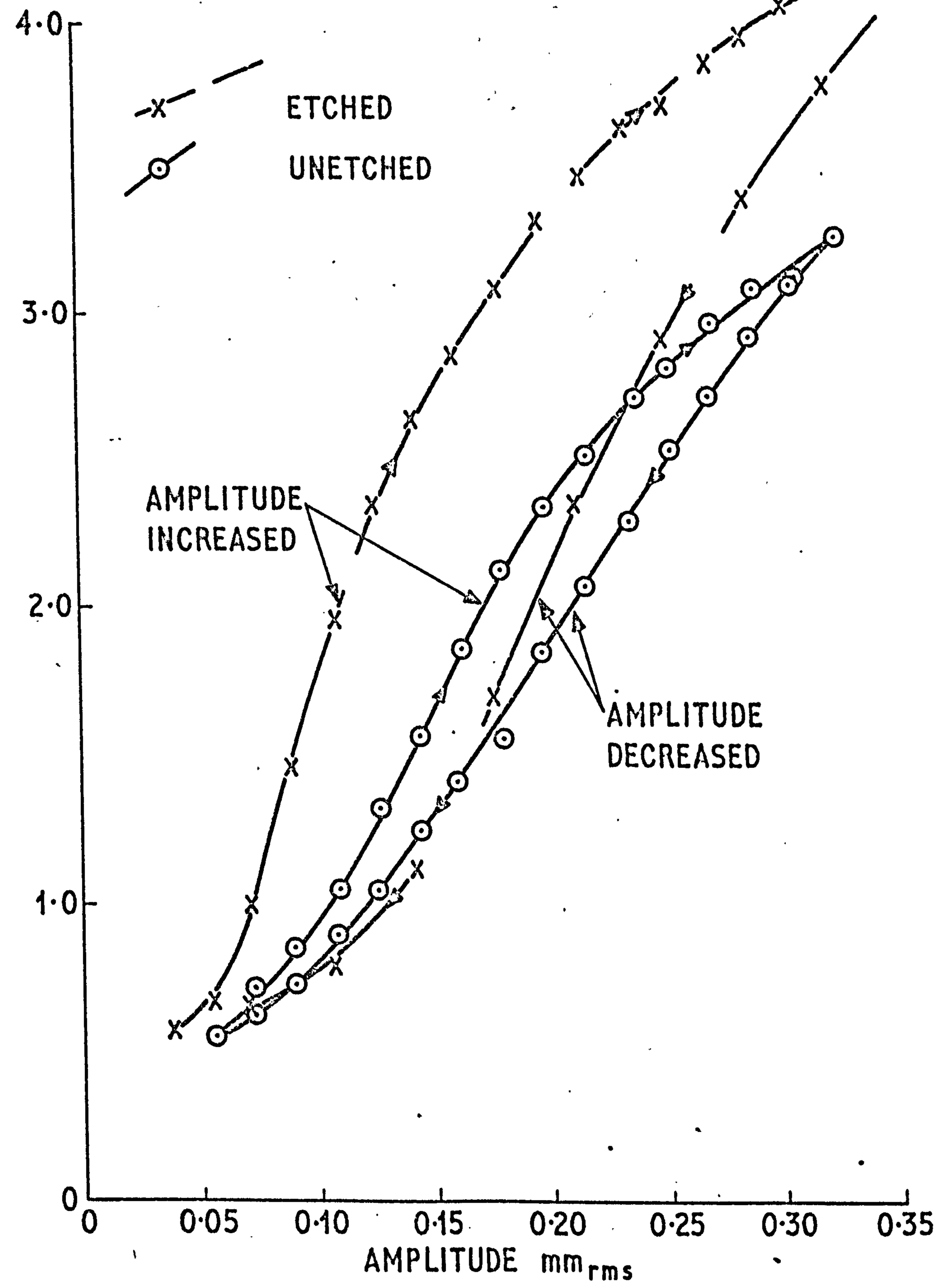

SPECIFIC DAMPING CAPACITY VERSUS AMPLITUDE OF OSCILLATION AT 0·83Hz (UNBONDED SPECIMENS)

FIG. 55

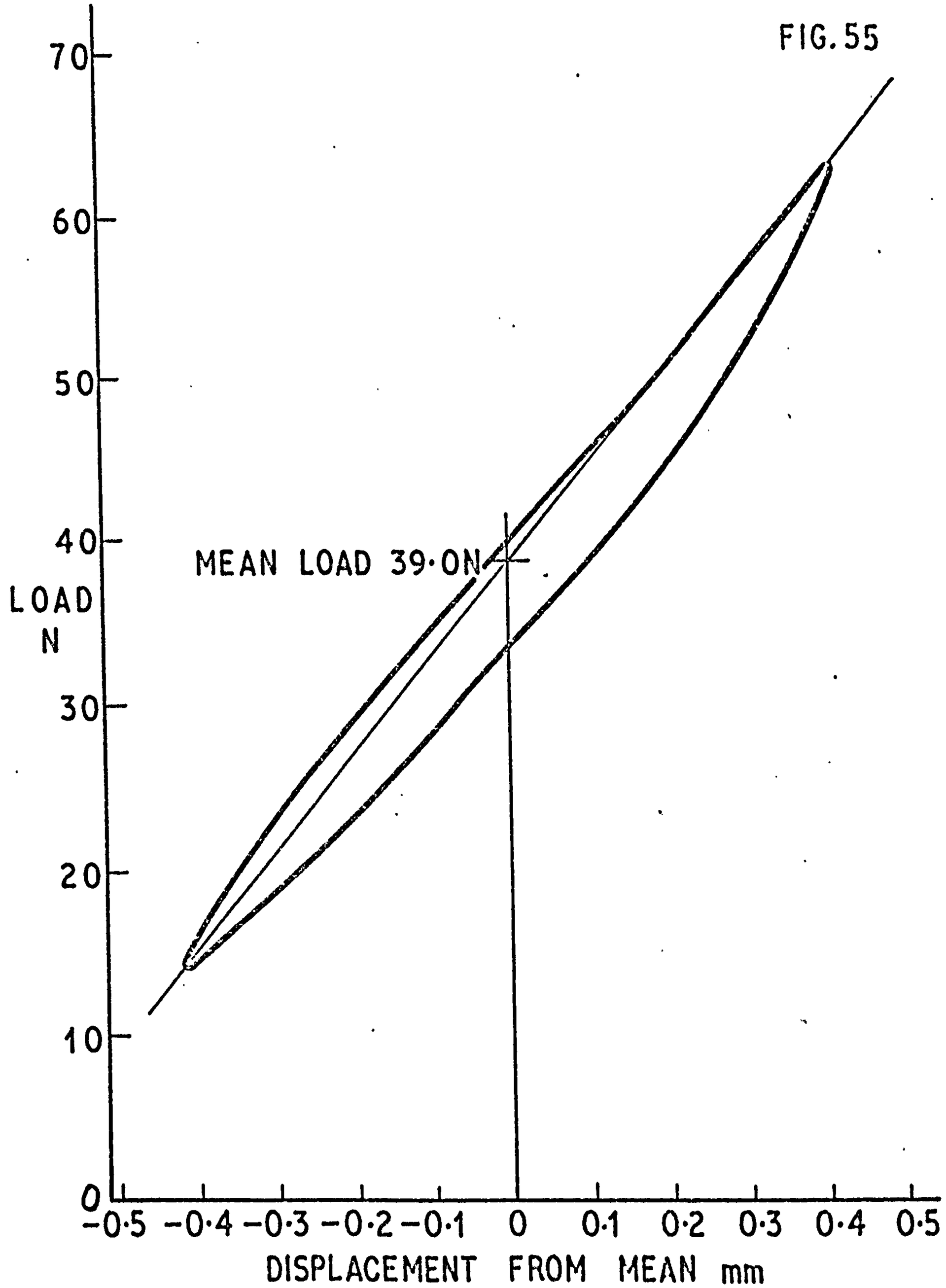

SAMPLE OF HYSTERESIS LOOP FROM BONDED SPECIMEN WHICH SHOWED LOWER STIFFNESS AND HIGHER DAMPING THAN OTHER BONDED SPECIMENS — THE INTERMEDIATE SPECIMEN

FIG. 56

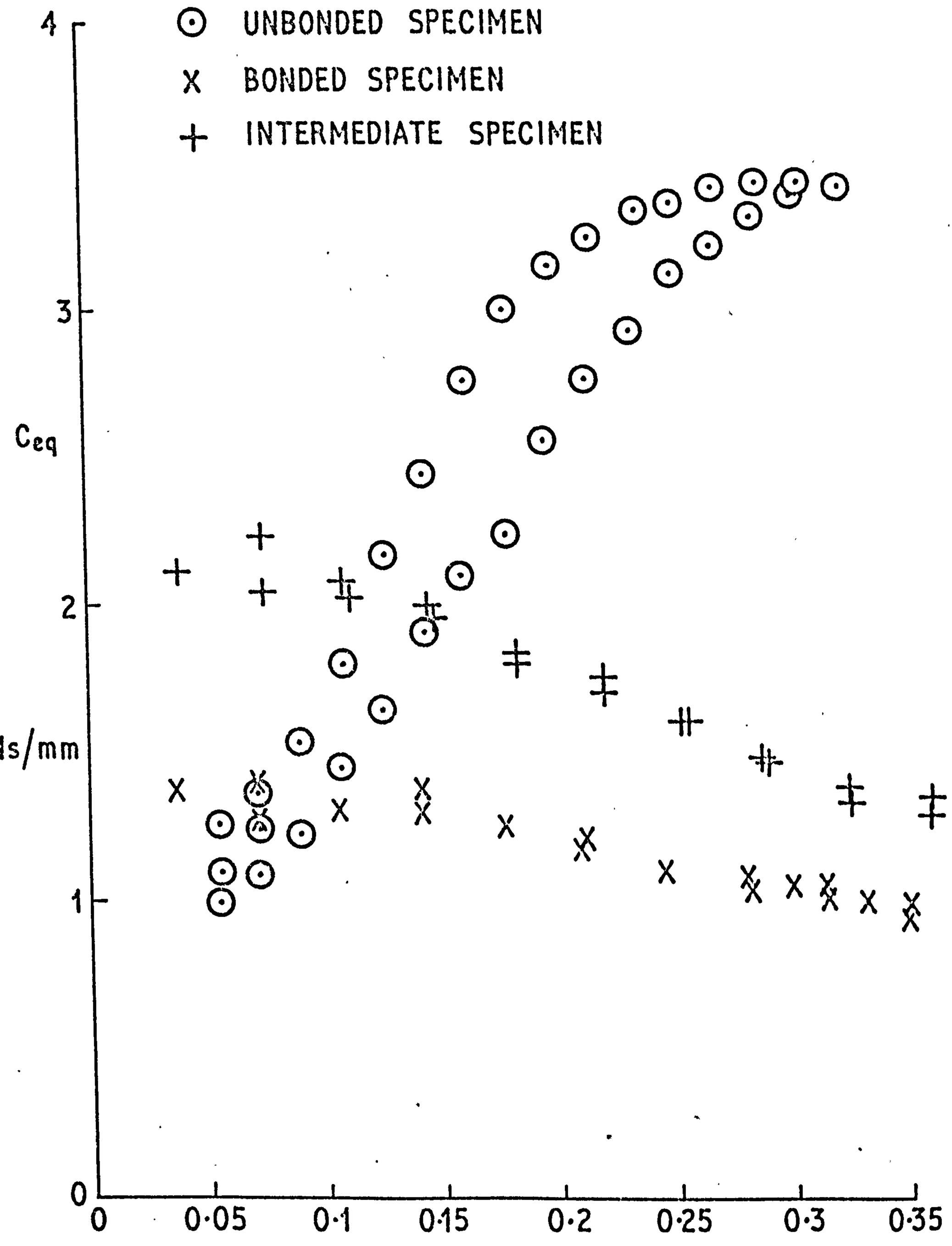

COMPARISON OF EQUIVALENT DAMPING CONSTANTS
CALCULATED FROM EXPERIMENTAL RESULTS

FIG. 57

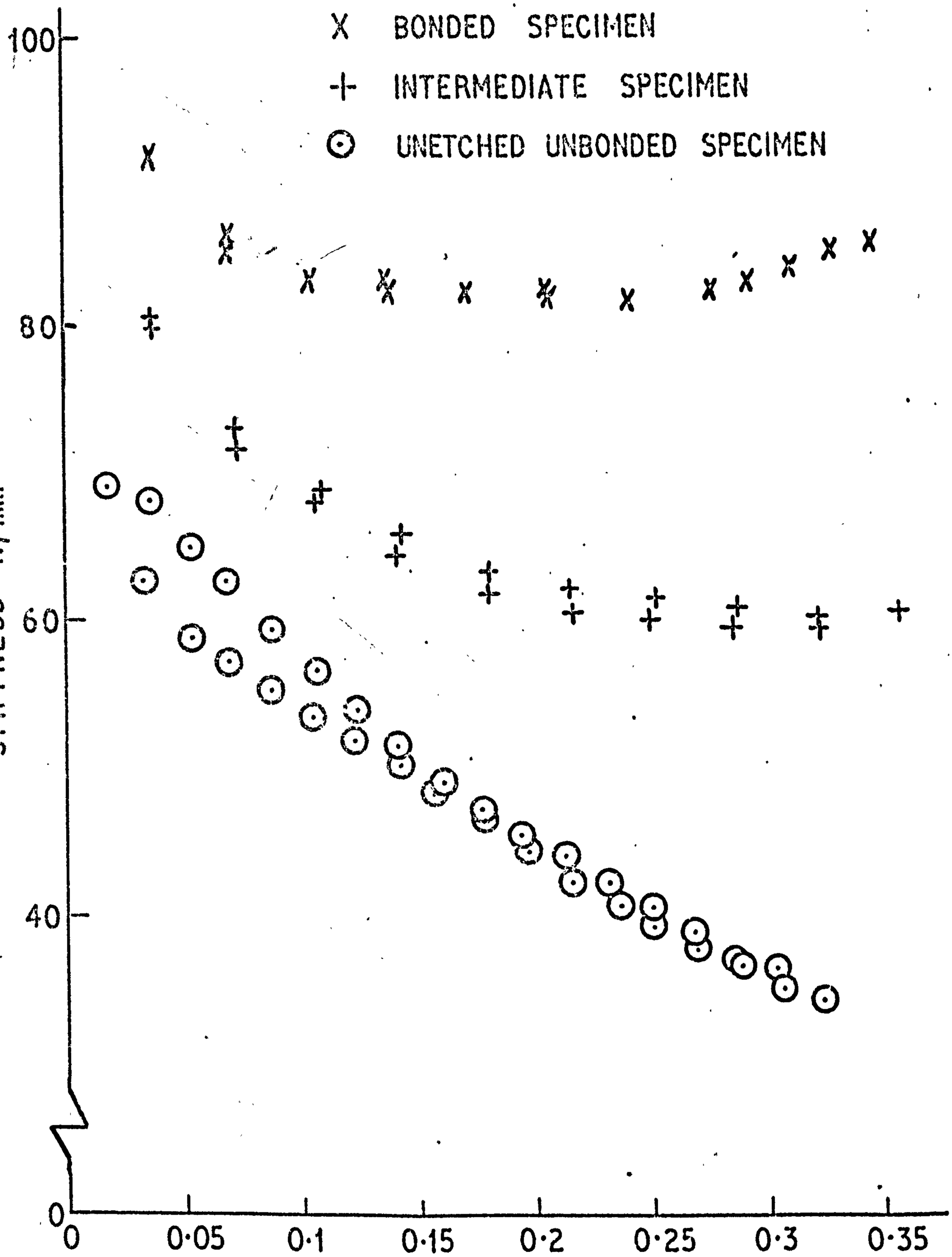

COMPARISON OF STIFFNESSES OF BONDED, UNBONDED, AND INTERMEDIATE SPECIMENS

FIG. 58

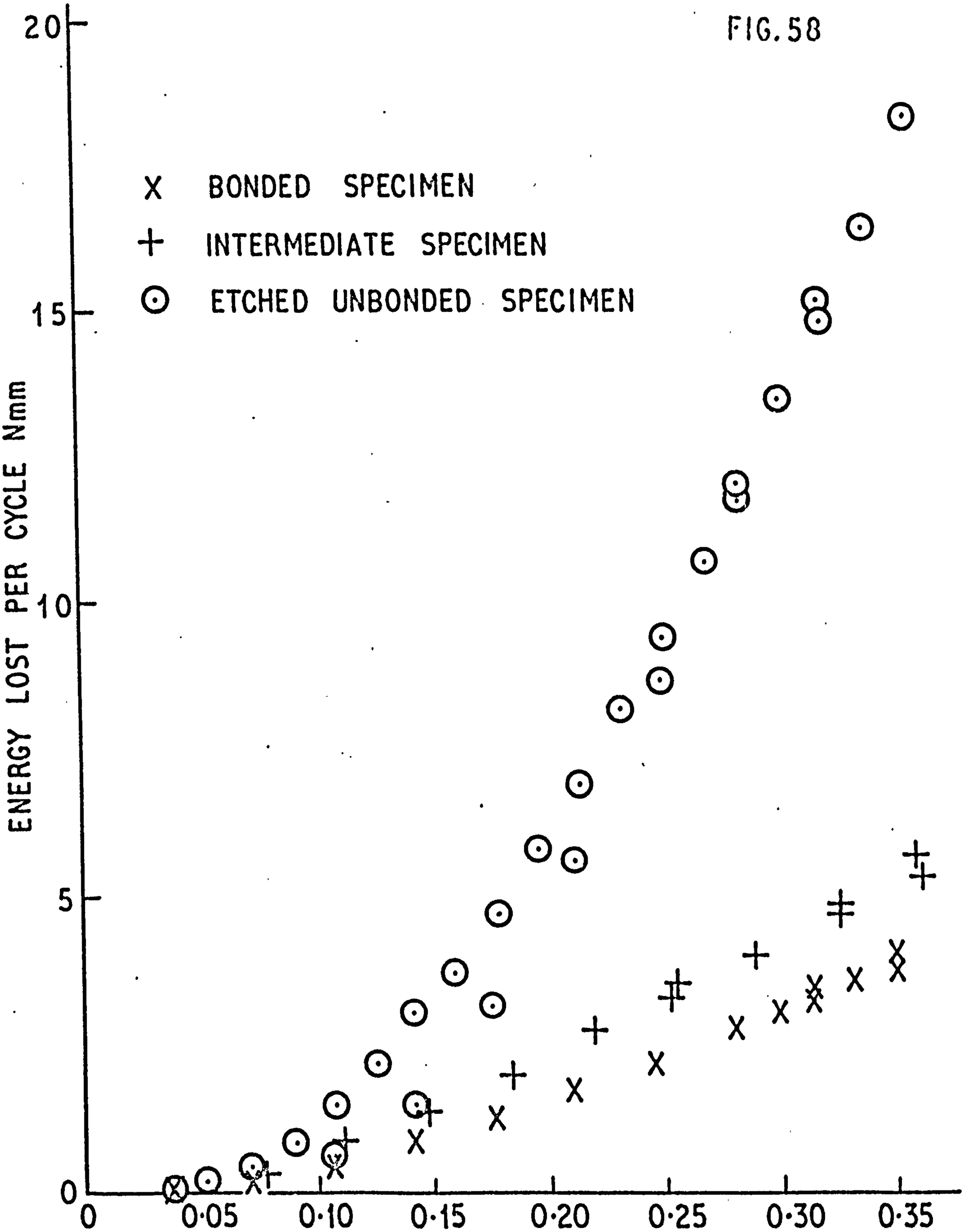

COMPARISON OF ENERGY LOST PER CYCLE OF BONDED, UNBONDED, AND INTERMEDIATE SPECIMENS

FIG. 59

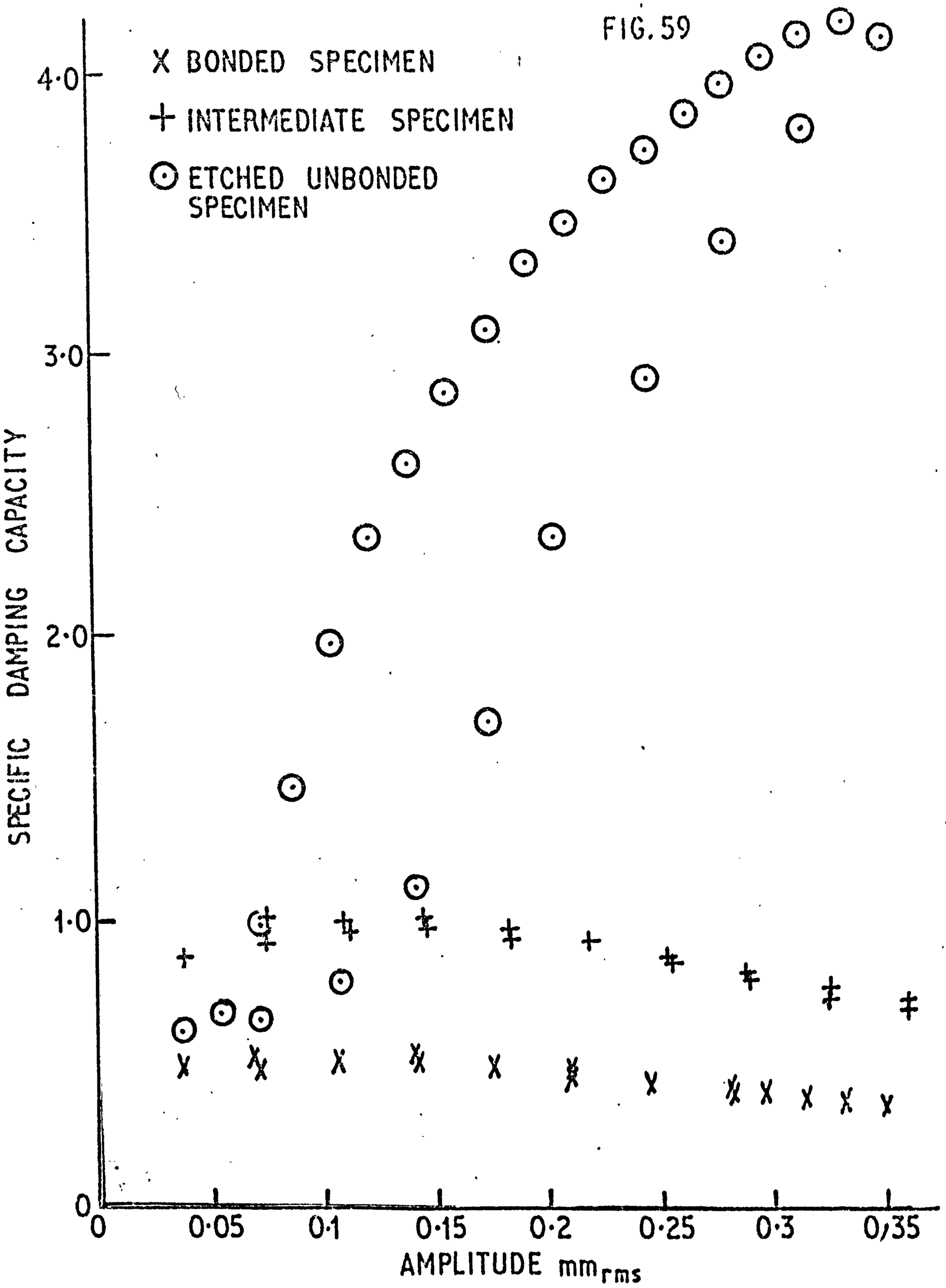

COMPARISON OF SPECIFIC DAMPING CAPACITY OF BONDED, UNBONDED, AND INTERMEDIATE SPECIMENS

FIG. 60

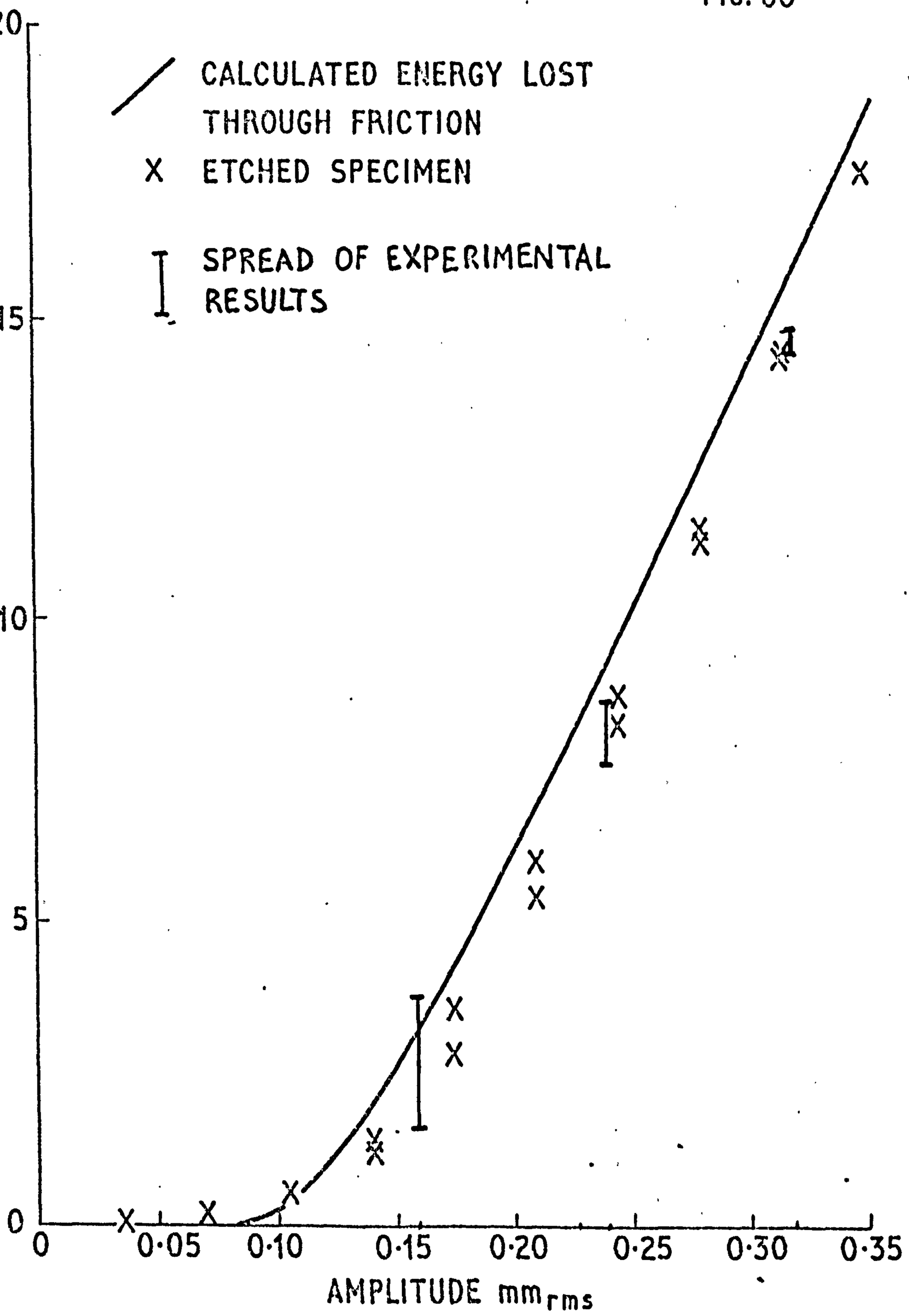

COMPARISON OF EXPERIMENTAL RESULT AND CALCULATED ENERGY LOST THROUGH FRICTION

FIG. 61

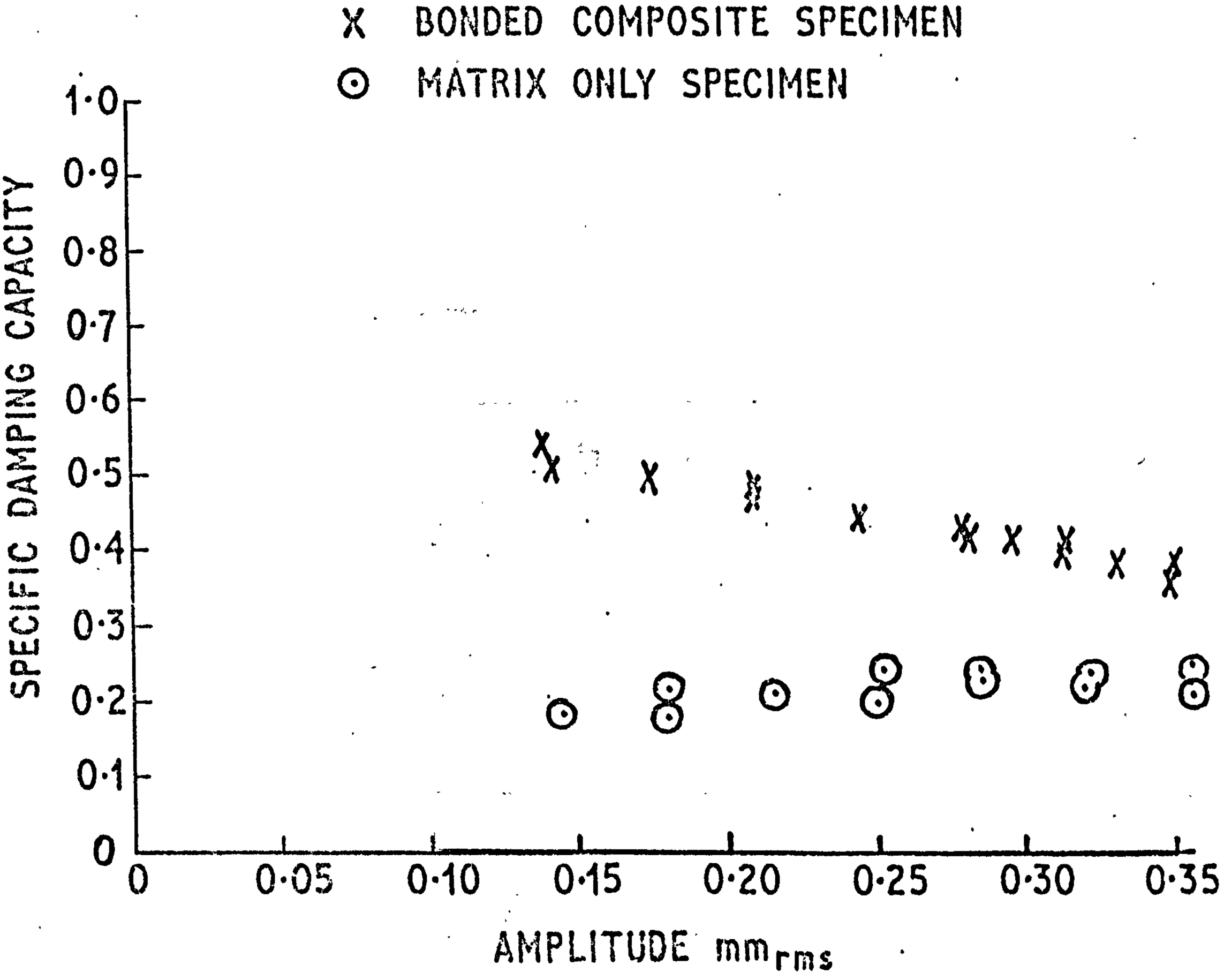

COMPARISON OF BONDED COMPOSITE SPECIMEN
SPECIFIC DAMPING CAPACITY
WITH MATRIX ONLY SPECIMEN

Specimen **S** is clamped to the back plate on the frame and to the mass **M** in both cases by the means shown in figure 63. The accelerometer **A** is screwed on to the mass **M** which in turn is screwed via force gauge **F** to vibrator **V** which sits on bridge piece **B** thus independently suspending vibrator and frame.

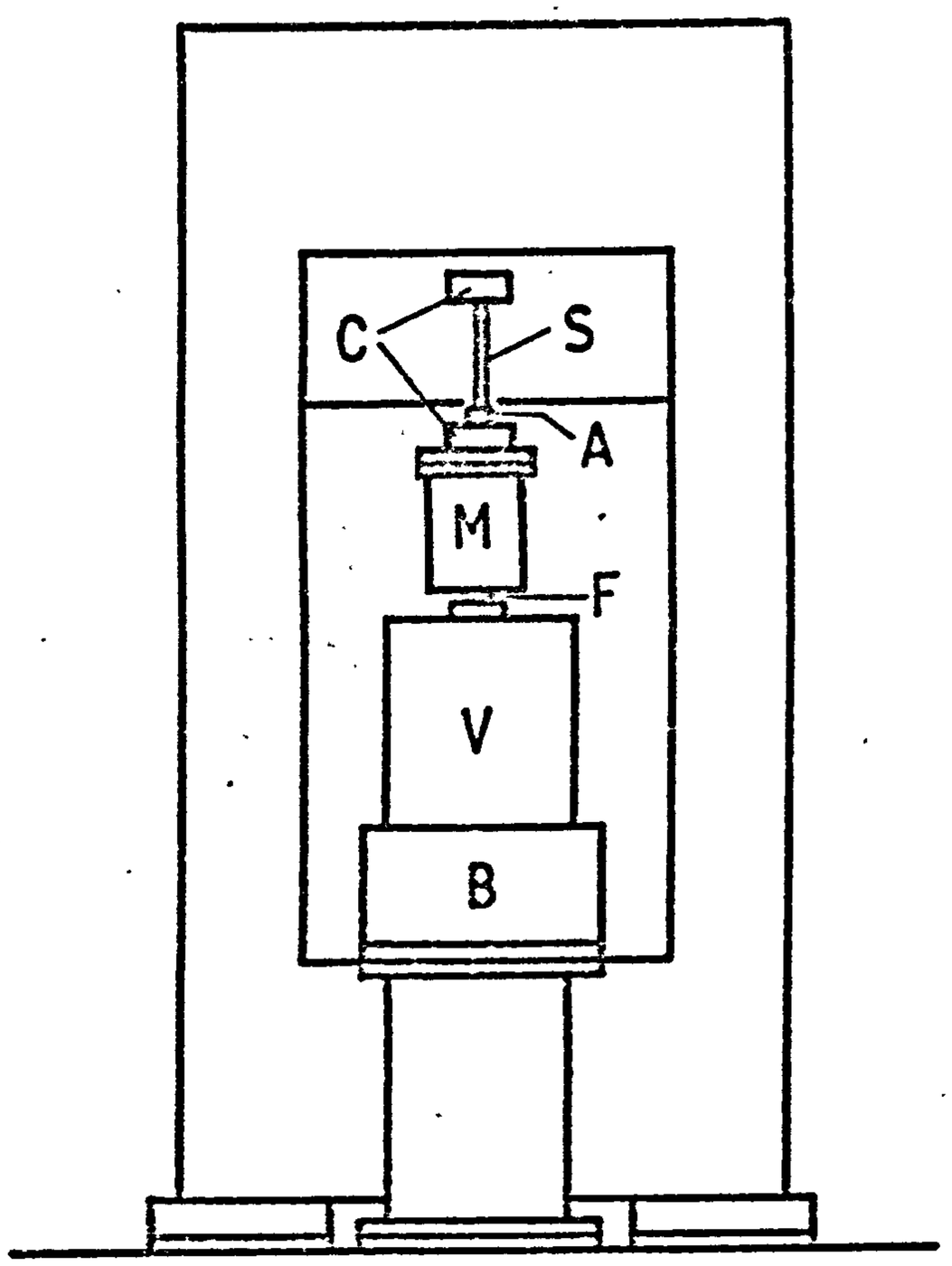

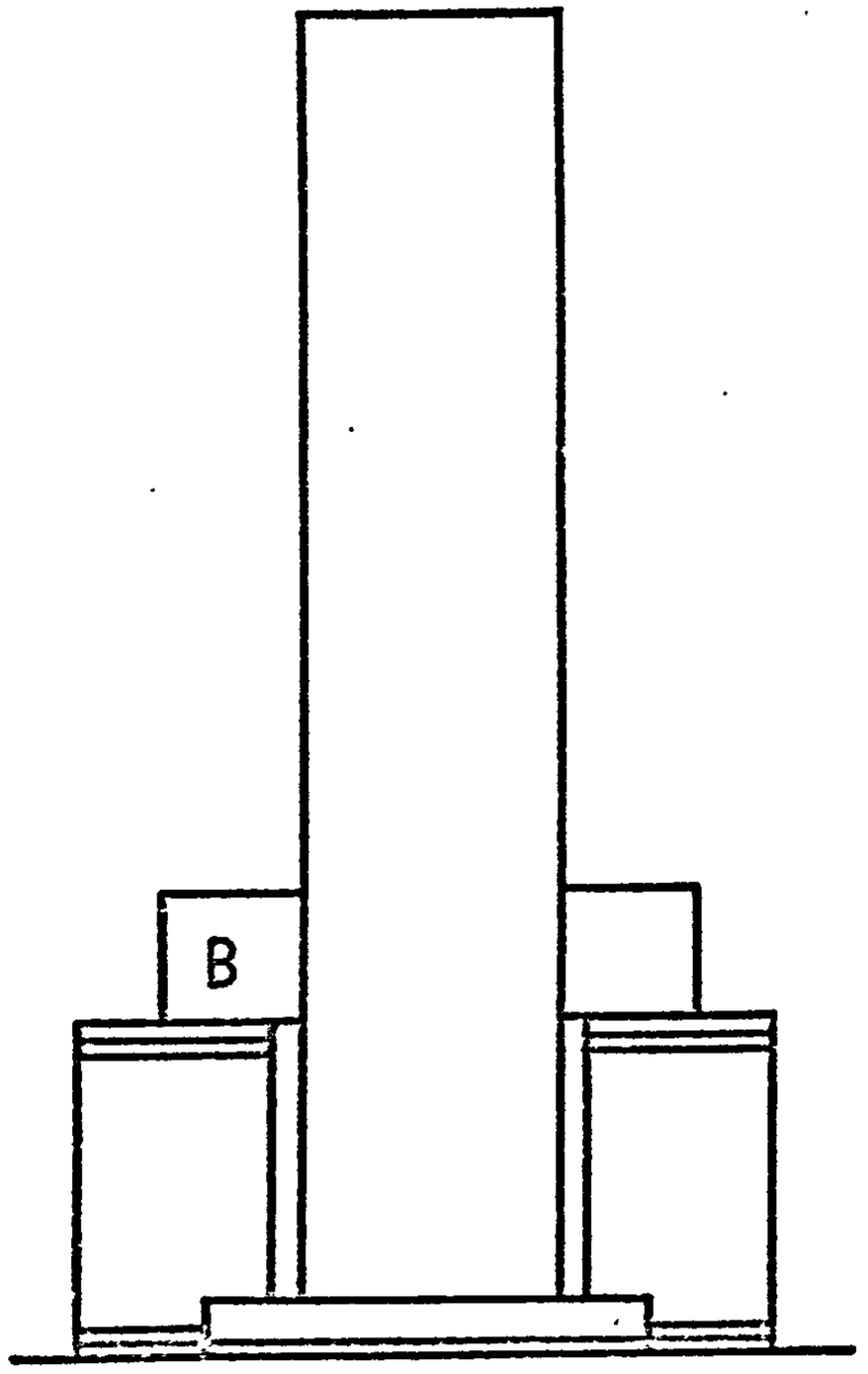

S SPECIMEN
A ACCELEROMETER
C CLAMPS
M MASS
F FORCE GAUGE
V VIBRATOR
B BRIDGE PIECE

FIG. 62

ELEVATION AND END VIEW OF VIBRATION RIG

FIG. 63

L LATERAL LOCATION BLOCKS

C CLAMPING BLOCK

B BRIDGE PIECE

S SPECIMEN

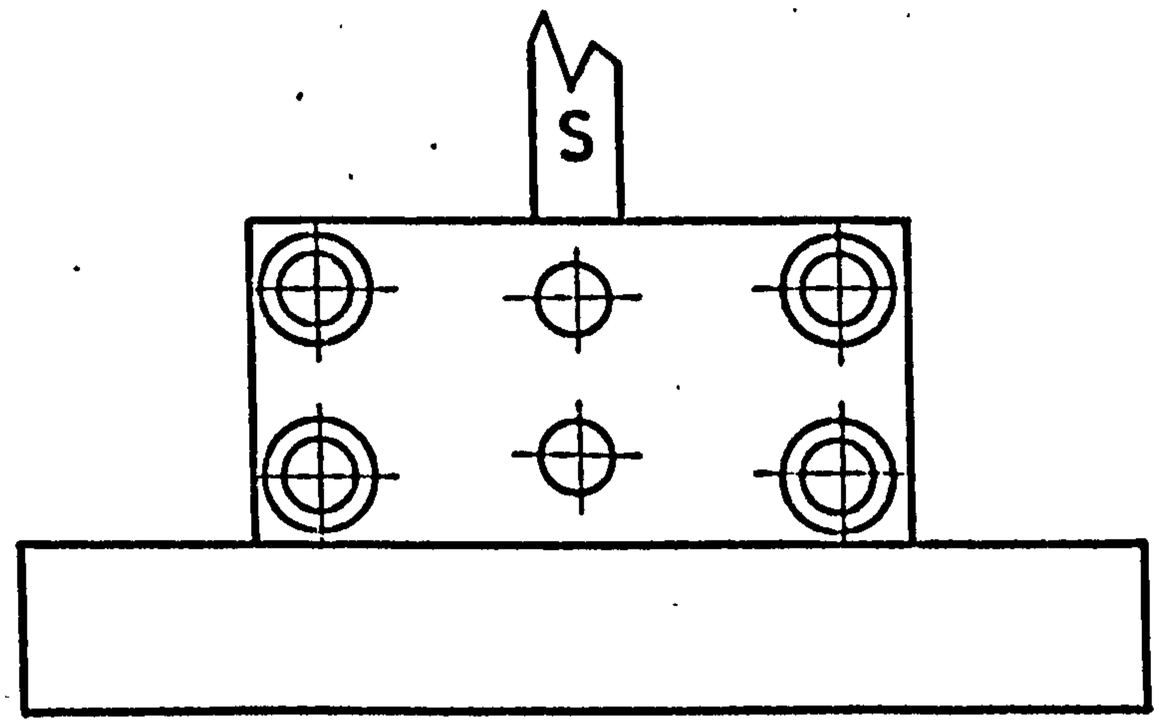

ELEVATION

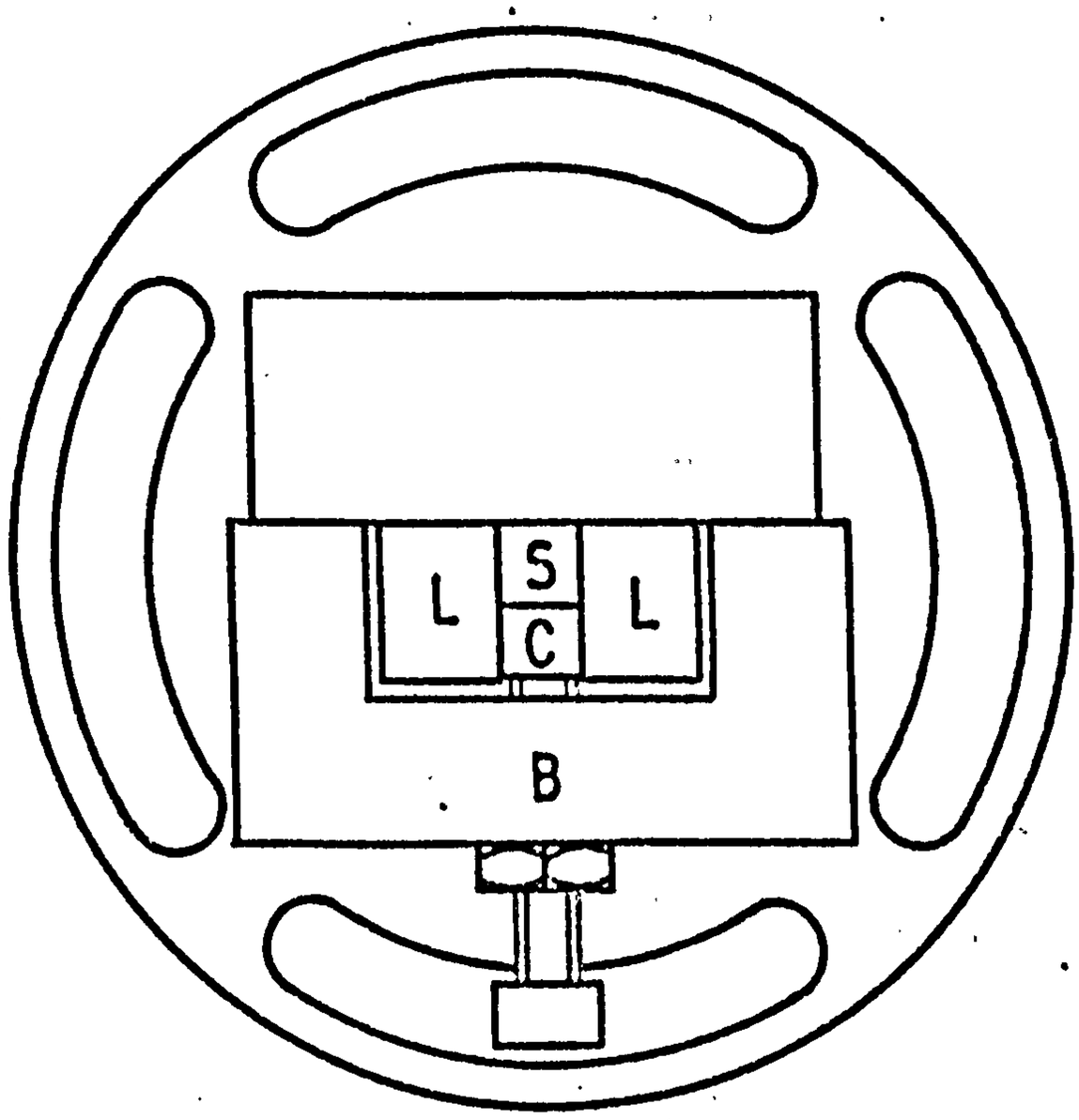

PLAN

DETAIL OF MASS TOP PLATE AND CLAMP

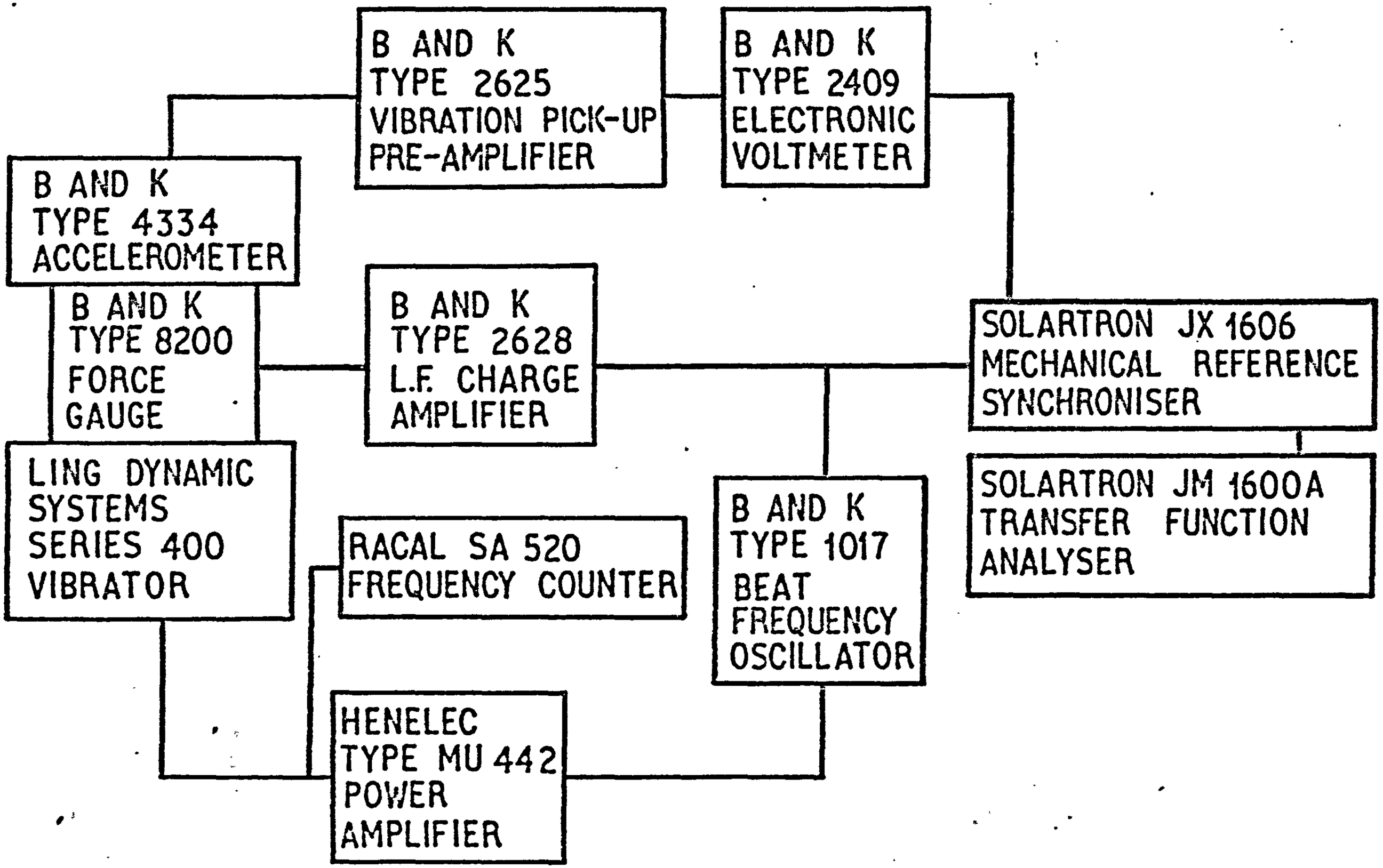

FIG. 64

SCHEMATIC ARRANGEMENT OF VIBRATION TEST EQUIPMENT

FIG. 65

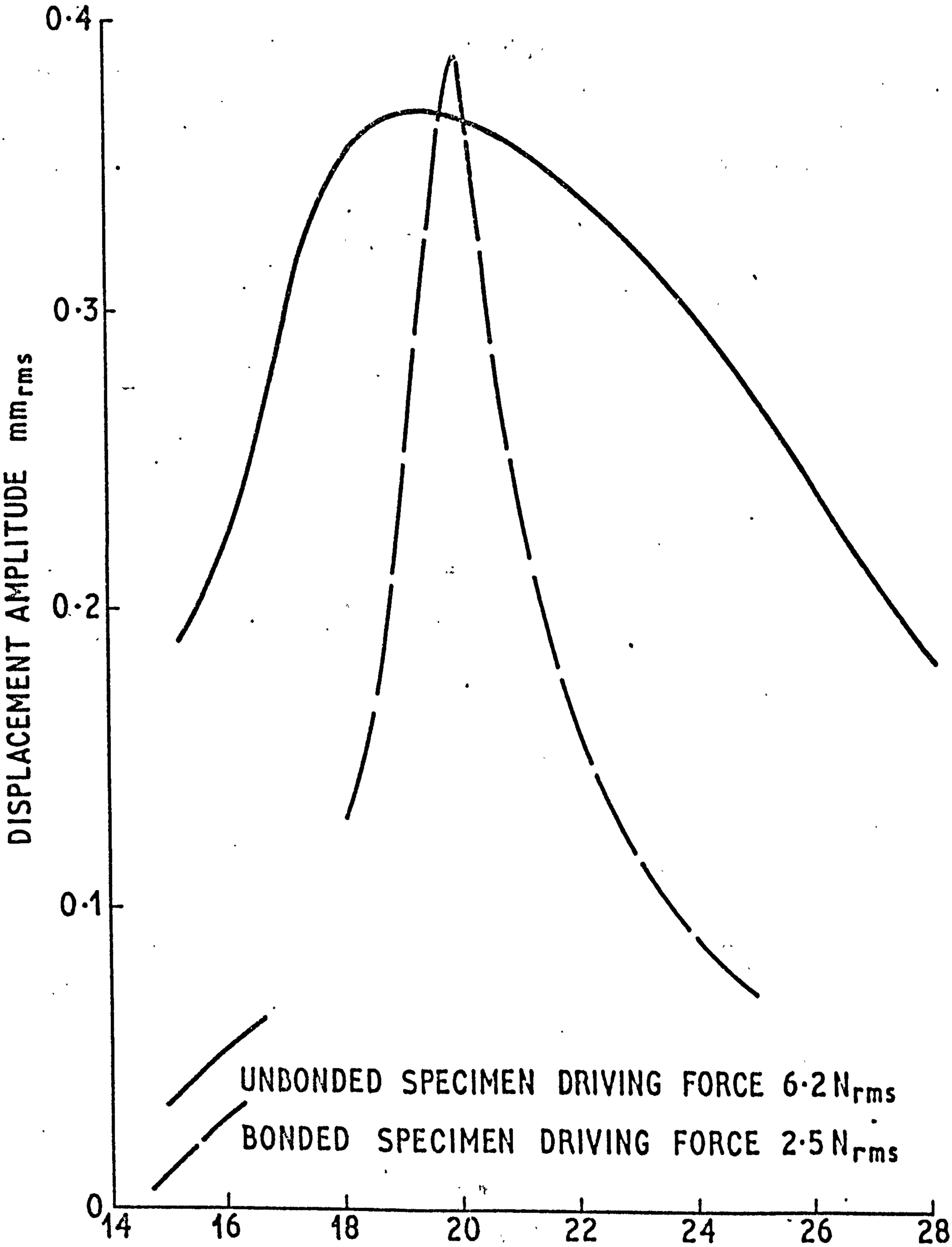

SAMPLE RESONANCE CURVES FOR BONDED AND UNBONDED SPECIMENS

FIG. 67

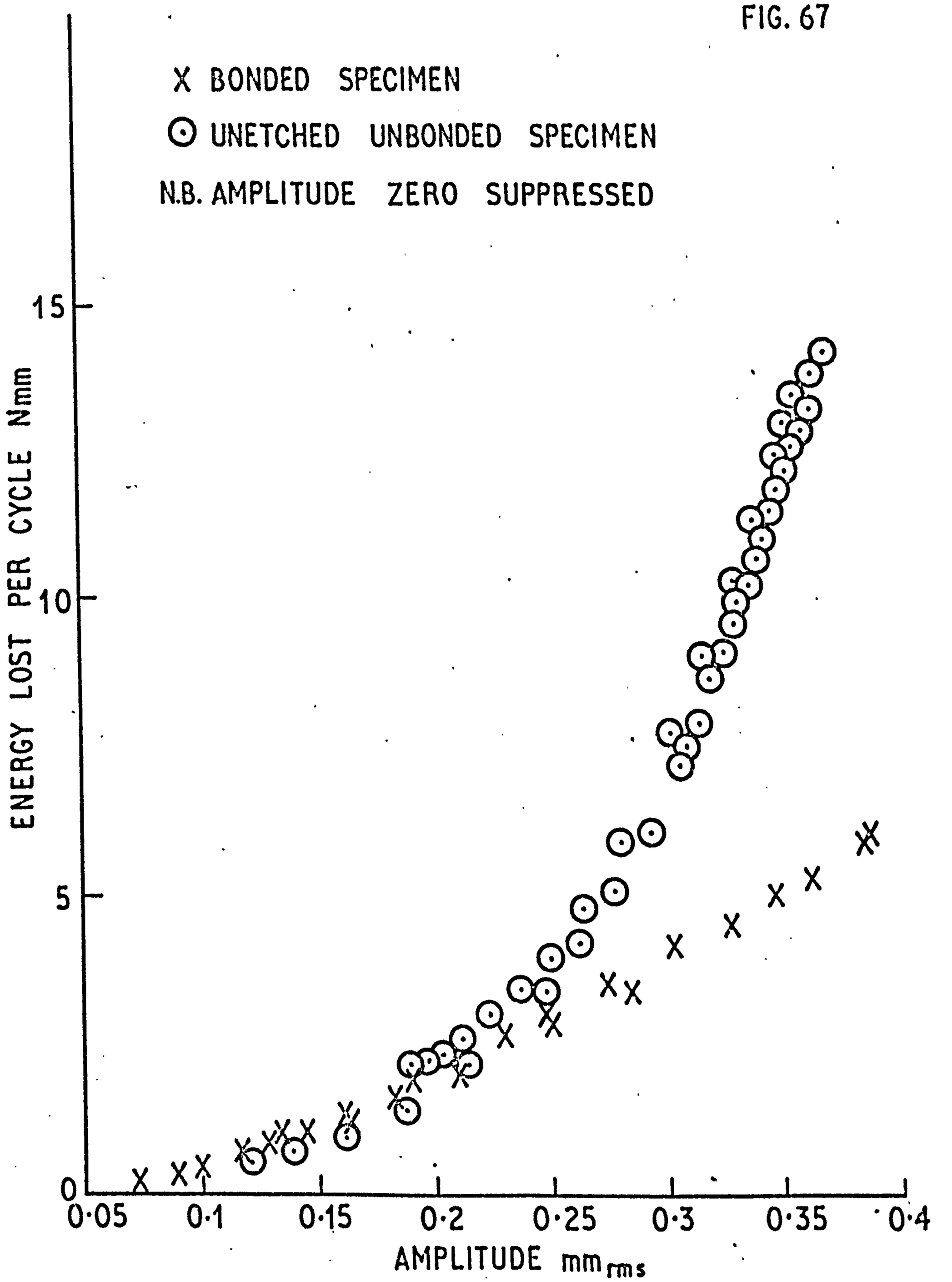

SAMPLES OF ENERGY LOST PER CYCLE RESULTS
FOR BONDED AND UNBONDED SPECIMENS

FIG. 68

BONDED SPECIMEN

ONE DEGREE OF FREEDOM SYSTEM TEST

0·83 Hz TEST

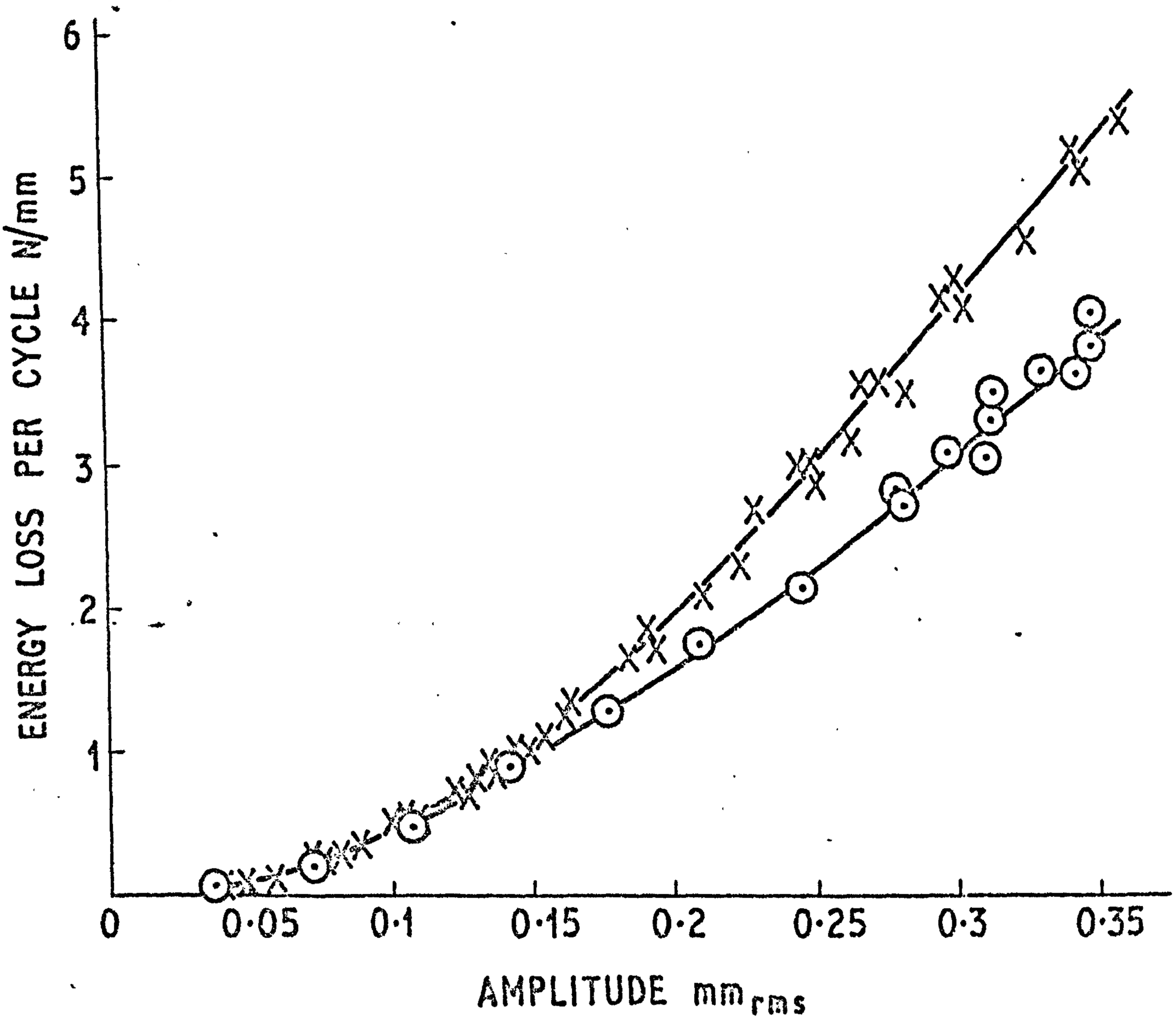

ESTIMATE OF ENERGY LOSS PER CYCLE

EXTRANEOUS TO SPECIMEN

VIBRATION TEST :- FIG. 69

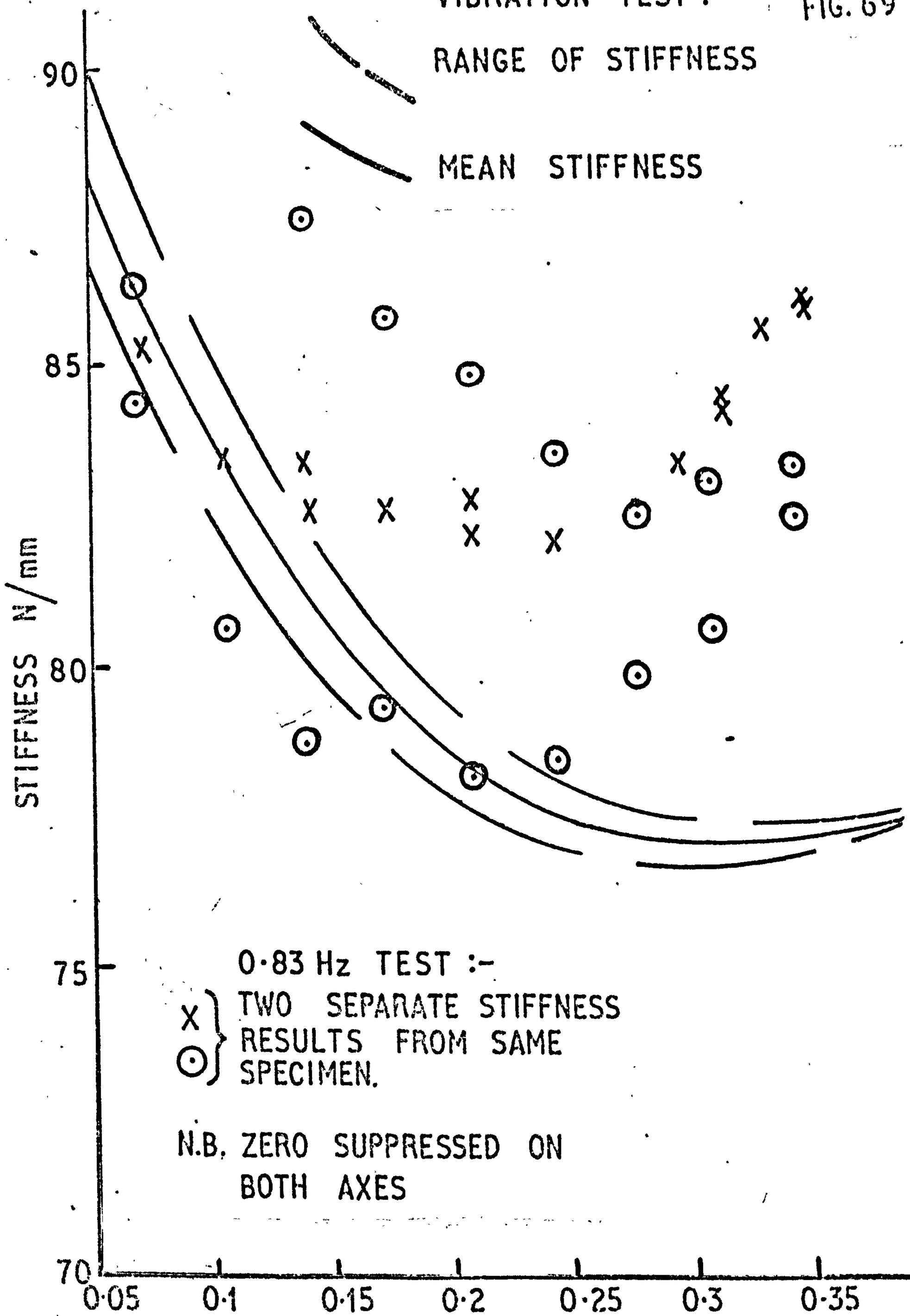

COMPARISON OF STIFFNESS RESULTS FOR BONDED SPECIMEN FROM VIBRATION AND 0·83 Hz TESTS

FIG. 70

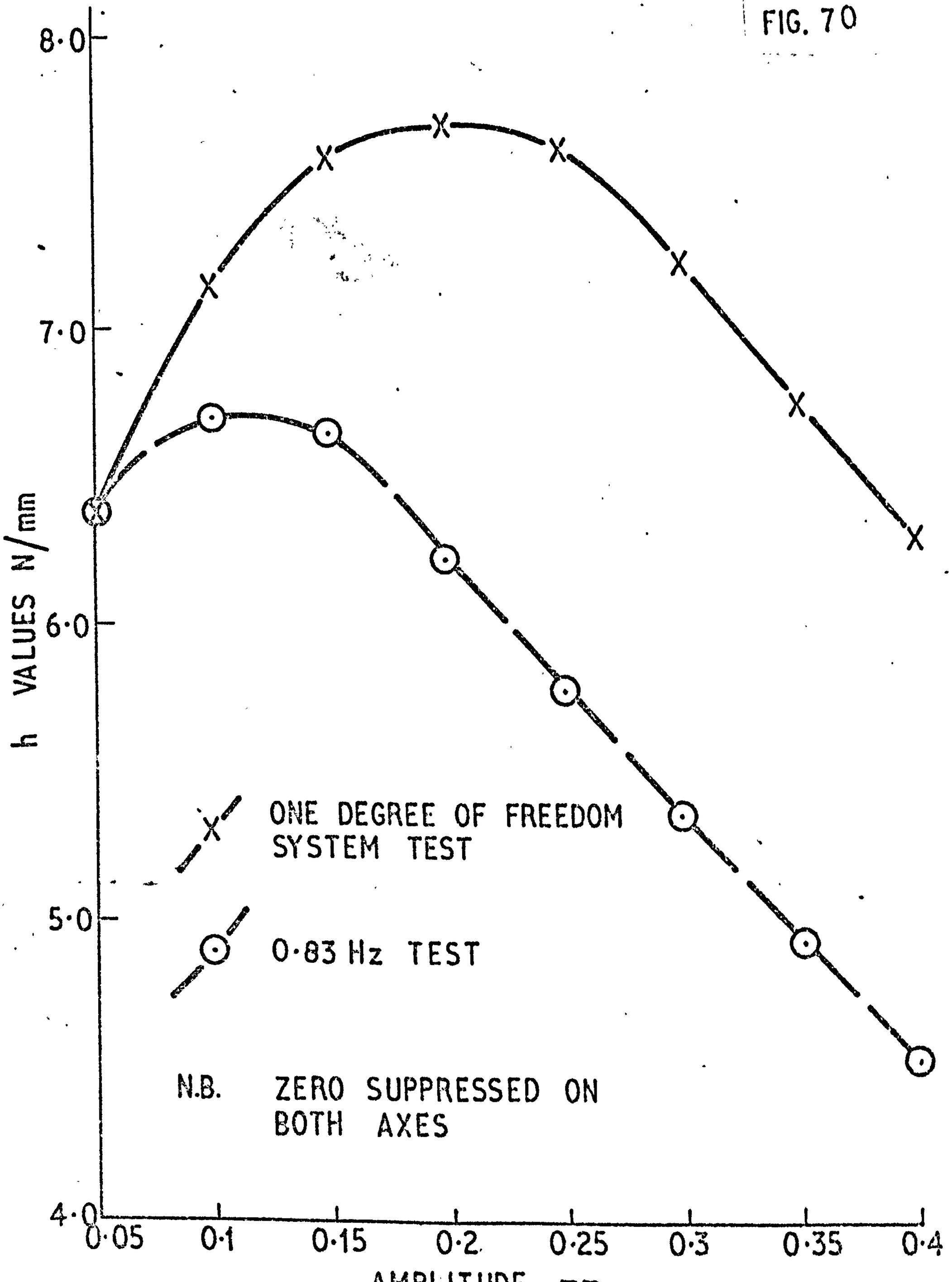

EQUIVALENT HYSTERETIC DAMPING COEFFICIENTS h
FROM VIBRATION AND 0·83Hz TESTS
(BONDED SPECIMEN)

FIG. 71

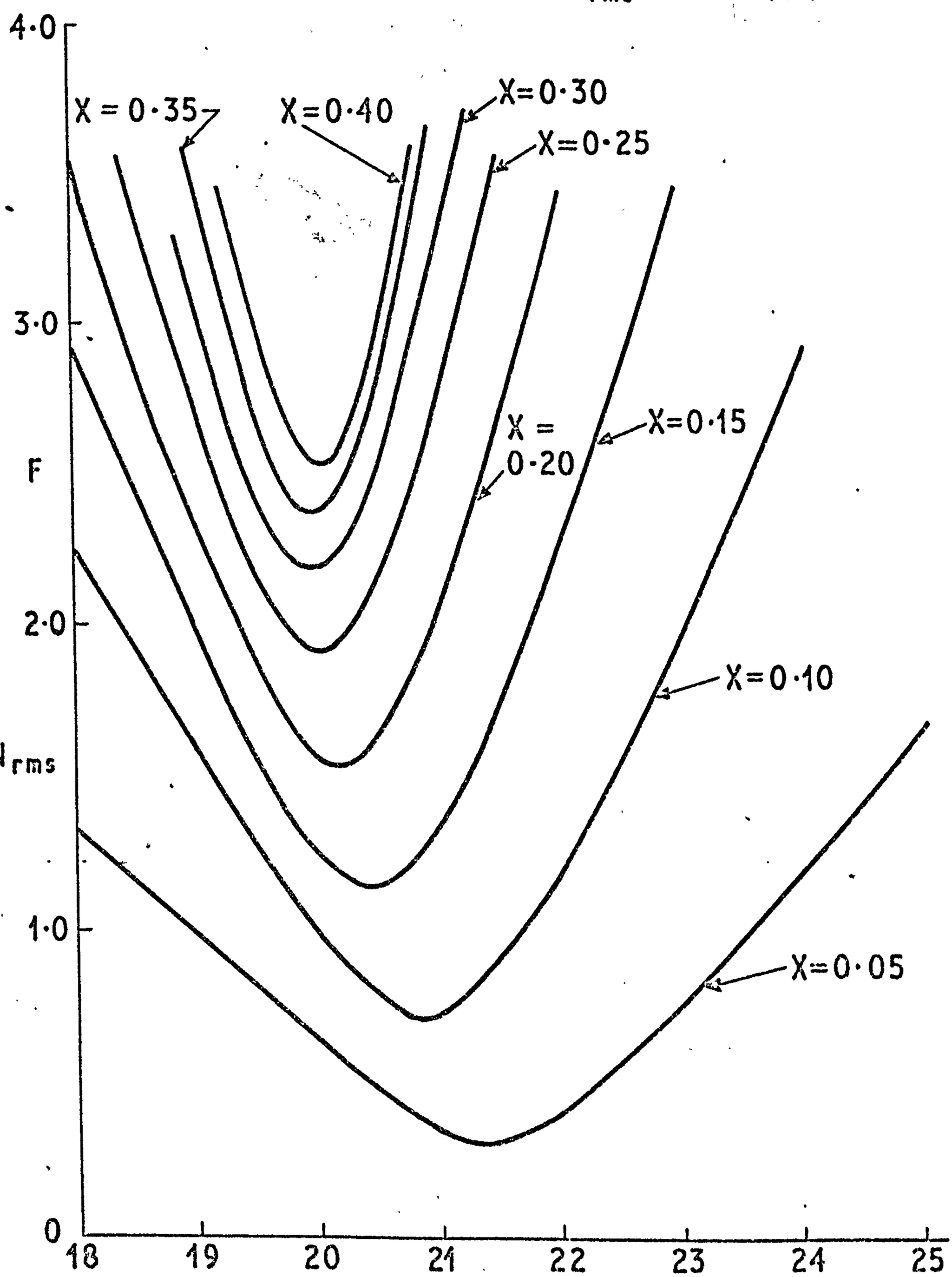

SAMPLE CURVES OF DRIVING FORCE, F AGAINST FREQUENCY CALCULATED FROM ONE DEGREE OF FREEDOM SYSTEM RESULTS

FIG. 72

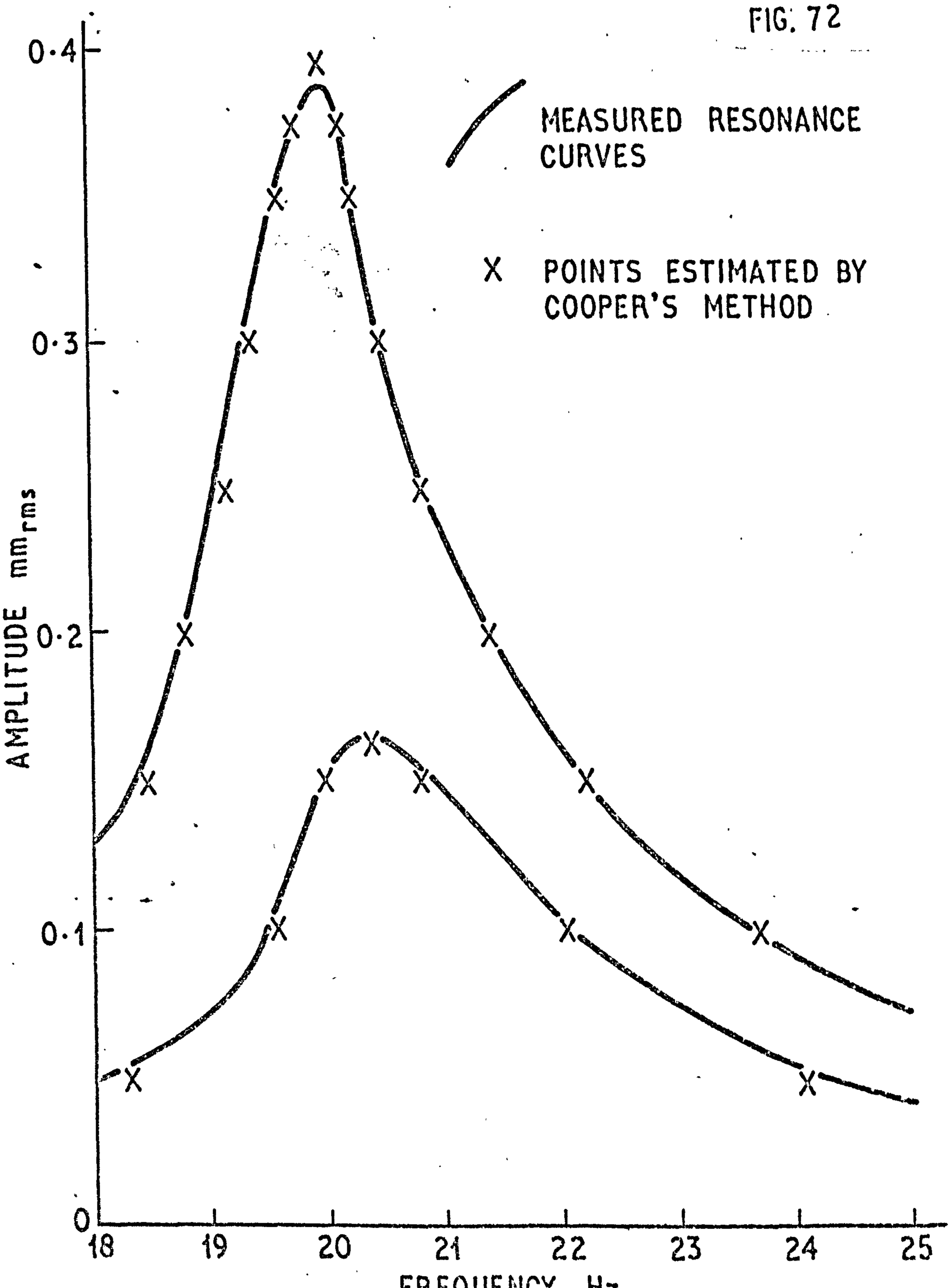

SAMPLE RESONANCE CURVES FOR BONDED SPECIMEN WITH POINTS ESTIMATED BY COOPER'S METHOD

FIG. 73

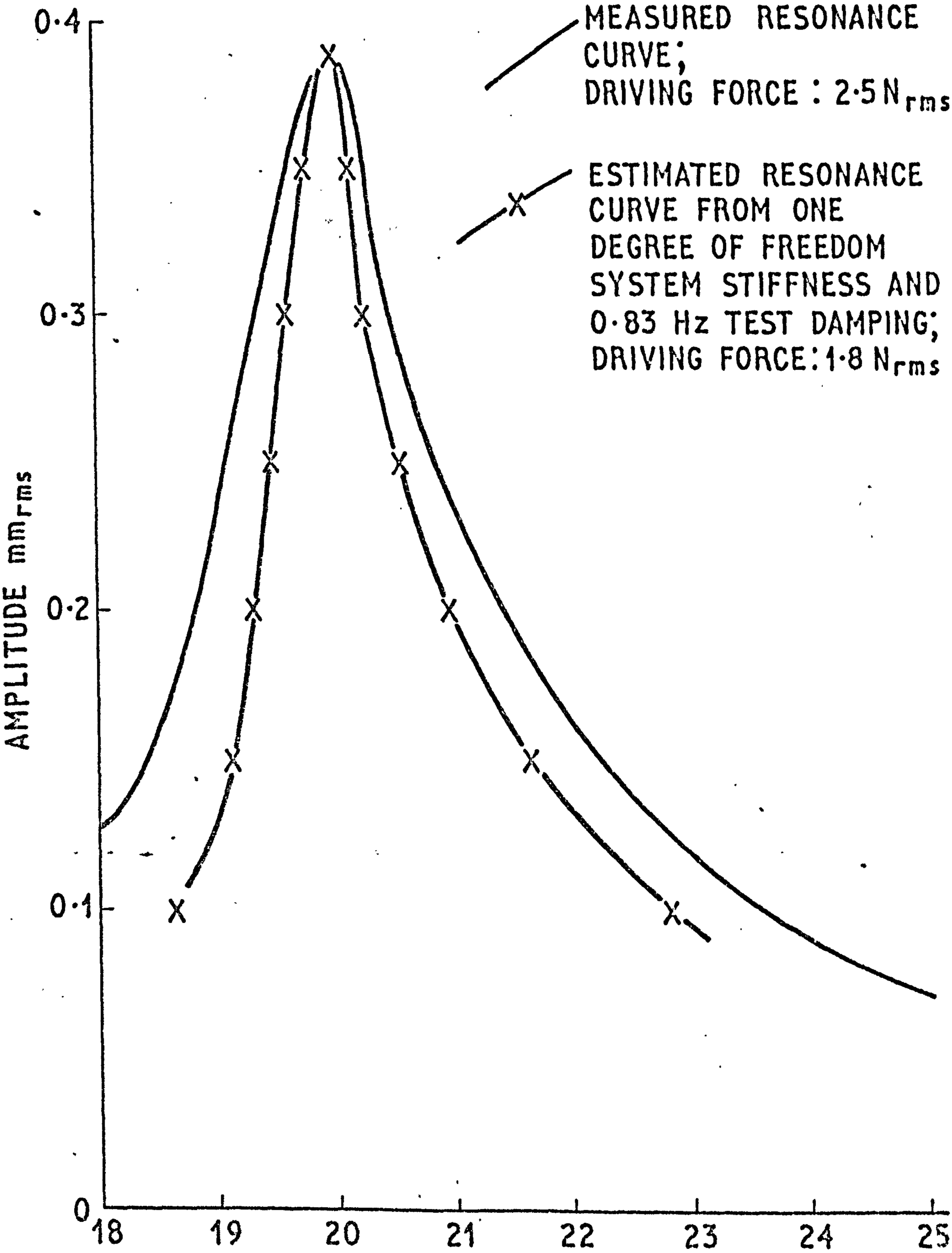

COMPARISON OF MEASURED RESONANCE CURVE AND ESTIMATED RESONANCE CURVE USING 0·83 Hz TEST DAMPING

FIG. 74

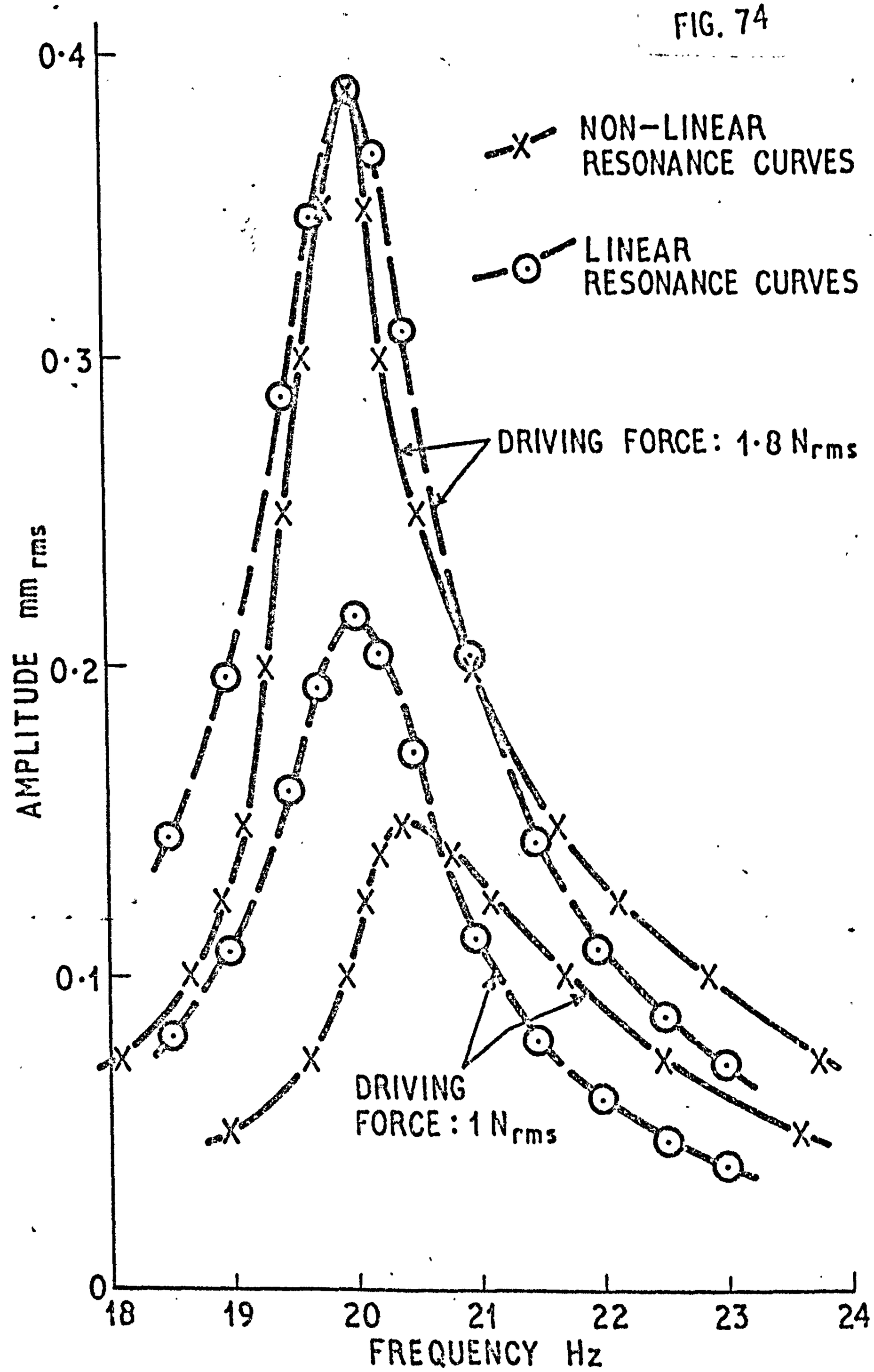

COMPARISON OF ESTIMATED NON-LINEAR AND LINEAR SYSTEMS RESONANCE CURVES

FIG. 75

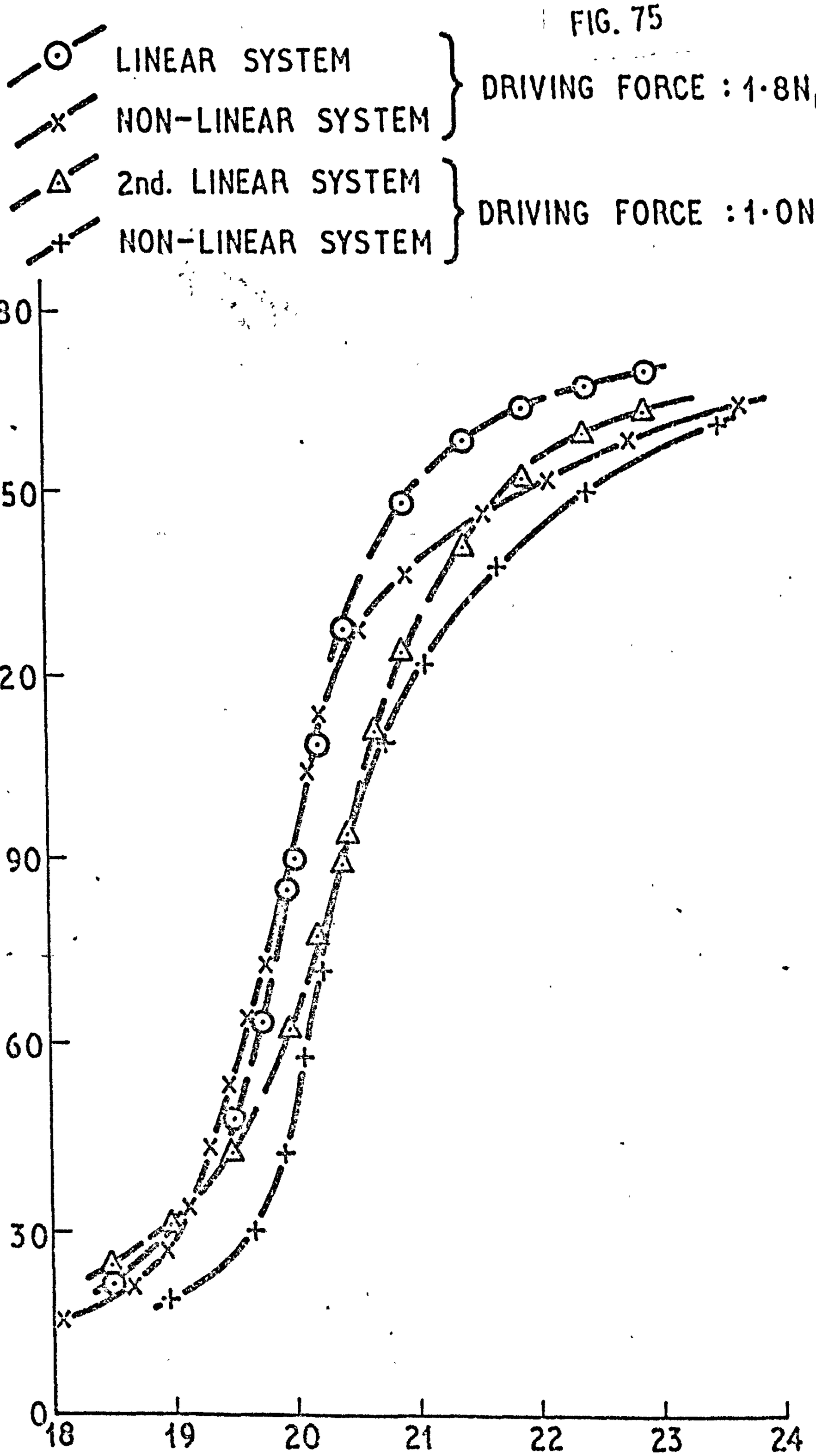

COMPARISON OF ESTIMATED NON-LINEAR AND LINEAR SYSTEMS : PHASE ANGLE

FIG. 76

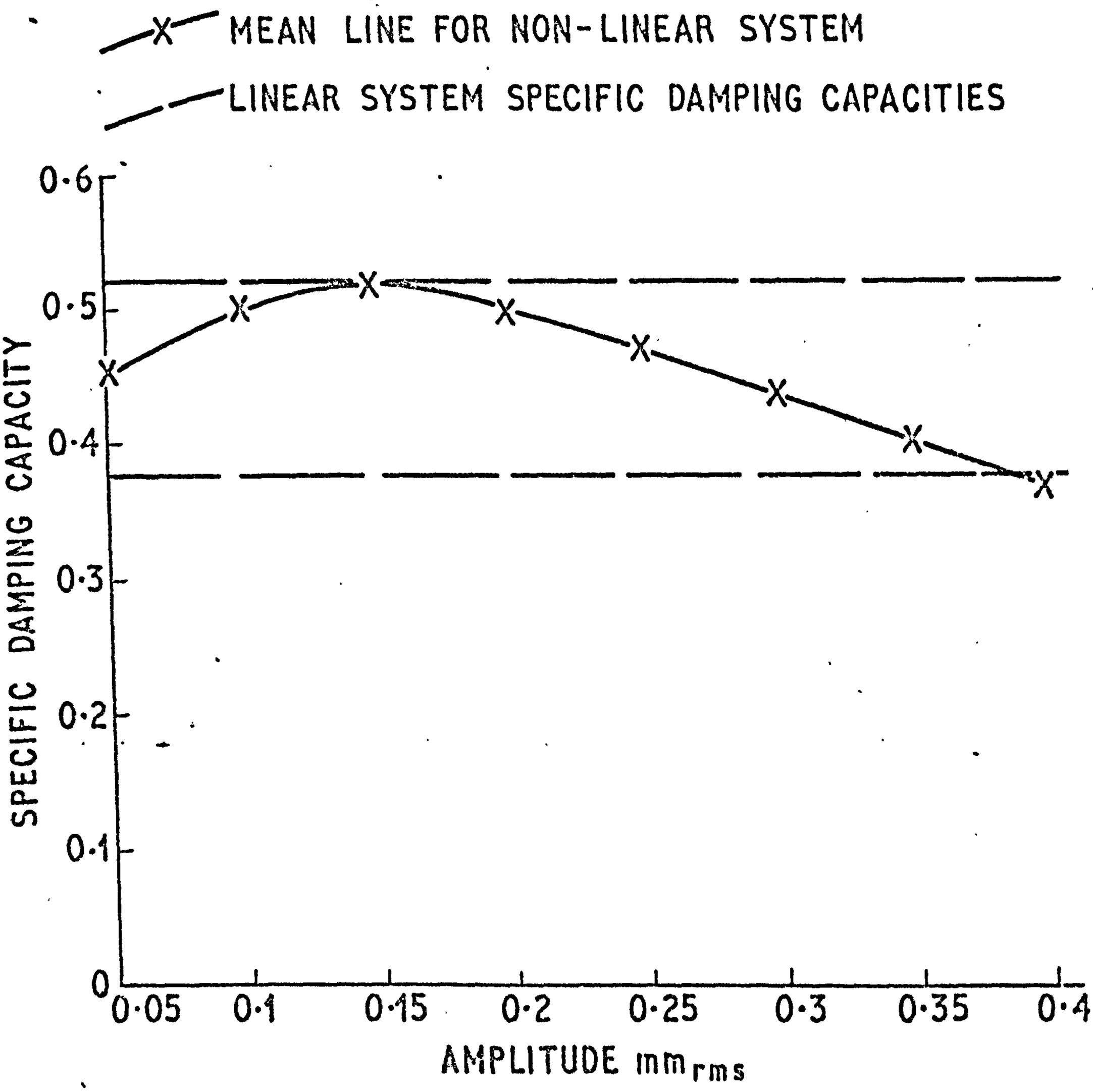

COMPARISON OF ESTIMATED NON-LINEAR AND LINEAR SYSTEMS : SPECIFIC DAMPING CAPACITY

FIG. 77

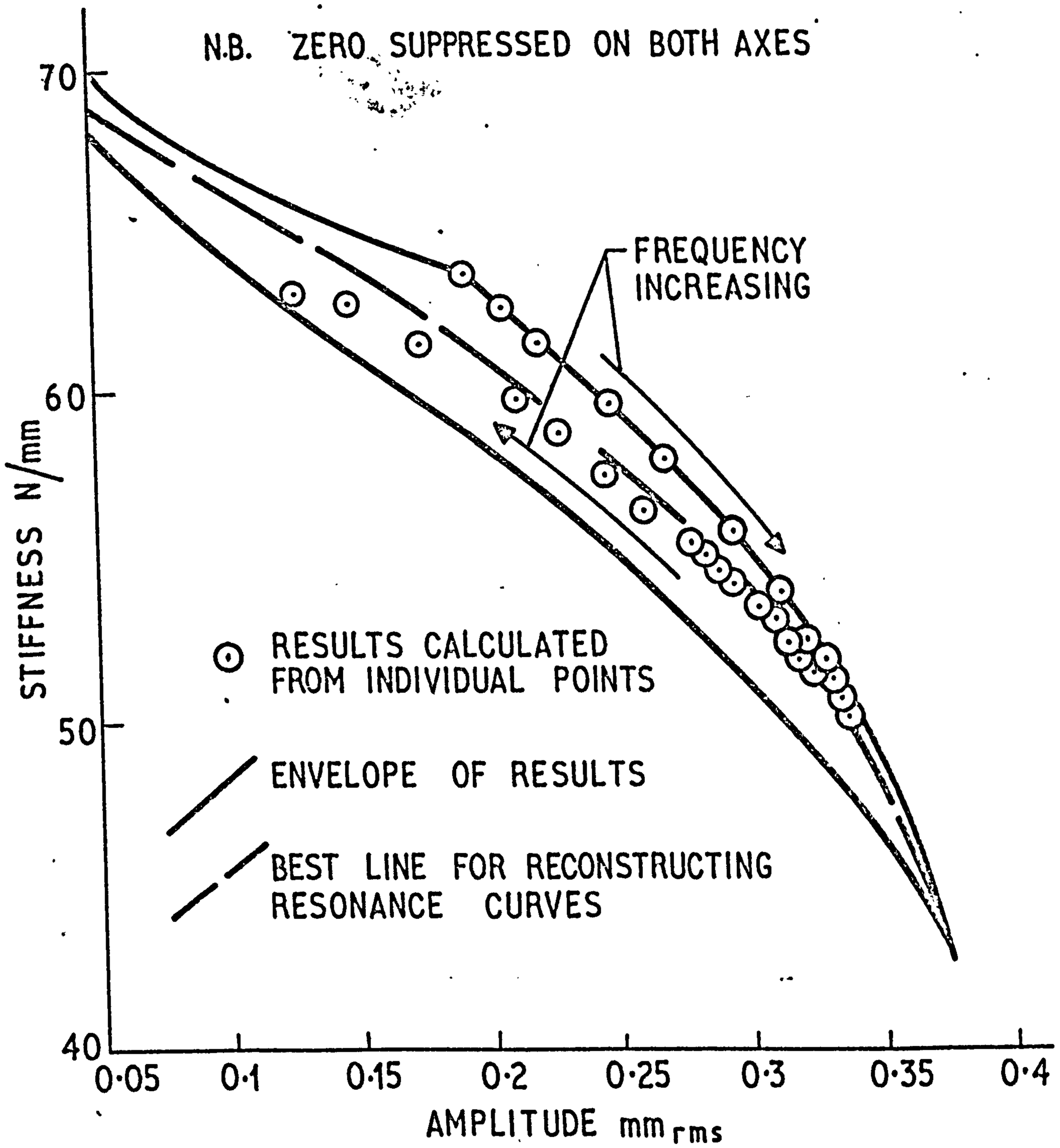

SAMPLE STIFFNESS AGAINST AMPLITUDE RESULT FOR UNBONDED (UNETCHED) SPECIMEN

FIG. 78

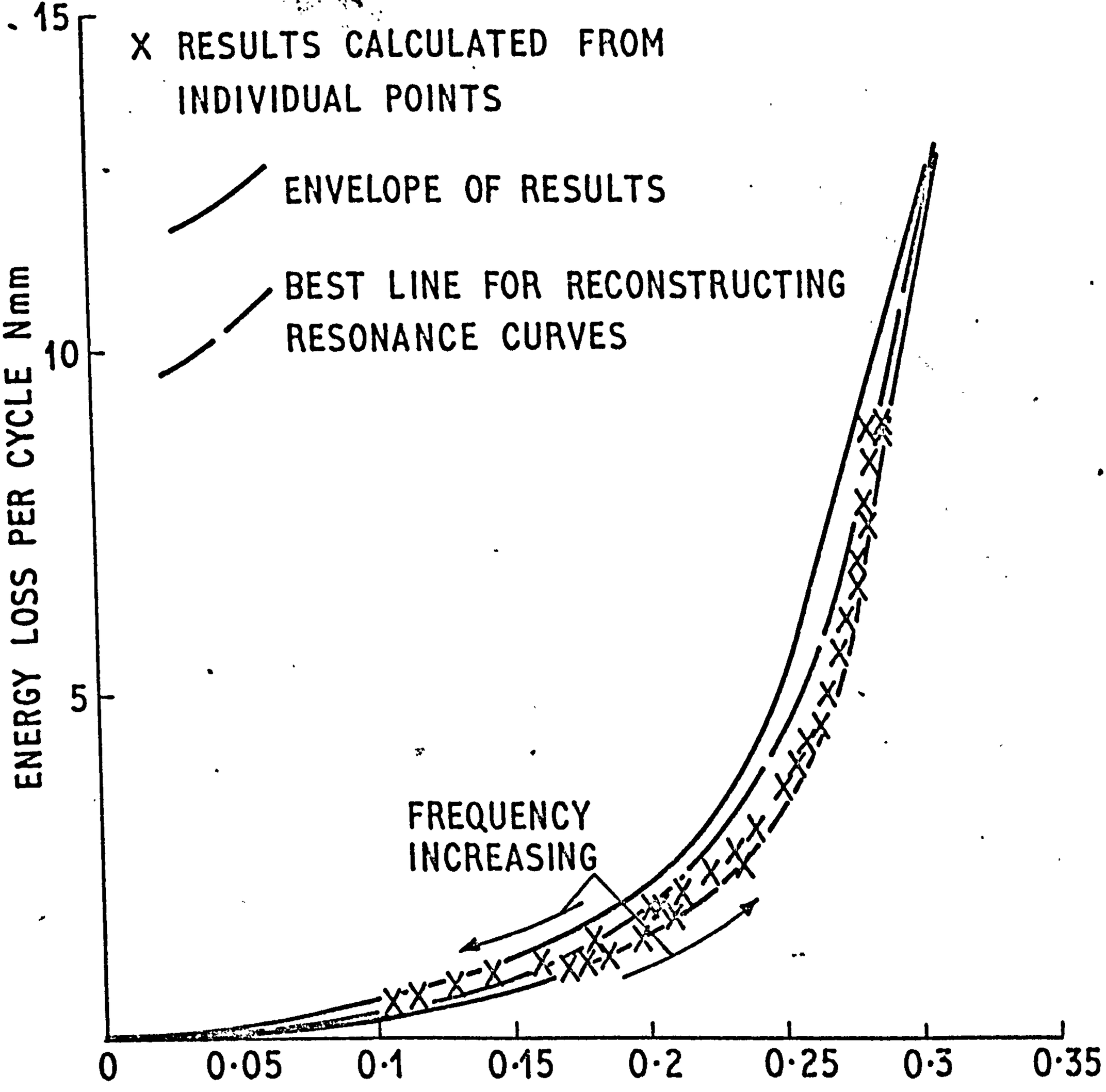

SAMPLE ENERGY LOST PER CYCLE AGAINST AMPLITUDE

RESULT FOR UNBONDED (ETCHED) SPECIMEN

FIG. 79

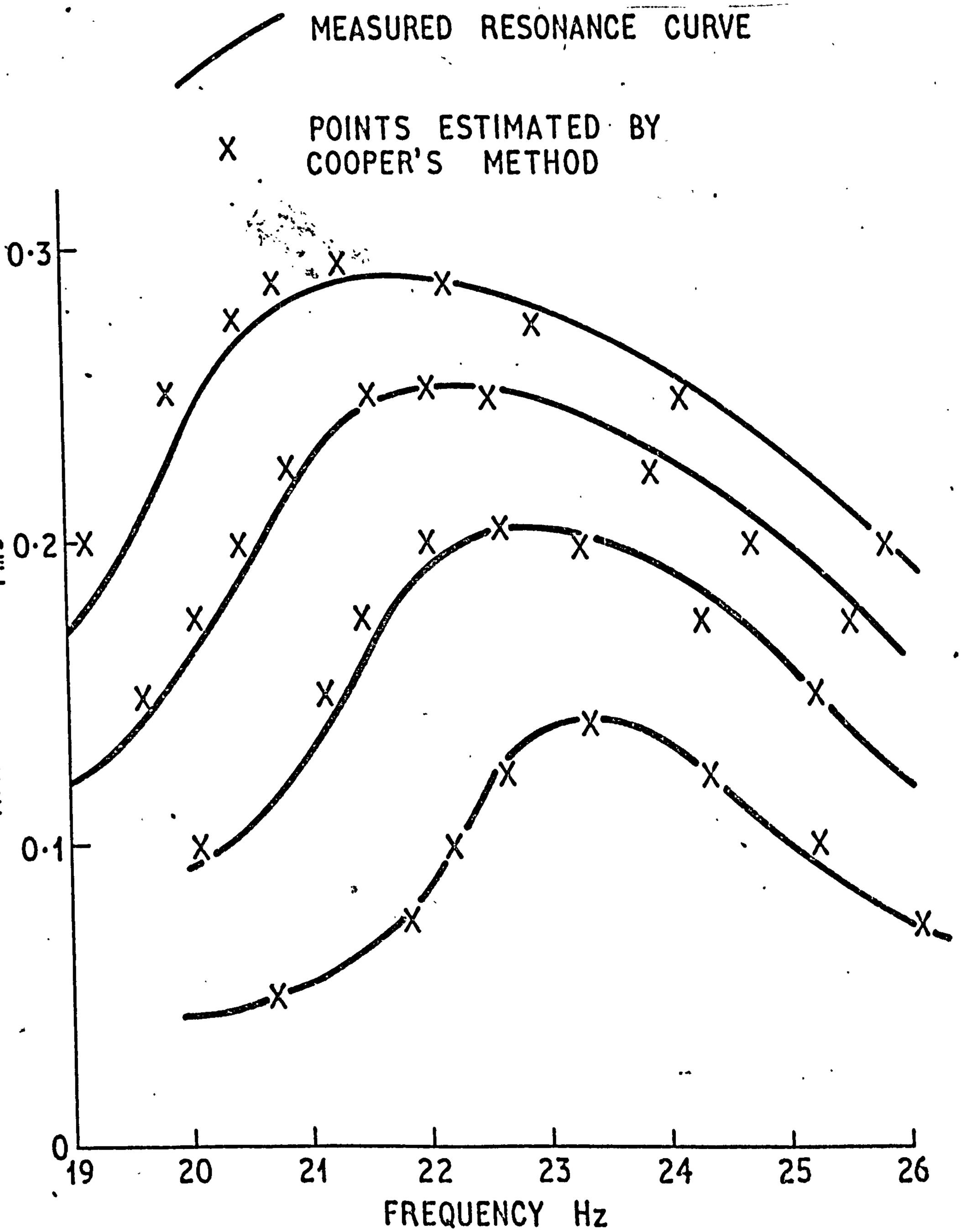

SAMPLE RESONANCE CURVES FOR UNBONDED (UNETCHED) SPECIMEN WITH POINTS ESTIMATED BY COOPER'S METHOD

FIG. 80

/ MEASURED RESONANCE CURVE

X POINTS ESTIMATED BY COOPER'S METHOD

\+ POINTS ESTIMATED BY COOPER'S METHOD (WITH DAMPING CORRECTION)

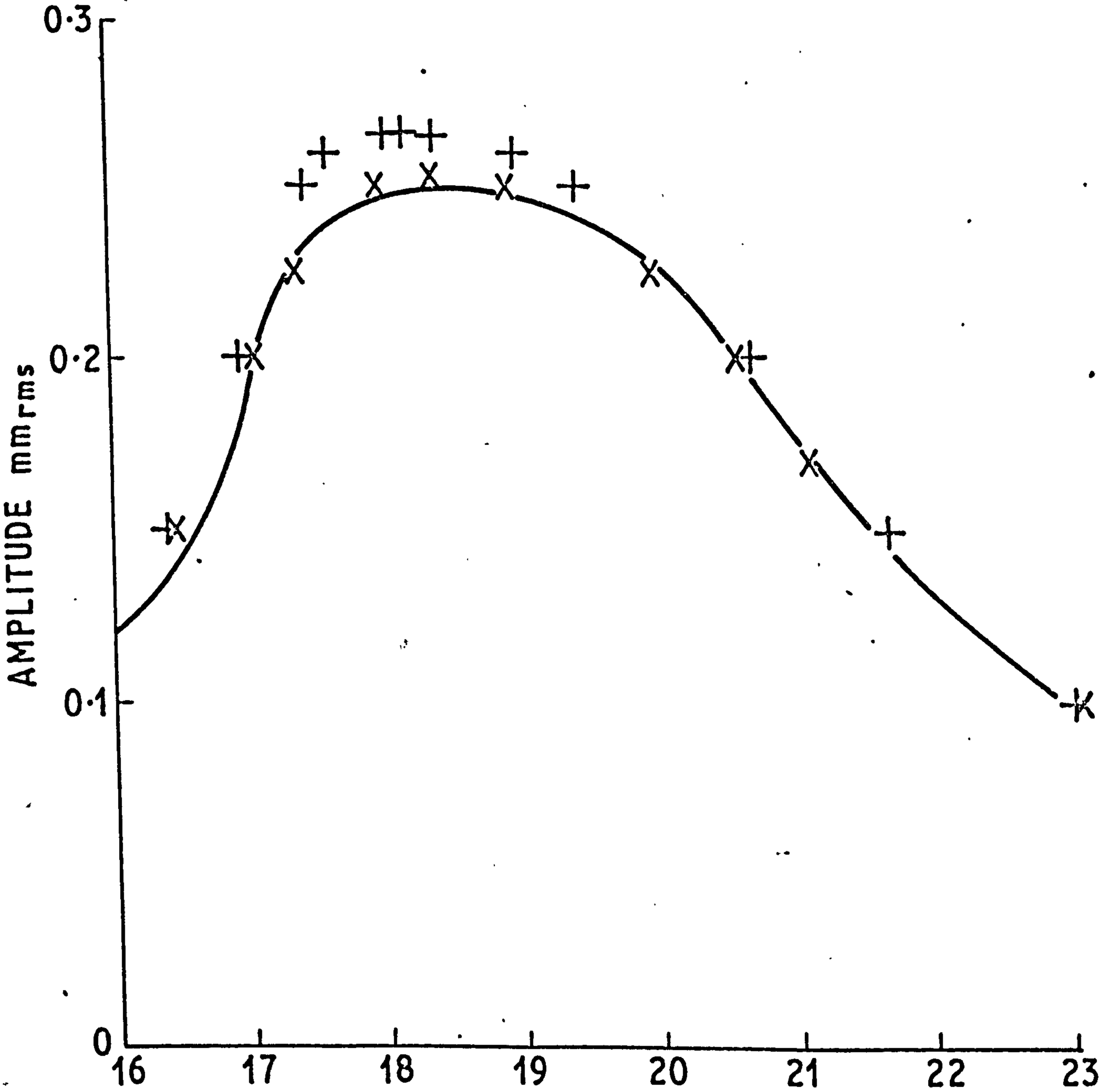

COMPARISON OF MEASURED RESONANCE CURVE AND POINTS ESTIMATED BY COOPER'S METHOD BOTH WITH AND WITHOUT EXTRANEOUS DAMPING CORRECTION

(ETCHED SPECIMEN)

FIG. 81

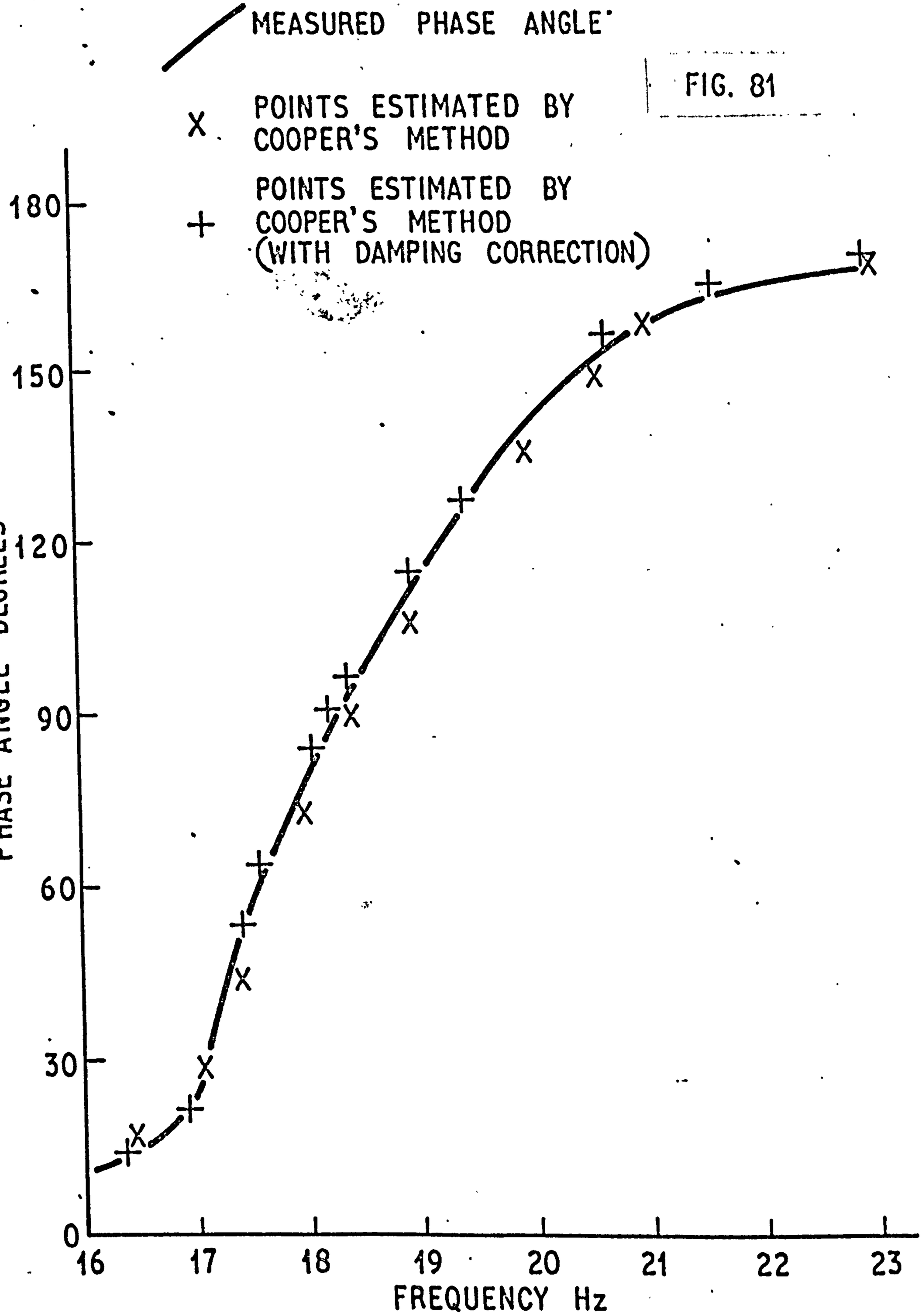

COMPARISON OF MEASURED PHASE ANGLES AND POINTS ESTIMATED BY COOPER'S METHOD BOTH WITH AND WITHOUT EXTRANEOUS DAMPING CORRECTION (ETCHED SPECIMEN)

FIG. 82

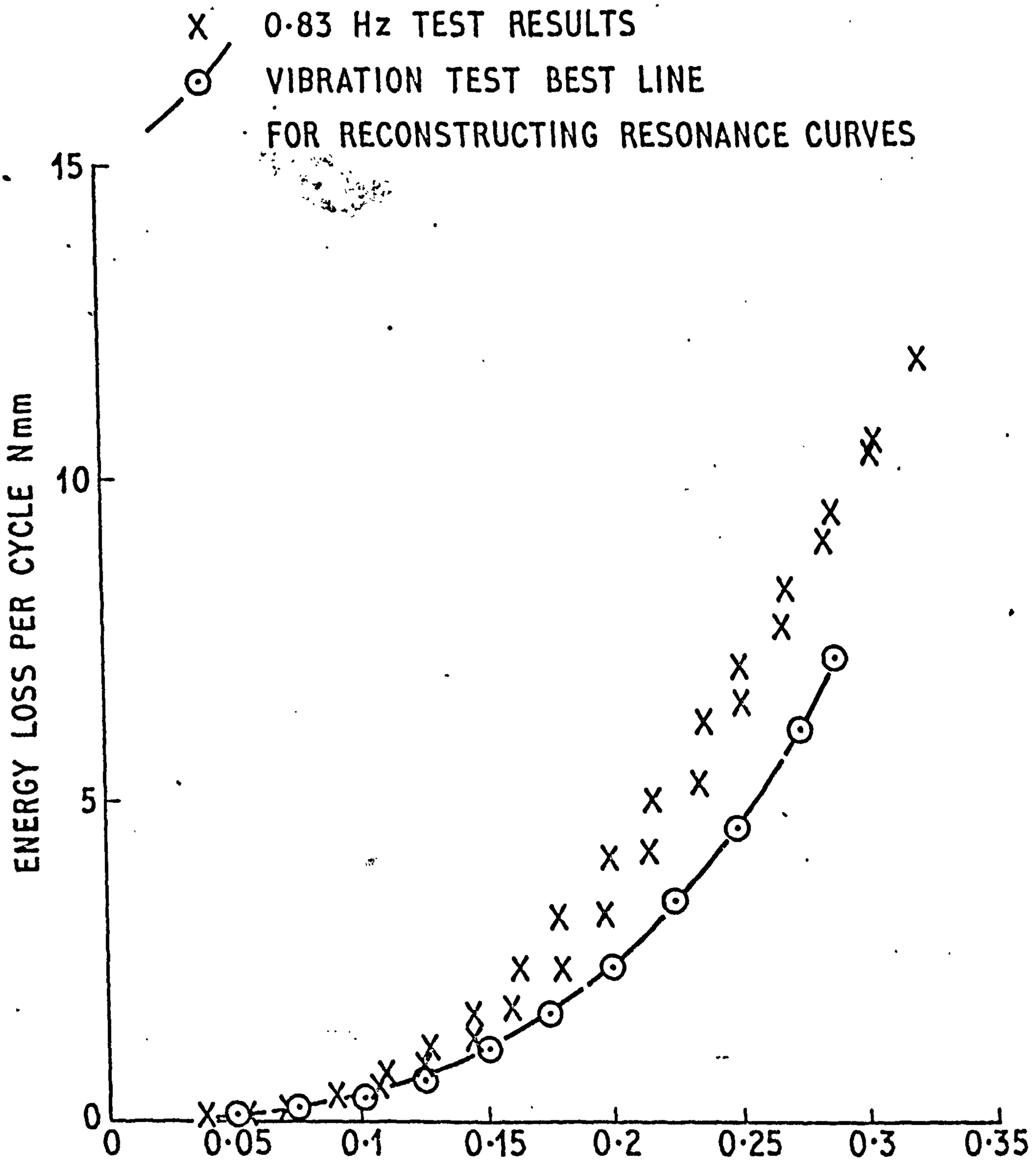

COMPARISON OF ENERGY LOSS PER CYCLE FROM 0·83 Hz AND VIBRATION TESTS (UNBONDED UNETCHED SPECIMEN)

FIG. 83

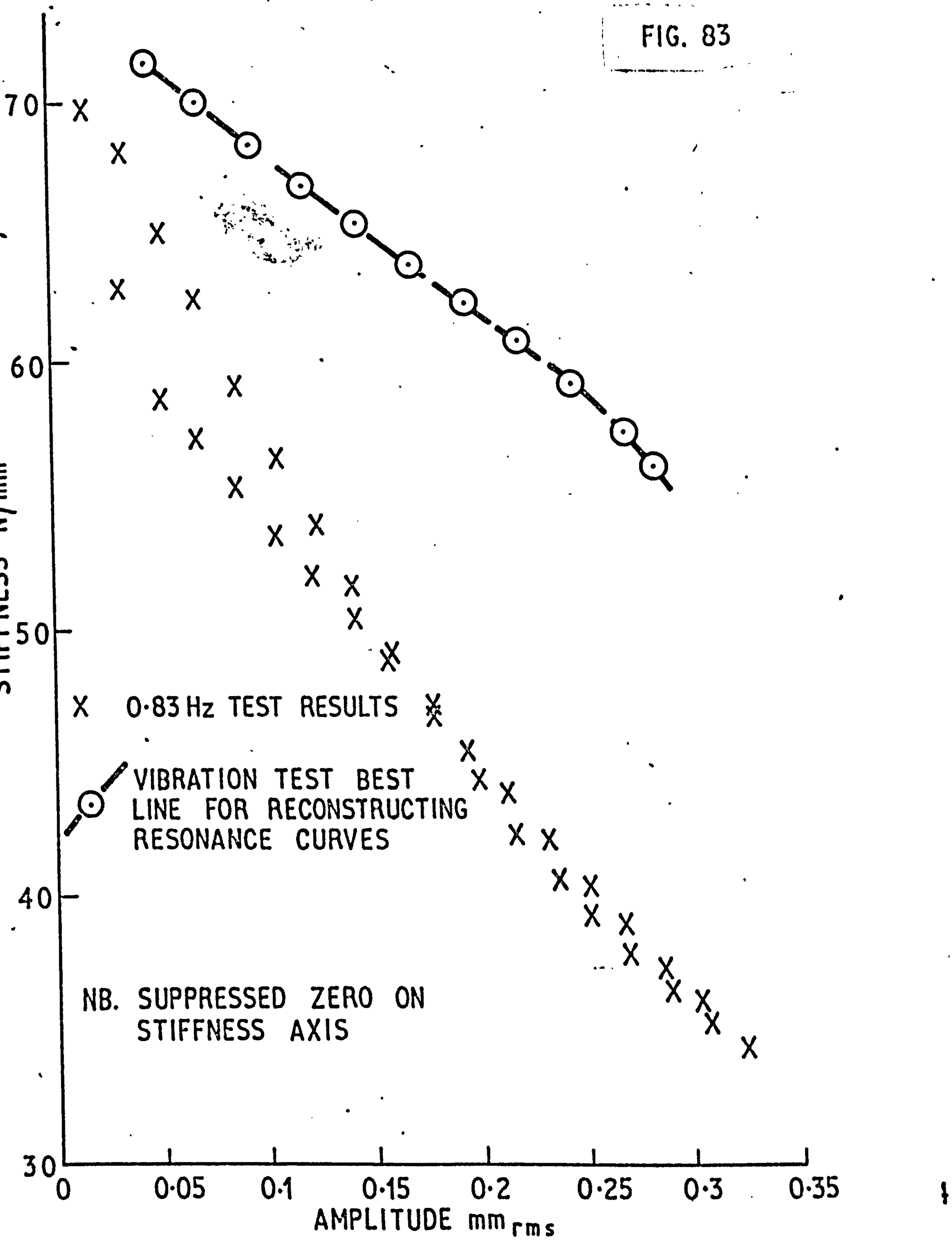

COMPARISON OF STIFFNESS RESULTS FROM 0·83 Hz AND VIBRATION TESTS (UNBONDED UNETCHED SPECIMEN)

FIG. 84

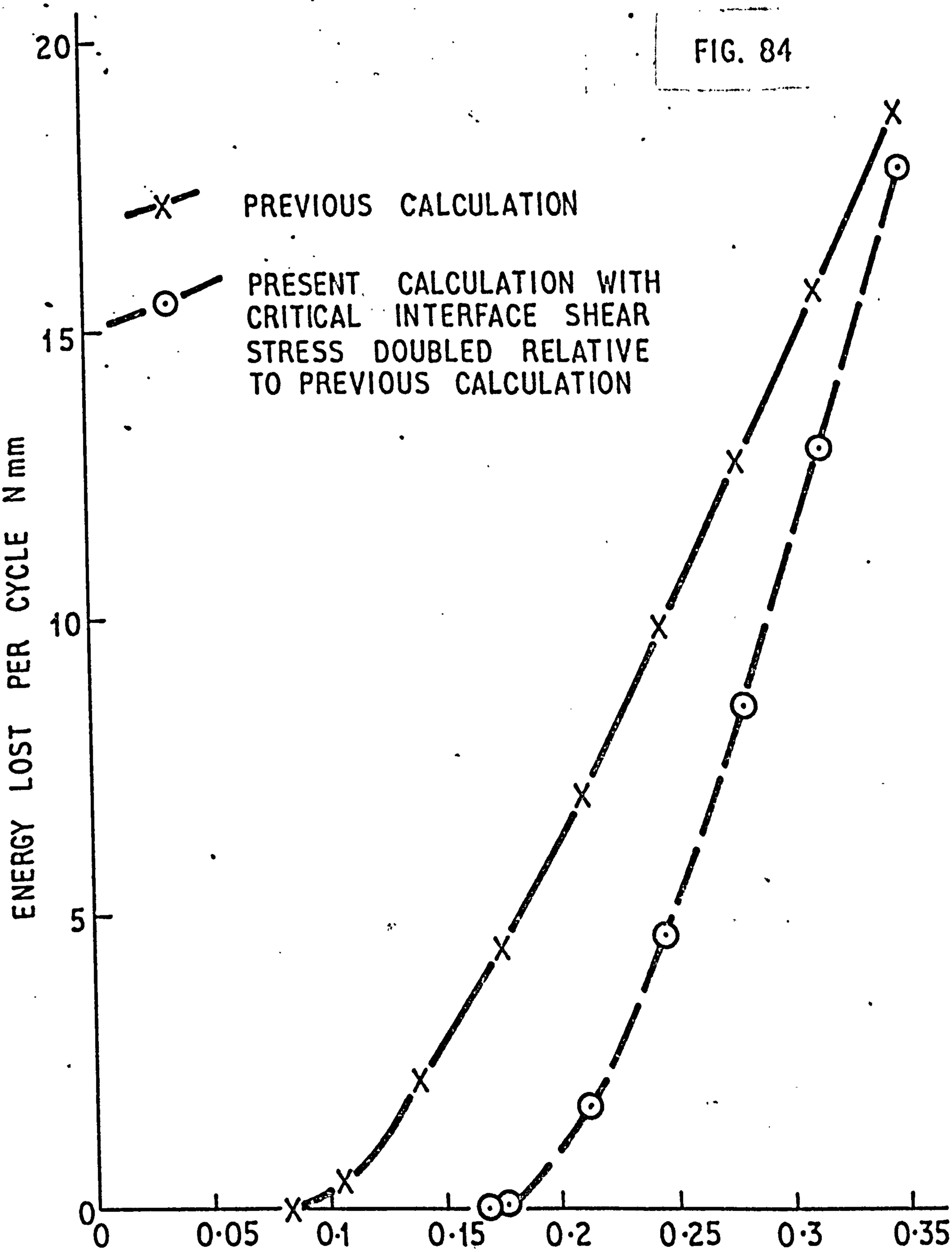

COMPARISON OF CALCULATED ENERGIES LOST PER CYCLE SHOWING EFFECT OF DOUBLING CRITICAL INTERFACE SHEAR STRESS

FIG. 85

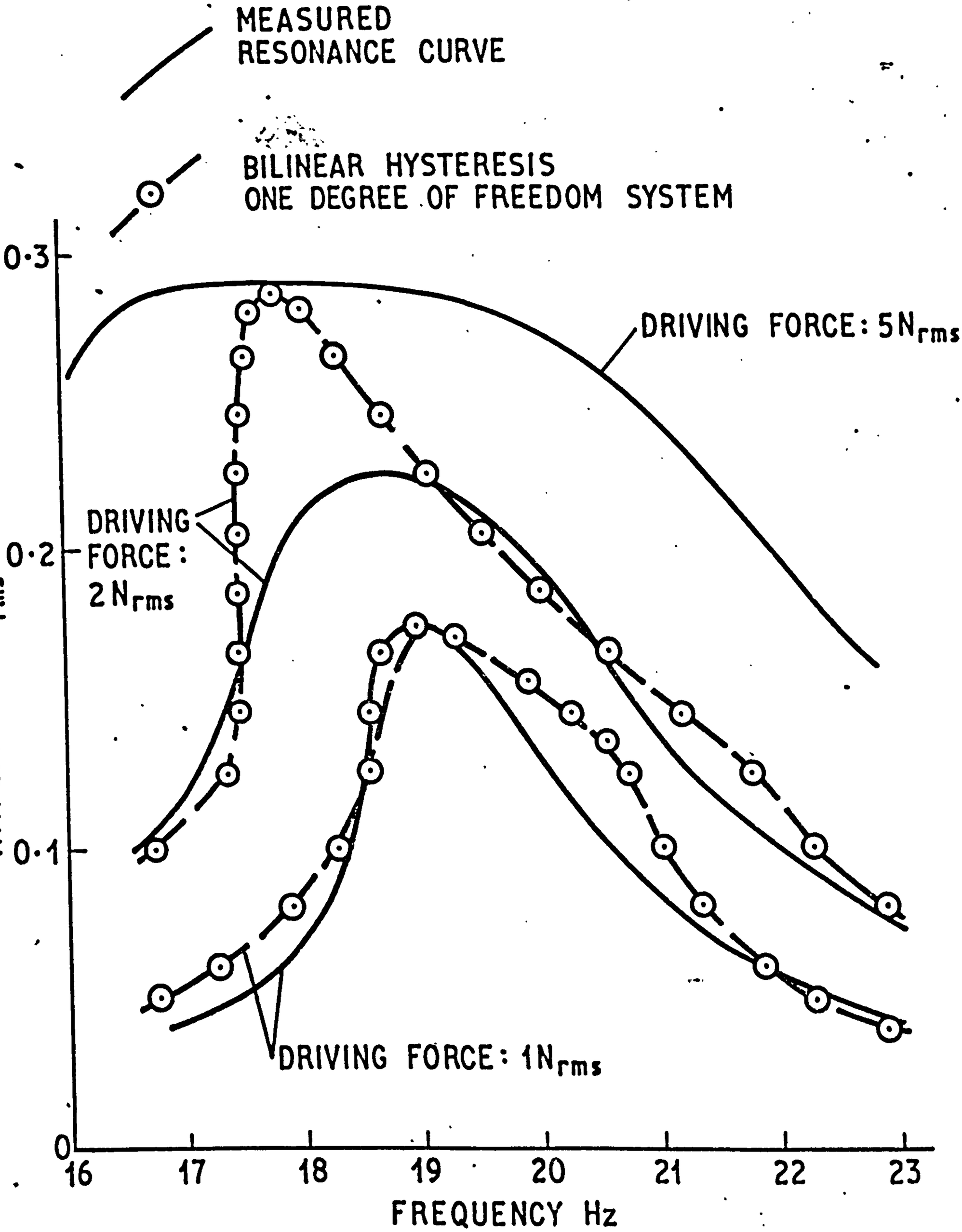

COMPARISON OF ETCHED SPECIMEN RESULTS
WITH BILINEAR HYSTERESIS ONE DEGREE OF FREEDOM SYSTEM

MEASURED RESONANCE CURVES

FIG. 86

LINEAR SYSTEM

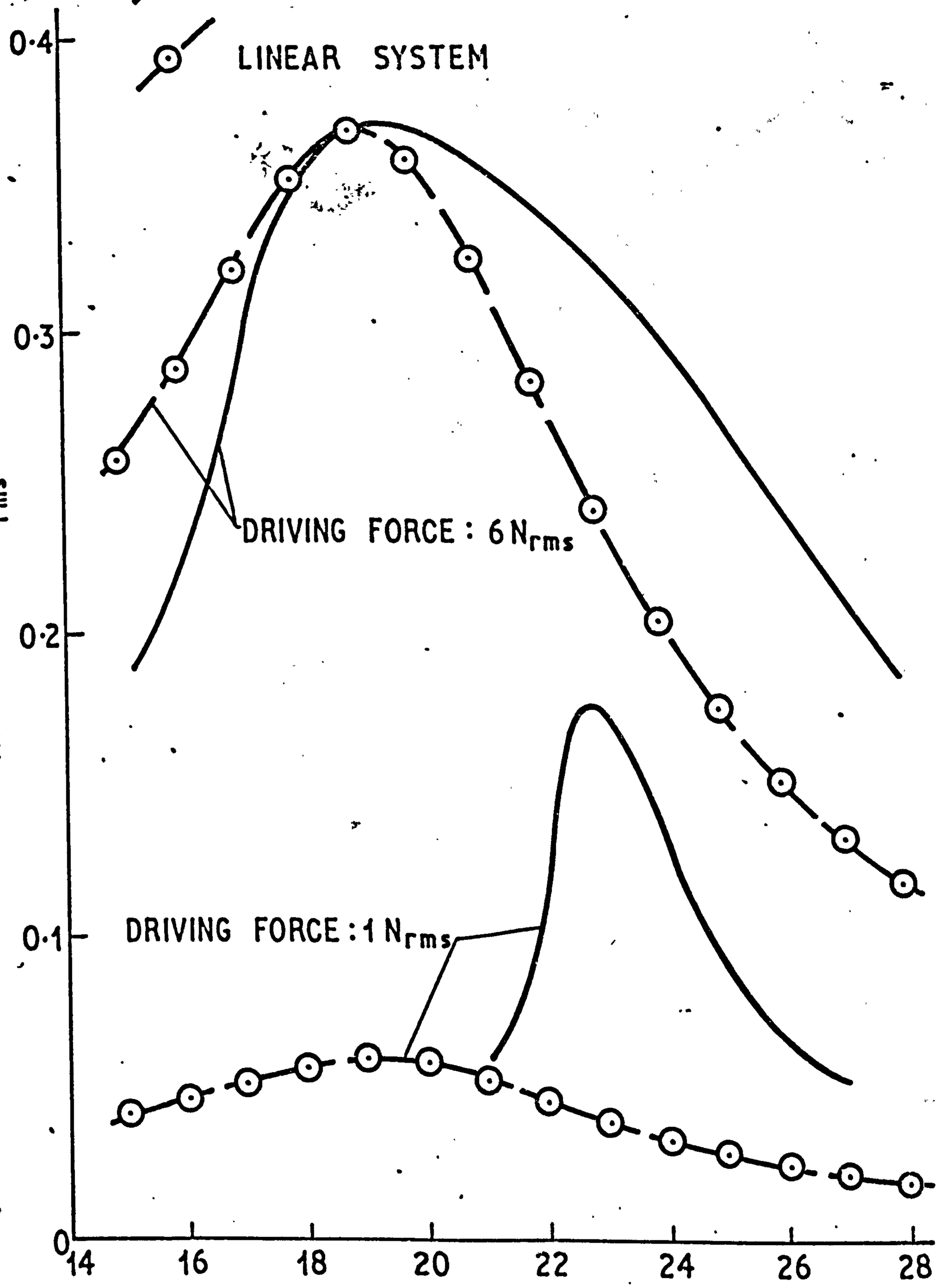

COMPARISON OF RESONANCE CURVES FOR UNBONDED (UNETCHED) SPECIMEN AND LINEAR SYSTEM

FIG. 87

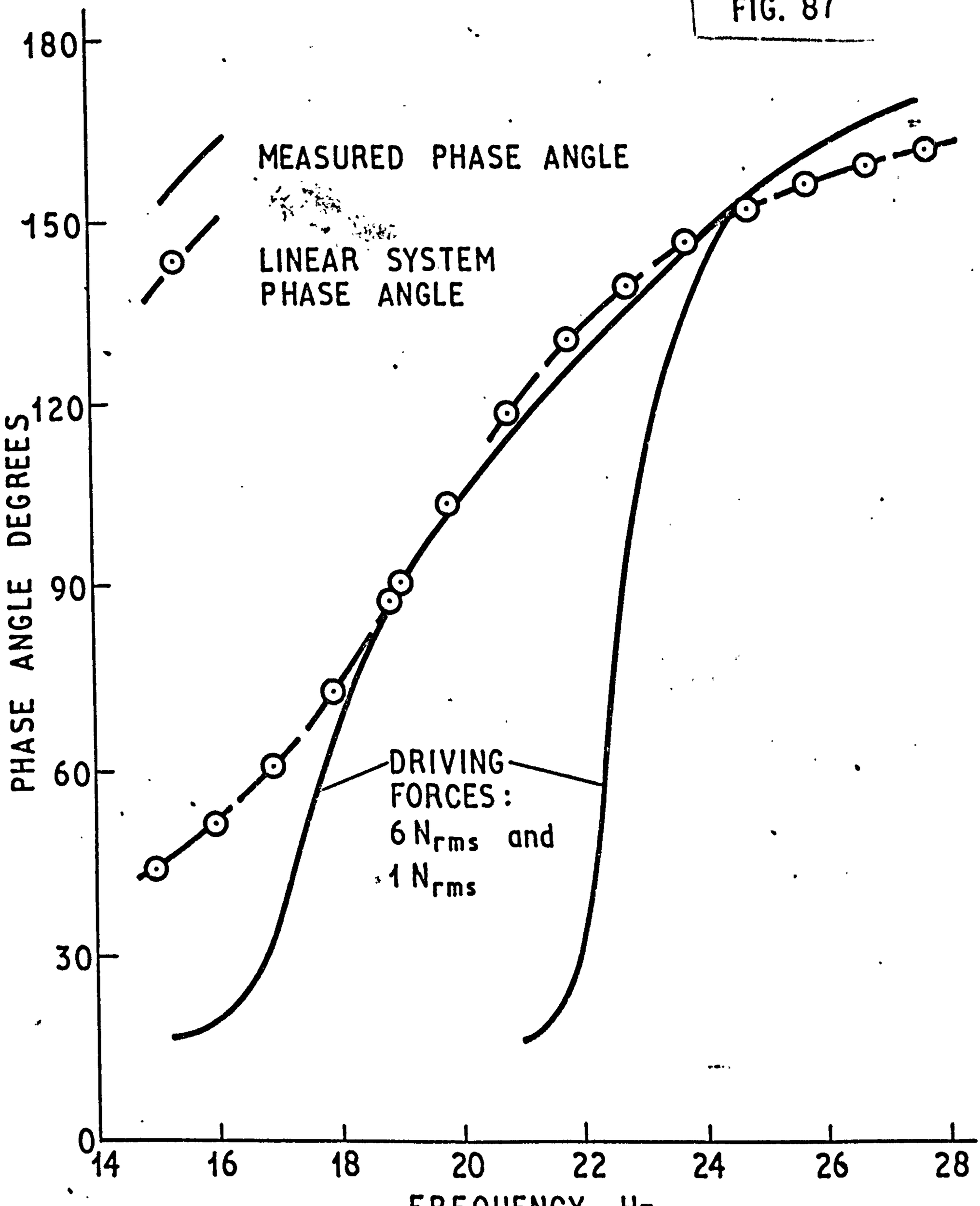

COMPARISON OF PHASE ANGLES FOR UNBONDED (UNETCHED) SPECIMEN AND LINEAR SYSTEM

FIG. 88

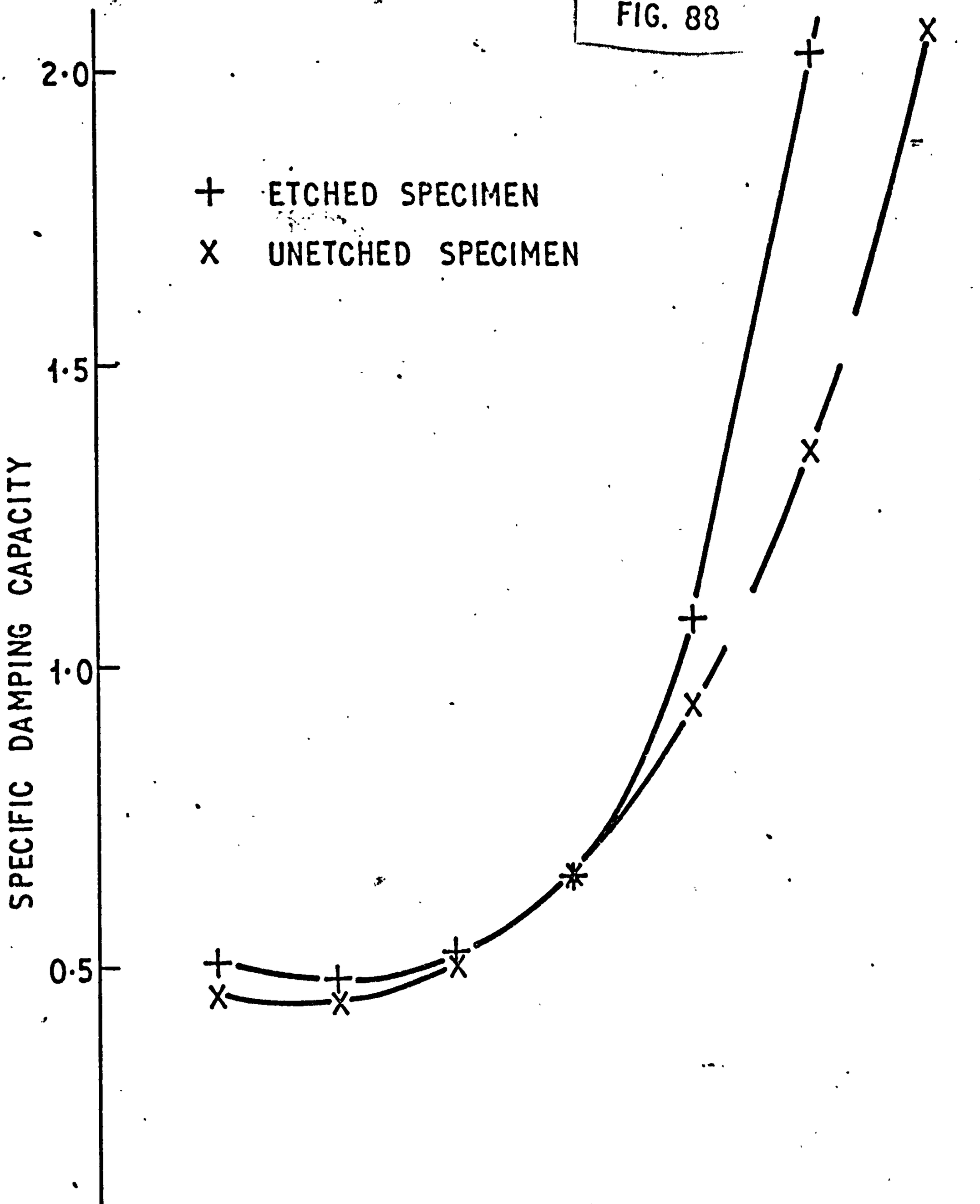

SPECIFIC DAMPING CAPACITY FROM BEST LINE
RESULTS FOR UNBONDED SPECIMENS

FIG. 89

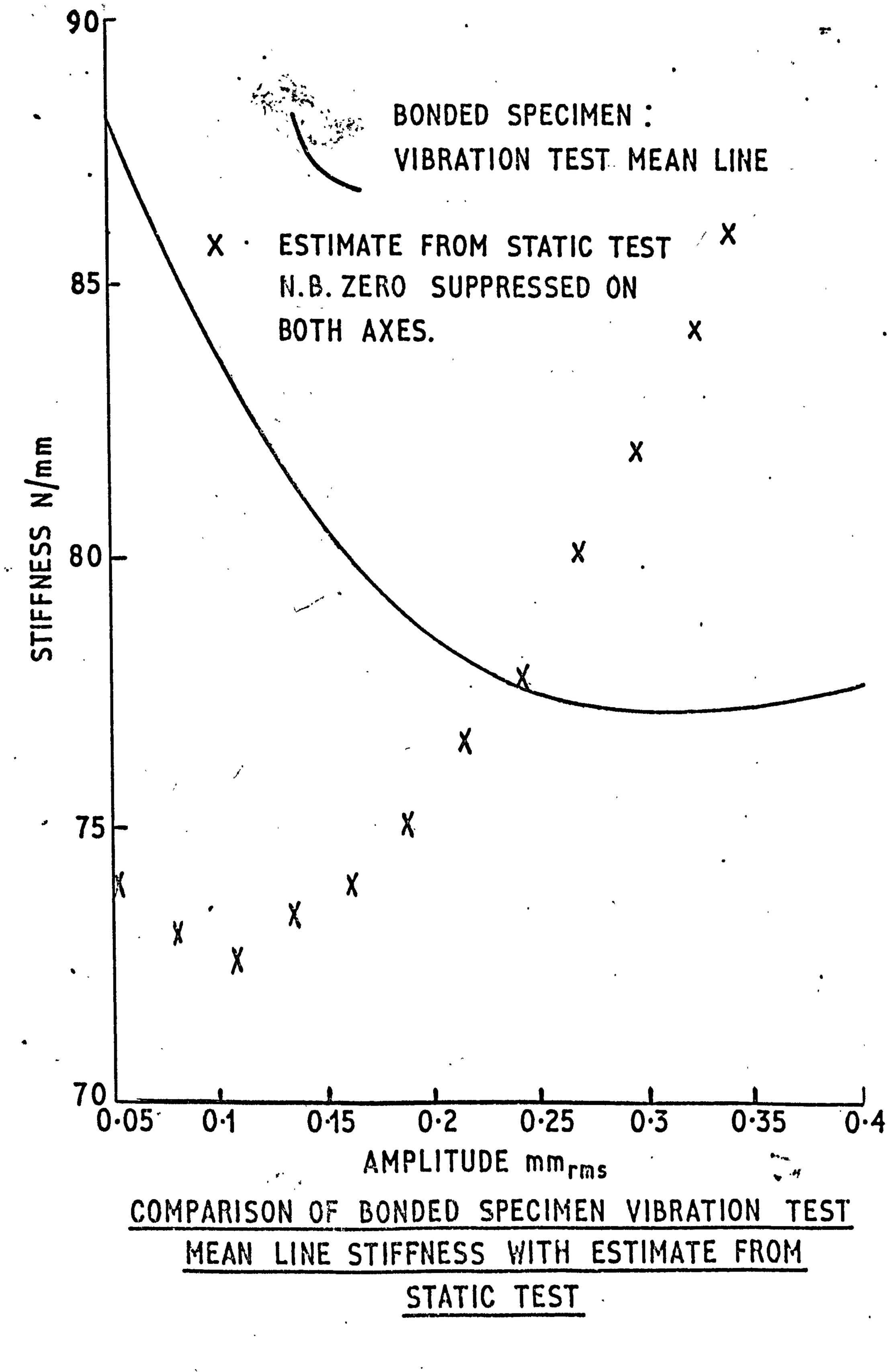

COMPARISON OF BONDED SPECIMEN VIBRATION TEST MEAN LINE STIFFNESS WITH ESTIMATE FROM STATIC TEST

Addenda

p. 27 Matrix Young's modulus

$$= \frac{\text{maximum load in cycle/specimen area } (= 40\text{mm}^2)}{\text{maximum strain in cycle}}$$

p. 28 The term "yielding" has here been applied to describe the phenomenon of bond failure.

p. 36 Figure 16 shows further yielding in the same loop. Figure 21 shows yielding in a loop subsequent to that which showed initial bond failure (e.g. figure 16).

p. 103 The resonant frequencies in the experiments were predominantly influenced by the stiffness of the specimens and the size of the mass used. Since it was desired to have large displacement amplitudes the mass sizes were chosen (3.05 and 4.885 Kg) so that the resonant frequencies were kept low at around 20 Hz. All the measurements were made in the range 14 - 30 Hz although the apparatus could have been used at slightly higher (but not lower) frequencies.

p. 106 1. It was assumed that the calibration of the accelerometer in the experimental frequency range was the same as at the calibration frequency (80 Hz). The measurement of the harmonics in the apparatus and the inferred calibration of the force transducer were carried out in the experimental frequency range (14 - 30 Hz).

2. It was assumed that, since the non-linearity of the specimens was not great, the variation in phase angle in any one cycle would not be great. Such averaging as may have occurred was carried out by the transfer function analyser over 100 cycles.

3. It is probable that the 170° phase distortion is made up from a phase shift of 180° and actual distortion of 10°.

p. 108 The particles do not move only in the axial direction of the bar due to Poisson's ratio effects.

GLASGOW UNIVERSITY LIBRARY